Author:
Young, James J

Title:
Flight control and performance estimation of wild free flying birds and implications for small-unmanned air vehicles

Flight control and performance estimation of wild free flying birds and implications for small-unmanned air vehicles

Jon James Young

A dissertation submitted to the University of Bristol in accordance with the requirements for award of the degree of Doctor of Philosophy in the Faculty of Engineering.

School of Aerospace Engineering, March 2023

Word count: 54,512

Abstract

Birds fly with apparent ease, remaining in control during manoeuvres despite large variations in wind conditions. They do this reliably, repeatably and efficiently. This thesis looks at the flight control of two species of bird, the lesser black-backed gull (*Larus fuscus*) and the red kite (*Milvus milvus*). Rotational stereo videography, a 3D multi-point tracking technique, is employed in the field to study the flight control of wild members of these species in free flight. The motion of the bird's wings and tail was related to the measured flight path to estimate flight control parameters, giving an indication of the control strategies being implemented by the birds. By examining the equivalent control laws for fixed wing aircraft this work highlights the features of the birds' flight control strategy which might enhance the performance of a gliding bird when compared to a traditional fixed wing aircraft with discreet trailing edge control surfaces.

Looking firstly at longitudinal control of flight path angle in gliding flight, it was found that the gulls used fore and aft movement, adjusting the effective sweep of their wings to control their longitudinal flight path angle when in steady glide. This result is interesting as it highlights the decoupling of pitch angle from longitudinal flight path control as is typically found in rigid body fixed wing vehicles. Secondly when making gliding turns the gulls kept their tails furled and used bank angle to adjust their turning radius much in the same way that rigid body fixed wing aircraft do. It was found that the equations of motion for rigid body fixed wing turning mechanics can be applied to model the gulls turning performance as in this case the tail played little roll in controlling turning flight. Conversely a very different result was seen in the turning performance of the red kites. These birds make active use of a widely spread and comparatively large set of tail feather to enhance their control in turning flight. In a straight glide the tail was seen to twist up to $\pm\ 30^o$ to help the bird to maintain its desired ground track and in steeper turns the tail was pro-versely deflected into the direction of the turn to enhance the effective amount of pro-turn force and to increase turn rate and reduce turn radius for a given bank angle. Turns at a lower bank angle made more use of this tail twist than turns at higher bank angles where a small change in wing angle has a larger effect.

The study of the birds inspired three novel control strategies: wing sweep for pitch control, wing twist for direct lift control, and wing rise/flap for variable lateral-directional stability. These three control schemes are implemented on a representative small unmanned aerial vehicle focusing on control about the principal axes using an articulating main wing, with freedom to rotate about the wing root. Wind tunnel testing and computational modelling using a vortex lattice method were used to study the flight dynamics and control potential of these strategies.

Wing sweep for longitudinal flight path control was found to be highly effective, particularly at higher angles of attack. This effective weight shift changes the moment arm between the centre of pressure and the centre of mass and can generate large pitching moments without making large changes to the angle of attack, as such dynamic manoeuvres such as end over end tumbles are achievable. Wing twist for roll control was found to be no more effective than properly sized ailerons, with the upgoing wing being pushed close to its critical angle and in extreme cases stalling and inducing control reversal. Symmetric wing twist for direct lift control has some transient benefits but effectively changes the longitudinal trim position of the fuselage as the wing adopts a new setting angle, its effect was of limited benefit. Finally, being able to dynamically vary the wings dihedral / anhedral angle in flight can profoundly affect the lateral direction stability of the vehicle. High dihedral angles stabilise the spiral mode and excite the Dutch roll mode and might be beneficial in environments where the vehicle would be subject to strong and variable lateral gusts.

To conclude, birds fly quite differently from three-axis, rigid body fixed wing vehicles and some elements of directly controlling the main wing may be beneficial for small unmanned aerial vehicles that demand high levels of agility performance in unsteady flow fields. Having articulated wings and tails extends the flight envelope of 'fixed wing' vehicles, traditional design rules become less applicable and new performance metrics and control concepts are required to fully exploit the benefits over a fixed wing design.

To my beautiful wife Imogen
Who has given me unwavering support to pursue my passion
You are my inspiration, I love you.

Acknowledgements

This thesis could no have been completed with out the support of so many and here I would like to thank them for their contributions. Thank you to my family, friends and colleagues who have supported me over the last six years and to all the people who listened to me talk about gulls, kites, camera systems and aviation. In particular I would like to pay special thanks to the following groups and people for making this possible:

Thank you to the members of the University of Bristol flight lab and the bio-inspired flight research group, for all the support and encouragement when things weren't going well and for being a second opinion when the first clearly had it's issues. In particular, thank you to Dr. Sergio Araujo-Estrada and Dr. Jonathan Stevenson, for your advice, answering all my questions with regard to PCB and aerodynamic design. Thank you to Andrew Hughes for assistance with access to Fenswood farm which was used for testing and storage of all my equipment and thank you to Lee Winter and Russ Eyre for their assistance in setting up the wind tunnel laboratory. Thank you to Dr. Tom Richardson for your support of the flight testing and for allowing me the opportunity to develop of the undergraduate gliding flight experience course.

Thank you to Dr. Emmanuel de Margerie of the University of Rennes for introducing me to the rotational stereo videography methods, for demonstrating your system and for providing support and feedback whilst I developed the new device.

To my supervisor Dr. Shane Windsor, your support since my final undergraduate year through to the completion of this PhD has been fantastic. Thank you for encouraging me to apply to return to the University of Bristol and for providing me with direction in my choice of research project. This thesis would not have been possible without your ongoing academic, financial and personal support. Thank you for taking the time to meet with me and to discuss ideas over the last six years and for supporting me in my career choices. Your knowledge and approach to supervision has and will continue to inspire me. I've learned a lot studying under your supervision and will use those lessons for many years to come, thank you.

Thank you to my parents, Carol and David and my brother William, you have always supported my choices in life even when they seem to be taking me in circles. Thank you for your ongoing support, for listening to everything I have to say about birds, flying and aviation and for financial support, allowing me to use your home to write, without which this would have been so much more difficult.

Above all, thank you to my beautiful wife Imogen. I couldn't ask for a more patient and supporting partner. Thank you for putting up with my life choices, whilst I took us round the country. Thank you putting up with me working long hours and for being away from home. You are my rock and I couldn't have done any of this without you, I love you more than anything.

And finally thank you to gulls and kites of southern England, they were disagreeable subjects at times, but this wouldn't have been possible without them.

Declaration

I declare that the work in this dissertation was carried out in accordance with the requirements of the University's Regulations and Code of Practice for Research Degree Programmes and that it has not been submitted for any other academic award. Except where indicated by specific reference in the text, the work is the candidate's own work. Work done in collaboration with, or with the assistance of, others, is indicated as such. Any views expressed in the dissertation are those of the author.

SIGNED: Jon James Young ..... DATE: 23/11/2022 .....

Jon James Young
March 2023

Table of contents

List of figures

List of tables

Chapter 1

Introduction

1.1 Small Unmanned Aerial Systems and Nature's Flyers

Small Unmanned Aerial Systems (sUAS) make up one of the fastest growing markets in Aviation [1]. The low cost, low risk development cycles of small expendable aircraft are driving innovation in the design of future airborne platforms. These vehicles are moving away from rigid body aerodynamic structures as derived from scaled down traditional aircraft. A lightweight vehicle can exploit different aerodynamic properties which apply at low Reynolds numbers [2]. Birds are well suited to flight at low Reynolds numbers in turbulent environments [3]. Many species navigate the landscape with ease, remaining in control as they move between perches in cities or manoeuvre through dense forests hunting prey, they cope with variations in wind [4], respond to gusts [5] and some species exploit the energy available in the fluid to soar making use of thermal buoyancy, orographic uplift and dynamic shear layers to extract energy and minimise energetic expense [6]. They do this reliably, repeatedly and with apparent ease.

The early pioneers of human flight looked to natures aerialists for inspiration, now with advances in material science, aerodynamics and controller design it is time to do so again. Early flight concepts from the likes of da Vinci, Caley, Lilienthal, Langley and the Wright brothers took inspiration from birds to design their aircraft; the general arrangement and in particular the first aerofoils [7]. However, it became apparent that these bird derived wings were not well suited to the higher Reynolds number flight regime the early pioneers were exploring and as human aviation advanced the focus turned to flying higher and faster. The physics that governs these flight regimes has since been well investigated and there are a variety of engineering references and models available if you wish to design an aircraft to operate at higher order Reynolds numbers. Not so for flight at smaller scales.

Whilst aeronautical engineers changed focus, bird flight continued to be of interest to biologists and the aerodynamics and flight mechanics of a variety of species is part of established literature [8]. Bird flight is varied as different species are subject to a variety of external pressures. The evolutionary process results in an animal that is well suited to the full variety of tasks it must accomplish to survive and reproduce and as such its body isn't necessarily optimised for the simple task of flying as efficiently as possible [9]. As with all forms of natural motion it is possible to identify a variety of flight strategies distinguished by the motion of the wings. These strategies broadly fall into one of three categories (Figure 1.1) [10]:

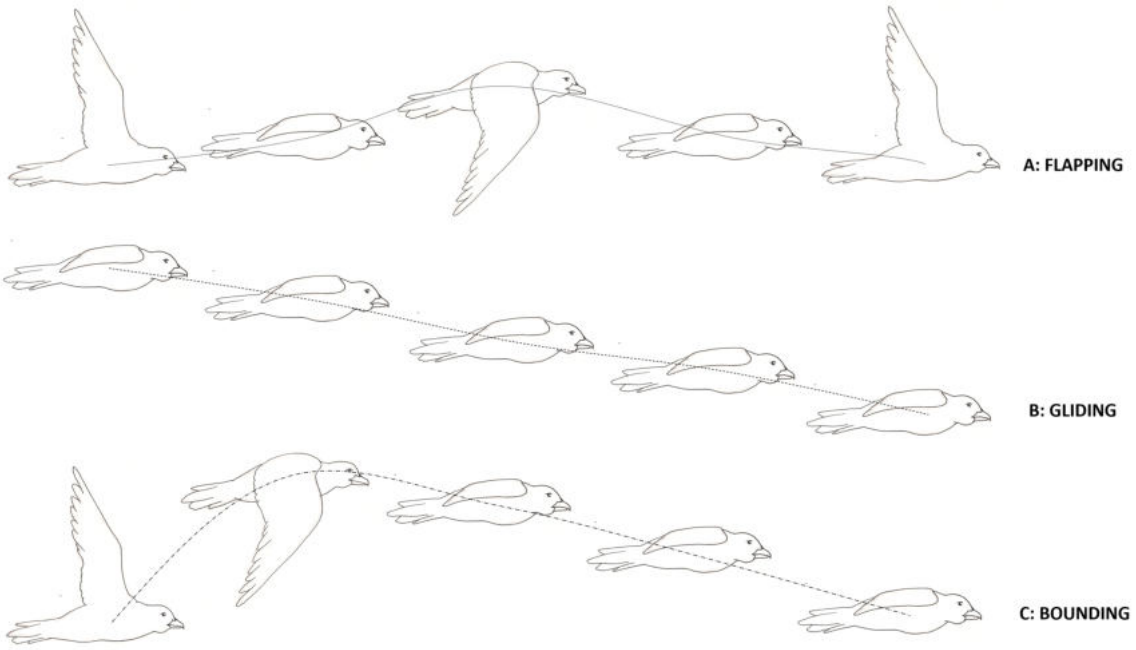

Fig. 1.1 The different flying gaits exhibited by different birds. A: Flapping, B: Gliding, C: Bounding

Flapping - A cyclic wing motion comprising of a downstroke and upstroke, the gait of the wingbeat varies to provide the required thrust and lift to achieve the desired flight path.

Gliding - A quasi-static wing position generates a resultant aerodynamic force that overcomes the birds weight and drag, birds that adopt this strategy achieve the lowest levels of energetic cost.

Bounding (Flap-Glide) - A combination of the aforementioned strategies which provides the bird with more control of it's flight path at a lower energetic cost than a continuous flapping cycle.

Of the three flight strategies, birds optimised for gliding and soaring flight are the most relevant to the design of a UAS with an independent propulsion subsystem. The wing of a bird in a steady glide can be modelled as a quasi-rigid body (albeit one which has deformed under aeroelastic load) with a fixed geometry and control inputs through a manoeuvre can be modelled as a series of discreet updates to this geometry in time[11].

Quantifying the flight performance of a bird requires simultaneous measurements to be made relating the control inputs the animal is making to changes in it's flight path. Various techniques have been developed in the pursuit of a better understanding of birds in free flight. Early efforts were largely observational and qualitative, relating the macro-motions of flights to environmental factors. The first recordings were made by plotting the path of a bird along mirrors [12]. More recently radar, radio tracking and optical methods have been used to attempt to quantify and record the flight path of birds at scales covering large scale migrations to individual soaring or perching manoeuvres [13]. These techniques employ Altitude - Azimuthal measurements in relation to the observer and provide detailed flight paths in a relative coordinate system. Global positioning system (GPS) receivers offer the highest temporal and spatial resolution measurements of the flight path of a bird in free flight outside of a laboratory environment [14]. Combining GPS with miniaturised inertial reference systems (IRS) represent the current state of the art when making measurements of flightpaths and body forces in free flight outdoors.

Measuring changes to the geometry of the lifting surfaces that reflect control inputs requires more control than has typically been achievable in a field environment. Coupling a controlled environment such as a wind tunnel or flight corridors with high resolution imaging techniques: motion capture and videogrammetry, it is possible to make more detailed measurements of changes in geometry [15][16].

Traditional flight mechanics for 3-axis rigid body aircraft relate external forces and inertial properties to the kinematics and consider aspects pertaining to a nominal steady state flight condition. Such states are representative of a particular phase of flight, for example: straight and level, constant speed coordinated turns and constant speed climb or descent

Unmanned aerial systems designed for small sensor payloads and operating with flight parameters similar to those of medium sized soaring birds are becoming common place, performing missions where human operation is undesirable due to the dull, dirty or dangerous nature of the task [17]. These aircraft are expected to operate in all weather, in dynamic obstacle rich environments and with uncertainty of position. Birds perform live their lives and operate day and night in this environment with ease.

This work investigates what features enhance the performance of a bird when compared to a traditional fixed wing aircraft subject to three axis control.

1.2 Project aims and objectives

The aim of this project is to evaluate how a gliding bird controls it's flight path and to explore novel control arrangements based on actuation of the primary lifting surfaces when applied to Unmanned Aerial Systems. Gliding flight was chosen because of the reduced order parameters and for the ability to reliably identify repeat manoeuvres in wild birds. It is a requirement to achieve stable straight and level flight with any aerial vehicle, additional manoeuvring functions are supplementary to this requirement. This project specifically addresses the following research questions:

1. How can the flight performance of a bird in free flight be quantified whilst performing a wide variety of normal flight manoeuvres without inhibiting natural behaviour?

2. What parameters define the control scheme of the bird, how are the primary lifting surfaces actuated to achieve the desired flight path and are there any quantifiable control laws observable?

3. What affect does a primary lifting surface with a higher degrees of actuation freedom have on the flight performance on a small unmanned air vehicle?

4. How does the actuation of secondary lifting surfaces affect the control of the flight path?

To answer these questions this work develops on existing measurement techniques by using multi-point tracking technologies to make measurements of a bird's flight path and the position of key markers on the body through a series of flight manoeuvres. The information from these flight tracks identifies features of the birds morphology that are effecting the control of the flight path. This information provides the basis of the development of a series of experimental sUAV platforms that incorporate an articulate wing, hinged at the root, inspired by the forearm layout of a medium sized soaring bird. Further development of the flight model is extended to more novel control system layouts in simulation.

To answer these research questions the following objectives were undertaken:

1. Develop a multipoint tracking system to make measurements of a free flying bird, recording the flight path and position of the primary lifting surfaces remotely on wild animals with no hardware attached to the subject (Chapter 3)

2. Analyse the birds techniques to control its flight path in a variety of flight manoeuvres focusing on longitudinal and lateral flight performance and control (Chapter 4 / Chapter 6)

3. Investigate the effect of articulating a primary lifting surface at the wing root, inspired by the function of the birds shoulder joint, increasing the freedoms and magnitude of control forces available to the sUAV platform (Chapter 5 / Chapter 6)

4. Consider how a bird inspired articulating wing might contribute to future UAV design (Chapter 7)

1.3 Contributions

This thesis has three main contributions. First and foremost this thesis presents an improvement to a 3D position measurement technique that is able to simultaneously measure flight path and fit a reduced order geometric model of the bird's morphology to make estimates of control surface position at discrete points in time. The Rotational Stereo Videography method (RSV) is an extension of existing technologies [18] and uses stereo imaging and angular encoding to combine multipoint tracking with spatial and temporal filtering to allow for quantitative measurements of flight path and control derivatives to be made from high definition video recordings of free flying wild animals. The equipment is low cost and can be easily replicated using consumer accessible cameras and optics, it is field portable, can be rapidly deployed to new locations and requires only minimal calibration using in-situ or external reference points. This method serves to provide the data capture required for the second contribution.

The second contribution is an assessment of the flight control strategies observable in two species of native British birds and describes the longitudinal and lateral-directional control characteristics. An assessment of the longitudinal flight path control of the gulls (*Larus fuscus*) in gliding flight is presented and it was found that the birds use their main wing for longitudinal control, this is in opposition to the traditional control schemes employed in three-axis flight control which requires an empennage with discrete surfaces to achieve similar results. One of the main observations was the decoupling of the body from the wing which breaks a key assumption in the rigid body equations of motion for aircraft and in this case it was necessary to consider appropriate variable substitution to apply existing equations of motion to the birds flight paths. In addition the lateral-directional control and turning performance of the Red Kite (*Milvus milvus*) is observed to again be quite different to both the gulls and three-axis control. Kites in gliding flight make substantial use of their tail surface as a means of control. When turning they use their tail surface to augment the effect of banking the main wing to increase turning authority at low speeds and low angles of bank. In this manner the kites use their tail to modulated side-force in a turn at a constant bank angle.

Finally this thesis presents a series of articulated wing designs to validate the use of bird-inspired control schemes on small unmanned air vehicles. Three different main wing articulation schemes are considered: wing sweep for pitch control, wing twist for direct lift and roll control and variable wing dihedral for dynamic adjustment of lateral stability. Each wing articulation design has been validated through wind tunnel testing and it's control effects examined using numerical analysis via a 3D vortex panel method. Wing sweep was found to be a powerful control input for controlling vehicle pitch attitude, particularly at high angles of attack when traditional control surfaces begin to lose effectiveness. Wing twist is useful for adjusting the trim angle by varying the setting angle between the wing and the fuselage, in addition its use as a form of direct lift control showed promise but no real benefits were seen in roll control. Variable dihedral can dramatically change the lateral stability characteristics of the wing and may be useful to reconfigure for suppressing lateral directional modes in some situations.

Overall this thesis contributes a demonstration of the application of bird-inspired control schemes to smaller vehicles which require substantial control power at lower flight speeds. It does this by presenting a novel multi-point tracking system which was developed using low cost consumer grade equipment and can be rapidly deployed in the field. This system allows for the analysis of the motion of the primary and secondary lifting surfaces on the bird and how these impact the flight path. By applying articulating wing and tails in future control schemes the flight envelope of small winged UAVs may be extended.

1.4 Document structure

Chapter 1: Introduction - An introduction to small unmanned air vehicles and bird flight. This chapter lays out the aims and objectives of this research and the contributions of this thesis.

Chapter 2: Background and literature - A brief discussion of the operating requirements for small unmanned aerial vehicles and the fundamental forces acting on both aircraft and birds. This is followed by a discussion of bird flight specifically focusing on how they differ from engineered flying machines. The next section presents a short history of research into quantifying bird flight parameters and the development of observational measurement techniques to establish the background of the 3D tracking technique employed in this thesis. The final section looks at bio-inspired flight and how bird control techniques might be adapted to service the established rigid body flight parameters and to summarise the position of this research within the established literature.

Chapter 3: Remote measurement of flight path and pose - This chapter describes in detail the Rotational Stereo Videography tracking technique and presents the results of the lesser black backed gull study. The technical setup of the camera, optics and encoding system are described in detail including the basis of the stereo depth measurement methodology. The estimation of control parameters from video data requires considerable processing and the full methods for extracting flight path, kinematic properties and estimating the birds pose to extract control surface position are described in this chapter. Due consideration is given to the expected sources of measurement error and the ways to reduce it as much as possible. This chapter explains how RSV can be applied to flying birds and the typical results which it can output as well as the limitations imposed by the underlying assumptions.

Chapter 4: Longitudinal and lateral control of gliding flight - The RSV system is used to collect flight data of Lesser Black Backed gulls from flights around the Bristol Harbourside located in central Bristol, UK. The results comprise of an assessment of both longitudinal and lateral flight control strategies. In straight and level gliding flight the results indicate a correlation between wing sweep position and the birds flight path angle, indicating a possible longitudinal control law.

Chapter 5: Bird inspired control schemes using the main wing for flight control - This chapter is a study into the effect of using an articulated main wing for primary flight control. The chapter starts with a recap of traditional three axis control and establishes the wing root articulation as a basis for an alternative method of flight control. Three separate wing articulation mechanisms which each restrict the articulation to a single degree of freedom comprising of sweep, twist and dihedral are presented. The effect of these control schemes were validated with wind tunnel tests and further analysed using a vortex panel method. Each articulation has an associated control scheme and the effectiveness of each control scheme is discussed in relation to traditional discrete surface control.

Chapter 6: Lateral control using a variable twist tail - Red kites use their tails to control their turns. This chapter specifically looks at a the effect that a twisting tail has on the turning flight of the red kites. The introduction establishes the role of the birds tail as an aerodynamic surface along side other considerations, the birds tail is contrasted against the empennage structure found on engineered aircraft. The observational results show that the tail plays a very active role in controlling the turning flight of the red kites and a variety of control schemes are considered. Measurements from Rotational Stereo Videography reveal the range of motion of the tail and the way it is actuated in gliding turns to effect control. Analytical modelling of the tails establishes the expected forces and moments such a surface would be capable of generating and compares this to traditional empennage control surfaces. This chapter discusses the requirement for lateral and vertical control and stabilising surfaces and how an articulating tail may be applied to the design of a small unmanned air vehicle.

Chapter 7: Summary and Conclusions - The final chapter in this thesis discusses the highlights of this body of work, summarising the key contributions and contains a final discussion of how implementing articulated main wings and tails along with bird inspired control schemes might influence the design of small UAVs in the future.

Chapter 2

Background and Literature

2.1 Requirements for small unmanned air systems

Small unmanned aerial vehicles are expected to function in wide range of environmental conditions. The low mass and inertia of these small vehicles place large demands on the control system to operate in turbulent environments. Turbulence and it's effects influence the guidance particularly at low altitudes and in proximity to obstacles and terrain [19]. Turbulence within a fluid is identified by random variations in pressure, temperature and velocity [20] and it manifests in various structures at a range of spatial dimensions and temporal frequencies. These turbulent flows are highly irregular both in structure and time, typical structures are rotational and diffusive and can cascade through scale domains over time.

To some extent the characteristics and onset of turbulent flow are predicted by the Reynolds number (Re), the ratio of inertial to viscous forces in the fluid (Equation 2.1). These forces are modelled as the product of fluid density (ρ), the mean fluid velocity (U), a reference length ($\bar{c}$) and the dynamic viscosity of the fluid (μ).

$$R_e = \frac{\rho \bar{c} U}{\mu} \tag{2.1}$$

Some UAS systems operate at Reynolds number consistent with turbulent flow and at a scale susceptible to many of the turbulent structures found in lower atmosphere.

The scale of vehicle attitude control power needed to stabilise flight in a dynamic atmosphere should not be underestimated. Gusts regularly exceed the maximum safe airspeed of some vehicles, gusts of more than 10 m/s can be experienced due to convective activity [21] generated by local depressions, thermal heating and storm activity. A relatively large convective cumulus cloud with a volume of 1 km^3 and a density of 1 g/m^3 contains approximately 500 tonnes of water [22], the force this mass of moving air can impart on a small flying vehicle is significant.

Gusts are difficult to detect, can be temporally and spatially variant and act upon the airframe with forces that can potentially overcome even the most powerful of conventional control surfaces [23]. A gust can disrupt a vehicle's flightpath and ability to maintain station, thus affecting the outcome of its mission. In the take-off and landing phases and any other situation that requires flight in close proximity to the ground, structures, vehicles or people, there is a real risk of collision and damage.

Large manned aircraft have the advantages of scale. Primary lifting surfaces are sized such that most of the high frequency, low amplitude atmospheric turbulence is averaged out across the lifting surface - affecting the aircraft's flight path but preserving the body orientation [24]. More massive aircraft have higher mass moments of inertia. This property increases the rise time in the response to external perturbation giving control systems time to measure the change and apply a corrective input. Despite this, there are strict limits placed on the operational environment of these aircraft to prevent an upset condition and a loss of control. Anywhere these aircraft operate in close proximity to the ground or other obstacles there are systems in place to provide information about the properties of the atmosphere at the location to assess whether the aircraft will be within the operational envelope. In most cases because of the scale of the aircraft, generalised meteorological information comprising of pressure, temperature and wind velocity are sufficient to properly estimate the expected levels of turbulence [25]. Systems to detect and measure these parameters are both predictive and reactive and are present locally on the aircraft and at remote stations but it is clear from continuing incidents that cite turbulence as a contributing factor that better forecasting and response is needed to enhance the safety of aircraft [26].

Smaller UAS do not benefit from these advantages of scale. Their lifting surfaces are at scales comparable to the typical turbulent structures found in cluttered environments. The lower mass airframes have smaller mass moment of inertia resulting in faster rise times in response to external perturbations. Many of the systems needed to detect and measure the expected turbulence are either not accessible remotely due to the uncertain nature of the theatre of operation or the technology's mass budget is inconsistent with the payload fraction of the airframe as the technology is not easily scaled down. An attitude control system for a small unmanned air vehicle must be capable of stabilising flight in significant turbulence. Requirements of such a system include: Minimising path divergence for flight in confined space and maintaining controlled flight in ground effect and obstacle wakes [27]. To achieve these functional requirements the system must maintain sensor pointing accuracy in the presence of uncertain turbulence and must minimise it's load on the system in terms of mass and power budget [28]. Conventional sensors provide some of this functionality but further sensor research indicates a requirement for novel sensors to provide the predictive control required to achieve high levels of agility in strong turbulence [29].

A combination of passive dynamic stability, derived from design features that promote an inherent tolerance to gust level, active attitude control systems and advanced sensor suites, will provide the basis of a vehicle that is truly robust to uncertain atmospheric turbulence and resilient to gusts.

2.2 Flight Mechanics of rigid body aircraft

A classical assumption made when analysing the motion of a fixed wing aircraft is that the aircraft is comprised of rigid bodies whose geometric relationship to each other remain fixed and do not deform under loading and that the body as a whole is free to move in space. The motion of the body and the forces applied to it are condensed to a single point to simplify the mathematics. The centre of gravity is typically chosen as in steady flight all forces acting through this point should sum to zero.

2.2.1 Fundamental forces

A powered aircraft reacts it's weight with an aerodynamic lift force and that which obtains it's lift through the action of an primary lifting surface and not from buoyancy (as is the case with dirigibles) nor from a substantially vertical element of thrust (as is the case with rockets) is considered to be acted on by four fundamental forces acting through the centre of gravity. These forces being Lift (L), Weight (mg), Thrust (T) and Drag (D):

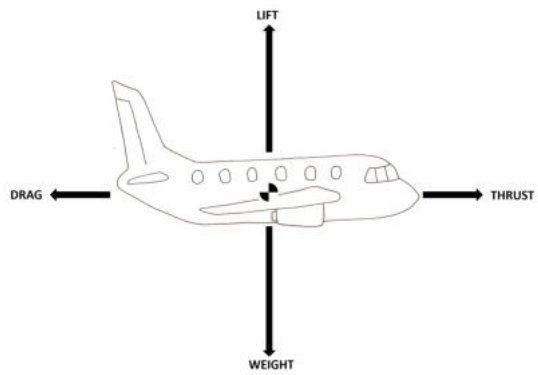

Fig. 2.1 The four fundamental forces acting on a flying body subject to aerodynamic lift

Steady level flight is defined such that the vertical component of the aerodynamic force, Lift, is equal and opposite to weight and the component parallel to the free-stream direction, Drag, is equal and opposite to the thrust.

2.2.2 Reference frames and degrees of freedom

To establish the motion of the aircraft through space and to resolve the forces acting on the body it is necessary to establish a number of different frames of reference.

This body moves through space in relation to an Earth centred frame of reference, with the origin at an arbitrary location. Defined by 2D position XY usually by Geocentric coordinates: Latitude and Longitude, and by a vertical component either as an altitude measured above mean sea level or as a height above a reference datum position on the ground.

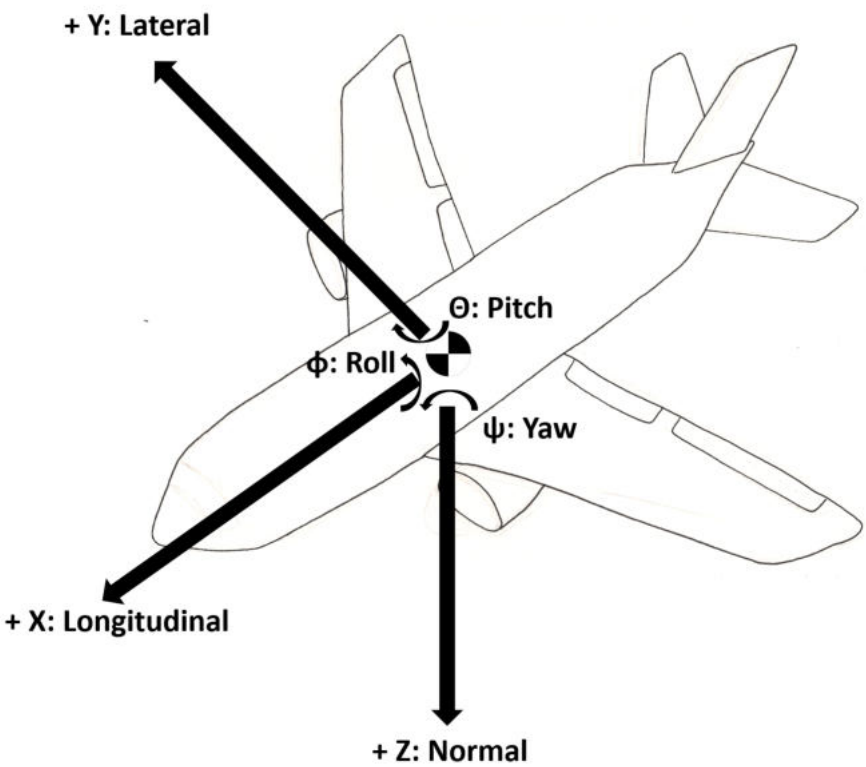

Fig. 2.2 Principle axis of the aircraft aligned with the fuselage centreline, wing axis and normal vector.

Using Cartesian coordinates the aircraft can be considered to have a Body frame of reference, with the origin at the body Centre of Gravity defined by three axis:

Longitudinal Axis: Positive X is forward along the fuselage plane of symmetry.

Lateral Axis: Positive Y is perpendicular to the X axis and by convention on the starboard side.

Normal Axis: Positive Z lies on the plane of symmetry below the aircraft perpendicular to the XY plane.

The relative position of this body centred frame is typically measured with reference to the Horizon. A flat plane orientated perpendicular to Earths gravity vector at any point over the earths surface, with an arbitrary axis origin and orientated by convention to True North. The transform between the Earth frame and the Body Frame is described using three Euler angles:

Roll (ϕ): A rotation about the longitudinal axis with reference to the horizon.

Pitch (θ): A rotation about the lateral axis with reference to the horizon.

Yaw (ψ): A rotation about the normal axis. When referenced to true north it is known as a heading.

In addition there is a final frame of reference defined by the relative wind acting on the aircraft. Through this we define the aerodynamic forces acting on the body.

The transform between the Earth frame and Wind frame is described using three Euler angles:

Angle of Bank (ϕ): With reference to the horizon.

Flight path angle (γ): With reference to the horizon.

Track angle (TRK): With reference to True North.

The transform between the Body frame and Wind frame is described using 2 Euler angles and these properties are proportional to the aerodynamic forces acting on the body:

Angle of Attack (α): The angle between the average chordline and the relative wind in the XZ plane.

Angle of Side-slip (β): The angle between the body centre line and the relative wind in the XY plane.

The three coordinate systems: body referenced, earth referenced and wind referenced and the transforms between them are conventional standards [30]. Where this thesis deviates from standard appropriate definitions are provided.

2.2.3 Stability and Control

A traditional fixed wing aircraft comprises of a fuselage connected to a primary lifting wing located close to the centre of gravity and an empennage with a vertical and horizontal stabiliser [31]. This arrangement is a result of a long standing requirement for longitudinal and lateral static stability required in manned aircraft. Arranging the centre of gravity to be close to the aerodynamic centre of the primary lifting surface minimises the moments induced by the majority of the lifting force reacting the aircraft's weight. Placing the secondary lifting surfaces aft of the centre of gravity the surfaces produced stabilising moments when perturbed. The long moment arms enhance control effectiveness for a given surface area. Aircraft designed to be flown without computer control augmentation are typically statically stable and either dynamically stable or have low frequency dynamic modes that are easily controllable by a pilot. The control scheme used in powered flight is essentially unchanged since its inception. 3-axis control was pioneered in a patent by the Wright brothers [32] as a means to "to provide efficient means of guiding the machine in both vertical and horizontal directions".

Fixed wing aircraft maintain a substantial velocity along the longitudinal axis throughout the flight envelope. This longitudinal airflow acts on the primary surfaces to produce the lift that reacts the vehicles weight. Additional secondary lifting surfaces are used to introduce control forces and moments. These secondary surfaces may be discreet surfaces or flapped segments of a primary surface. By varying the position of these surfaces the local aerodynamic properties can be altered, imparting roll, pitch and yawing moments to the airframe which are used to control the vehicle's trajectory through space. Three primary flight controls are used: Ailerons provide roll moments through asymmetric deflection of flaps on the primary wings trailing edge. Elevators provide pitching moments via deflection of a flap on the horizontal stabiliser. Yawing moments are achieved through application of the rudder.

Translational forces can be achieved through varying engine thrust and high drag devices but these are substantially limited to acting along the longitudinal axis. As such traditional fixed wing aircraft as described do not achieve true translational control independent from the lifting force required to maintain aerodynamic control.

2.2.4 Limitations of 3-Axis control

Three axis control works well when directing the aircraft to follow a specified flight path in still air. However, many of the perturbations encountered by an aircraft act in direction that is out of the plane described by the vehicles flight path. When using 3-axis control the aircraft has the ability to control its rotations around its velocity vector but it cannot directly respond to an out of plane translational perturbation. Instead, pitch and yaw inputs combined with changes in thrust or drag are used to manage the change in angle of attack or side-slip to correct for out of plane translational perturbations. Whilst some aircraft use additional secondary flight controls or reaction based control systems to add translational degrees of freedom and to decouple the effect of aerodynamic controls surfaces with respect to forward velocity there are very few vehicles that use the primary lifting surfaces to achieve additional control axis.

However if we turn attention to nature, birds wings are more dynamic, flexible and configurable than any engineered solution. Birds achieve remarkably robust control in the most dynamic environments at a scale comparable to small unmanned air vehicles and they don't use the traditional 3-axis system to achieve it.

2.3 Bird flight

Why study bird flight? Flight it seems is perhaps the most economical way to move through space. Of the circa thirteen thousand species [33] of warm-blooded vertebrates over ten thousand of them have taken to the skies. Birds are not alone when displaying mastery over movement through the air. Arguably the most successful users of the air are the nearly 1 million species of insects that inhabit the planet. The extant species account for 90 percent of all species on earth and most of these are flight capable. Bats (the only mammals to have grown wings) are capable flyers, with some studies claiming the likes of the Brazilian free-tail to have the record for the fastest flying animal in horizontal flight [34]. Indeed, there are other animals who use the air for locomotion, some marsupials, reptiles and even fish are known to take to the air for brief periods, supported by aerodynamic lift but it is birds who perform the greatest aerial feats at the scales, mass and speeds comparable to small unmanned air vehicles.

Flight through an atmosphere in motion presents a variety of issues [4]. How to deal with component flows, detect wind directions and gradients? Birds demonstrate remarkably robust flight skills in highly dynamic, uncertain environments where the forces acting to oppose their motion can vastly exceed their own mass and strength. They exploit the energy available to them and perform energy harvesting to extend their flights over great distances. Soaring birds exploit thermal updrafts, orographic lift and shear layers to reduce their own energy expenditure [35]. To perform these manoeuvres they must control their flight path with precision and do so with a variety of modified, feathered limbs and tails. How often do you see a bird crash on take-off, be blown into a building or collide whilst in formation?

They can fly in all weathers, day or night and with feathers missing.

2.3.1 How do birds differ from rigid body aircraft

The dynamics of bird in flight are very different to the mathematical models applied to rigid body aircraft. Whist in certain phases of flight, e.g. a straight glide some similar assumptions can be made, holistically the flight model is dynamic and varies between species and with the flying gait.

Birds still have to balance their weight and overcome drag but they do not decouple thrust and lift in the way a rigid body aircraft does [36]. Instead a variable resultant aerodynamic force from both the main wing flapping and tail surface contributes to propulsion and lifting the bird. The various component parts of the bird can in no way be described as rigid. The positional relationship between the various geometries is variable in its configuration and elastically flexible in its response under loads. Indeed attempting to fit a coordinate system to the body for analysis is not a trivial task. For most of the flight envelope there is no plane of symmetry through which to define an axis. Wings change shape and are employed asymmetrically to effect control. Birds rely heavily on visual navigation [37] and so stabilise their head to the horizon, this combined with flexible wing root joints makes defining reduced parameters such as Euler angles very difficult. The wings are comprised of skin and feathers, feathers are non isotropic in there structural and aerodynamic properties, they are flexible and porous to the flow. Where as rigid body aircraft have individual control surfaces to affect individual control axis the response of a bird is highly coupled. The mass distribution of a bird is very different to that of a typical rigid body unmanned air vehicle [38] with variable rotational moments of inertia.

These differences make comparisons in performance between birds and unmanned air vehicles difficult. It is necessary to quantify the performance of the bird in such a way that can be directly related to the mathematical models described by rigid body flight dynamics.

2.3.2 Quantifying bird flight performance

Ornithology, the science of birds, a vast field encompassing ecology, physiology, behaviours and mechanics amongst others has been the subject of research for generations. Indeed, some of the oldest Stone Age cave drawings are of birds. When it comes to the assessment of bird flight mechanics, methods of research have evolved with technological advancement and can be broadly split into several categories:

1. Observational – Research conducted making physical observations of subjects, both captive and wild. Using both the naked eye and enhanced with various optics.

a. Flight path following

b. Morphological studies

c. Qualitative descriptions of migrations / behaviours / manoeuvres

2. Experimental – Aerodynamic characterisation of avian wings, photogrammetric measurements in flight

a. Using trained birds in bird-flight arenas and wind tunnels

b. Using deceased and taxidermy birds

3. Theoretical – Flight dynamics modelling using the latest engineering methods

a. Derivation of kinematic equations of bird flight

b. Application of classical aerodynamic theory to birds

c. Computational fluid dynamics modelling of bird aerofoils and wing plan-forms

2.3.3 Measurements of flight path

Most of the very early observational work regarding bird flight, does not delve into the mechanics, and it was Leonardo da Vinci's Codex on the Flight of Birds [39] in the late 1600s that formed the first real investigation into this form of locomotion.

Up until 1914, research on the flight of birds had been largely observational and qualitative in its description. This early work looked at the various wing configurations used by gulls and vultures in different phases of flight [12] In pursuit of a technique to better understand the soaring flight of these birds Hankin developed the earliest known technique of recording the flight path of a free-soaring bird. This technique involves tracing the movement of the bird along a horizontal mirror.

Various technologies have been employed to track birds since, making recordings of flight paths and ground referenced speeds. By combining this information with wind and weather information useful information on airspeeds and path planning has been obtained. Many authors, Williams et al. [40] and Bruderer and Stedinger [41] , made use of tracking radars capable of identifying individuals birds. Others have used the relative separation of a chase aircraft [11] and on large scales simply visually tracked migrating flocks over great distance [42]. Recently the implementation of miniaturised GPS electronics has made such large-scale tracking of individuals possible.

In an effort to develop a low-cost tracking system to be implemented at ranges $<$ 1km Pennycuick in 1982 introduced a device based on a coincident image rangefinder combined with altitude - azimuthal encoders (alt-azi) and eight-bit computing that could track a bird in a spherical coordinate system relative to the device. Due to its similarity to an architects Theodolite he named it the Ornithodolite [43]. Delinger and Willis [44] built upon this stereoscopic method using a variation on the altitude - azimuth ranging model. Delinger and Willis opting for phototheodolites and using calibrated standard object lengths. They used this device to measure the position and relative bank angle of birds in flight from the recorded video. Tucker [42] made use of an Ornithodolite to make measurements of the flight paths of African White-Backed Vultures and noted equivalences in the way both large soaring birds and humans approach landing. Pennycuick then iterated the design of the Ornithodolite and the latest versions are based on a pair of laser range finding binoculars the same used by

the military to target artillery munitions [45]. It is important to note the distinction here that Ornithodolites do not capture images or video, they record only a single timestamped position measurement, making them useful for recording flight paths but require supplemental methods to simultaneously measure the morphology of the bird and record behavioural traits.

Altitude - azimuth ranging is one method to track an object in spherical coordinates, another is multi-sensor triangulation. Theriault et al. [46] used multiple pairs of fixed calibrated stereo-cameras and videography methods to better understand the mechanics and behaviours of the flights of cliff swallows. The ability to record behavioural information in video whilst tracking the bird through space without mounting any hardware onto the bird is an important feature of videography based techniques, researchers no longer need to capture or train birds for flight research. However, the multi-camera setup requires multiple operators and time to setup and provides a limited volume of interest. Issues of camera syncing and stereo-calibration must be overcome as well as prior site surveys to locate camera spots. It is not an appropriate technique to be rapidly deployed by a single operator in any environment.

In order to perform behavioural observations in inaccessible environments with portable equipment and minimal setup times, a device is needed that combines the portability and single-person operation of Pennycuick's Ornithodolite with the video recording Hedricks multi-camera triangulation method.

Rotational Stereo Videography (RSV) combines the stereo ranging and alt-azimuth encoding of the ornithodolite for animal tracking with high definition video recordings of animal behaviour in the wild (2.3).

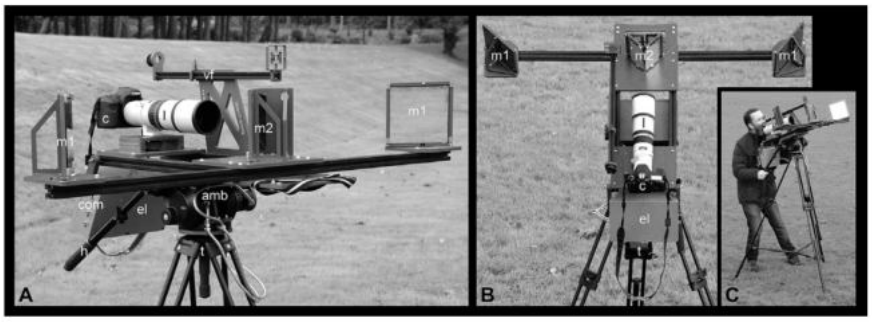

Fig. 2.3 First prototype Rotational Stereo Videography device by deMargerie. (A) The RSV device setup. (B) Mirror geometry showing primary and secondary reflectors and main camera body. (C) Device in operation. Figure reproduced from [18]

The RSV employs a single camera and a Wheatstone stereo setup to eliminate the issues of multi-camera time –synchronisation and can track an animals position to within 1cm at 10m. This methodology is discussed in more detail in chapter three.

2.3.4 Measurements of aerodynamics and control

Experimenting with birds is not a trivial task. Most animals by their nature are non-compliant with people. Two approaches to enforce a condition on an animal is either to use trained animals or to use cadavers in an experiment.

It takes years to produce highly trained individuals capable of performing manoeuvres consistently and repeatedly. Having trained animals in a laboratory environment is beneficial in that it allows for controlled experimentation and can generate reliable and reproduceable data. However in some cases the behaviours of captive trained animals have been shown to depart from the behaviour of wild animals [47]. Examples of using videography techniques on birds in controlled flight arena include looking at common manoeuvres such as a sharp turn [48] and perching [49] both of which use multiple synchronised camera setups to interpret the mechanical perspectives of such manoeuvres.

Deceased animals are much easier to work with. Lentink [50] used wing pairs from deceased common swifts (*Apus apus*), mounted on a force balance in a wind tunnel to measure the aerodynamic forces at play. This technique has since been developed and it is now possible to measure such forces in vivo by using an aerodynamic force platform which supports a contained measurement volume, in which a live specimen can be subject to the test conditions [51]. Whilst information gleaned from deceased animals is useful, in practice the exact wing geometry will depend on how the taxidermy wing is set and will not be the same shape as that assumed when the wing in balancing aerodynamic forces with muscular loads. To be certain of a wings flight geometry it must be recorded in free flight. To do so is not trivial. The first of such efforts in measuring the wing profile sections of free flapping house sparrows (*Passer domesticus*) [52] and free-gliding starlings (*Sturnus vulgaris*) [53], in a wind tunnel, by means of stereo-photogrammetry. Other methods use FARO non-contact surface measurements and NVision three-dimensional laser scanners to extract wing geometry and combined this with fitted models taken extracted from video frames to compute flight-dynamics models for level-flying seagulls, cranes and geese [54]. More recently this technique has been applied to measure the aerofoil profiles of free-flying Steppe Eagles (*Aquila nipalensis*) [55] . Such profiles have allowed them to dissect gross wing morphing and aerofoil properties of a perching bird of prey. With access to trained birds it is possible

to fit them with inertial measurement units like those that are used in traditional UAV autopilot systems, not for control, but for characterisation of accelerations and angular rates. Captive Steppe Eagles have been used to present the first measurements of 3D accelerations and turn rates in free flight. This system makes kinematic measurements of a variety of avian manoeuvres, including: banked turns, wing tucks, pull-ups and gust response in flight [56]. In order to take aerodynamic measurements of the fluid it is possible to use particle image velocimetry, measuring the displacement of a particle seeded fluid to determine fluid velocities to infer aerodynamic properties of flying birds in a controlled environment [57]. This technique provides perhaps the most visually interpretive method of examining the aerodynamics of free-flying birds.

2.3.5 Bird flight physics and aeronautics

Bird flight mechanics, aerodynamics, morphology, wingbeat kinematics, muscle activity and sensory guidance are often considered separately. However it is the interfaces between these systems that are of the greatest interest to designers of future bird inspired systems [58].

Defining the performance metrics to quantify the performance of a bird is not straight forward [59]. Systems engineering principles deconstruct the functions of a system to simplify the design and analysis of individual components. A typical unmanned aerial vehicle might be comprised of a payload housing, an aerodynamic lifting surface, a propulsion system, a sensor system and a control system. This segregated systems way of working is difficult to map onto nature as most biological components perform multi-functions and have complex interactions. For example, separating a passive deformation of a birds wing under load from a deliberate active control input is difficult to do without the knowledge of the control laws and signals being used by the bird. Something that is difficult to measure from an external perspective.

To be able to quantify the flight performance and relate this to improvements in engineered systems a common set of performance metrics and handling qualities must be defined for both the bird and the unmanned aerial vehicle.

2.4 Bio-Inspired flight

Engineering and physical modelling methods are now being applied to provide new insight into the flight characteristics. The stability of birds have can be considered both regarding gliding [60] and flapping [61] flight. Traditional engineering metrics of flight stability (static margin, specific excess power, thrust to weight ratios) can only be strictly applied at fixed flight conditions where an equilibrium angle of attack is specified. Using quasi-static and blade element methods they provide a set of physical characteristics indicant of stable fliers and note that there is nothing inherently destabilising about flapping flight.

Overall wing aerodynamics can be assessed using low-order modelling approaches. Either by using curve fitting and linear regression to estimate taper factors [62] or apply lifting line methods to investigate the performance of the wing [63]. Such approaches have made interesting discoveries concerning aerodynamic efficiency and how discrete feathered wings compare to continuous aerodynamic surfaces. Common approaches consider wings in free-flight but birds typically display the most desirable flight characteristics when interacting near the environment. By modelling the mechanics of flight in separate aerodynamic regimes such as ground effect [64] it is possible to comment on how many species of bird use such techniques to vastly extend their glide and reduce the energetic cost.

Often the avian wing is partitioned to simplify the mathematics, focusing only on what are considered interesting area of flow: around primary feathers forming slotted wing tips, wing-tail interactions and highly cambered wing surfaces (both span wise and chord wise). Drooped wing-tips, contra to the upward swept tips often employed on manned aircraft are very common in flight-generalist species. When looking at the adoption of droops in gliding gulls [65], it is found that this configuration relates favourably with pre-existing flapping wing kinematics and establish maximal lift-to-drag ratios.

When comparing all bird species to engineered flying vehicles the lack of a vertical stabiliser is apparent. Very few of our aircraft are capable of flight without a vertical tail, they generally demonstrate poorly damped yaw modes and all require electronic stabilisation and control systems. Birds plan-forms are perhaps most like these flying

wing designs, as such a lot of interest has been generated, looking at how the slotted-wing tips, tail effects and wing movements are used to control yawing motion. When considering the yaw stability of birds, deriving a dynamic stiffness metric, it would appear that birds can achieve stability by having dynamic stiffness which is sufficiently high for controllable flight even though the birds possess low lateral static stability [66]. The birds use their wing tips [67], in combination with their tail surface [68] to generate and modulate a yawing moment with which to alter their flight path.

When compared to manned flight the avian strategy is quite different. Birds typically exhibit a high level of aerial agility. This level of aerial agility can be contributed to several factors:

- Extensive distributed sensing systems
- Fast reaction times
- Highly efficient actuators
- Massive control power afforded by morphing primary flight surfaces
- Passive self-stabilising aeroelastic lifting surfaces
- Adaptive learning

Much work is ongoing in the field of distributed sensing and advanced controllers but fundamentally flight control for fixed wing aircraft has not changed in since it's inception.

2.4.1 Three axis flight control

For the past one hundred years manned fixed wing flight has for the most part subscribed to the three axis flight control system pioneered by the Wright brothers in the early 1900s [69]. The principle of three axis flight control is to effect controlling moments around the aircraft's three principle axis whose origin exists at the aircraft's centre of gravity. Motion around the longitudinal axis is referred to roll, motion about the lateral axis as pitch and motion about the normal axis as yaw.

Affecting control about these three axis allows the pilot to steer the aircraft through three dimensional space. In addition to the main wing generating lift additional stabilising surfaces (horizontal and vertical stabiliser) are used to trim the aircraft's attitude in flight. To generate the control forces, physical control surfaces alter the lift produced on the primary flight surfaces (main wing) and on the secondary stabilising surfaces. Ailerons act differentially as a pair on the main wing to generate rolling moments about the longitudinal axis. An elevator acts with the main wing to induce a pitching moment about lateral axis. A rudder (or rudders) yaw the aircraft about the normal axis. Additional control surfaces are sometimes employed to directly affect lift production (flaps, slats, spoilers) and some aircraft arrangements move the position of a control surface (i.e. Canards – Elevators positioned ahead of the centre of gravity) or combine control surface functions (i.e. Elevons – Elevators and ailerons as a single surface). Fundamentally these systems all work to provide three axis flight control.

2.4.2 Rotary-wing flight control and similarities to flapping flight

Rotary wing aircraft pose an additional layer of complexity for flight control systems. However many parallels can be drawn between a rotary wing system and a flapping wing system. Both systems rely on highly dynamic wing motions to generate the necessary lift, both have very different aerodynamic regimes depending on whether they are in powered or gliding/auto-rotating flight, both readily exploit non-linear aerodynamic effects, both make use of at least three degrees of freedom of actuation in their main lifting surfaces and both rotary and flapping aircraft make use of their main lifting surfaces as the primary flight control surface. Helicopters and autogyros make use of a swash plate to actuate the main flight surfaces for control purposes. In 1920 Juan de la Cierva developed the first articulated rotor hubs. The rotor hub uses a 3-hinge arrangement to balance lift and drag forces on the rotor disk and to actuate flight control [70].

- **Flapping hinge** – Out of plane varies lift distribution around the rotor disk
- **Lead-lag hinge** – In plane varies drag distribution around the disk
- **Feather hinge** – Control axis alters blade angle of attack

These three hinges allow for three axes of freedom in the rotor disk, with the counter-torque being provided by thrust from a tail rotor. Two control inputs, the cyclic (azimuthally variable) and collective (azimuthally constant) are mixed through a swash plate (rotor-stator control coupling) to vary the rotor pitch azimuthally around the disk. The control forces are transmitted to the blade through a pitch link and the pitch (feathering angle) of each blade is the only rotor hub element actuating control. The flap and lead-lag hinges are passively active, allowing the blades to dynamically adjust their flap and lead-lag angles based on the lift and drag distribution around the rotor disk. These passive hinges are necessary for a stable rotor system. Whilst the articulated rotor hub hinges are necessarily stabilised by the centripetal acceleration of the mass of the rotor blades a similarly articulated wing root may be stabilised in more conventional wings. Biological joints use a mixture of ligaments, tendons and muscle tissue to support and stabilise joints whilst enabling them to carry loads. Having articulation in three planes would give a bird or a vehicle direct control over the wings' effective dihedral, by flapping the wing, the position of the centre of pressure, by sweeping the wing (lead-lag), and, the local angle of attack, by twisting the wing (feather).

2.4.3 Avian flight control

Birds make use of their primary and secondary flight surfaces to control their flight [71]. The main wing and tail work together to coordinate flight. Unlike engineered fixed wing aircraft, birds do not have a control scheme based on discrete control surfaces. The main wing and tail morph in conjunction to provide control in roll, pitch and yaw however they also demonstrate direct control over heave, surge and sway through creative flapping patterns. Birds also demonstrate multiple methods for effecting control, for example initiating a turn can be achieved through wing twisting, extension and primary feather control, the tail is also employed to affect roll control, the exact method and combination of control inputs varies depending on a number of factors including weather, obstacles, competition and may others.

A bird's wing is a modified forelimb. The arrangement of the skeletal structure in an avian wing is analogous to the arrangement of a human limb. The main wing consists of two segments (Figure 2.4): The arm wing comprised of the Humerus, Radius and Ulna, and the hand wing comprised of Carpals, Metacarpals and Phalanges.

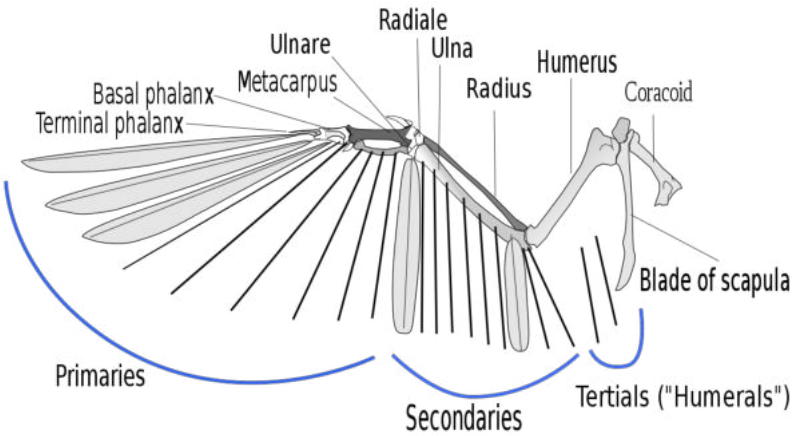

Fig. 2.4 Avian wing skeleton showing the modification of the forearm bones [72]

Large muscles in the chest provide the primary power for flapping flight; the pectoralis and supercoracoideus muscles. These are supplemented by smaller muscles attached to the forearm to provide finer flight control, these muscles are in five pair groups; the biceps brachii, extensor metacarpi radialis, flexor carpi ulnaris, triceps brachii and the scapulohumeralis caudalis (Figure 2.5).

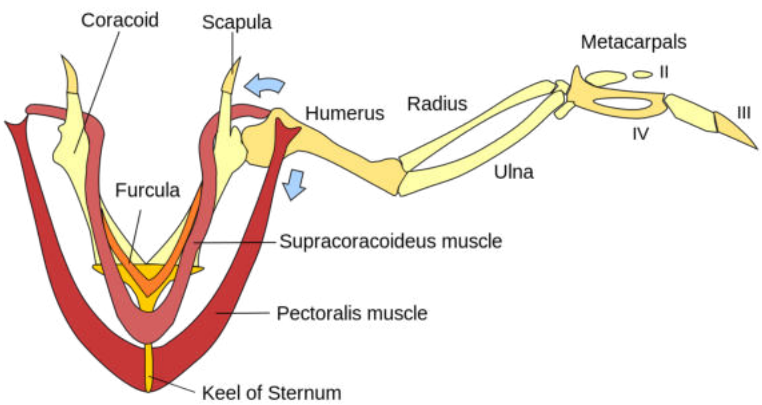

Fig. 2.5 Avian wing flight muscle arrangement showing the primary flight muscles and the forearm muscles [73]

The shoulder serves as a multiple degree of freedom wing root. It transmits loads between the flight muscles (affixed to the breast) and the wing. The Sternum (breast-bone) connects to the Scapula (shoulder blade) via the Coracoid and Furcula strut structure. This junction mates with the proximal Humerus to form the shoulder joint (Figure 2.5).

The elbow joint exists between the Humerus and the Radius, Ulna pair.

In the wrist the carpals and metacarpals are fused, forming three distinct digits. The Alula (thumb) projects along the anterior of the wing, it is independent of the other fused digits.

The various muscles, joints and connective tissue form structures which limit and couple the degrees of freedom which translates into the restrictions on the wings range of motion, the extent of which varies by species and by body mass [74].

Feathers cover the surface of the wing to form the lifting surface. Bird's wing feathers are split into four groups [75]:

1. **Primaries** – Long flight feathers growing from the hand wing

2. **Secondaries** – Long flight feathers growing from the arm wing

3. **Tertials** – Innermost feathers that rest atop the secondaries

4. **Coverts** – Overlapping feathers that form the wing surface lining

Together the main wing primary, secondary and tertial feathers are collectively referred to as Remiges. Tail feathers are known as Rectrices.

2.4.4 Jointed wings

Jointed wings are a massive research topic [76]. Novel materials, mechanisms and actuators are in development which, when coupled with complex control strategies shall provide a step change in aerodynamic control. A bird's wing is the product of millions of years of evolutionary pressure. Much of this may be attributed to environmental factors but social interactions have obviously had a strong effect on the development of some species wings. It is therefore a necessity to separate the aerodynamic advantages from the aesthetic influences that have shaped the bird's wing. The most interesting feature of the overall wing is the jointed nature of its design. The arthroscopic wing bears a resemblance to the rotor hub arrangement employed in helicopter design. A bird's shoulder is essentially a three degree hinge, giving freedom of movement in flap, sweep and twist, this three degree pivot is then repeated at the wrist, with the elbow providing an intermediate third hinge point providing a single degree of freedom, relative sweep between the Humerus and forearm. The system as a whole is coupled subject to the arrangement of bones, muscle and tendons but fundamentally the control inputs can be thought of as flap, sweep and twist angle demands for each discreet ball joint hinge.

2.4.5 Morphing wing UAVs

Aircraft morphing is a term which describes any significant in-flight change in the shape or configuration of the aircraft structure which effects the flight dynamics. Changes can be continuous or discrete with finite step changes in surface position. Typically a morphing structure will trade enhanced flight performance with increased weight and complexity of the underlying structure. Wing morphing is of primary interest with considering it's application in flight control and can be classified by how it affects the wing structure [77]. Rotational morphing of the wing either in-plane or out of plane generates asymmetric pressure distributions which impart control moments. In-plane rotation of the wing, variable sweep, effects longitudinal dynamics. Out of plane rotations, variable dihedral and variable twist effect the lateral-directional dynamics. Multi-jointed wings might have multiple degrees of rotational freedom [78]. Telescopic morphing of the wing changes the dimensions of the wing either through the actuation of discrete surfaces, exposing more wetted area to the flow or through deformation of the structure allowing for continuous changes to the wings profile. Examples of telescopic morphing include span-extension which can be achieved without discrete moving parts [79]. Compliant morphing describes changes to the aerofoil profile without the use of discrete hinges. This may involve changes to the thickness distribution and camber of the aerofoil in flight, changing the response of the wing at different angles of attack. Aeroelastic models of active aerofoils couple the structural parameters and the aerodynamics of compliant morphing structures [80].

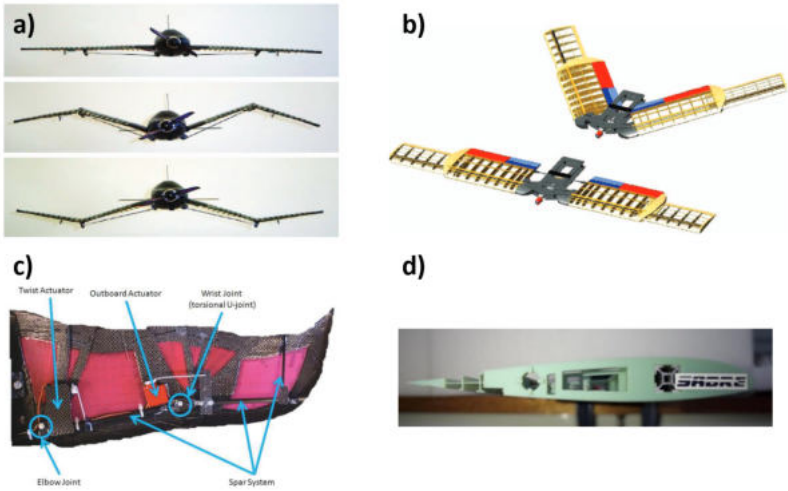

Fig. 2.6 Examples of different morphing wing concepts: a) Gull-wing morphing [81], b) Telescoping, variable sweep wing [82], c) Multi-span variable sweep [78], d)Active camber fish-bone aerofoil [80]

Figure 2.6 illustrates just some of the concepts that have been conceived to allow a typically rigid wing to morph and vary some aerodynamic parameter. One of the main challenges is to maintain a continuous aero-surface whilst allowing for motion in the underlying structure. The mechanisms which drive the changes in geometry can be external (such as those seen on the gull-wing vehicle), internal (the telescopic structure) or achieved through material compliance (the fish-bone). No matter the method of actuation each concept modifies the plan-form of the wing and aerofoil without a discrete flap.

2.4.6 Conclusion

When first looking to develop flying machines the inspiration came from nature and from studying the flight of birds. However the applicability of the mechanics and aerodynamics at work on the scale of a bird is limited when considering large and heavy manned and unmanned aircraft, they do not occupy the same flight regimes. Now as technology is shifting to smaller autonomous platforms operating close to the surface in complex environments and inclement weather, bio-inspired design and strategies are once again in consideration. Most work modelling the bird has been from observational assessment supplemented with specific laboratory based testing. It has been very difficult until recently to make accurate trajectory and body position measurements in a substantial working volume needed to capture manoeuvres at low spatial frequencies. Tracking technologies have advanced to the point where this is now possible. As UAVs have gotten smaller and the strength to weight ratio of materials has increased, compliant morphing mechanisms which would have been untenable on larger scale aircraft are now optional solutions and are being actively considered for their benefits over traditional flight control schemes. By making quantitative measurements to assess the types of control schemes being used in natures flyers and applying this to novel design elements this research considers what features of birds innate aerodynamic geometry can be used to enhance flight control of small unmanned UAVs.

Chapter 3

Remote measurement of flight path and pose

3.1 Chapter Summary

In this chapter a technique for multi-point flight path tracking using Rotational Stereo Videography (RSV) is presented which can be used to assess the behaviour, kinematics and flight mechanics of wild birds in flight. Point position is tracked in spherical polar space, using a pair of angular encoders and a low cost stereo imaging setup for range finding using a consumer grade digital mirror-less camera and optical mirror setup. The hardware is portable and rugged enough to be employed in field conditions and requires minimal setup and calibration. This method is the latest iteration of a series of devices know as ornitheodolites, it is developed in house with fully custom data processing scripts to process a variety of different flight path tracks. The RSV system fills the gap between long range strategic tracking using GPIRS backpacks, which requires capture and handling of wild birds and laboratory based studies which require trained birds in a highly controlled environment. Because RSV is portable it enables study of wild bird populations in their natural environment with minimal interaction between the researcher and subjects. The system outputs timestamped, 3D positions for as many points as are uniquely identifiable on the bird. The position data is filtered spatially using a convolution of a Savitsky-Golay function with the raw data, random error is reduced by using time averaged datasets. Using a reduced order morphology model fit to four morphology landmark points, it is possible to estimate pose and construct a bi-variate model describing the morphing wing of the gull in flight in terms of the wing-line sweep and rise. Flight mechanics equations derived for fixed-wing rigid body aircraft can be used to describe the flight mechanics of a non-rigid body in gliding flight. Because RSV captures video, evidence of in-flight behaviours is also captured. This approach provides a way of quantifying the kinematics and flight control strategies of birds in flight based on reconstructions of the flight path and pose estimation from stereo video, angular encoding and epipolar geometry. Rotational stereo videography serves as the method of data collection for Chapters 4 and 5.

3.2 Chapter Structure

This chapter introduces Rotational Stereo Videography (RSV) as a means to make time referenced position measurements and pose estimation of an object in a 3D volume as a function of stereo video, angular encoding and epipolar geometry. First the physics and epipolar geometry which underpin the RSV method are discussed followed by the hardware implementation of the camera, optics and encoder system, including the data logging protocol and synchronisation methods. The system calibration, video post processing, sub-pixel template matching and data smoothing are discussed to derive the timestamped 3D position data. The method used to collect flight paths and fit a wireframe model using multi-point 3D position information is discussed along with the methods limitations and estimates of the levels of error and uncertainty. A worked example of the post processing of the data is presented to reveal kinematics and pose estimation, this concludes the methods. Finally the methods used are reviewed and suggestions made for improvements based on the outcomes of fieldwork in this and later chapters.

3.3 Introduction

As our small unmanned aerial vehicles begin to infringe on the flight envelope of natural flyers the relevance of their aerodynamic solutions returns to prominence. The challenge now is to make quantifiable measurements of natures flyers and use these to define specific design features of aerodynamic devices, lifting surfaces and control effectors. Cadaver birds and taxidermies wings have been used in wind tunnels to make detailed measurements of aerodynamic properties [83][50]. These are however typically arranged in a notional pose based on qualitative measurement, the preservation process also changes the structural and material properties of the wings and there is no connection with an actual measurable flight path response. At large scales, GPS tracking records flight paths, a useful resource for behavioural or large-scale kinematic analysis but this methodology provides no connection to the body pose and the position of the flight control surfaces [84]. At smaller scales birds can be outfitted with motion tracking features and recorded in a flight arena [16], this provides quantifiable measurements on flight path and pose however the confined nature of these environments limit the types of manoeuvres that can be studied [15].

A system based on visual tracking and 3D reconstruction from stereo imagery provides a way to make simultaneous measurements of flight path and body pose at ranges up to and exceeding 100 metres from the point of observation. The methodology used in this chapter is derived from Rotational Stereo Videogrammetry [18] and allows for time stamped multi-point positioning in 3D space. By fitting a wireframe model to a number of tracked points an assessment of the body pose can be made alongside a measurement of the flight path. Time derivatives provide velocity and acceleration measurements and vector analysis allows for a quantifiable metric of the position of various flight control and lifting surfaces to be defined.

3.4 Methods

3.4.1 Rotational Stereo Videography

Rotational stereo videography is a technique for positioning an animal relative to a device within a 3 dimensional coordinate system [18]. Using timestamped relative position measurements it is possible to derive body velocity and acceleration relative to the device. Assuming the device is fixed stationary to Earth and has known coordinates within the absolute Earth coordinate system and aligning the device azimuth and inclination axis relative to Magnetic North and the Horizon respectively, the position, velocity and acceleration measurements become ground referenced in the Earth Cartesian system (Figure 3.1).

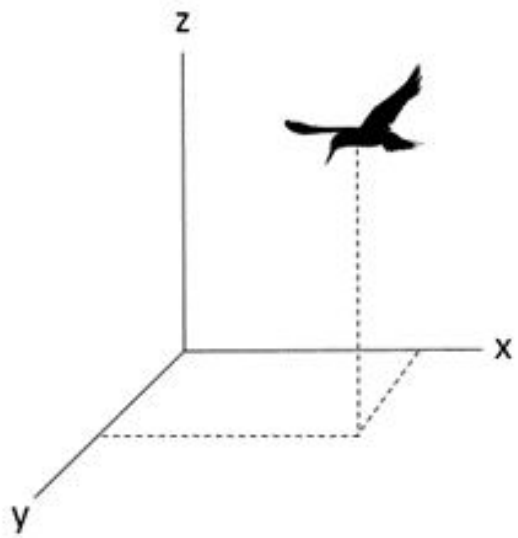

Fig. 3.1 Position of an object in 3-dimensional Cartesian space

The primary functions of the Rotational Stereo Videography (RSV) system are to observe the bird in flight and identify aerial manoeuvres, record the 3D position of the bird in these manoeuvres, fit a pose model to the birds morphology and make a record of the exhibited flight behaviour. The functional relationship of the RSV system is depicted in (Figure 3.2).

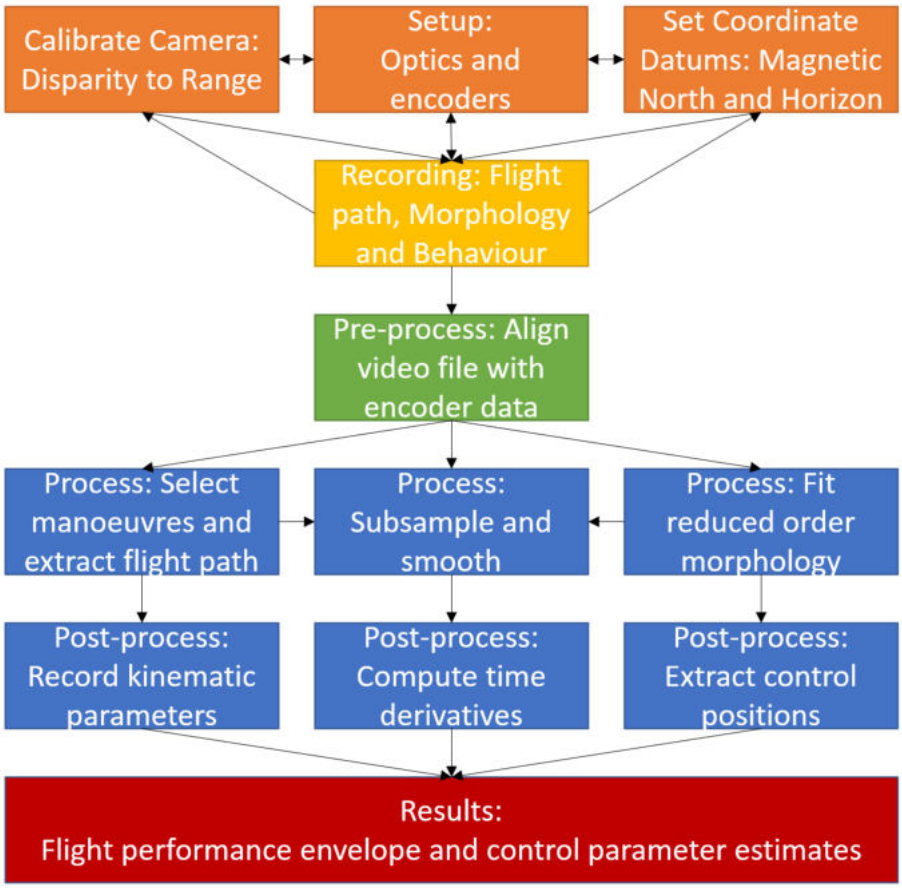

Fig. 3.2 Functional flow diagram of Rotational Stereo Videography (RSV) system depicting functional dependencies

3.4.2 Contributions to Rotational Stereo Videography

The RSV system presented in this chapter is an original system based on the work of Dr. DeMargerie [18] who provided input and support. DeMargerie's version of the ornithodolite, the latest in a line of bird tracking devices, and supporting software is capable of making single time stamped position measurements of an objects track and provides supporting video for behavioural analysis. This new RSV system, presented in this thesis is capable of tracking any number of points on an object and can fit a morphology model to these points to track both the flight path and pose of the object. The optical system has been improved to refine tolerances and improve the accuracy of measurement. The hardware has been completely redesigned based on the requirements of the optical system presented in this chapter and the software is custom and developed from first principles using epipolar geometry and camera intrinsics.

3.4.3 Coordinate system

The position of an object over local distances is usually described in a Cartesian coordinate system. Consider a point P in Cartesian space. The location of P is a function of its translation along three coordinate axis as a tensor of three signed vectors.

$$P = f(x, y, z) \tag{3.1}$$

Cartesian representation of position is useful from the point of view of an external observer of a system and is the representation of choice for three dimensional position data. However when it comes to making 3D position measurements it is difficult to directly measure the (x,y,z) components of an object relative to an instrument situated at the origin. Instead the positional measurements are made in an alternative coordinate system before transforming these into Cartesian space. Using a rotational instrument located at an origin the ideal coordinate system of choice is Spherical Polar Coordinates (Figure 3.3).

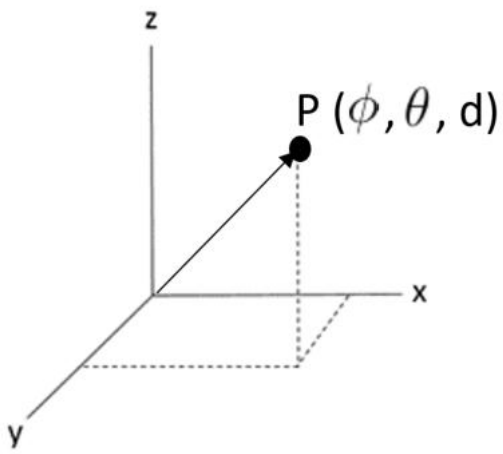

Fig. 3.3 Spherical polar coordinate system as centred on an arbitrary point of origin

Consider a point P in Spherical Polar space. The location of P is a function of its rotation about an azimuth (ϕ) and inclination (θ) axis and a scalar range parameter d.

$$P = f(\phi, \theta, d) \tag{3.2}$$

This representation of position is useful as physical methods exist for directly measuring each tensor coefficient. Azimuth and Inclination can be measured using angular encoding and the distance d using a variety of range measuring techniques including laser-ranging, radio return or in this case Epipolar geometry.

3.4.4 Epipolar geometry

Epipolar geometry relates properties of a 3D point to the 2D image plane in a stereo camera setup. Stereo ranging uses Epipolar geometry to measure the range to a point in 3D space by measuring the difference in the points position in a pair of stereo images made using visual planes in a known geometric relationship. Epipolar geometry works on the principle of corresponding projections. If there exists a feature of a 3D object projected onto a visual plane X then there will be the corresponding feature projected onto an offset point on an offset visual plane X' (Figure 3.4).

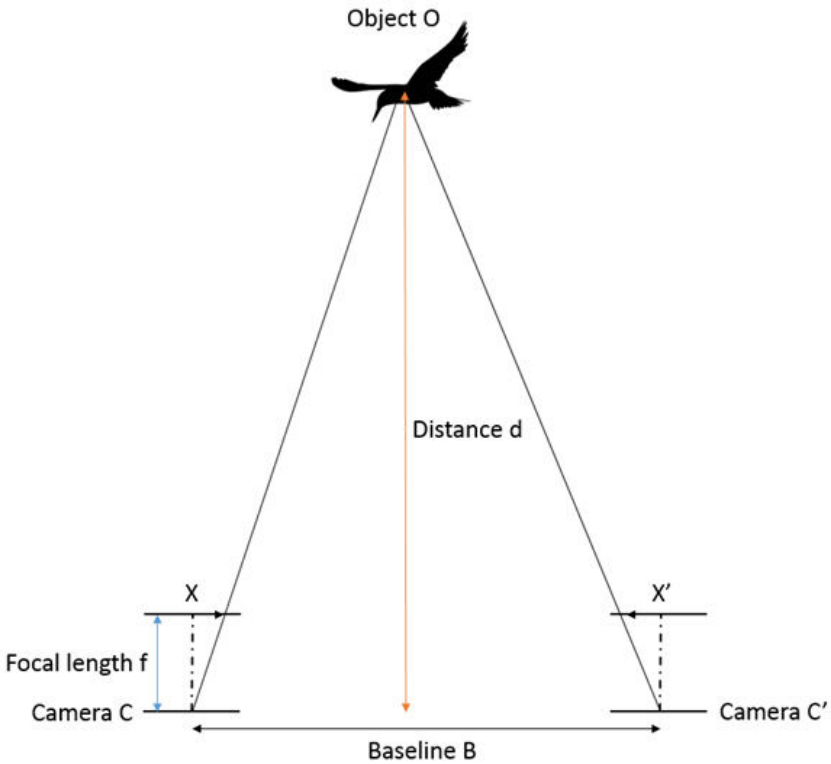

Fig. 3.4 Geometric relationships on the Epipolar plane can be used to calculate distance d using the difference of the intercepts on visual planes X and X' and the known baseline and focal lengths to build similar triangles

The difference in position of the point in the stereo images $(x - x')$ is known as the point disparity (s) and can be measured in the image coordinate frame (Figure 3.5).

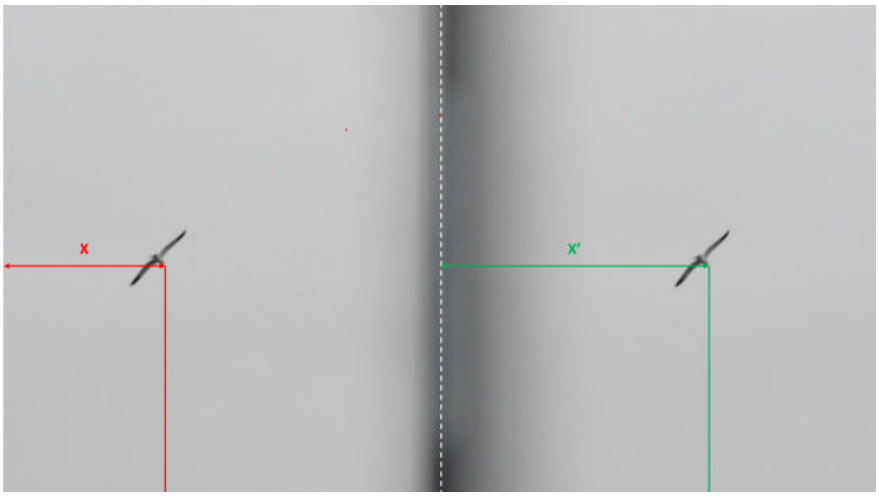

Fig. 3.5 The horizontal disparity in between two images of the same object in the epipolar plane as measured from the left hand edge of each half-image. By convention disparity is measured as $s = x - x'$ and the sign depends on whether the object is within or beyond of the convergence length of the offset image planes (Negative beyond the convergence length).

The plane formed by the conjunction of the visual planes and the object in question is known as the Epipolar plane. The distance between the visual planes is the Baseline (b) and the range from the centre of the baseline to the object is the distance (d). If the object and the visual image pair both lie on the Epipolar plane the calibration between the disparity measurement $s = (x - x')$ and the range (d) is reduced to a two dimensional problem with variables baseline (b) and focal length (f). The physical disparity (s) is a function of the pixel disparity ($u - u'$), where u is the position of the object as measured in number of pixels, and the pixel width (P_w) as determined by the sensor size and the resolution accounting for pixel binning. Using the rule of similar triangles we can derive the relationship between the offset image and the distance to the object (Equation 3.3).

$$\frac{(b - s)}{(d - f)} = \frac{b}{d} \tag{3.3}$$

Rearranging (Equation 3.3) to solve for d:

$$d = \frac{fb}{s} \tag{3.4}$$

Given a fixed calibration fb and measuring the disparity of an object between the stereo image pairs we can use equation 3.4 to compute the objects range distance d.

3.4.5 Optical system

Stereo vision requires a pair of offset image planes to measure the lateral disparity between feature points and hence compute object distance. The capture of a pair of image offset planes requires a pair of cameras. These cameras and associated lenses must be identical in optical quality and function and must be synchronised to trigger simultaneously. If they are not identical then the calibration matrix is extended to account for asymmetry in the camera intrinsic properties and this increase the complexity of the computation. If the cameras are not correctly synchronised the temporal variance between the image pairs distorts the lateral disparity measurement leading to an incorrect calculation of object distance. The solution to issue of doubling up on equipment was to use a single camera system coupled with a stereoscope. Reducing the system to a single camera also eliminates the need for synchronisation and temporal disparity distortion in the resulting image pair.

A Wheatstone's stereoscope arrangement (Figure 3.6) was used to project a pair of laterally offset images, across a mirrored prism, through a single lens onto a single frame. The Wheatstone's stereoscope setup using two distal primary mirrors reflecting of two central secondary mirrors positioned at 90 degrees to each other. This setup was used to recombine two images taken from different points of view and are viewed by each eye independently to visualise the images in 3D. The left and right half images then correspond to the X and X' visual planes respectively.

Drawbacks of this setup include halving image width, pixel count and field of view and introducing additional mirror alignment issues that can induce a vertical disparity between the left and right half images. The primary and secondary mirrors were initially aligned using a laser to minimise error, however flexing of the support structure during use introduces mirror pointing errors. This effect is evident by the introduction of vertical disparity between the half images. Any vertical disparity between the two half images is removed using image rectification in post-processing.

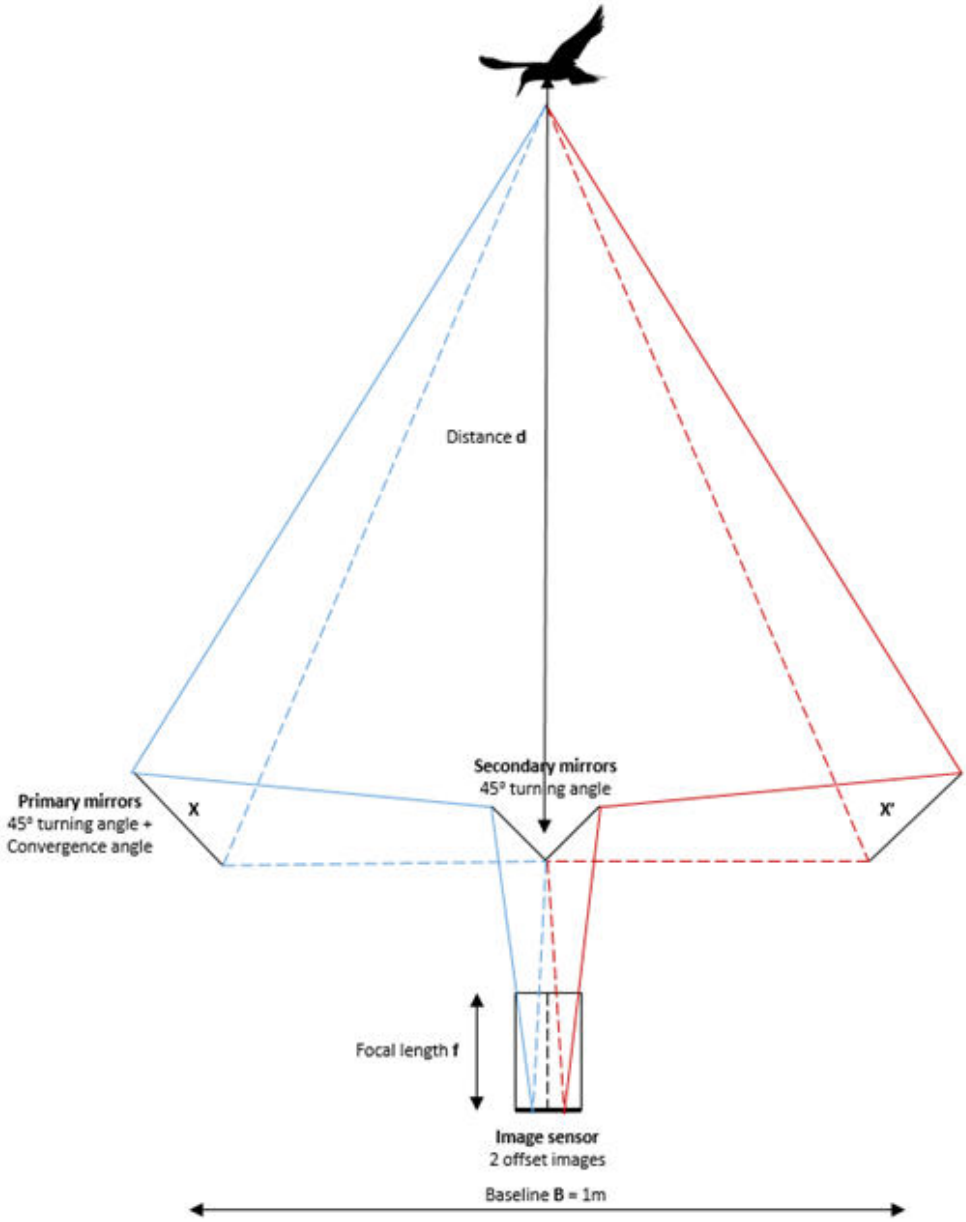

Fig. 3.6 Single camera optical setup using a Wheatstone stereoscope arrangement to allow for a single sensor to record both half images.

The stereoscope comprises of a pair of primary reflecting surfaces that serve as the independent visual planes. These are displaced at a baseline distance of 1 m to maximise baseline separation whilst maintaining a portable system. The choice of a 1 m baseline also simplifies the mathematics. The primary reflecting surfaces are levelled and convergence at an angle that is set based on mean working distance. Light is projected onto a secondary reflective prism comprised of a pair of bevelled mirrors. This secondary prism is then the focal target of the main camera lens. The mirrors are sized accounting for the minimum magnification of the lens that is the minimum focal length, which accounts for the maximum required reflective surface area. Because each half mirror system projects a half image on the sensor the image pixel density and field of view are half what they would be if using a two camera system. The Wheatstone mirror system is considered mathematically equivalent to the base two camera system in Figure 3.6 and the general physical arrangement is displayed in Figure 3.7. This arrangement produces a double offset image pair with each offset image occupying half of the image sensor.

The convergence angle on the primary mirrors was necessary to centrally position the object within the half image at the mean working range. It essentially fixes the focal set point, the distance at which the object will be in the sharpest focus. For sizing considerations the convergence angle was neglected as compared to the major 45° turning angle the convergence is small and was accounted for in the reserve over-sizing factor.

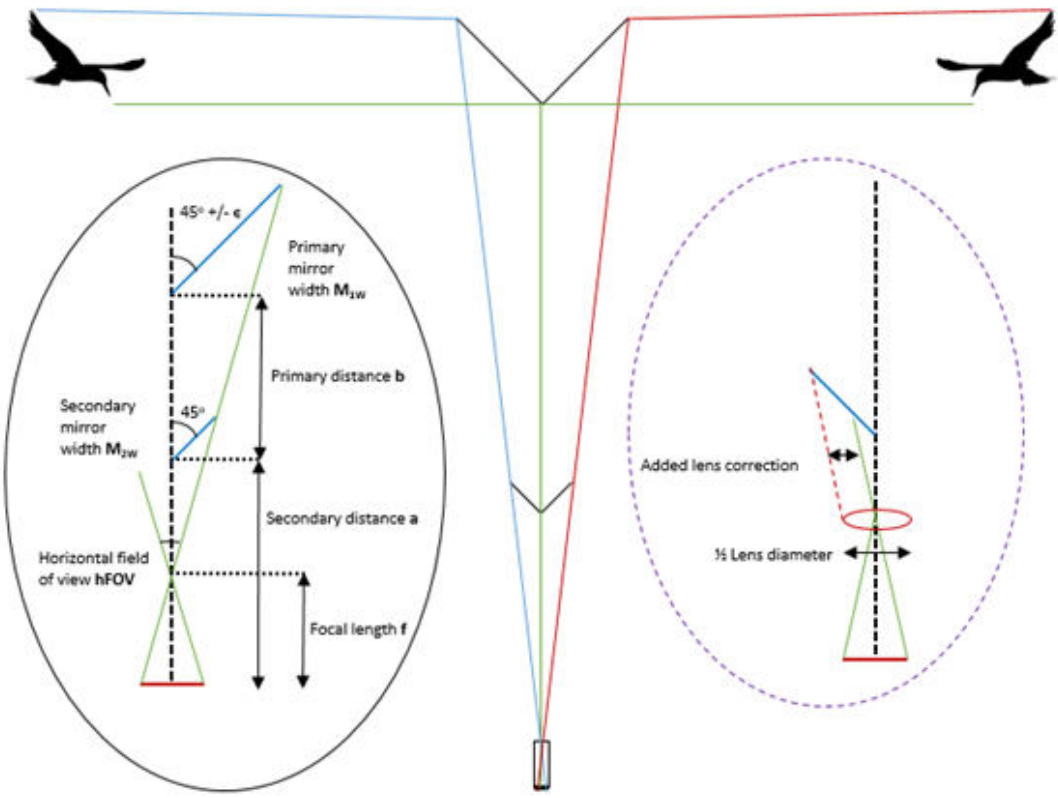

Fig. 3.7 Mathematically equivalent optical setup of the epipolar geometry, showing sizing of primary and secondary mirrors (inset left) and the camera lens correction (inset right)

Mathematically the mirror arrangement in Figure 3.6 can be considered equivalent to the one in Figure 3.7. This arrangement better highlights the similar triangles and makes the mathematics more intuitive. Primary and secondary mirror sizes are determined using camera intrinsic parameters and the geometric relationships portrayed in this arrangement, the specifics of which can be found in the Appendix - A.2.1.

3.4.6 Camera system

A high end digital single lens mirror-less camera, the Panasonic Lumix G DMC-GH4RH with a 16 megapixel sensor filming at full high definition, FHD (1920X1080) captures the video imagery. Video is recorded in full high definition at 50 frames a second, full specifications are available in Appendix - A.2.4.

3.4.7 Complete Rotational Stereo Videography system

Fig. 3.8 Complete Rotational Stereo Videography system setup in the field, the frame comprising Panasonic Lumix GH4 camera and optical mirrors and the video encoding head with data-logging and control.

Figure (3.8) shows the complete RSV system comprising of the optical frame and angular encoding video head. The tubular carbon frame and base plate form a rigid platform on which to mount the first surface optical mirrors. The mirrors have adjustable pointing via rear mount thumbscrews. The microcontroller feeds synchronisation clock signals to the camera and encoders and logs data to a removable SD card.

3.4.8 Observable working volume

The observable working volume or range of the rotational stereo videography system is governed by two assumptions:

1. Minimum working distance is determined by the maximum allowable object size in the image. Assuming a design species, the lesser black-backed gull has an average wingspan of 1200mm and that the maximum allowable object size to allow the operator to effectively track it is ¼ of full frame, in FHD recording mode the object must be projected onto < 4.5mm of sensor width.

2. Maximum working distance is determined by the maximum allowable object flight track error. The quantized positional error is found by summing orthogonal uncertainties quadratically for a given image width (IW) and calibration using equation 3.5 [18]. This is determined by the operator and is nominally set here at 0.2m. Flight paths at greater ranges will still be recorded but the track uncertainty shall exceed ± 0.2m.

$$d_{max} \approx 10\sqrt{0.2BI_wF} \tag{3.5}$$

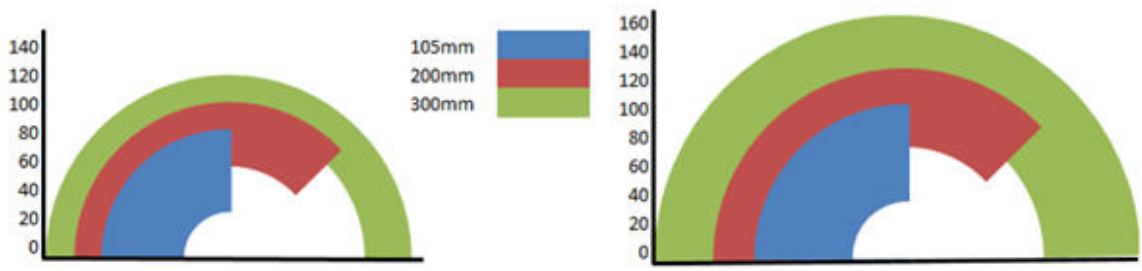

Fig. 3.9 Pictoral representation of maximum and minimum theoretical working ranges in meters of RSV system with 0.2m maximum allowable error with different focal length lenses at FHD resolution and UHD resolution

Because of the fixed system calibration the camera must maintain a fixed focal length for the duration of recording. A selection of three lenses provide a working volume coverage spanning 25-160 m as seen in Figure 3.9. Values available in Appendix A.2.5

3.4.9 Azimuth and Inclination encoding

The video head houses an encoding system to measure the azimuth and inclination angle components of the spherical polar coordinate system (Figure 3.3). These coordinates are calibrated to a zero reference. The RSV system calibration sets magnetic north and the gravity normal plane (the horizon) as the zero reference. Azimuthal angle is measured between 0-360° and inclination angle $\pm 90^o$. To make measurements of the azimuth and inclination angles the RSV system uses single turn optical encoders mounted to the video head (Figure 3.10). The 17 bit encoders provide an angular resolution of $\pm 0.01^o$.

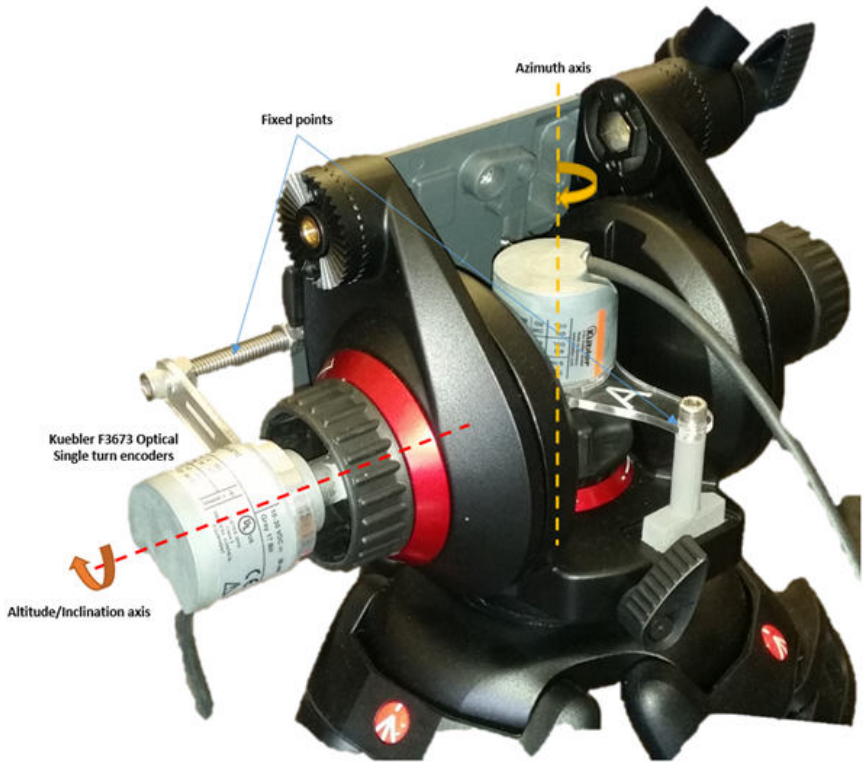

Fig. 3.10 F3673 single turn, optical angular encoders, mounted to a Manfrotto video head. Each encoder records the angular position of the video head about its azimuth and inclination in 17 bit gray format

3.4.10 Microcontroller and datalogging

Data-logging and camera triggering are controlled by a microcontroller (Max32, ChipKit, Digilent). Angular data is logged to the external SD card by the microcontroller. The microcontroller communicates with the SD card as a serial peripheral interface (SPI) device and makes use of specific high speed read/write hardware pins. The encoders communicate with the microcontroller using the Serial Synchronous Interface (SSI) protocol. SSI uses the RS485 transceiver standard to send data in response to a clock cycle. This allows a single clock output to drive the +- clock lines and a single data input pin to receive the ± data lines. The encoders share a common clock. Data is received in gray code format, most significant bit first, which is converted to decimal before being written into a csv file on the external SD card. Video is recorded on the camera's internal SD card and is connected to the microcontroller via the audio jack and via the remote trigger. To provide synchronisation between the video frames and the logged encoder data a synchronisation chirp is overlaid on the video audio track when the encoder logging is triggered to start and stop logging. Further details available in Appendix - A.1.

3.4.11 Video pre-processing

Videos are pre-processed by aligning the video frames with the angular encoder data-logs and cropping the video to length depending on the length of the manoeuvre sequence to be tracked. The video is broken into individual frames and stored as .tif files ready for processing in Matlab (Figure 3.11). Because of the single camera arrangement the stereo image is stored as one file. Before pixel measurements can be made the image is divided in two and stored as a temporary working file before being overwritten.

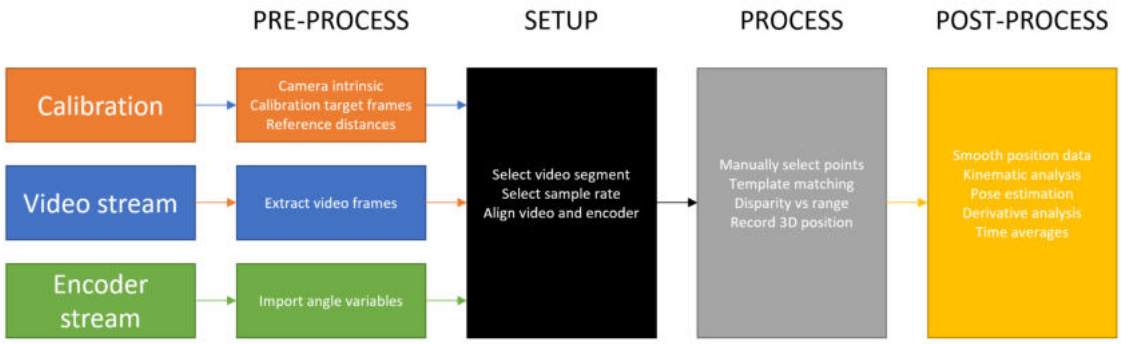

Fig. 3.11 Flow of data from three input streams: Calibration, Video files and Encoder files to Output datasets

3.4.12 System calibration

As previously stated the range measurement component of the spherical polar coordinates is derived from a calibration based on the epipolar geometry of the camera rig. The calibration consists of extrinsic properties such as the baseline and mirror convergence angles, and the intrinsic camera properties: FOV, focal length, sensor width, pixel resolution. The disparity range calibration is made by tracking multiple distinctive environmental targets or pre-placed fiducials at known ranges and fitting a curve to the points. The known range is established using a laser range finder accurate to 0.1m at all ranges where the RSV system is functional. By locating the fiducial or known feature in the calibration footage the camera intrinsic and extrinsic parameters are accounted for. The effect of lens field of view (FOV) and distortion is accounted for by tracking the fiducials across the full height and width of the sensor and producing a set of functions (Figure 3.13) from which to interpolate corrections for range and angular measurement based on the offset of the target from the optical centre of the image plane, the object in image (OII) correction (Figure 3.14).

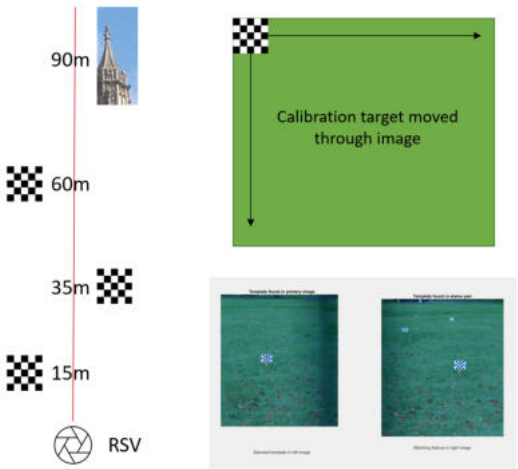

Fig. 3.12 Calibration targets are placed at known distances from the rig. Where a target cannot be placed a prominent feature can be used. Each target is tracked in a video file across the full image and template matching locates the matching target in the image. OII Disparity corrections are mapped at different ranges and different positions within the image.

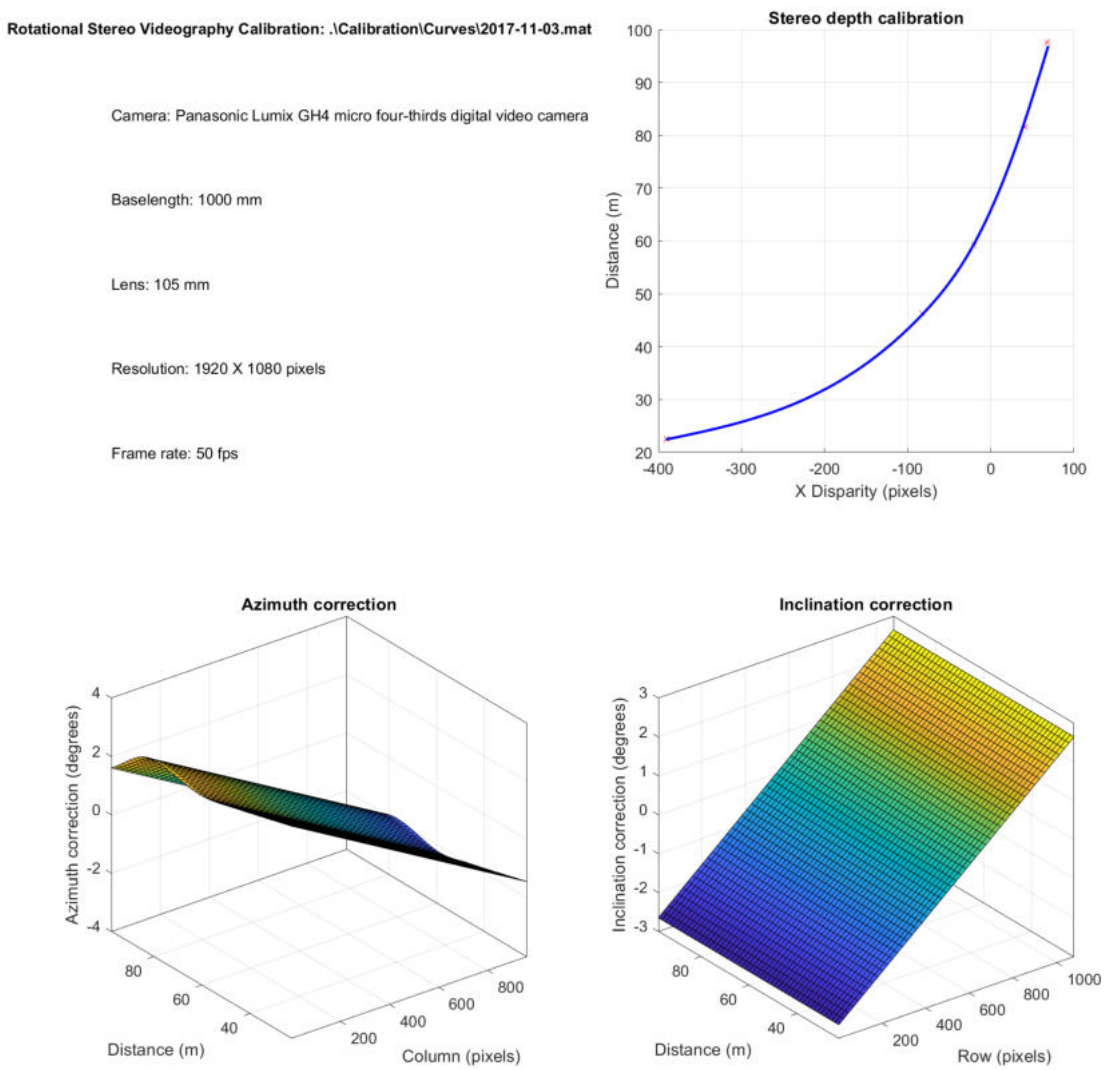

Fig. 3.13 Calibration function maps showing the stereo depth calibration and the azimuth and inclination corrections to be applied to correct for camera FOV and lens distortion

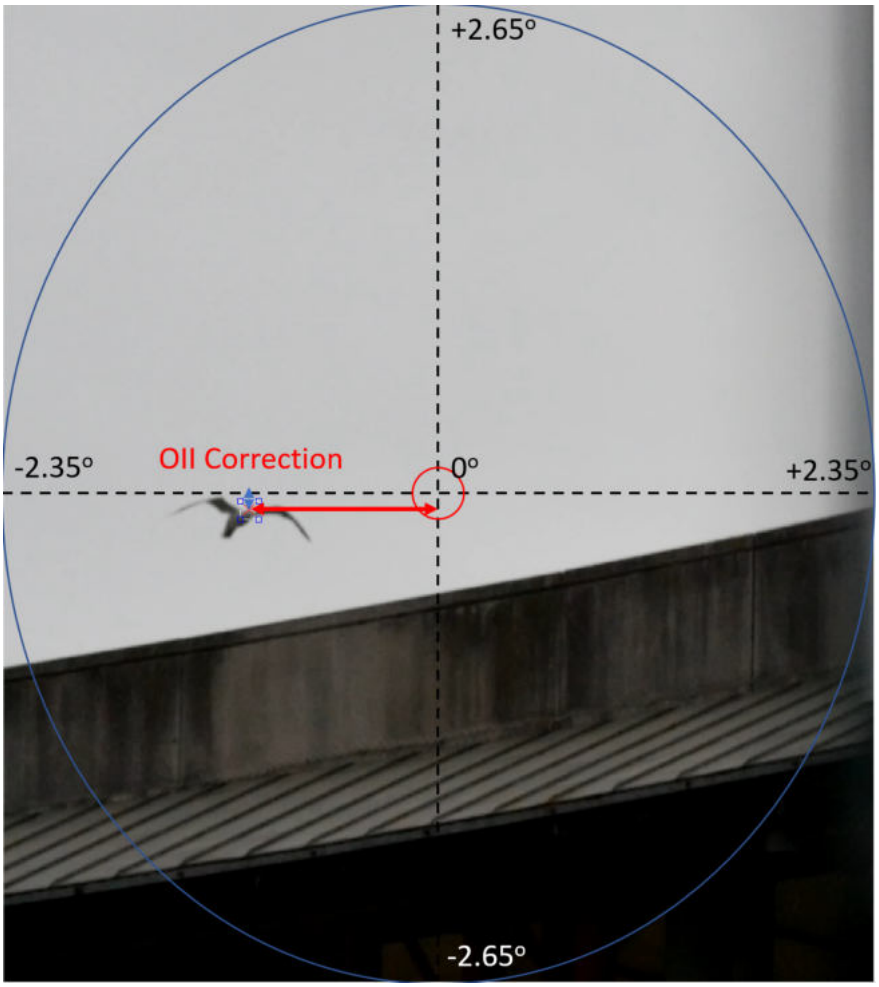

Fig. 3.14 Object in image correction, built as a function of the lens FOV and mirror convergence point. Correction applied to angular position data for off-centred location of target point in the image

The calibration file is an object structure containing the raw calibration points, range-disparity curves, OII correction curves and camera properties. Because each location requires adjustments to the rig for expected mean measurement range, size of target and environmental conditions the calibration can vary significantly between setups and as such the system requires a new calibration for each field session (Figure 3.15).

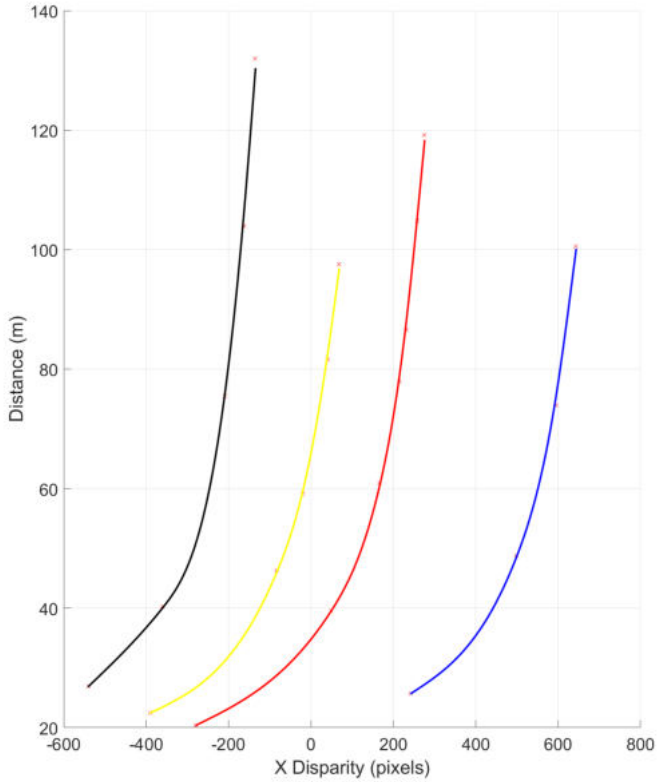

Fig. 3.15 Comparison of four separate distance-disparity calibrations for the RSV system. Note the shape of the calibration curve remains constant but is laterally shifted in each case. This lateral shift is caused by changing the mirror convergence angles to set the zero disparity point based upon the expected measurement range for the session.

Figure 3.15 shows four different calibration curves with the mirrors converging at different focuses (X Disparity = 0). Each experiments mirror convergence angle is set to approximately the middle of the expected working range. The yellow and red calibration curves show two different working range calibrations, the yellow curve showing convergence at 60m and the red curve showing convergence around 38m. The black and blue calibration curves indicate the extremes of mirror convergence. The black line has the mirrors convergent close to infinity so all disparity is negative and the blue line has the mirrors tightly convergent such that all disparity is positive. Large disparity increases range resolution but also increases the error in each measurement.

3.4.13 Flight path tracking

The RSV software component is written in Matlab and has various modules for different functions, see Appendix - A.3 for examples. The path tracking module loads in individual frames and the corresponding rig encoder pointing angles for that frame. A single target requires one point to be digitised and tracked in each frame (or in each sub sampled frame if a lower sample rate is acceptable). The tracking methodology requires the user to select one point to be tracked on the target in each successive half-frame. By convention the user selects the target in the left half-frame. When selecting the point to be tracked the user is selecting an image template of a predetermined sized to be matched in the right half frame (Figure 3.16).

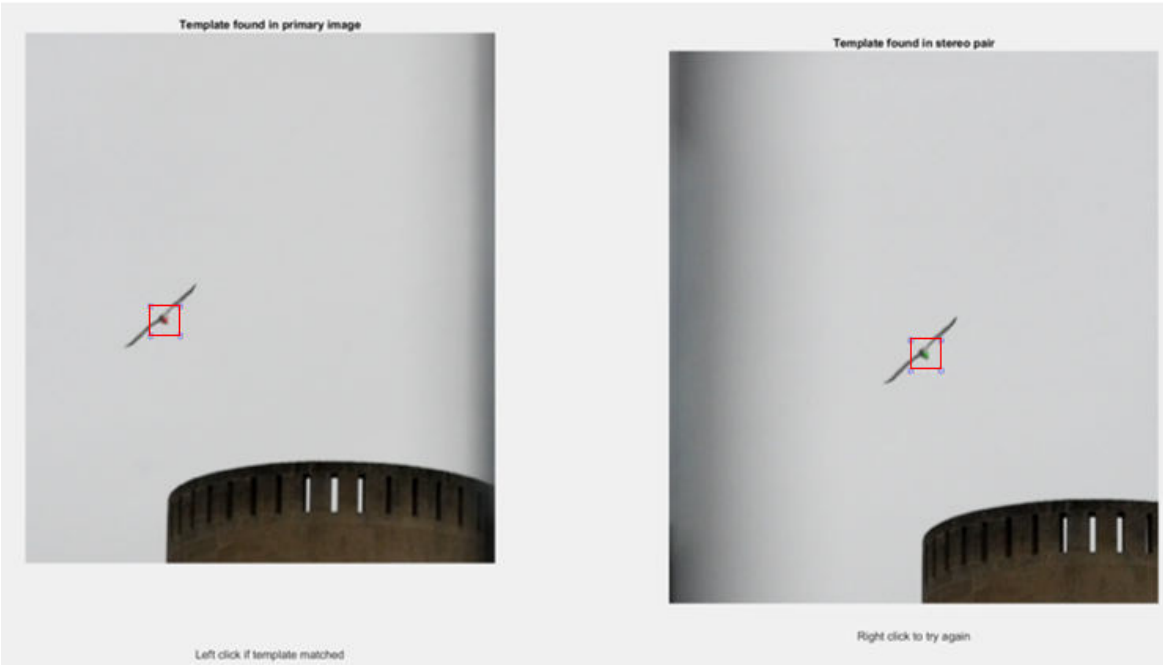

Fig. 3.16 The template is selected by the user in the left half-image, here the template size is exaggerated for clarity, typically the template is less than five pixels square. Normalised cross-correlation algorithms compare the template to the right half image and generate a matrix of coefficients based on how similar the template is to the windowed image.

The centre point of the template is established in each half-frame stereo image by processing a 2D normalised cross-correlation of the template matrix and the image matrix and finds the peak correlation coefficient within the image matrix and defines this as the target point. Specifically the function used is based on fast normalized cross-correlation, a technique developed by Industrial Light and Magic [85]. The process calculates the cross-correlation in the image spatial domain and calculates the local sums. The local sums are then normalised and used to calculate correlation coefficients.

$$\gamma(u,v) = \frac{\sum_{x,y}[f(x,y) - \bar{f}_{u,v}][t(x-u,y-v) - \bar{t}]}{\left\{\sum_{x,y}[f(x,y) - \bar{f}_{u,v}]^2 \sum_{x,y}[t(x-u,y-v) - \bar{t}]^2\right\}^{0.5}} \tag{3.6}$$

The implementation is described by equation 3.6, where, f is the image, $/bart$ is the template mean and $\bar{f}_{u,v}$ is the mean of $f(x,y)$ in the region under the template.

To further improve the resolution of the disparity measurement a sub-pixel matching method is used which fits a 2nd order polynomial to the nine points surrounding the local correlation maximum and returns the position of this new maximum (Figure 3.17).

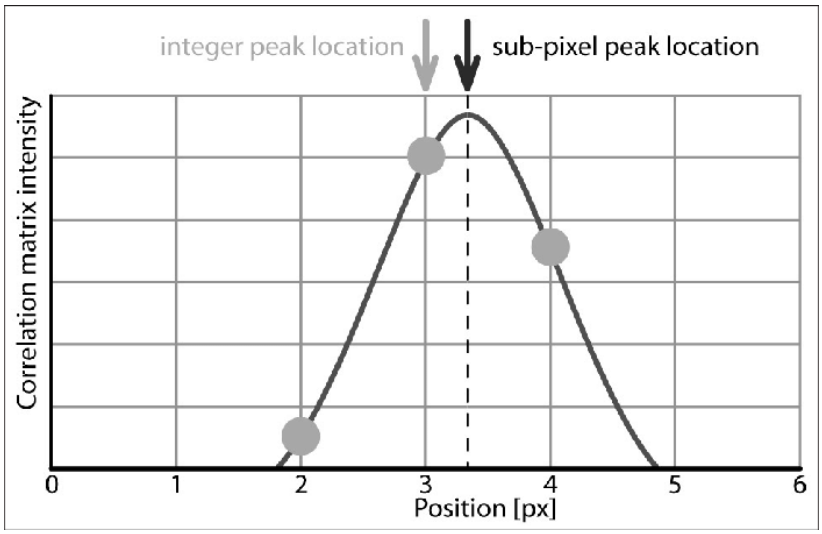

Fig. 3.17 Sub-pixel matching technique which uses a polynomial function fit to the matrix of correlation coefficients to infer a peak between pixel locations. Figure adapted from [86]

The location of the sub-pixel correlation maxima establishes the X and X' coordinates in the left and right half-frame images and the difference between them computes the X axis disparity between the target in the two images. Because of the vertical alignment of the mirrors and the assumption that the mirrors and object are all points on the epipolar plane the Y axis disparity $y - y'$ should be small. Any non-trivial values are indicative of a mirror alignment issue.

Using the calibration curve the X axis disparity equates to a target range distance d. The X and Y positions in the left half image along with the range and calibration curves allow for the determination of the object-in-image angular corrections required to correct for the off-centred position of the target within the image. The OII correction is added to the azimuth and inclination angular measurements to complete the spherical polar coordinate tensor. The process is iterated for each frame in the manoeuvre until a complete track is obtained.

3.4.14 Estimating error in the point tracking and data smoothing

The stereo systems range estimation is subject to an error of depth resolution, how much measurable change in depth is related to distance and change in disparity [87]. The depth resolution error in stereo (e_{stereo}) is shown to be:

$$e_{stereo} = \frac{d^2}{bf} \cdot s \tag{3.7}$$

where d the distance to target, b the baseline, f the focal length in pixels and s the matching disparity error in pixels. The baseline and focal length are fixed system constants. The disparity error in pixels is a function of the cross correlation peak matching algorithm and due to the sub pixel technique can be reasonably assumed to be half a pixel. As such range error is proportional to the range squared and is the largest component of error.

Angular measurement error for a single turn encoder is a function of the optical encoder bit rate (N) plus the deviation of the point of maximum correlation and the true target point in the image. It can be assume that in the event of a distinctive texture on the point to be tracked that the error due to maximum correlation is small and hence the angular error is simply:

$$e_\phi = e_\theta = \frac{2\pi}{2^N} \tag{3.8}$$

In terms of displacement the azimuthal and inclination errors are described as errors in meridian and parallel and are a function of the angular error and target distance.

$$e_{meridian} = d\tan(e_\phi) \quad \text{and} \quad e_{parallel} = d\tan(e_\theta) \tag{3.9}$$

The total effect of the error of the independent variables on the position measurement can be computed as the root mean square of the component errors. For the RSV system the total theoretical error is therefore modelled as a total positional error (TPE).

$$e_{TPE} = \sqrt{(e^2_{stereo}) + (e^2_{meridian}) + (e^2_{parallel})} \tag{3.10}$$

Constant error manifests as a positional offset and over short distances. This will in-

duce small errors in the derivative data and its effect will propagate with each derivative. This error is small and will not affect the trends in the dataset. However random error noise at very high sample rates propagates when post processed and conceals the true trends in the manipulated data. To reduce the random noise present in the dataset, smoothing can be used to reduce the volatility in derivative data. Visually the smoother tracks are easier to interpret. The smoothed data has reduced noise peaks due to random error spikes when differentiated to compute other parameters. When smoothing the positional dataset filters are applied to the raw polar positional data tensor. No further smoothing is applied so as to avoid over-smoothing the data and removing features from the results. To preserve higher order features in the signals a Savitsky-Golay moving average filter [88] is used to smooth the data sets (Figure 3.30).

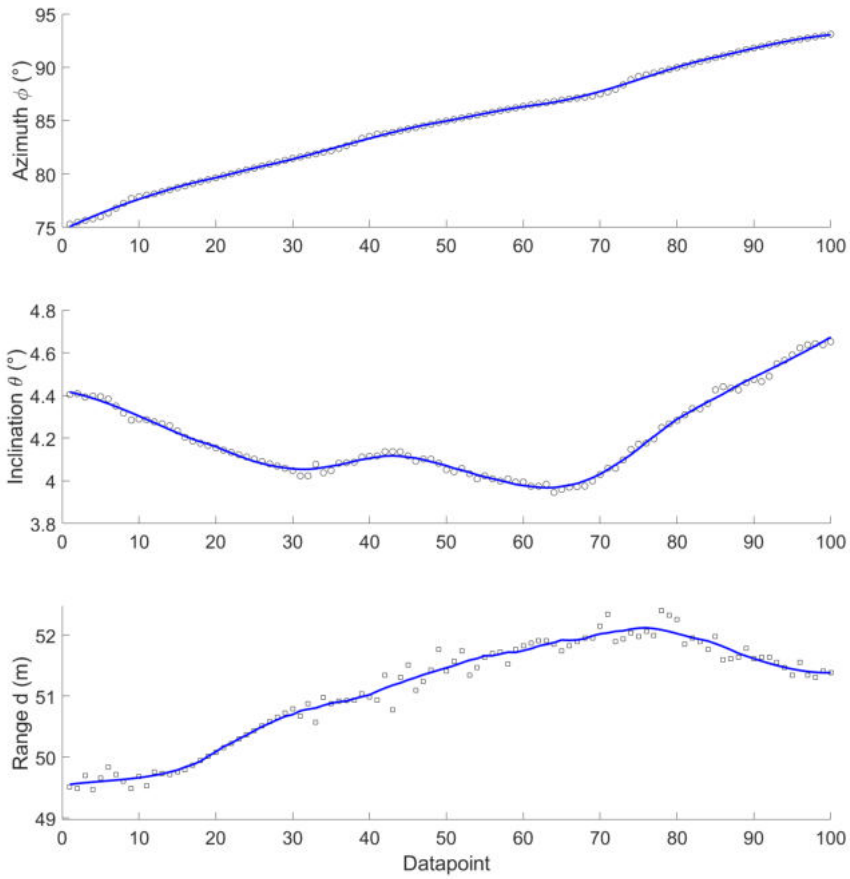

Fig. 3.18 Savitsky-Golay moving average filter applied to a typical raw RSV output data (ϕ, θ, d)

This method uses a two parameter convolution of a high order polynomial fit over a sliding window of data points. A third order polynomial is used to allow for inter-point regression and a window size of less than one half the length of the shortest manoeuvre of interest is used to satisfy the Nyquist sampling condition. This last condition makes the smoothing parameter dependant on both sample rate and the physical behaviour of the object being tracked. Other smoothing methods including moving average filters and singular spectrum analysis filters were considered but ultimately rejected due to the inconsistency in applying the smoothing parameters and the need to manually tune smoothing parameters for each flight track where the justification for the selection of the smoothing parameters was inconsistent. The Savitsky-Golay method produces consistent smoothing and the selection of the smoothing parameters is justified by the time period of the manoeuvre being assessed.

3.4.15 Measurements of experimental error

The RSV system was benchmarked against the theoretical error by using a known object following a prescribed object track. Measurements are made at three separate ranges and the computed position compared to the known position of the object at this location. Depth resolution and in-plane pixel matching error were measured separately to better understand the component error. The total error is taken as the root mean square sum of the component error.

$$e_{Total} = \sqrt{(e^2_{in-plane}) + (e^2_{out-plane})} \tag{3.11}$$

The experimental setup for benchmarking the RSV system error uses a tennis ball of standard dimensions moving through two prescribed tracks at ranges in between system calibration points. The prescribed tracks are an in plane orbit of radius one metre and an out of plane orbit of radius one metre. The tracks were produced by placing a rotational tripod head atop the prescribed point whose range was measured using a laser rangefinder. The tennis ball was affixed to an arm such that the position of the centroid of the ball was 1 metre from the centre of rotation. The arm was then moved through the orbit manually three times to produced three separate measurements of each orbit whilst the camera recorded the position at 50 frames per second.

Each object track is digitised manually to produce a series of points that sit on the in-plane and out of plane orbits. These points are then compared to a known cloud of points on the surface of a 1 m radius sphere representing the physical track of the object around the orbits. The point cloud is generated with an orbit centroid positioned at a range corresponding to the range as measured by the laser range finder. The points sit on a horizontal plane and vertical plane as determined by a spirit level and orbit with a radius of one metre. The point cloud for each orbit is comprised of $2n$ points where n is the number of experimentally measured points, taken during the error experiments. The comparative points are equispaced around the orbit. A nearest neighbour search is performed to determine the distance between the measured points and the closest relative point in the point cloud (Figure 3.19).

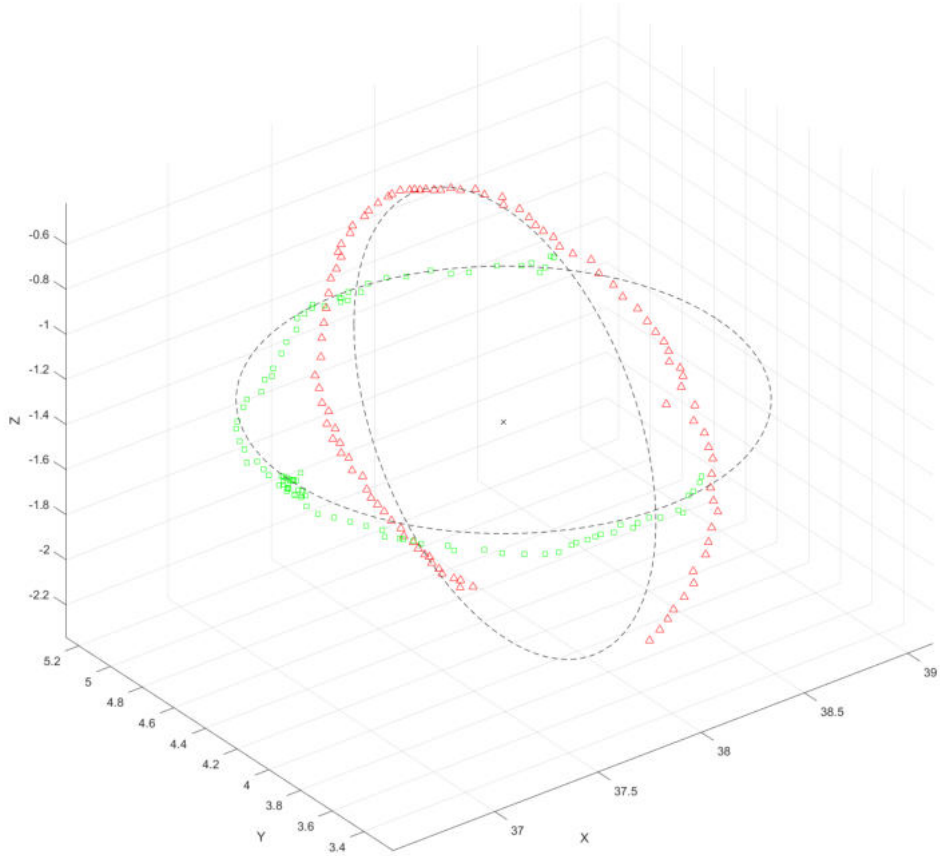

Fig. 3.19 In image plane points (Red) and out of image plane pints (Green) tracked about an orbit of radius 1 m. The measured points are then compared to an artificially generated point cloud affixed to a sphere of radius 1 m whose centroid is positioned at a distance measured using a laser range finder.

This distance is resolved into components on the epipolar plane and the image plane giving values of experimentally measured error in depth and for the object in image (OII) correction.

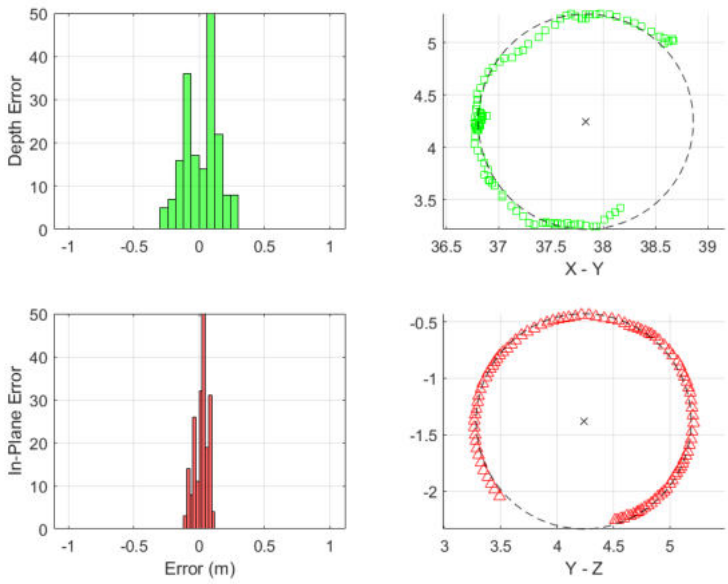

Fig. 3.20 Measured error histogram at 38m with measured points displayed against the associated point clouds for comparison

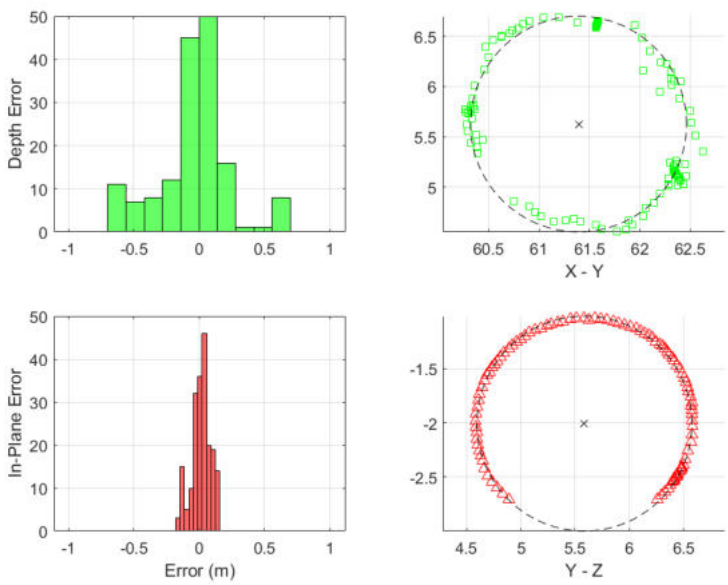

Fig. 3.21 Measured error histogram at 61m with increasing depth resolution error

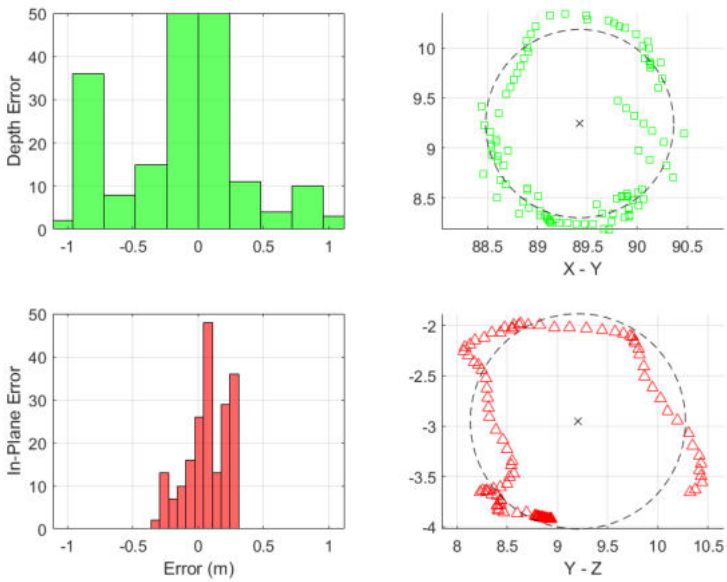

Fig. 3.22 Measured error histogram at 89m, approaching the maximum theoretical range of the device. Large growth in depth resolution error and difficulty tracking the object in plane due to the reduction in the number of pixels associated with the object

Figure 3.20, 3.21 and 3.22 are RSV measured error histograms showing out of plane (depth resolution) error and In-plane (Object in image) error and the associated points and point clouds for comparison. Measurements made at 38, 61 and 89m, within the calibrated range of the RSV device. At 61m note how the number of points affected by depth resolution error is increasing when compared to the measurements made at 38m whilst the in-plane, Object-in-image error remains roughly constant. At 89m approaching the maximum theoretical range of the device , the depth resolution error is growing as the object is represented by fewer pixels. The Object-in-image error is also now growing as the template matching technique has fewer pixels associated with the intended object.

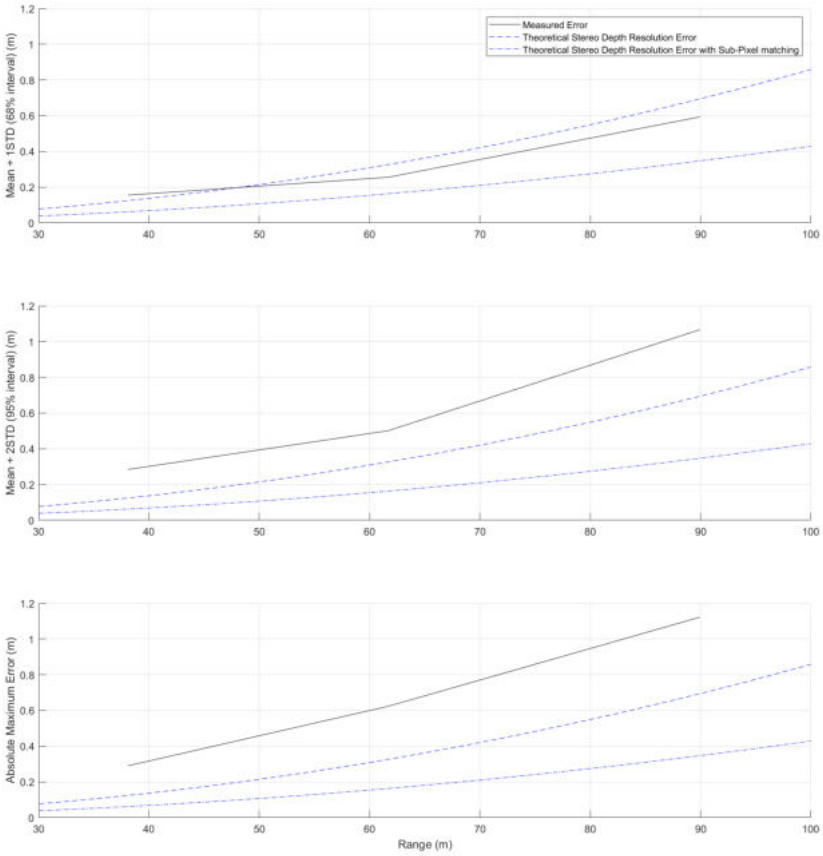

Fig. 3.23 Measured error as a function of range compared with theoretical error resolution

In accordance with the theoretical error (Equation 3.10) , the theoretical error of the RSV system can be modelled as a quadratic function of range. Figure 3.23 plots the mean and absolute maximum measured error against the error models both without and corrected for sub-pixel matching. The figure shows that the quadratic error model accounts for 68% of the measured error throughout the working range of the system. Whilst random errors sometimes exceed the modelled error by up to a factor of two these points are eliminated by subsequent smoothing of the position dataset account for less than 5% of the total dataset. This function is used to compute and record error as measured in the flight tracks made by the RSV and provides an estimate of confidence in the results.

An example of the error measurement in range along the flight path is shown in figure 3.24.

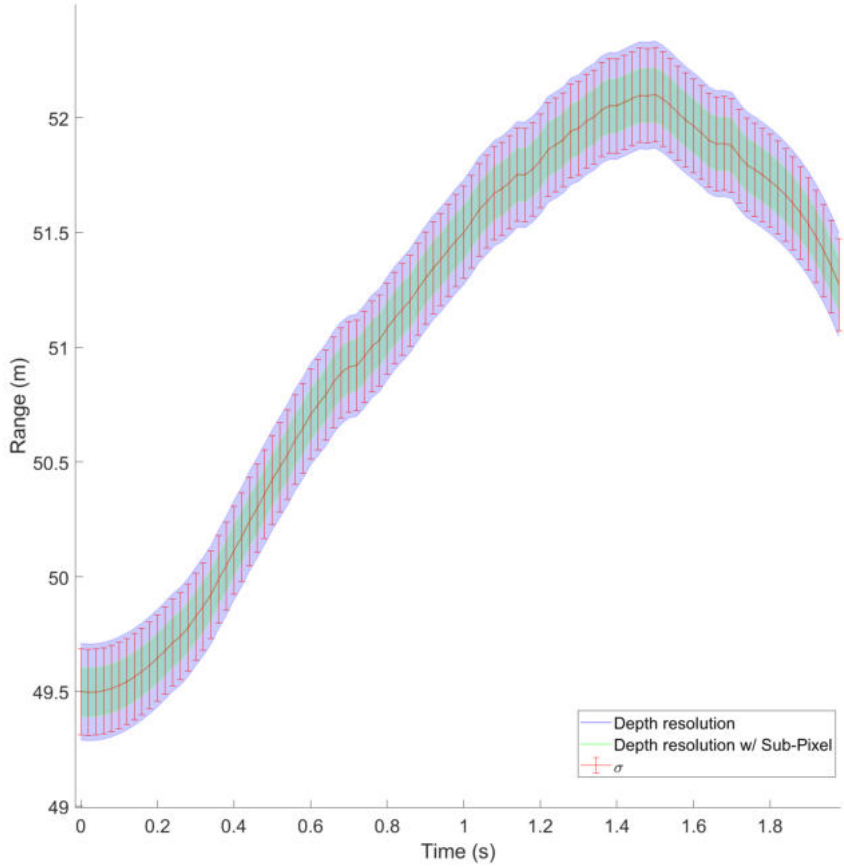

Fig. 3.24 Example of error estimation from a flight track near the maximum range of the RSV system with the 105mm lens. The area shaded blue shows the maximum theoretical error without sub-pixel matching. Green indicates the theoretical error with sub-pixel matching and red error bars showing two standard deviations from measured error such that 68% of the time the true value will lie within that range.

The total error in the point reconstruction can be considered to be a combination of random and systematic errors. The systematic errors are introduced both by the physics of the device as discussed and by the workflow in the setup and use of the system. The inherent range limitation imposed by the calibration between pixel disparity and the distance measurement means than the absolute values of point measurement may be consistently offset, however this will be consistent around the small area of focus at a given range. Given that the device is measuring relative positions whose relative range to each other is small in comparison to the relative range to the target, the error as a percentage of the total value will be broadly consistent so whilst the accuracy of the measurement will be reduced, multiple measurements will maintain precision. Other systematic errors such as those introduced by the primary structure oscillating at its natural frequency are harder to detect and hard to remove through smoothing, because of the level of accuracy of the device it is not conducive to making absolute quantitative measurements of derived data and instead the focus is on trends and gradients found in the resulting datasets. Random errors are most likely introduced by poor point tracking by the user, mitigation is provided by template match scoring and maintaining a sufficiently high level of match score between adjacent frames. These errors are easier to remove using averaging and smoothing and have less of an impact on the overall result.

3.4.16 Post-processing: Time based velocity and acceleration derivatives, flight path vector and energy equations

The RSV dataset outputs a 4 dimensional, time stamped position tensor with reference to spherical polar coordinates (ϕ,θ,d). The smoothed raw data tensor is then transformed into a Cartesian coordinate system (X,Y,Z) whereby the X axis is aligned with magnetic north and the Y axis is aligned with west. The Z axis is an altitude measurement aligned with the local gravity vector.

The 3D position data is timestamped, this allows for time derivatives of the positional data to be computed using a numerical difference method. Velocity and Acceleration derivatives are computed using a forward difference method.

$$u(t) = x'(t) = \frac{(x_{t+1} - x_t)}{t_{step}} \tag{3.12}$$

$$v(t) = y'(t) = \frac{(y_{t+1} - y_t)}{t_{step}} \tag{3.13}$$

$$w(t) = z'(t) = \frac{(z_{t+1} - z_t)}{t_{step}} \tag{3.14}$$

Velocity components (u,v,w) represent the component velocities along the axis (X,Y,Z) in the Cartesian coordinate frame. They can be combined to compute total velocity (V) and ground speed (GS).

$$V_{total} = \sqrt{u^2 + v^2 + w^2} \tag{3.15}$$

$$GS = \sqrt{u^2 + v^2} \tag{3.16}$$

The total velocity component represents the kinetic state of the animal with reference to a fixed ground based reference point. In the case of wind velocity being equal to zero this total velocity would equal the instantaneous airspeed as experienced by the bird. By summing this velocity vector with a known wind velocity component an approximation of airspeed is computed.

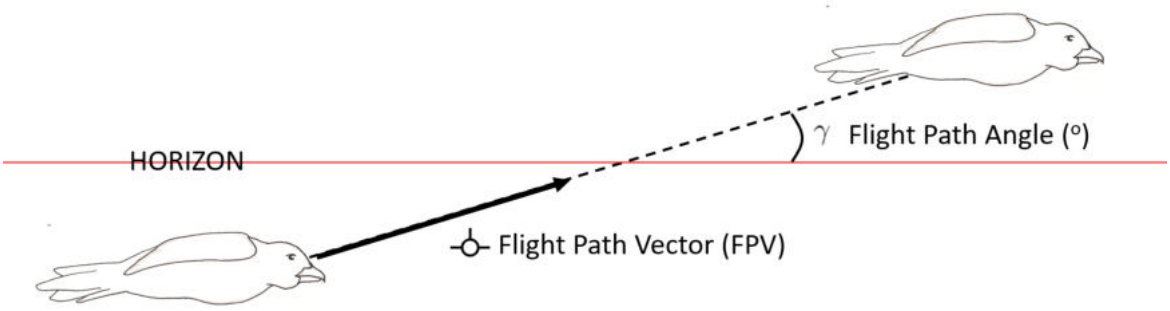

Fig. 3.25 Flight path vector and flight path angle as measured relative to the horizon. These describe the longitudinal motion of a bird / aircraft which has a non rigid relationship between the main wing and the body.

The instantaneous flight path vector (Figure 3.25) can be defined by two successive position measurements in space. With reference to a defined plane, the angle (γ) between the flight path vector and the plane is shown to be equation 3.17 where a is a vector between two successive points, $a = [\mathrm{x}_{t+1}$ - x_t, y_{t+1} - y_t, z_{t+1} - $\mathrm{z}_t]$ and b is the vector normal to the plane and in the case of the horizon, $b = [0, 0, 1]$.

$$\gamma = \arccos \frac{\bar{a} \cdot \bar{b}}{|\bar{a}| \cdot |\bar{b}|} \tag{3.17}$$

If the plane of reference is defined as a horizon plane normal to the local gravity vector or Cartesian Z axis, the included angle between this plane and the velocity vector is the instantaneous flight path angle (γ). For a bird in gliding flight this represents the geometric measurement of glide angle as achieved over the ground. For aircraft with a rigid relationship between the main wing and fuselage this angle is equal to the pitch angle minus the angle of attack in still air.

Using equation 3.17 but instead defining b as a vertical plane parallel to Magnetic north, $b = [0, 1, 0]$, the angle between this plane and the velocity vector represents the magnetic track made good over the ground (TRK). Summing the magnetic track made good with the local magnetic variation as taken on the date of recording gives the track angle as referenced to true north.

Flight manoeuvres typically require an exchange of energy and excess power is a typical measurement for high performance manoeuvres. The gravitational potential and kinetic energy states of the object can be determined from the positional data, velocity and some basic assumptions regarding the mass of the object in question where E is energy and m is mass.

$$E_{Potential} = m_{bird} \cdot g \cdot z \tag{3.18}$$

$$E_{Kinetic} = \frac{1}{2} \cdot m_{bird} \cdot V^2 \tag{3.19}$$

$$E_{Total} = E_{Potential} + E_{Kinetic} \tag{3.20}$$

Time derivatives of energy between successive position compute the power (P) being expended in that timestep (t).

$$P = \frac{E_{t+1} - E_t}{t_{step}} \tag{3.21}$$

3.4.17 Post-processing: Kinematics

Turn performance is expressed as kinematic parameters including: the radius of curvature (r), the rate of turn (ROT) and the lateral force due to centripetal acceleration (a_c). Instantaneous curvature is computed as a function of velocity and acceleration (A).

$$r = \frac{(1 + V^2)^{\frac{3}{2}}}{|A|} \tag{3.22}$$

This represents the instantaneous radius of turn between two data points and allows for turn performance to be considered. The other parameters important for quantifying turn performance: Rate of turn and lateral force can be described kinematically using small angle assumptions.

$$RoT(^\circ/s) = \frac{V}{R} \cdot \frac{180}{\pi} \tag{3.23}$$

$$a_c = \frac{V^2}{R} \tag{3.24}$$

3.4.18 Multipoint tracking: Pose estimation

The flight path tracking method can be extended to track multiple points on a single object to determine the geometric relationship between the points. A wireframe model can then be fitted to the points to establish the measurements of distance between points and angles between assumed rigid bodies. These measurements are representative of the position of the birds main lifting surfaces and reveal the relationship between limb motion and body response along the flight path. To estimate the pose of the main flight surfaces and relate them to the flight path requires multiple points to be tracked to define rigid body reference and the position of the surfaces of interest. Here four points are tracked to define five body points (Figure 3.26) where the body centroid is defined by the conjunction of the four points.

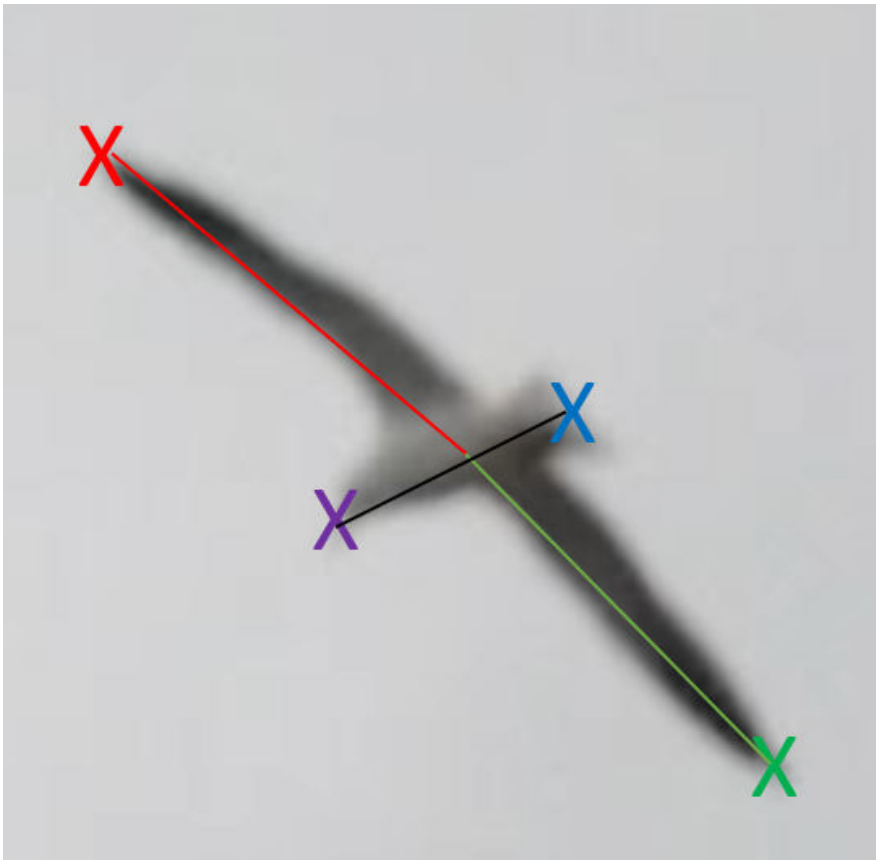

Fig. 3.26 Four points tracked on the bird in each frame: Head - as defined by the beak, Port/Starboard wingtips - as defined by the wingtip feather textures, Tail - as defined by the base of the tail feathers. Body centroid defined at 50% distance between head and tail.

Additionally a body centroid is defined at the midpoint on the vector connecting the Head position to the Tail position at each time step. This assumed wing centroid was arbitrarily selected for the reduced order model fit as the true wing root position cannot be determined from this dataset.

Two rigid body vectors are defined to provide a reference from which to compute geometric body angles. The body vector is defined by two points: the head and the tail and is the vector between them. It is a rigid body from which to compute the body Euler angles in relation to the world coordinate system and is analogous to the longitudinal body axis as defined for an aircraft. The total wing vector is defined as the vector parallel to the vector connecting the port wing tip to the starboard wingtip passing through the body centroid point. It is an assumed rigid body axis connecting the wing-tips and is used as a reference axis for measurements of wing angle deflection as well as measurements of wing span. The port/starboard wing vector connects the port/starboard wing-tip to the body centroid. It is an assumed rigid body used to define quantitative wing motion and deflections relative to the body and total wing vector.

The pose of the bird is estimated as a vector analysis between the body and world reference planes (Figure 3.27) where by:

Pitch (θ) is defined as the angle between the body vector and the horizon plane normal to the local gravity vector.

Roll (ϕ) is defined as the angle between the total wing vector and the horizontal plane normal to the local gravity vector.

Yaw (ψ) is defined as the angle between the body vector and the North-South vertical plane aligned with magnetic North.

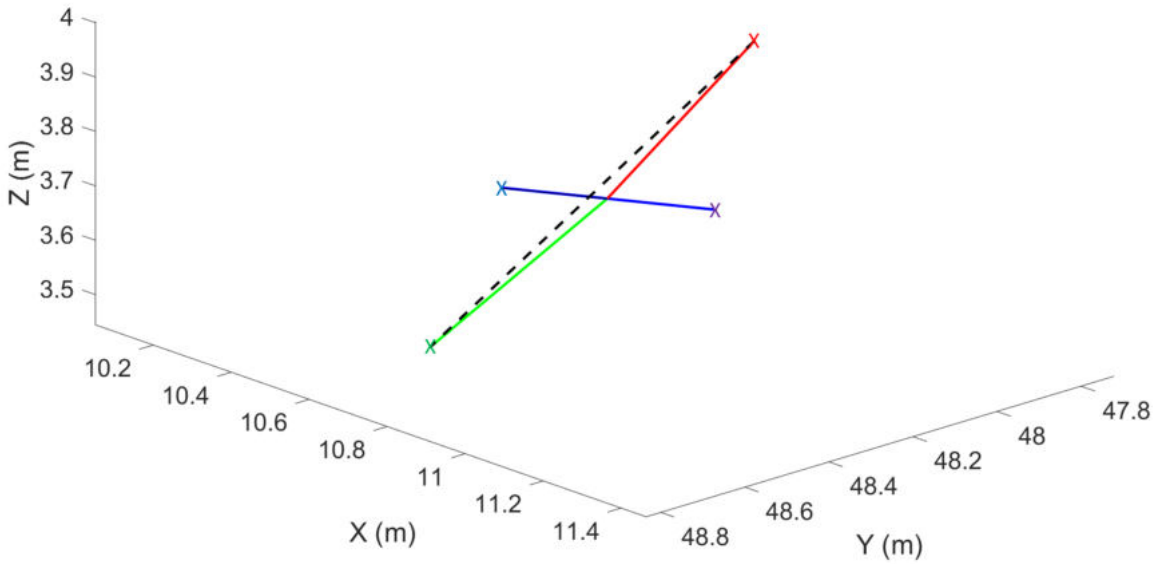

Fig. 3.27 Defining pseudo rigid body pose angles using geometric relationships between tracked features to establish parameters from which to build a flight model. Body vector (Blue), Port and Starboard Wing-lines (Red,Green), Total wing vector wing-tip to wing-tip(Black dashed)

The position of the primary lifting surfaces in relation to the body are analogous to control inputs and are defined by a vector analysis between the body axis and the port/star wing vectors and a local measurement plane (Figure 3.28):

Wing-sweep (ζ) is defined as the included angle between the port/starboard wing vector and the body centroid in the plane defined by the wing-tip, head position and the common body centroid.

Wing dihedral (δ) is defined as the included angle between the port/starboard wing vector and the total wing vector in the plane defined by the two wing-tips and the body centroid.

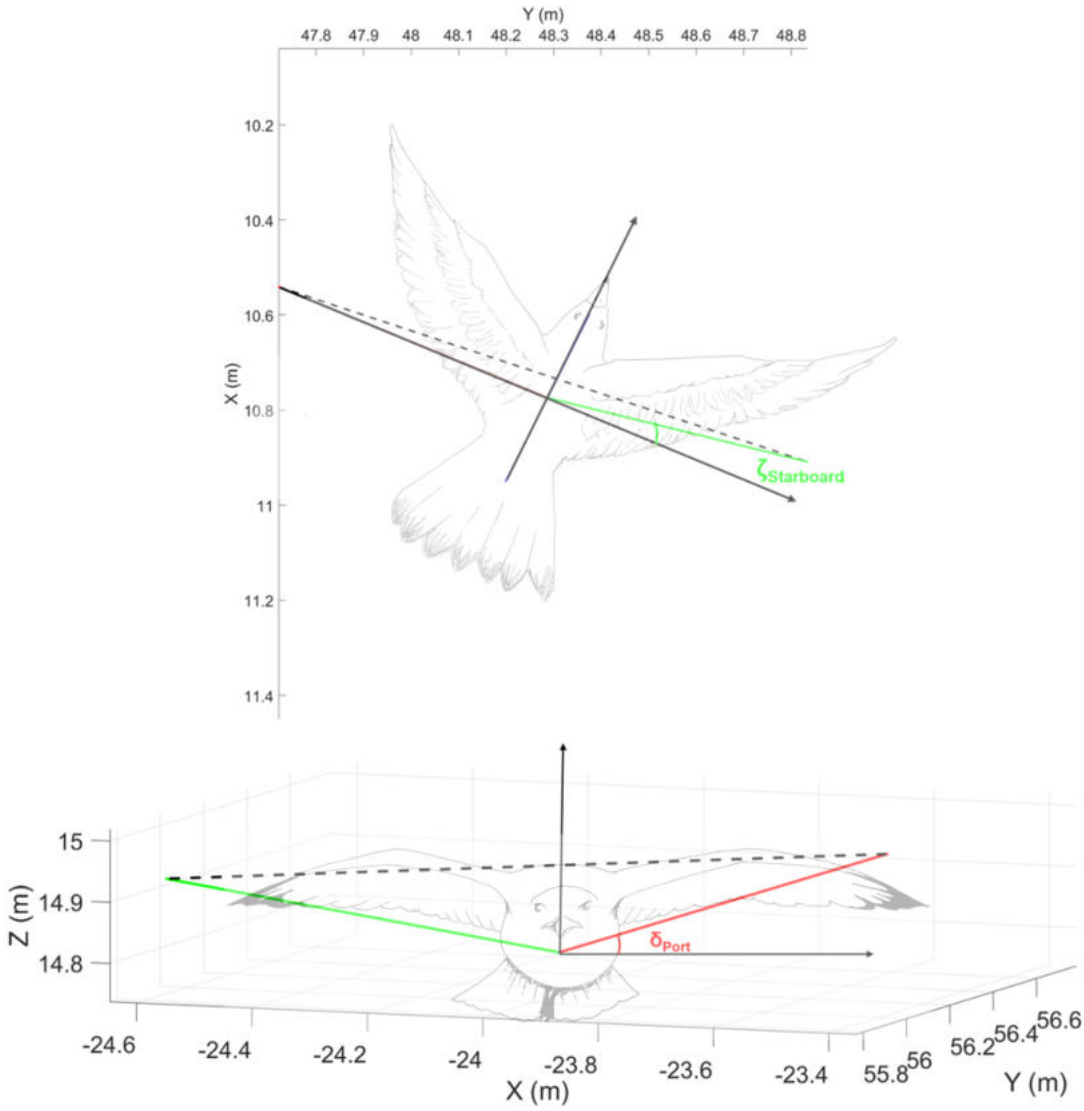

Fig. 3.28 Bi-variate model of wing geometry as defined by wing-sweep and wing dihedral. The red and green lines depict the average port and starboard wing lines.

This reduced order wire-frame model greatly simplifies the geometry of the bird. It reduced the highly complex arrangement of feathers, joints and underlying musculature into a model where by the critical points could be determined reliably using the RSV system. Assumptions made about the pose introduce new errors and the couple of motions that mask the true motion of the wing. Because of this the dataset cannot be used to make any absolute quantitative measurements. The reduced order model has a many input, single output mapping to the underlying geometry which limits its use to cases where the bird maintains a steady pose. The manoeuvres analysed in

later chapters are predominantly steady and flapping gaits were specifically excluded for this reason.

Due to shadowing effects it is not always possible to determine the body angles of the bird. In cases where the body vector cannot be reliably determined it is replaced by the flight path vector making the assumption that angle of attack and side-slip are small and thus a forward iteration of the velocity vector should provide a good directional analogy for a body axis given that body length is an unimportant parameter. The substitution of the bird's velocity vector to define a notional body line raises the assumption of symmetry of the bird in flight. Casual observation shows that the bird is not always aligned with the direction of flight, the head is often turned out of the free-stream and the measured asymmetry in the position of the main wings suggested a variation in span-wise flow across the body. However in these circumstances the offset of the body line will manifest as a rotation about the birds centre of gravity, which is close to the assumed centroid of the model, fit at fifty percent of body line. The impact of the offset of the assumed body line from the measured body line would in this case be small. In addition the shadowing effect that requires substitution is prominently evident when the bird is posed such that it is head on to or flying away from the camera system, these sequences were not selected when processing manoeuvres for analysis. In any case it is the relationship between the flight path and the control surfaces which is of primary interest.

3.5 Example of manoeuvre data processing

In this section an example of the RSV system results is presented. Starting with an input image (Figure 3.29) and by selecting features on the bird in each half image, the following figures are examples of the type of data outputs and represent an analysis of a manoeuvre sequence.

Fig. 3.29 Example input image taken from a gull flight recorded by the RSV system. This image frame will have a corresponding set of encoder values indicating the direction the camera was pointing relative to the datums. The image is timestamped.

3.5.1 Flight paths

Typical trajectory of a flight path track recording as measured in spherical Polar co-ordinates are presented in figure 3.30.

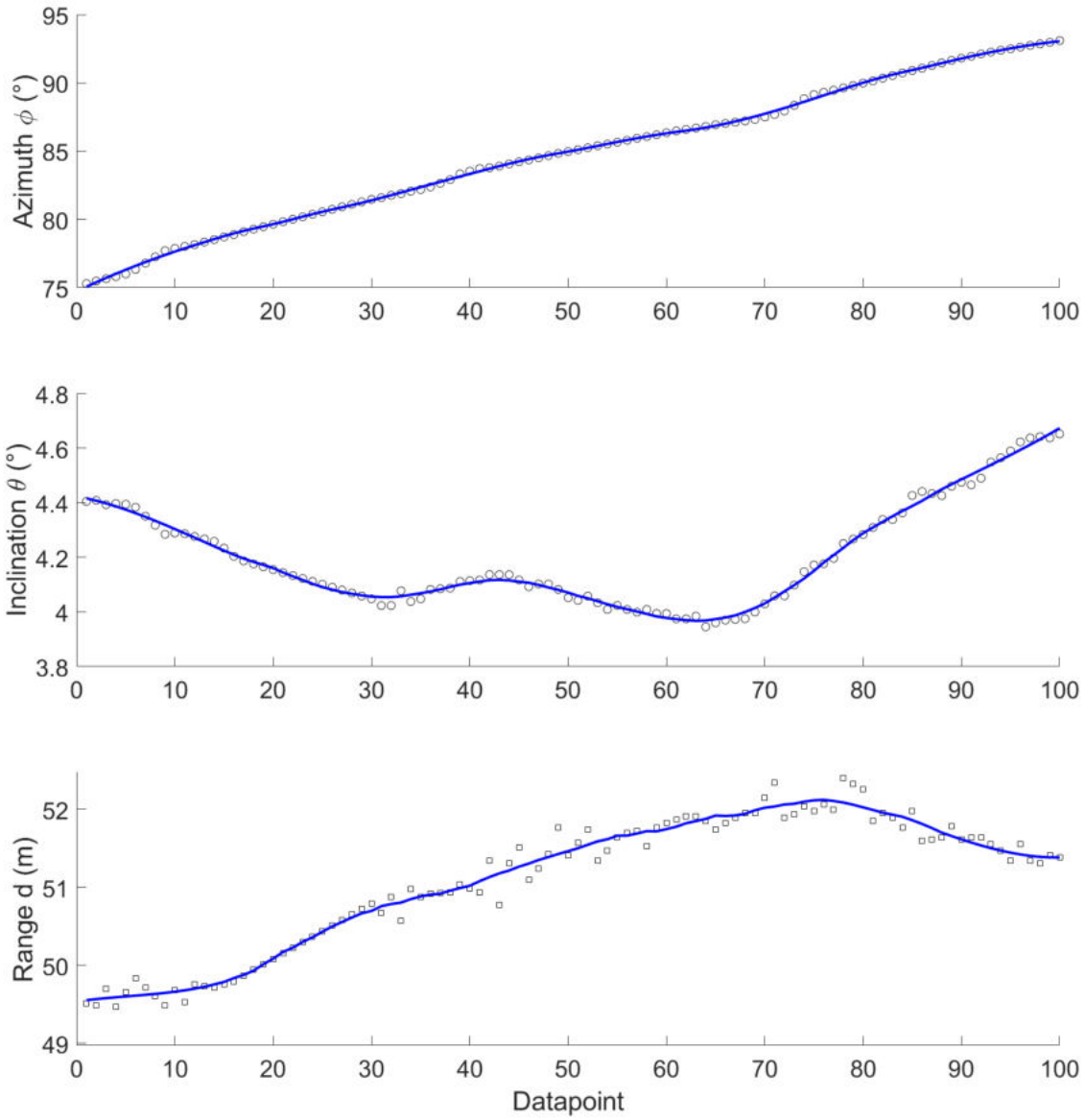

Fig. 3.30 Spherical polar RSV output data (ϕ, θ, d) presented as individual time series.

The spherical polar data as transformed to Cartesian data, four examples of sequences from gull flight data are shown in figure 3.31.

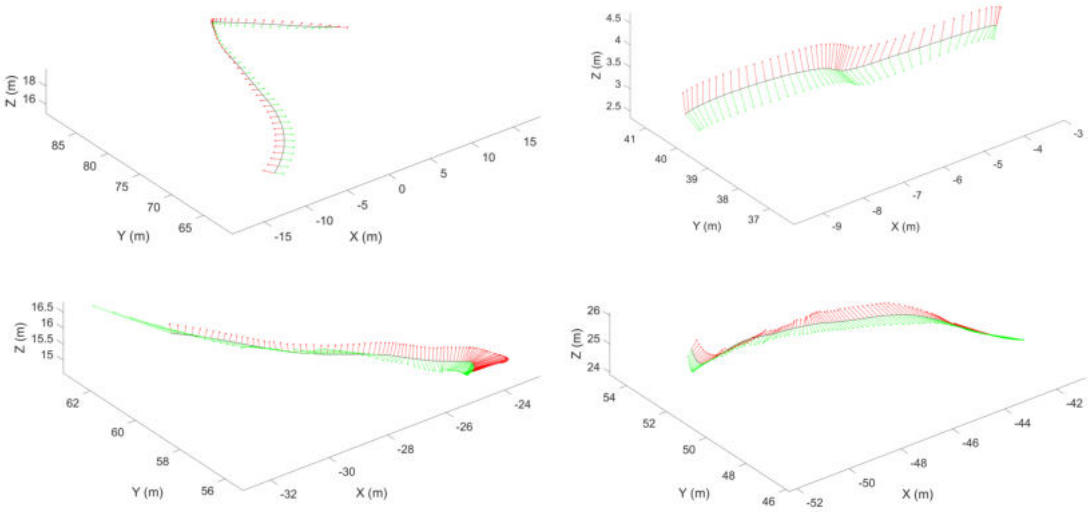

Fig. 3.31 Examples of gull flight paths in 3D Cartesian space. Each track is a series of successive measurements of the bird in time. The red and green lines are each positions wing lines and the black track line traces the progression of the body centroid.

This 3D information can be represented in as a 2D ground track and as 1D time sequences as seen in Figure 3.32 with x, y and z positions with respect to the time step.

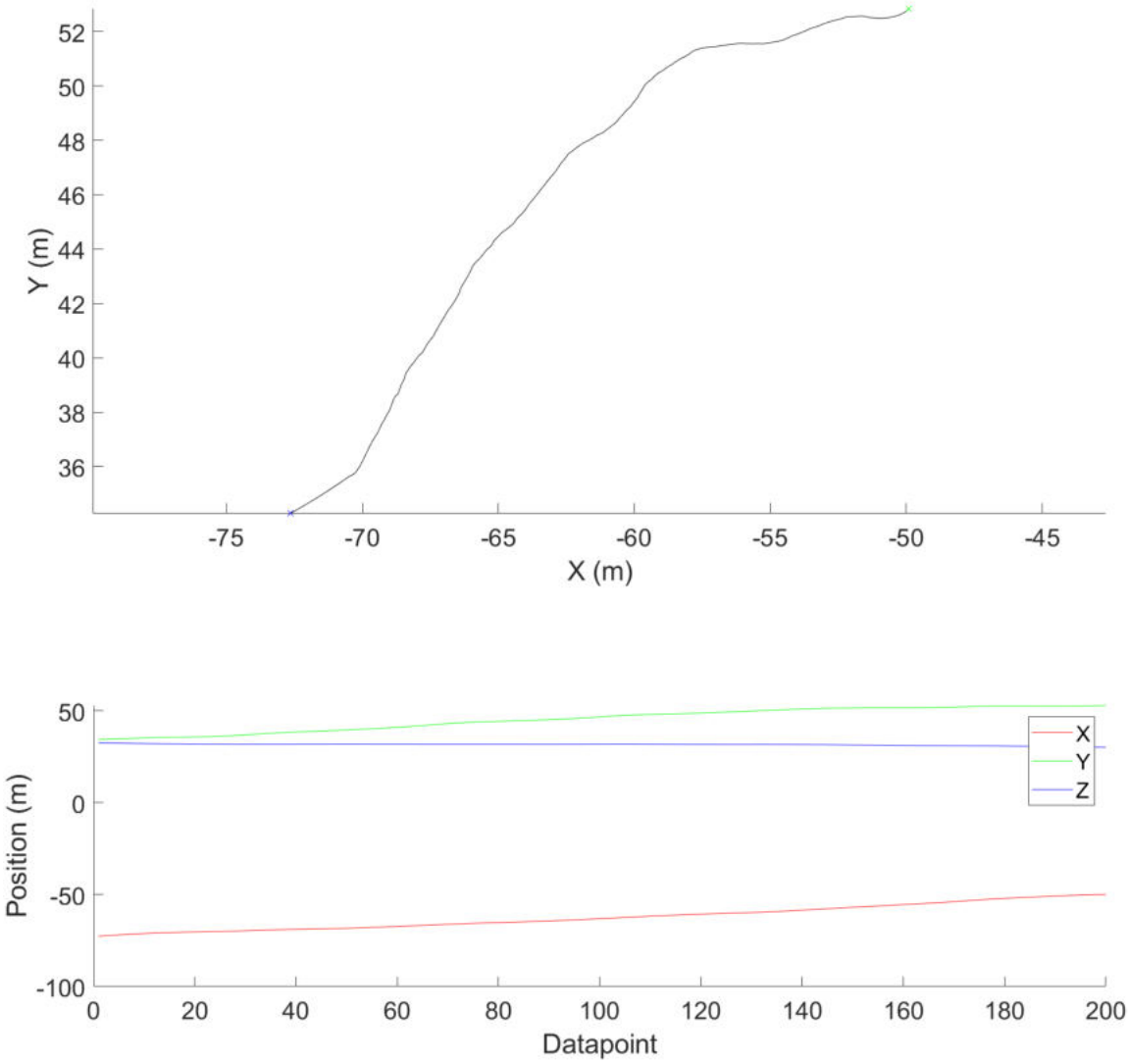

Fig. 3.32 Cartesian representation of flight path viewed top down and as a time series representation of the positional components.

3.5.2 Flight dynamics

Time based derivatives of position data are computed using a forward difference method and can be plotted as a function of time (Figure 3.33).

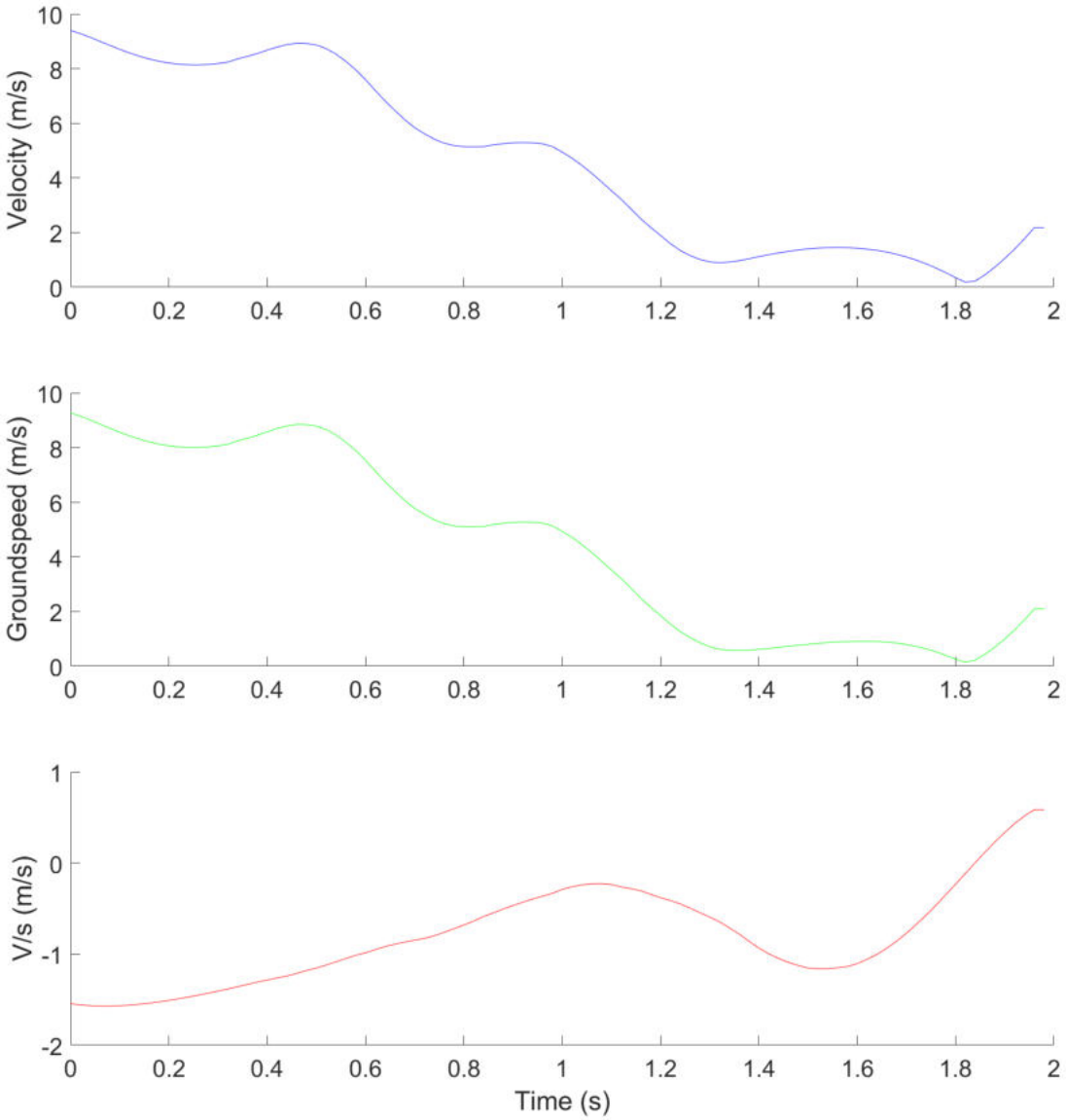

Fig. 3.33 Velocity components as calculated from time derivatives of positional data and summed for total velocity V, ground speed GS and vertical speed VS

Velocity components can be examined individually or geometrically summed to give a total velocity V or a ground speed component and a vertical speed component. Second derivatives of position data with respect to time gives acceleration information (Figure 3.34) that can be handled in a similar manner to the velocity data and is is normalised by acceleration due to gravity (g = 9.81 m/s^2) and expressed in terms of multiples of this factor G.

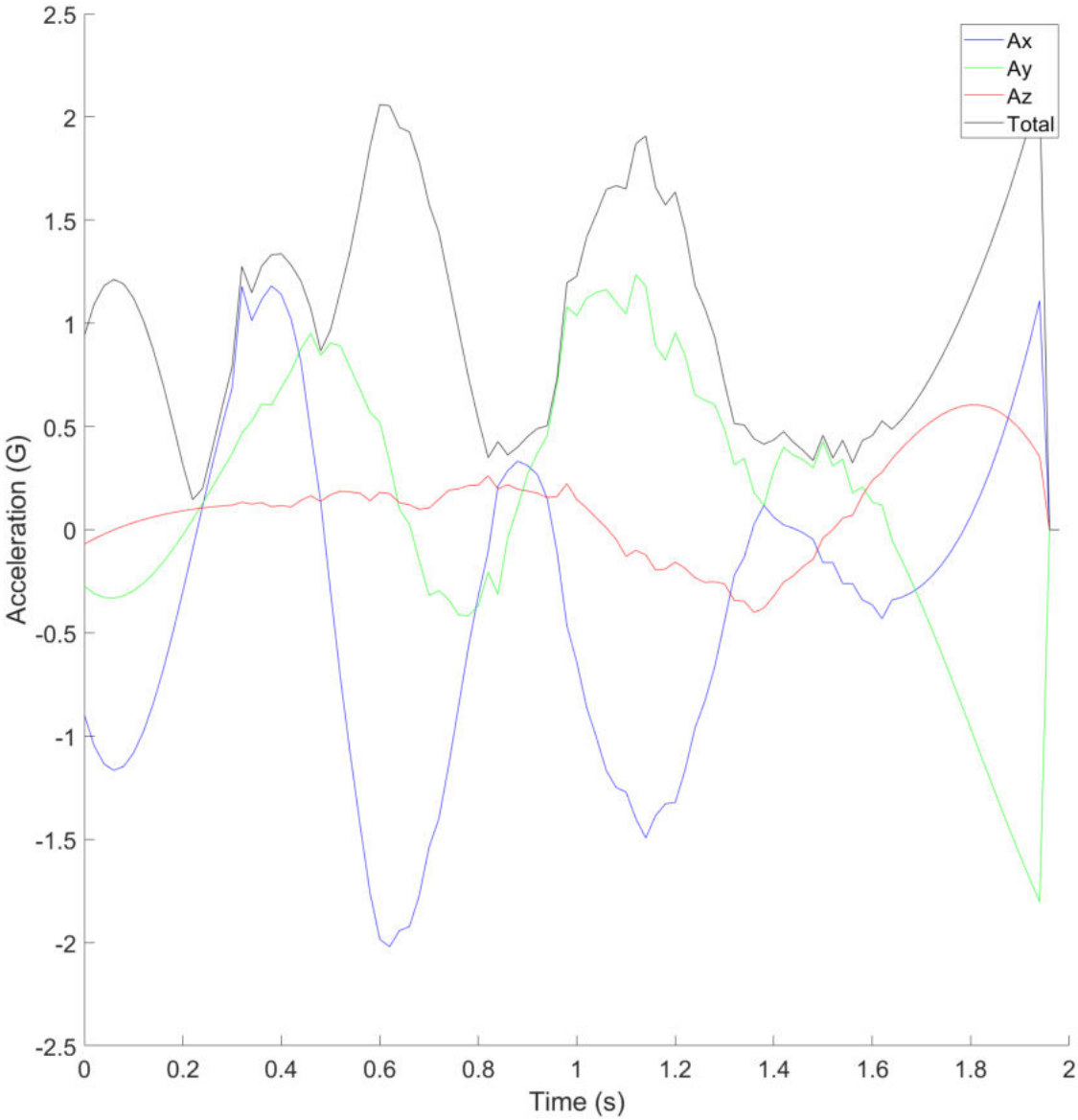

Fig. 3.34 Time series of acceleration data as computed using second derivatives of position with respect to time. The second derivative amplifies noise in the signal and requires a smooth input.

Similarly using an assumption of unit mass to account for the unknown mass properties of the bird it is possible to extract metrics for the energy and power flow throughout the manoeuvre. Figure 3.35 shows the changes in total, potential and kinetic energy throughout a manoeuvre.

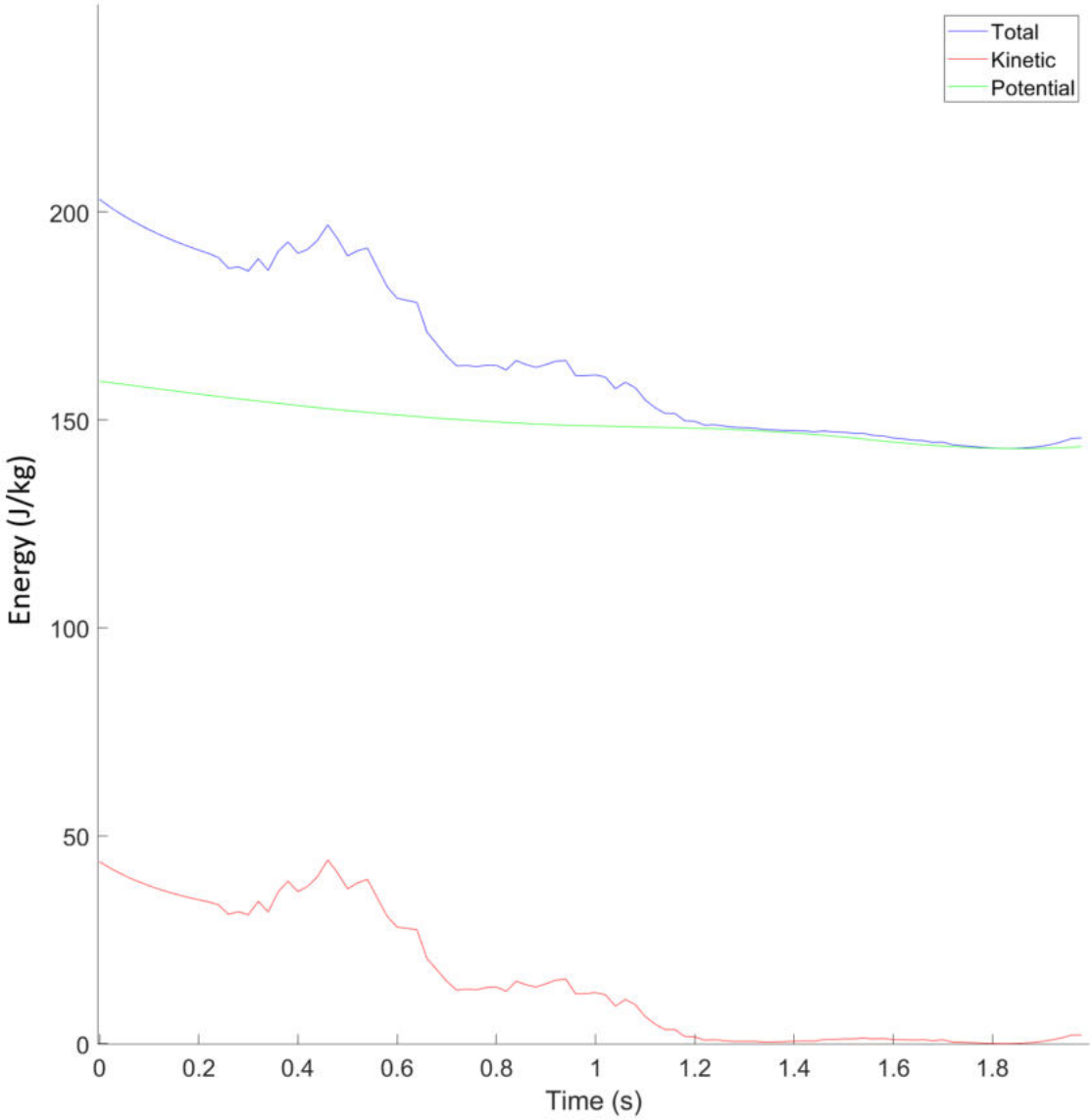

Fig. 3.35 Time series of normalised energy state as computed using the position and velocity state of the bird.

This is useful for analysis as much of the fixed wing manoeuvring involves trading kinetic for potential energy and vice versa. Power at each time step is computed as the time derivative of the energy flow where by positive power indicates a gain in system energy and negative power an expenditure of energy by the bird.

3.5.3 Kinematics

Kinematic analysis of the flight path provides perhaps the most useful insight into the control laws at work in simple manoeuvres such as a steady glide pitch up / pitch down or the initiation of a fixed-wing turn. Using the kinematic equation 3.22, the instantaneous curvature of the flight path can be related to the body pose. Other important parameters are derived by measuring the angle change between the flight path at each time step and the change in the flight path in relation to fixed datums such as the horizon or North - South axis. The flight path angle describes the physical trajectory relative to the horizon and the Track relates the flight path to the North-South plane (Figure 3.36).

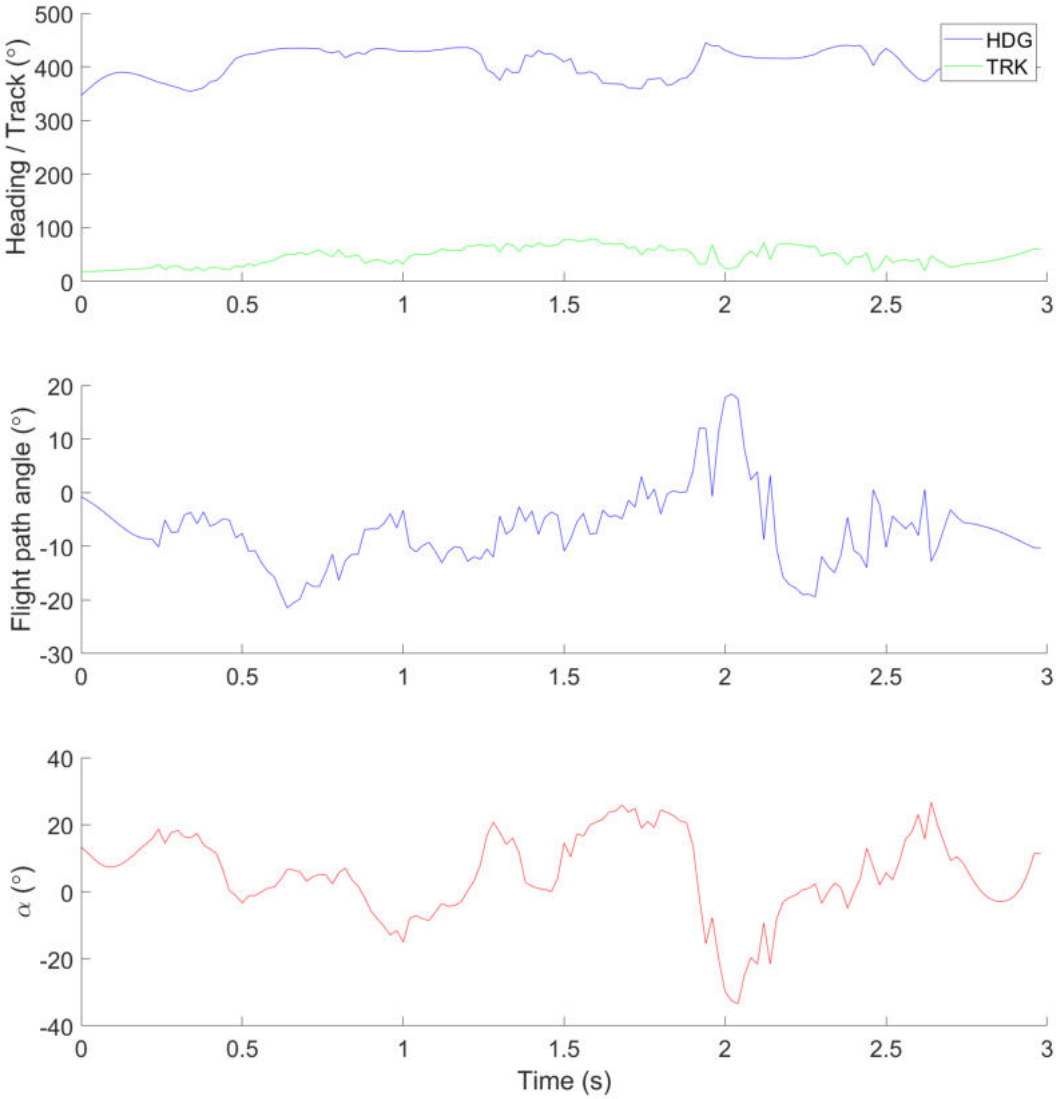

Fig. 3.36 Time series of heading / track relative to magnetic north, flight path angle relative to the horizon and a pseudo angle of attack as defined by the difference between body angle θ and the flight path angle. Note this is not representative of the α as experienced by the wing

In addition to the instantaneous curvature data as calculated for the flight path from velocity and acceleration data an average turn radius for turning manoeuvres can be computed by using a circle fitting algorithm to fit to the flight path providing a more average measure of turn performance.

3.5.4 Pose estimation

Pose estimation provides the body angles relative to the Horizon and North-South planes. Wing spread is defined as the length of the vector connecting the wing tips. It should be considered separately to wing span as if doesn't account for the additional degrees of freedom along the wings but it does give a quantifiable measurement of the spacing between the wing tips. This property is useful as it should be somewhat constant in straight and level gliding flight and it should have a cyclic property in flapping flight whereby the wave length seen in the time series data corresponds to the flapping frequency of the bird, for gulls this cycle is typically 3.5Hz [89].
The body angles as defined by pseudo rigid body assumptions are plotted as a time series (Figure 3.37). Roll, pitch and yaw are defined by vector analysis between the wing-line and the horizon (roll), the body line and the horizon (pitch) and the body line and the flightpath (yaw). These are used to define the bird pose in reference to the earth coordinate system and are the basis for flight path analysis.

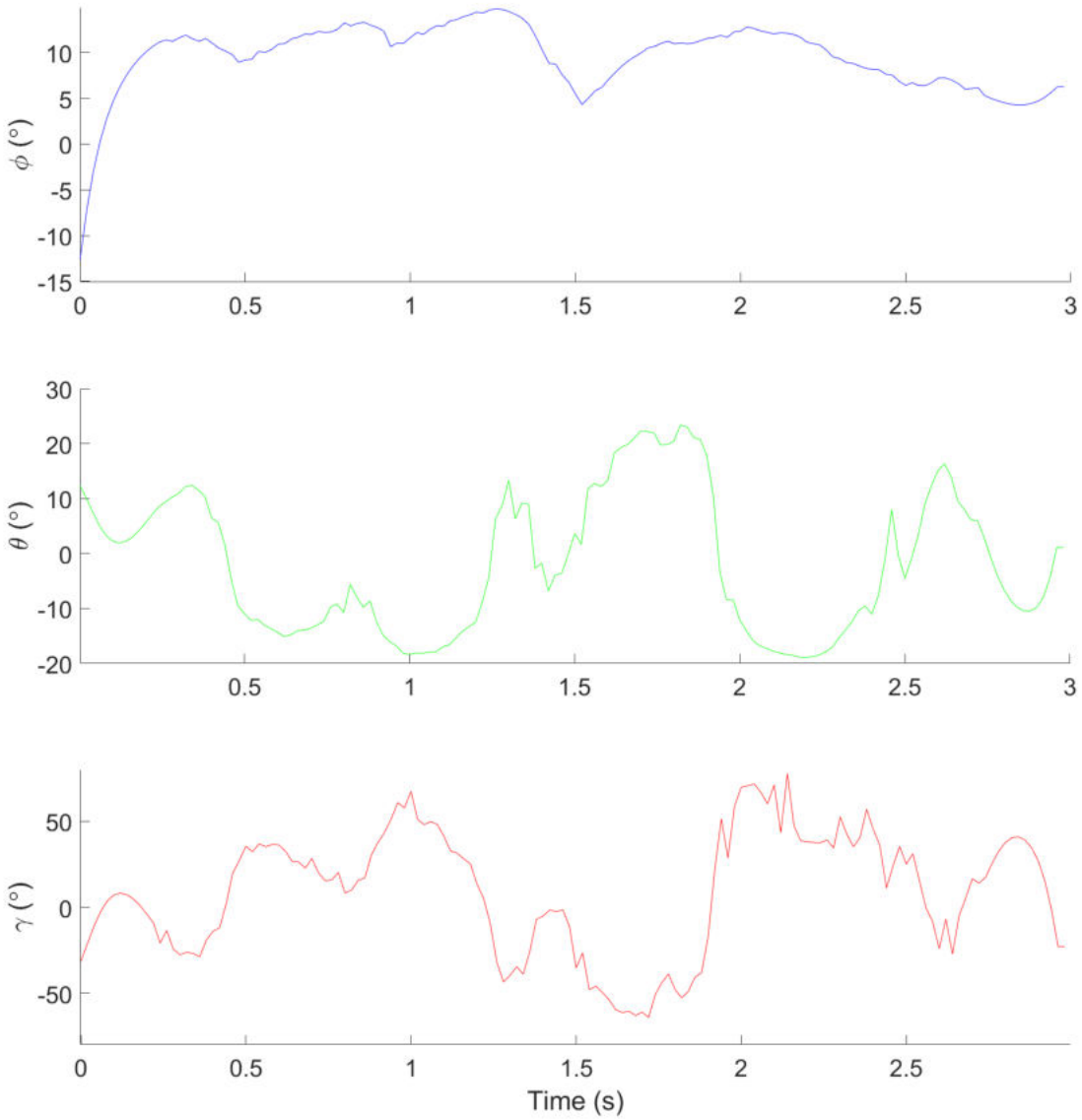

Fig. 3.37 Roll, pitch and yaw angles of the pseudo rigid body angles presented as a time series for the section of flight path tracked.

The pseudo-sweep and dihedral angles are used as quantitative metrics for the control inputs made by the main wing. By reducing the complex degrees of freedom to just these two parameters it is possible to represent the range of motion of the highly flexible structure more simply and to look for correlations between the wing motion and the body response in terms of quantifiable measurements. The sweep and dihedral information can be expressed as a time-series (Figure 3.38).

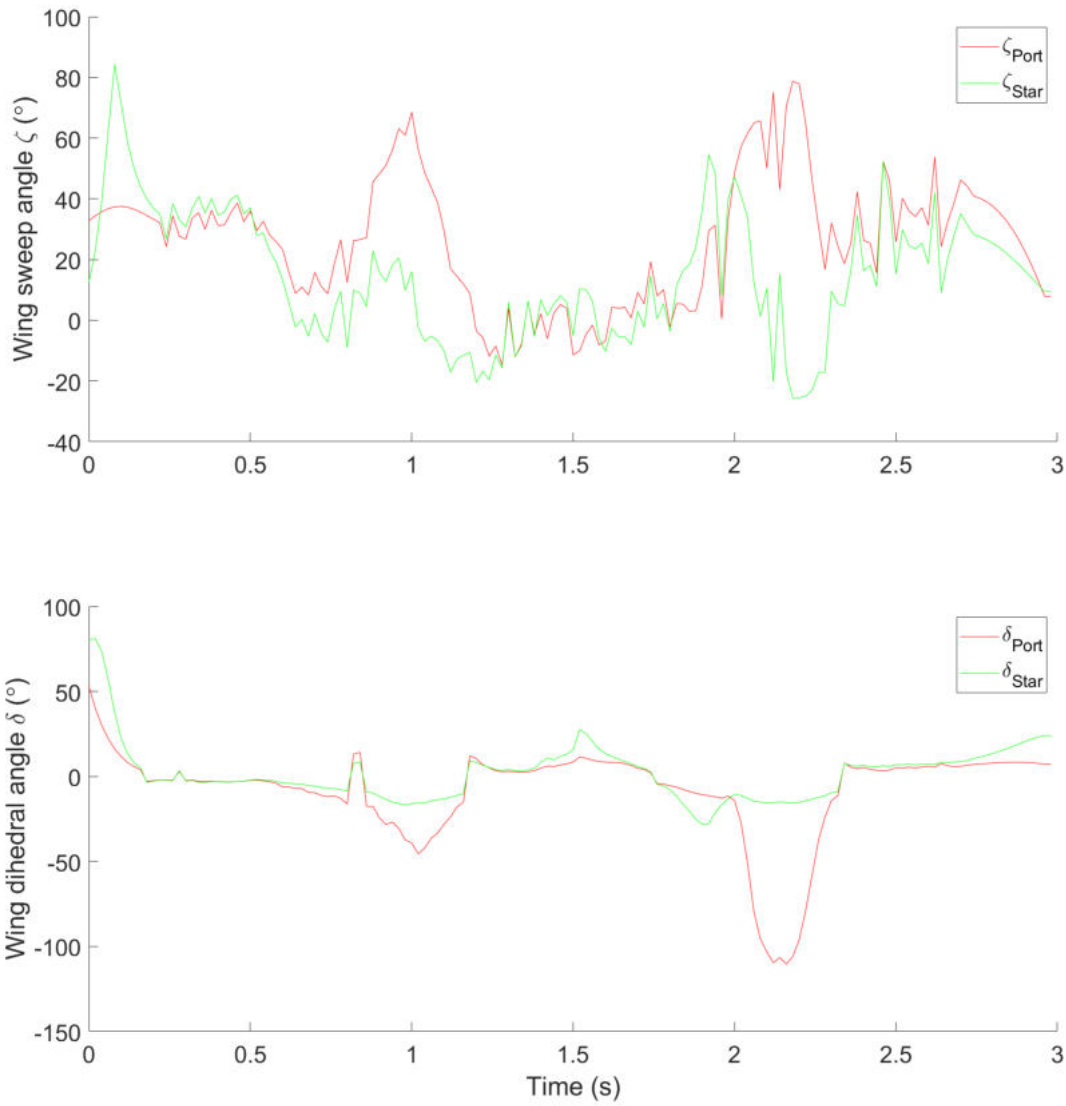

Fig. 3.38 Wing sweep ζ and dihedral δ as a time series. These two variables form the basis of a bi-variate model describing the wing geometry as a simplified set of parameters for analysis.

3.6 Discussion

3.6.1 Review of methods

Ornithodolites and fixed camera stereography are tracking techniques that can be used to track the flight path of birds in the field and to study in-flight behaviours using measurements taken from free-flying wild animals in an uncontrolled natural environment with minimal interference and thus minimal impact on the behaviour of the animal. To complement the tracking of flight paths, studies of the mechanics of birds in flight have been made using supplementary aerodynamic data provided by cadaver preparations or by controlled load measurements using birds flying in a wind tunnel. The most complete assessments of the control of bird flight have been conducted in laboratory environments which do pose some restrictions on the bird natural behaviours due to the confined flight space. A Rotational Stereo Videography system couples the multi-point tracking techniques with pose estimation and reduced order morphology model fitting to allow for simultaneous measurements of flight path kinematics and body pose. Filming locations and days were selected based on criteria to minimise the effects of external influences, such as environmental effects (wind, updrafts etc...) on the flight paths that were being observed. The remote nature of the method is subject to other limitations such as having no real aerodynamic data for the gulls wings, and relying on assumed mass characteristics based on sample measurements of the species in question.

The RSV technique has inherent depth resolution error that scales with the square of the range. At longer ranges it becomes more difficult to track the target in the image when it's size is reduced to just a few pixels. In these scenarios any background clutter in the image can make it very difficult to reliably get a positive template correlation peak, even with the sub-pixel matching techniques. This reduction in image size of the target can be mitigated by using higher magnification lenses with longer focal lengths but these in turn make it more difficult to manually track the target in the frame (due to the high zoom level). In this work the smoothing filter was applied consistently across all data points, using a sliding cubic function over a fixed window size, defined by behavioural frequencies. A possible improvement in this area would be to use a dynamically variable window size based on the range to the target as the points more distant from the camera require the most smoothing. Gain scheduling the smoothing

filter in this way is something seen in other bird tracking works [90] and would be a suggested improvement to the technique.

Pose estimation as attained from a wire frame model fit to multiple tracked points is a novel contribution to the field, using relatively few points taken using consumer grade camera equipment it is possible to construct a bi-variate wing model that captures the principle components. However this model fitting method is subject to maintaining a viewing angle in which all points can be reliably tracked. Too often the viewing angle from the single camera position arrangement means that one or more of the points can be out of view for a number of frames. The RSV system currently linearly interpolates between the last and next seen positions of the points which is acceptable if the point is only out of view for a small number of frames but becomes a poor estimate when the point is out of view for much of a manoeuvre. Currently this case is handled by excluding entire segments of manoeuvres where this point shadowing is experienced which results in a lot of unused data. An improvement to the method would be to update the estimated position of the shadowed point using the average direction vector of the target centroid. This method would essentially satisfy the laws of conservation of momentum and would preserve the flight path of the point in relation to the body centroid if not the other points.

When fitting the wireframe model any out of plane motion is difficult to reliably measure. As discussed the depth resolution error is proportional to distance squared. In a situation where one wing tip is directly out of the image plane, the error associated with this point is maximal when compared to the other wing-tip which is towards the observer in the image plane. In this scenario the length of each wing-line as measured from the centroid will be subject to different levels of error and will result in the out of plane wing-line being measured as relatively longer than the into plane wing-line. This difference in length also effects the measured included angles which are solved geometrically and so differ for each wing-line, which in reality may be equal. Again this scenario is dealt with by manually excluding whole manoeuvre segments where this condition is likely to occur. To improve system tracking robustness with regards to depth resolution error propagation, it may be possible to bound the wireframe model to have a symmetry constraint for manoeuvres where high levels of asymmetry are not expected although this would in turn hide any asymmetric properties of the birds flight and so would only really be useful in non-turning flight.

To help mitigate the probabilistic error and to increase the signal to noise ratio, particularly in the second time-derivative acceleration measurements, smoothing in the form of time-averaging applied to a continuous flight track is applied by fitting a third order polynomial over a data window corresponding to half the period of the manoeuvre of interest within that track (Nyquist Savitsky-Golay smoothing). This time-averaging is based on the assumption that the control signals would be stable over the window of the manoeuvre whilst the random error in the measurements is probabilistic and so the signal to noise ratio will be boosted in this case.

From these suggested improvements the easiest to implement would be to allow for the template window and smoothing gain to be dynamically varied with the range measured. Some experimentation would be necessary to select robust strategies for doing this and it may be that an iterative approach would be best, perhaps using limits on the path gradient as a cost function to limit the process. Furthermore, hardware improvements that increase the out of plane stiffness would help to reduce some of the vertical bouncing observed in use when the device is subject to high rates of rotation. Lighter mirror components distal from the central mount would further improve the structural properties of the device.

3.7 Conclusions

Rotational Stereo Videography is an effective method of analysing bird flight mechanics because of it's ability to simultaneously track the birds flight path and fit reduced order morphology models to the image of the bird. Because the source of the position information is based on a video recording, there is the additional benefit of recording a visual record of flight behaviours alongside the dataset. The RSV system presented in this chapter is the latest iteration of a series of devices described as Ornithodolites and it is the first instance of a technique which, using a single camera, can fit a reduced order morphology model to a free flying wild bird with no markers affixed to it's body. The system is low cost and portable and can be constructed on a low budget with readily accessible tools and materials. Flight path and animal pose are computed by tracking multiple points on the bird. The time stamped flight track and the bird's pose allow for an assessment of how changes in the birds morphology effect its flight path. The amount of error present in the 3D position measurements is small and is a function of the square of the range to the target and the accuracy of the pixel matching. This limits the working volume of the device to around one hundred metres which covers the vast majority of flight manoeuvres demonstrated by the gulls (chapter 4) and red kites (chapter 6) but does limit its use as a means of qualifying behavioural traits. The Rotational Stereo Videography setup is a low cost solution for path tracking and pose estimation in the field and is the source of the datasets used in chapters 4 and 6.

Chapter 4

Longitudinal and lateral control of gliding gull flight

4.1 Chapter Summary

In this chapter, the RSV method described in the previous chapter was used to gather a dataset from free flying lesser black backed gulls to asses their flight control characteristics. The gull dataset comprises over 100 flights from 89 recordings over a four day period. The gull's pose was extracted from four data points having tracked the head, body, tail, port and starboard wing tips and the reduced order wire frame seagull model was fit to these points. The control parameters wing-line sweep and wing-line rise, as previously described are extracted and compared to the kinematics of the flight path at the time point. From this it is possible to construct an envelope of control motion and flight performance and compare this to a traditional fixed wing UAV. The gulls glide polar as determined from this dataset is in line with that seen in other literature. In terms of longitudinal control the gulls appear to use wing sweep to control their rate of change of longitudinal flight path angle in steady gliding flight. The flight path angle is a better measure of longitudinal flight performance compared to pitch angle for a gull because the relationship between the gull's body and wing is not rigidly defined. This result conforms with the qualitative observations that the gulls are gliding with furled tails which are unlikely to contribute to longitudinal control and with existing observations of gulls changing their static stability by sweeping their wings in the glide. In terms of lateral control the gulls glide with furled tails. Their turn performance aligns with that predicted using rigid body turn analysis for a fixed wing. Gliding turns are initiated by rolling into the turn and load factors as estimate by turn radius are in line with those a similarly sized fixed wing UAV would experience.

4.2 Chapter Structure

This chapter introduces the gulls use of wing sweep for longitudinal flight control. It begins with a description of the experimental location and gives description of the RSV method as employed for this study focusing on the two aspects of the study, measuring the kinematics and the wing position of the gulls in flight. The results section covers the main metrics of the dataset including maximum and minimum values as well as averages for the kinematic properties of the flight path. The gulls flight performance envelope is discussed including comparing the glide polar measured in this dataset to that in established literature. The main wing's range of motion as described by the reduced order wire frame model are given in the form of histograms, indicating upper and lower limits as well as the most commonly used ranges. The effect that these wing variables have on the longitudinal control are presented to support the hypothesis that gulls use wing sweep for longitudinal control. The effect of variable wing dihedral on the bird is discussed but no conclusions are drawn from this dataset. In discussion the dataset is used to construct a manoeuvring velocity - loading diagram, a representation of the flight envelope, which is compared to a comparable small manned UAV. The gulls control strategies involving wing sweep for longitudinal control and wing rise for variable lateral stability are presented and compared to traditional control setups. Turning performance is considered based on the kinematics of the flight path and compared to the lateral performance of a small fixed wing aerial vehicle.

4.3 Introduction

Studies have shown that gulls use the extension and flexion of their wings to adapt their longitudinal stability whilst in the glide [83]. These studies have assumed static geometries and examined their effects on the longitudinal control parameters, such as changes in pitching moment and static margin [91]. Here in this study changes in the birds flight path and changes in the wing geometry are measured in free flying wild birds in their natural habitats. The lesser black-backed gull were observed soaring in the Bristol harbourside area in the south-west of the United Kingdom. These gulls frequent the harbourside location throughout the day for its variety of perches and for its foraging opportunities.

Fig. 4.1 Location of the Bristol harbourside in the UK and the position of the filming location on the harbourside [92]

This chapter uses a dataset recorded using the rotational stereo videography technique described in Chapter three. Lesser black backed gulls were tracked to record their flight paths and the RSV technique fits a morphology model to a series of points to analyse how changes to their wing geometry effects their flight path. Three different hypothesis are presented:

1. Gulls use fore and aft motion of their wing to control their longitudinal flight path angle and that this can be decoupled from the body pitch angle. This fore aft movement of the wing centre of pressure can form the basis of a longitudinal flight control law.

2. Gulls vary the amount of dihedral whilst they glide to effect both their lateral direction stability and to control their vertical speed through gusts.

3. The turning performance of the gulls can be modelled as a rigid single main wing and the lateral performance is proportional to bank angle.

The dataset consists of gull flights which have been down selected and segmented to expose instances of straight and level gliding behaviour from which the longitudinal flight path angle and the wing positions can be derived. This dataset can then be used to look for correlations between wing position variables and changes in the flight path forming the basis of a gull-inspired control law derivation.

4.4 Methods

The flight data was collected using the rotational stereo videography rig and processed using the accompanying software as discussed in the previous chapter. The dataset was collected across four days from two different camera setup positions on the west and east side of the harbour. The RSV rig was setup to define zero degrees azimuth angle as magnetic north and zero degrees inclination angle as the earth centred horizon. This translates to Cartesian coordinates with fixes in a north - east - normal coordinate system. Calibration of the RSV system used a series of pre placed fiducial targets as well as distant unique building features with known ranges measured using a laser range finder.

Fig. 4.2 Rotational stereo videography rig in use

Fig. 4.3 Observed gull behaviour at Bristol Harbourside, Bristol, UK.

The Bristol harbourside location was selected due to it's dense gull population, its topography and it's accessibility (Figure 4.3). With it's high foot traffic, open waterway and numerous high building perches the area attracts a large number of gulls from multiple species. The site is a natural flying area surrounded by buildings acting as artificial barriers and a high concentration of birds performing a variety of behaviours. This dataset is comprised of flights made by lesser black-backed gulls. The surrounding buildings serve to provide an artificial boundary to the area establishing a volume in which the RSV system can be calibrated and the flights can be determined to start and finish as a bird flies across this boundary. This maintains the flight paths within the known calibration range of the device. For the purpose of the analysis each flight is treated as independent, however due to the large number of gulls manoeuvring in the area there is no guarantee that all flights were from different individuals.

4.4.1 Flight paths

Fig. 4.4 Sample of recorded flight paths

The RSV system was used to track wild flying birds in their natural environment (Figure 4.4). As such there were no controls in place over the nature, duration and range of the flight other than those enforced by the environment. A wide variety of flights were recorded to allow for further down select looking for specific flight manoeuvres and features. The flights were recorded from different aspects so as to account for the occlusion of various parts of the geometry throughout the flight. For longitudinal flight the primary component of motion of interest is the flight path angle or the angle made between the flight path and the horizon. Flight paths which display the required gliding behaviour were segmented out and the flight path angle was recorded alongside the wings position at that time. The 3D position data had previously been smoothed as raw data before the coordinate transform and so no further smoothing was required. The position data is ground referenced with respect to the RSV rig position, which in turn is aligned with magnetic north and the local gravity vector, because of this the flight path angle was measured with respect to the ground. To minimise the effect of wind on the flight path of the bird, filming was restricted to days with light and variable winds, as wind measurement was only possible at the RSV location and not at the birds location.

4.4.2 Wing range of motion

One of the main objectives of the RSV dataset was to capture *in-vivo* biometrics relating to the positioning of the gulls wings and how these might be used to make control inputs in gliding flight. The musculoskeletal linkages in the gulls wing means that there is a degree of coupling between the motion of the wing in different planes. There are various degrees of freedom, extension/flexion, pronation/supination and elevation/depression [91] these are coupled as the wing moves through it's range of motion. The wing is a modified forearm consisting of joints at its root (shoulder), mid-section (elbow) and distal segments(wrist). Each of these is free to move with coupled motion subject to the underlying tendon and muscle architecture. Additional structures such and the primary feathers and alula have compliance which allows them to move under load and in coupling with the other wing structures. All of these degrees of freedom are governed largely by the internal geometry of the skeletal-muscle system and have few external surface cues from which to define the geometry.

The lack external tracking cues and limitations of the RSV method made it difficult to assess the pronation/supination or twist of the wing and so a two degree of freedom, bi-variate model was fit to the wing. Using the bi-variate wireframe model described in the previous chapter the complex wing geometry is represented by just two variables: A pseudo-sweep angle ζ and dihedral angle δ. Using these two variables the model describes a variety of complex wing geometries composed of flexion and rotation of the manus, elbow and shoulder joints in the wing.

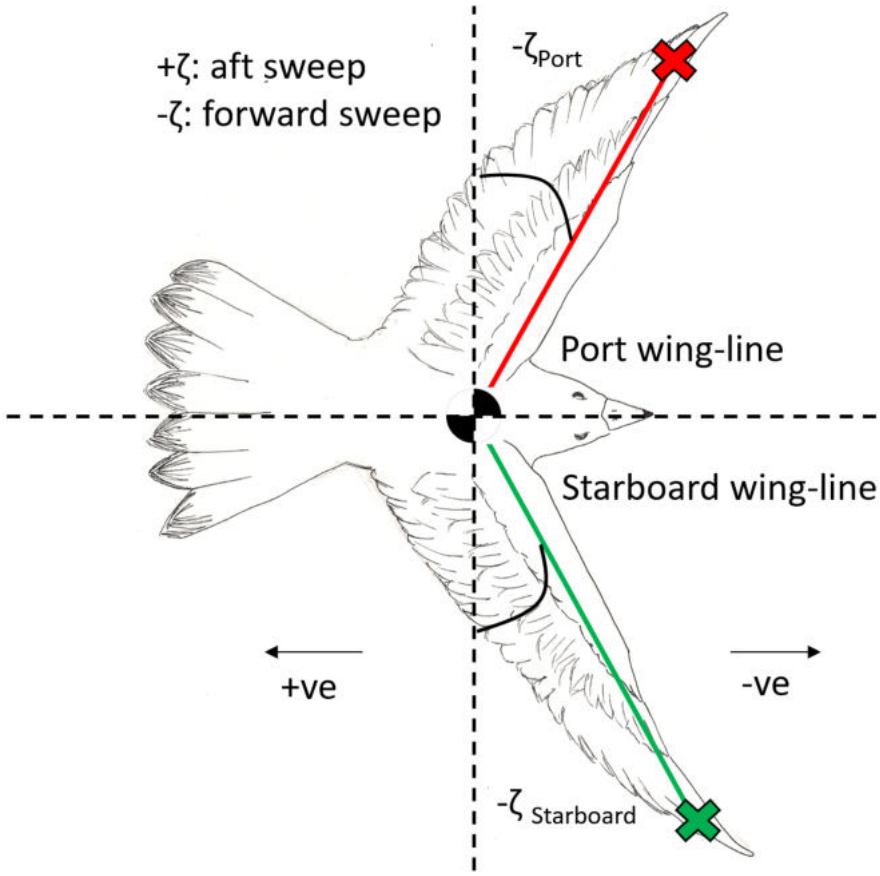

Fig. 4.5 Pseudo - Sweep angle ζ defined by the angle subtended by the wing-line and the longitudinal axis in the x-y plane.

Looking first at the pseudo-sweep angle ζ. This angle defines the fore-aft relationship of the wing-tip to centroid line, here after referred to as the wing-line, for the port and starboard wings. The magnitude describes the degree to which the wing-tip moves fore-aft with the relation to the centre of the body, but because the measurement is computed as a function of the dot and cross product of vectors and the inherent coupling between the joints of the wing the angular measurement of ζ in degrees also captures the amount of wing spread. This one variable can be used to describe the morphing of the wing from it's fully spread to a retracted swept pose. Hence, ζ is describing how the centre of pressure of the wing is moving fore-aft relative to the centre of mass of the bird. This couple is important statically when quantifying the longitudinal stability characteristics of the animal and dynamically in control of pitch. Additionally the aerofoil geometry will also be changing substantially with ζ and the position of the aerodynamic centre can be reasonably be expected to move in relation to the centre of mass and centre of pressure.

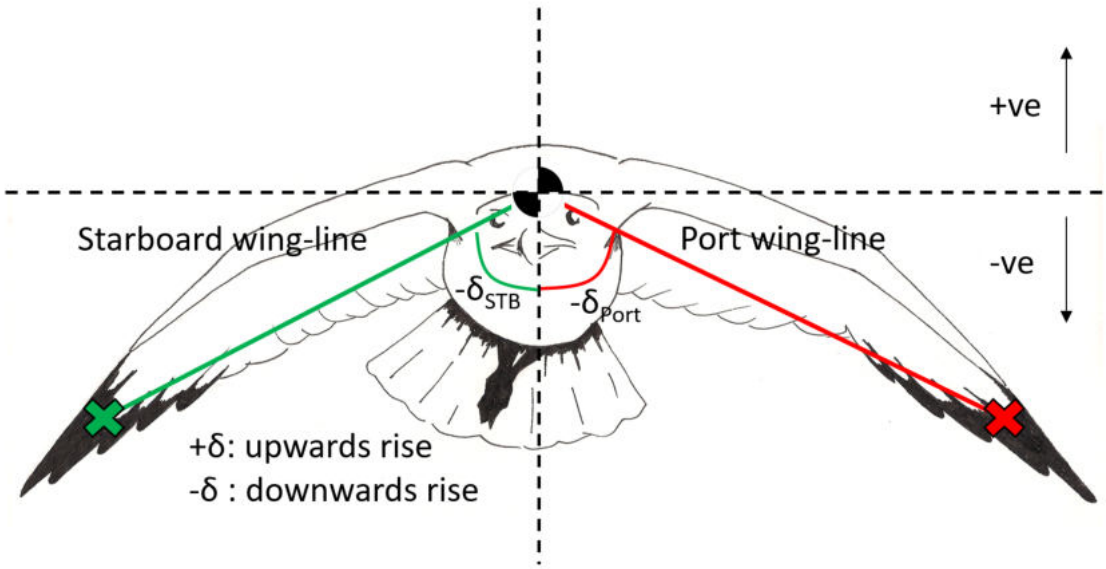

Fig. 4.6 Pseudo - Rise angle δ defined by the angle subtended by the wing-line and the normal axis in the z-y plane.

Deflection of the wing-line up-down in relation to the normal body axis of the bird is captured by the pseudo-dihedral angle δ. This biometric captures the flap cycle in flapping flight and the essence of the eponymously named gull-wing geometry in gliding flight albeit with a few issues. The gull-wing so commonly seen in the glide is a complex geometry comprising of rotations at the shoulder and flection-rotations at the elbow and manus joints, as such it is possible for the bird to achieve substantial deflection of the wing surface along the normal body axis both in the positive and negative sense with deformation around the manus whilst maintaining only a small change in the wing tip position relative to the centroid and the wing-line. In this case the wing spread is reduced, reducing the effecting span whilst maintaining the wetted area of the wing. It has not been possible with the RSV system to reliably track the number of points needed to properly capture this polyhedral deflection and so the variable δ and wingspread are used instead. By varying the polyhedral of the wing the gull is substantially altering it's aerodynamic properties in a way that effects both the lift distribution and the inertial properties of the wing. As such the deflection of the wing-line with respect to δ is an interesting variable to associate with possible control strategies being used by the gulls.

4.4.3 Turning mechanics

Gulls adopt a gliding gait when commuting to help extract energy from the environment and reduce their own energetic cost of transport [93]. When gliding the gulls morphology is adapted to maximise lift and minimise drag. They fly with their wing outstretched at maximum span and their tails furled and adopt a flight speed close to their minimum drag airspeed. This configuration is similar to that used by a conventional airframe modelled by rigid body flight mechanics [94], albeit minus the vertical tail. When turning, the direction of velocity is continually changing. The gulls when gliding are constantly descending through the air mass and vary their rates of turn. To simplify the mathematics the equations presented here, consider the turn as steady (that the rate of turn is constant) and constrained to a horizontal plane. A gull turning through an angle (ψ) with a radius (r) and velocity (V) is subject to aerodynamic forces in equilibrium with it's weight (W). The accelerations as experienced by the gull, the load factor (n), represent the increase in lift required to support the weight of the bird and provide the lateral force to initiate and maintain the turn. Described as multiples of gravity (g) the load factor and lateral load factor (n_{a_c}) are independent of the aerodynamic and inertial forces acting on the bird and are functions of the bank angle (ϕ) alone. Bank angle is poorly defined for birds whose wings are not rigidly constrained to the fuselage so the analysis here assumes the bank angle as being defined by a vector perpendicular to the body joining the wing-tip in relation to the horizon.

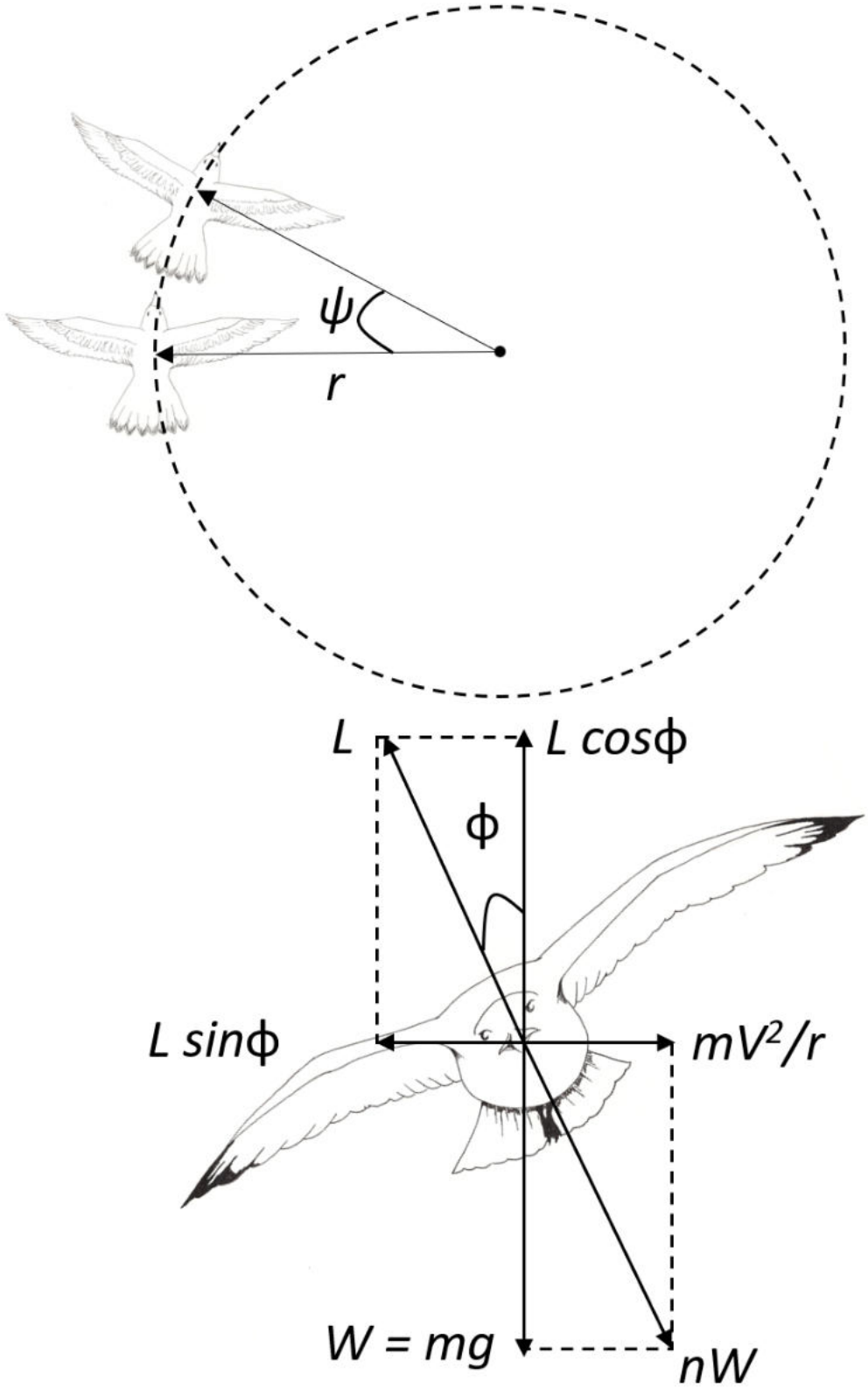

Fig. 4.7 Gull in a steady coordinated turn in the horizontal plane.

In the steady horizontal turn (Figure 4.7), the conditions of equilibrium are expressed as:

$$Lcos\phi = W = mg \tag{4.1}$$

$$Lsin\phi = \frac{mV^2}{r} \tag{4.2}$$

By combining equations 4.1 and 4.2 and rearranging, the turn radius is given by:

$$r = \frac{V^2}{gtan\phi} \tag{4.3}$$

And the corresponding rate of turn ($\frac{V}{r}$) is given by:

$$ROT(^\circ/s) = \frac{g\tan\phi}{V} \tag{4.4}$$

The centripetal acceleration (a_c) is the in-plane acceleration given by:

$$a_c = \frac{V^2}{r} \tag{4.5}$$

Substituting equation 4.3 into equation 4.5 and normalising with respect to gravity give the centripetal acceleration in terms of a lateral load factor (n_{a_c}):

$$n_{a_c} = tan\phi \tag{4.6}$$

4.5 Results

4.5.1 Flight paths

The data set presented here is derived from 117 flights from 89 video samples. The RSV system produces timestamped position information of multiple points. Here are six example flight paths from which flight path angle and wing position information are extracted.

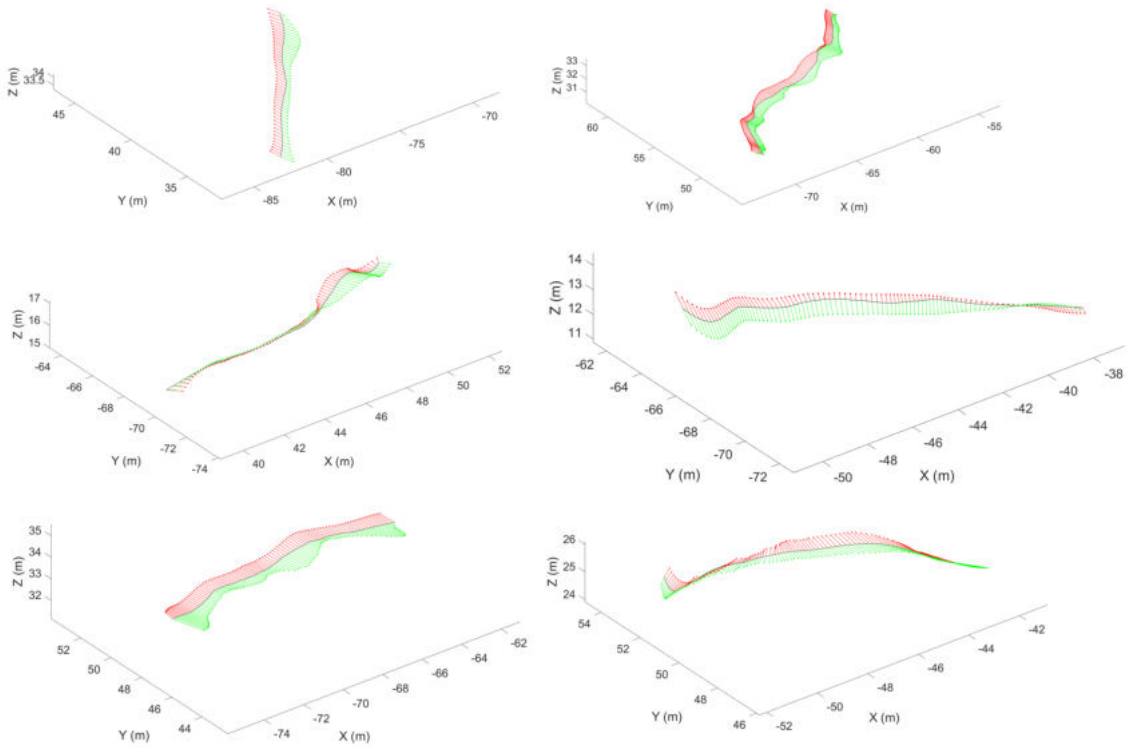

Fig. 4.8 Example gull flight path with wireframe overlay showing the typical manoeuvres from which flight path angle and wing pose can be extracted. The flight tracks are oriented such that the direction of flight is left to right. The black line indicates the path of the body, the red and green lines show successive positions of the wing line.

By taking the time derivatives of the position points it is possible to calculate velocities and accelerations, analysis of the flight path provides angular and radius information and body pose estimation give body variables. The flight envelope (Table 4.1) is characterised by measurements of the mean and maximum velocity, acceleration, rates of change of heading, flight path angle as measured from the flight paths.

Table 4.1 Flight performance envelope of *Larus fuscus* showing maximum, minimum and mean values from all measured segments from 117 individual flights

Performance Variable	**Mean**	**Std**	**Max / Min**
Velocity (ms^{-1})	9.47	4.59	27.44
Vertical speed (ms^{-1})	-0.41	3.10	+ 6.35 / - 9.45
Acceleration (g)	1.84	-	9.56 / 0
Rate of Turn ($°s^{-1}$)	0.94	49.78	93.90
Centripetal Acceleration (g)	0.48	0.77	3.58
Roll (°)	0.27	21.29	64.5
Pitch (°)	1.67	11.17	31.6 / -18.92
Flight path angle γ (°)	-2.15	15.69	78.10 / - 90.00
Roll rate ($°s^{-1}$)	-0.03	57.05	211
Rate of change of flight path angle ($°s^{-1}$)	-0.10	89.24	177 / -223

The mean speed of 9.47 m/s was close to one third of the maximum observed instantaneous speed of 27.44 m/s indicating that most flight recordings were well within the typical flight regime and not indicative of peak performance. The average recorded flight track was 20 - 30 seconds. For the purposes of analysis the manoeuvres were segmented into 2 - 3 second sequences and subsampling down from the full 50 Hz data rate was used when longer flight section analysis was required (typically a 2Hz sample rate was used for recordings up to one minute). Pose estimation fits a simple four point wireframe to the bird and the pseudo-sweep and pseudo-dihedral angles are measured. Kinematic analysis of the flight path establishes radius and thus turning performance.

4.5.2 Glide Polar and Flight Envelope

Using the velocity data as derived from the gull's data set it is possible to plot a glide polar for the gulls (Figure 4.9). The selection of flights to include in this dataset was constrained to contain only flights deemed to be in a steady glide.

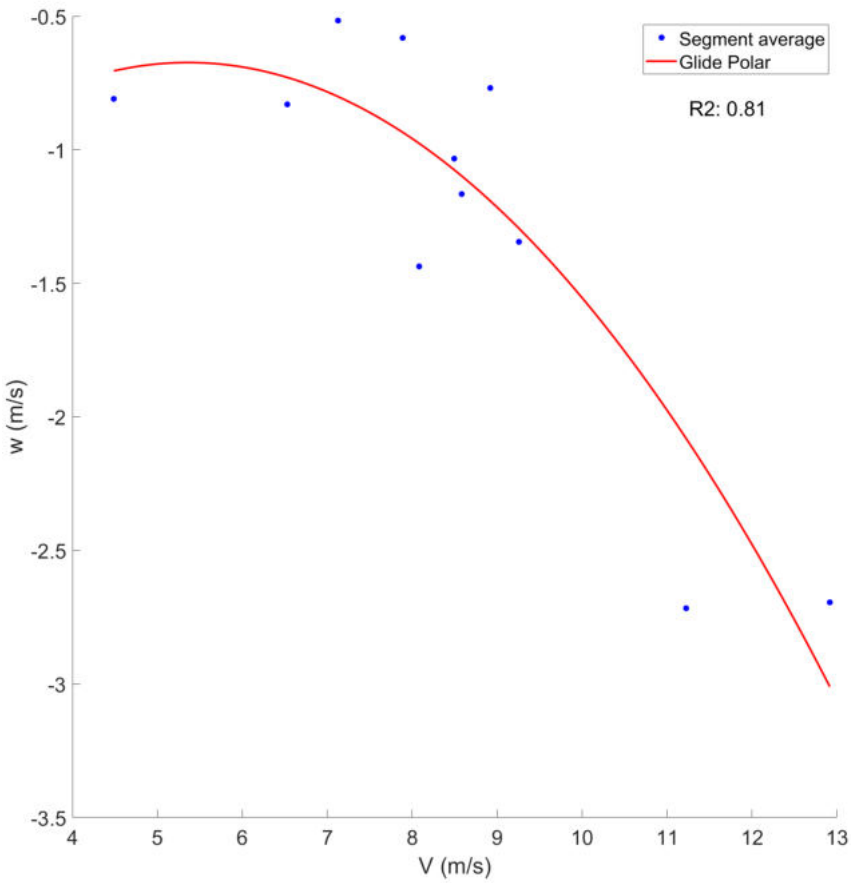

Fig. 4.9 Glide polar of *Larus fuscus* as measured from eleven flights. All velocity measurements are ground referenced which would account for lateral shift against other known polars.

Eleven Flights were included which met the following criteria:

1. **Mean Bank angle** $< 20°$

2. **w** < 0 m/s

3. **Gliding flight** - (Qualitatively not flapping)

The gulls glide polar is based off velocity measurements relative to the stationary RSV device on the ground with a simple vector sum of the spot wind at this location. Whilst all flights were recorded on low wind days to minimise the difference between measured ground speed and airspeed the exact effect of the local wind vector on the velocity is not known. It was not intended for this to be a true measurement of the birds polar but as a confirmation check that the results as measured by the RSV were sensible and in accordance with other sources of data. The measured polar shows a min sink of 0.5 m/s at 6m/s and a best glide of 8:1 at 8m/s. This polars low speed region agrees with existing polars of lesser black backed gull in literature [95] however the high speed region shows increased descent rates for a given airspeed. This is likely because the sample of manoeuvres selected for this analysis contain diving and climbing manoeuvres that don't conform to the assumption of a straight and steady glide. Whilst the small sample size prohibits detailed analysis of this polar the difficulty in obtaining flights that obey the aforementioned criteria set is in of itself evidence that the gulls spend a relatively low proportion of the flying time in straight steady glides in still air, preferring to instead adopt flap-glide gaits in transit and using gliding gaits to soar updrafts and to manoeuvre.

4.5.3 Wing range of motion

Using the landmarks tracked on the gulls wingtip and body centroid the range of motion acheived by the wing as described by wing sweep ζ and wing rise δ in flight recorded are presented in figure 4.10.

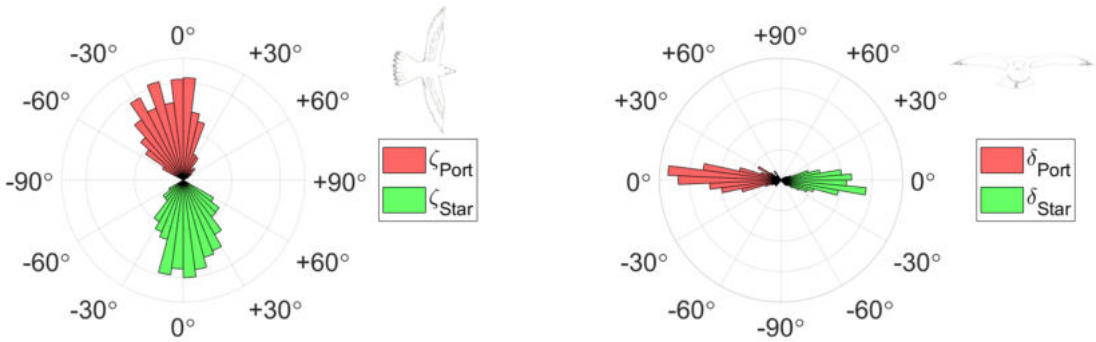

Fig. 4.10 Histogram of wing sweep and dihedral angles as measured by reducing the complex wing geometry to a bi-variable model, describing the average wing-line in sweep and dihedral. These histograms represent all measured segments from 117 flights.

Plotting a histogram (Figure 4.10) of the range of pseudo-sweep angles of the wing line (ζ) and the linearised polyhedral angles of the wing line (δ) it is possible to see both the extent and distribution of these biometrics taken from a series of straight gliding flights. The apparent asymmetry in this figure is a function of the total dataset being unbalance in terms of the number of flights observed with complete view of the bird. In this dataset there were more flights where the view of the starboard wing was occluded and this imbalance in the dataset is seen by there being proportionally more points for the port wing compared to the starboard wing. Attention should be paid to the relative limits and distribution of the histogram with each wing being considered in isolation. There is no inference here that the birds are flying predominantly in one direction or favour a particular wing. From this histogram the maximum range of motion of the wing-line sweep and wing-line dihedral is $\binom{-60^\circ}{-30^\circ} < \binom{\zeta}{\delta} < \binom{+60^\circ}{+30^\circ}$ respectively. The maximum range of deflection is symmetrical and the mean values of the angle and the standard deviation for wing-line sweep were aft $\zeta_\mu = 7.8^\circ \quad \sigma_\zeta = 26.6$ and for wing-line dihedral it was raised $\delta_\mu = 3.2^\circ \quad \sigma_\delta = 18.4$.

4.5.4 Forward motion of the wings and control of flight path angle in gliding flight

The configuration of the gulls wing is described by a large number geometric parameters. As such selecting an individual parameter for feedback control is difficult and so the method in this chapter uses a reduced order model to analyse the relationship between the the wing state and the resulting change in flight path. The reduced order model is bi-variate, comprising of the average wing-line sweep and dihedral angle as computed from the morphology model fit to the four tracked points on the bird. Pitch angle (θ) from the RSV data is unreliable for two reasons: firstly due to the constant occlusion of either the tail or head as the aspect of the bird changes in the image it is difficult to generate an accurate body line in every frame. Interpolating the body line introduces large position error. Secondly the relationship between the main wing and the body is not rigidly defined for the gull as the gull has the ability to pronate and supinate it's shoulder joint. This varying setting angle introduces an offset error which decouple the body pitch angle from the longitudinal dynamics. This section instead chooses to use the Flight Path Angle (FPA, γ) variable, which is a direct measure of longitudinal flight performance, to assess the relationship between changes in position of the birds wing morphology and changes in the flight path. The results presented here are comprised of the eleven flights comprising 33 seconds of flight time and represent climbing and descending manoeuvres, entering into or pulling up from a straight glide (Figure 4.11).

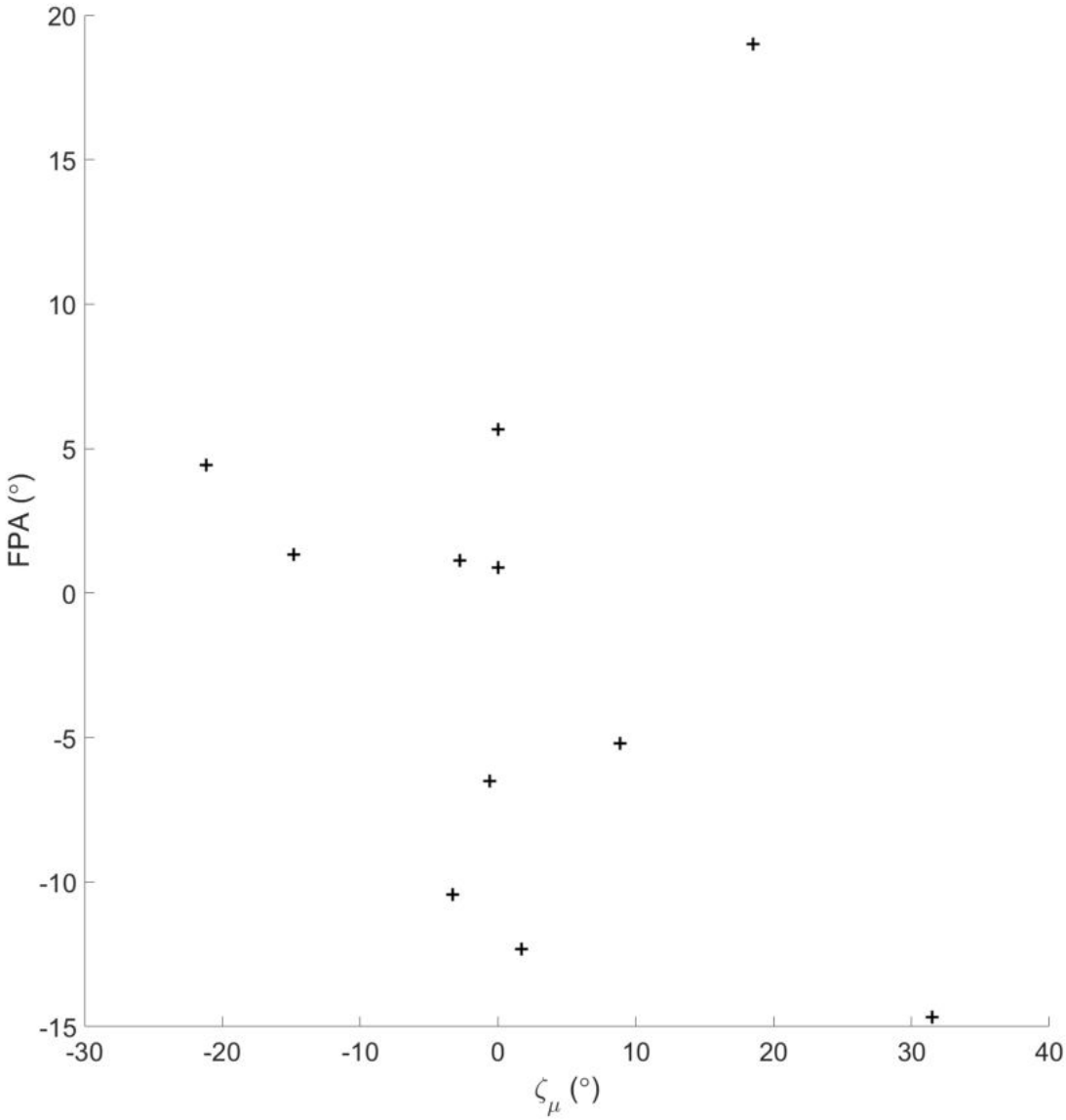

Fig. 4.11 Flight path angle vs Wing sweep angle showing a loose correlation

Figure 4.11 shows that whilst there is a loose relationship ($R^2 = 0.45$) between wing-line sweep and flight path angle there are significant outliers. A similar picture is seen if instead of looking at flight path angle the dependant variable is replaced with the vertical speed of the bird (Figure 4.12).

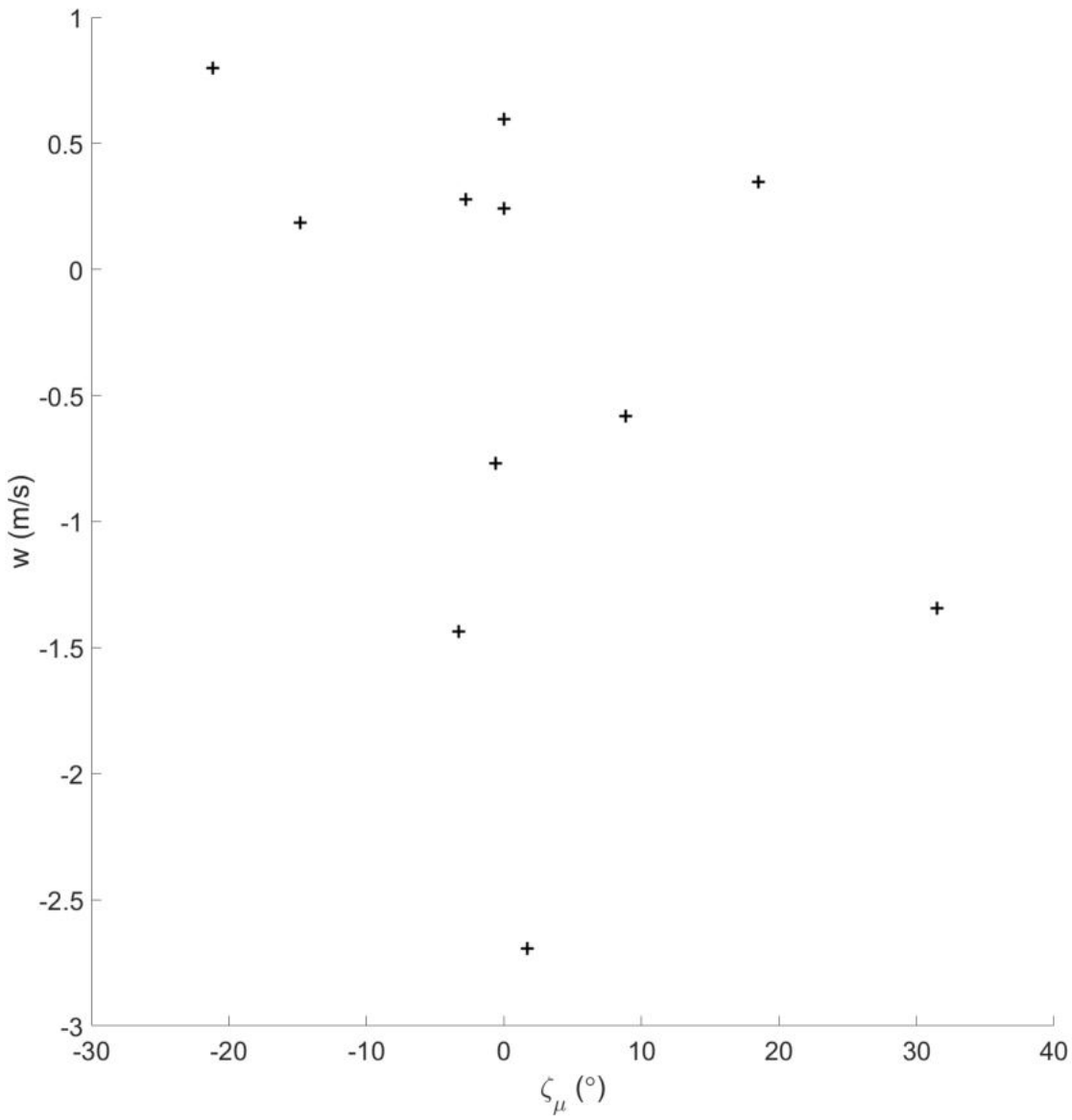

Fig. 4.12 Vertical speed vs Wing sweep angle showing a loose correlation

Instead of looking at absolute values we can instead look at rates of change on longitudinal variables.

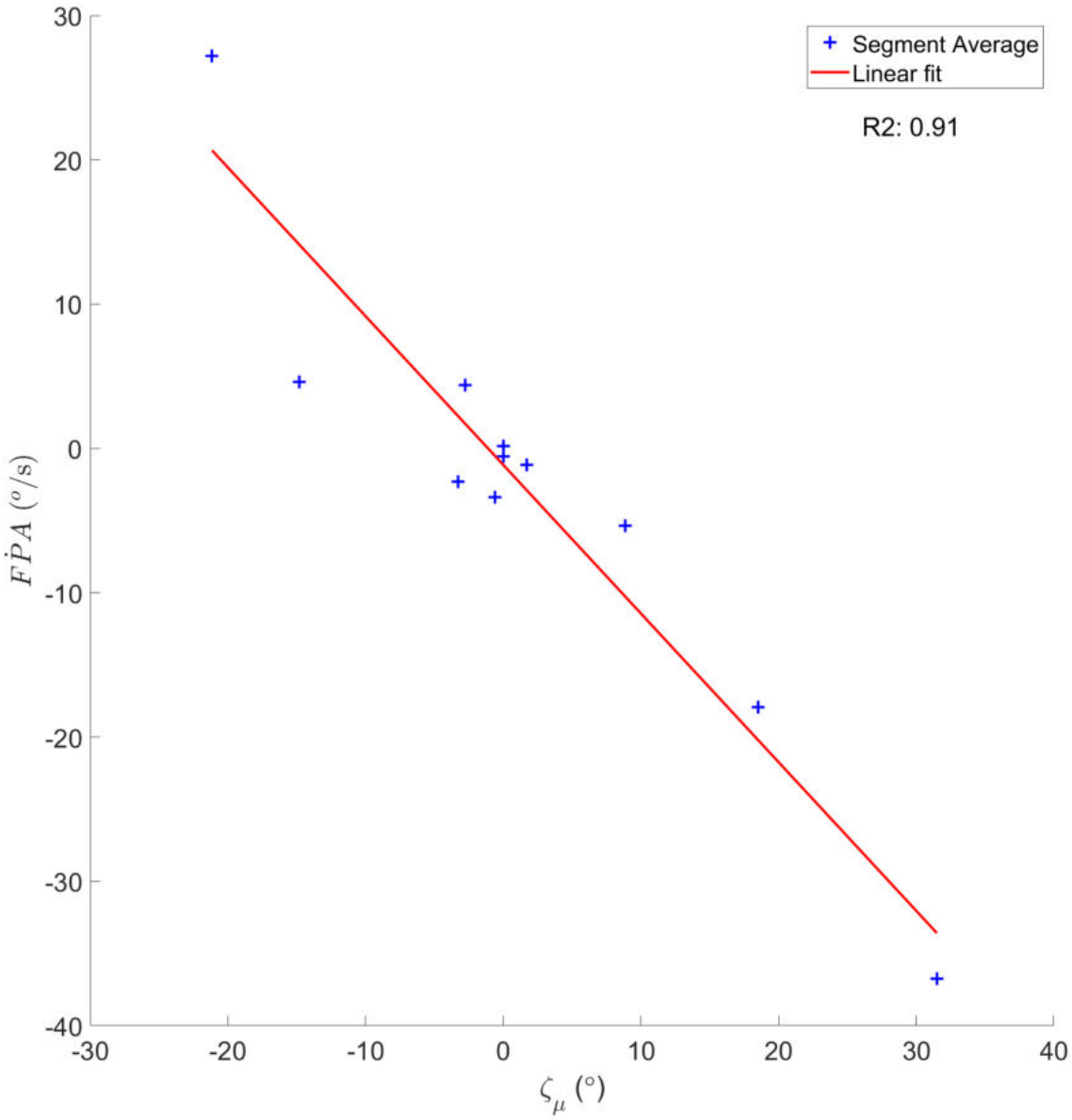

Fig. 4.13 Rate of change of flight path angle ($^o/s$) vs wing sweep showing a strong correlation

Here the relationship between wing-line sweep and the rate of change of flight path angle with respect to time is stronger ($R^2 = 0.91$) with the wing-line sweep accounting for over 90% of the variation in the FPA rate. This relationship satisfies the mechanics of the manoeuvre as demonstrated in Figure 4.13 and is measurable with a strong coefficient of determination.

This suggests that the gulls are using the relative change in the position of the centre of pressure on their main lifting surface as represented by the wing-line sweep, to modulate longitudinal guidance and control the rate of change of their flight path angle relative to the ground during pitch up and pitch down manoeuvres whilst in gliding flight.

4.5.5 Variable dihedral and changes in vertical speed and stability

Here the relationship between the wing-line rise angle and flightpath angle and vertical speed are presented.

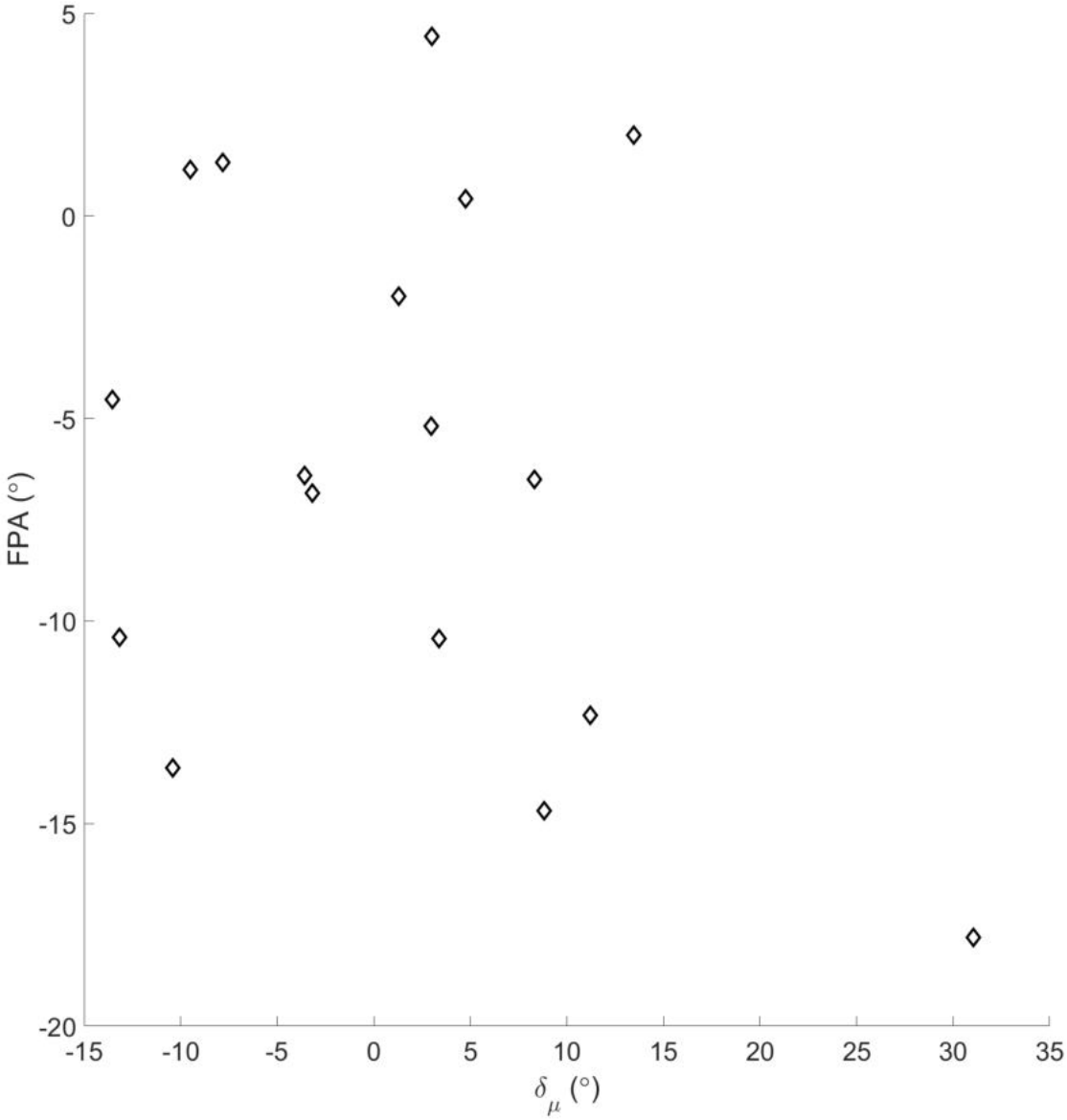

Fig. 4.14 Flight path angle vs dihedral

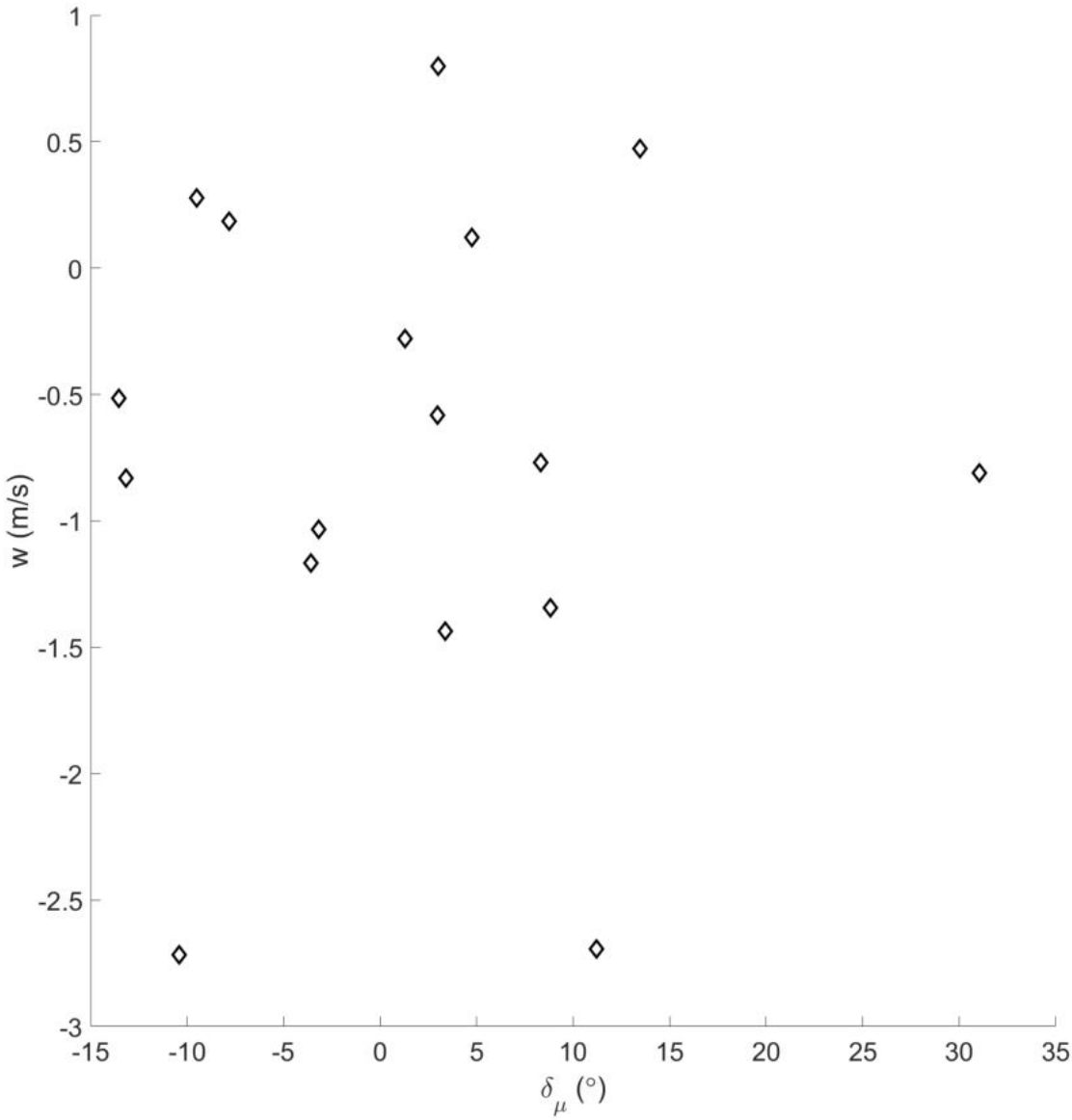

Fig. 4.15 Vertical speed vs dihedral

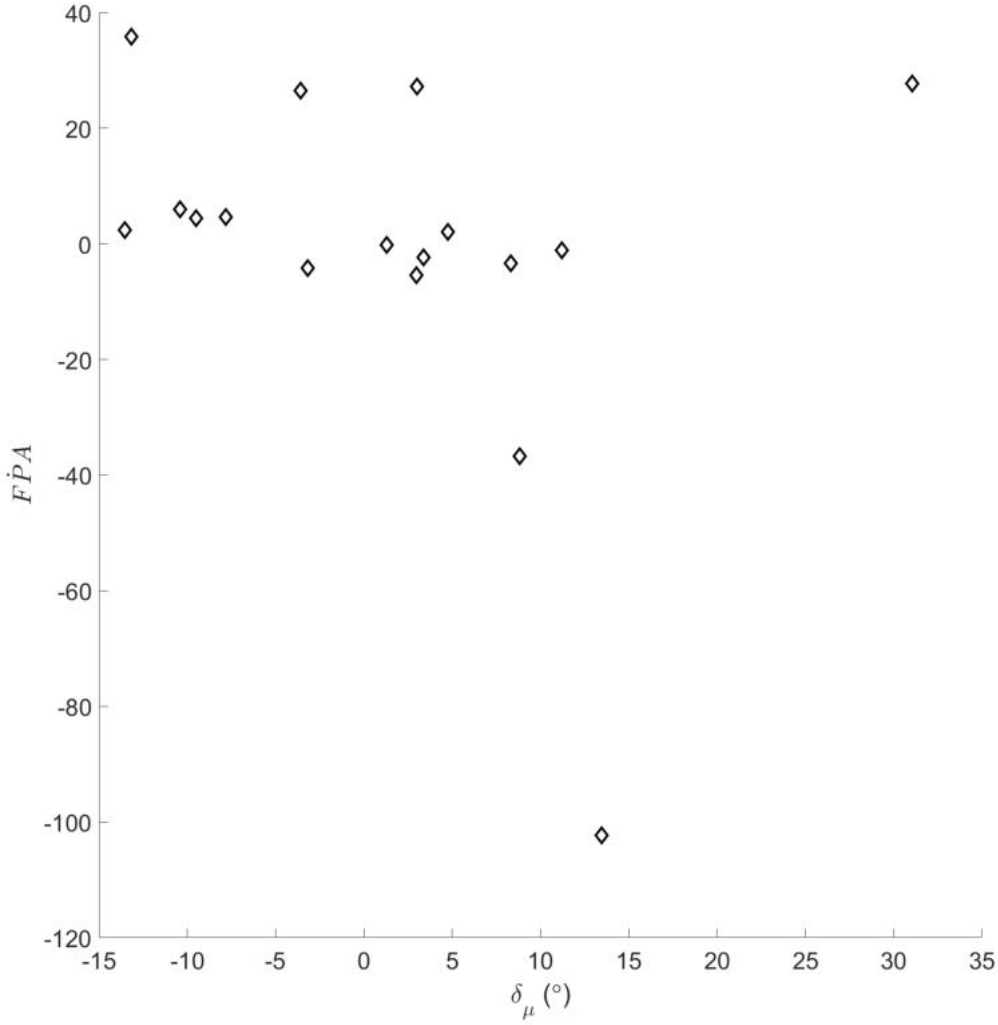

Fig. 4.16 Rate of change of flight path angle vs dihedral

As can be seen in figure 4.14 and figure 4.15 there is no statistical relationship between the flight path angle, vertical speed and the wing-line rise in this dataset. However this dataset was captured for the purpose of analysing the longitudinal dynamics and does not examine the change in pose whereby some species adopt very high dihedral angles. Figure 4.16 shows an almost constant null relationship between the wing-line rise and the rate of change of flight path angle. From this plot, for the case of the steady glide manoeuvres the amount of wing-line rise has no bearing on the flight path angle in the vertical plane. Because this dataset does not contain air reference positions it is possible that incorporating additional wind data would reveal a correlation.

4.5.6 Turning performance

The results presented here were selected from twelve flights consisting of gliding turns with no large changes in velocity (constant speed turns). To reduce the effect of wind on the metrics for turn performance, i.e. the turn radius is strongly effected by the wind, the parameters of interest are the rate of turn and the in-plane lateral load factor experienced throughout the turn accounting for the centripetal acceleration on the bird.

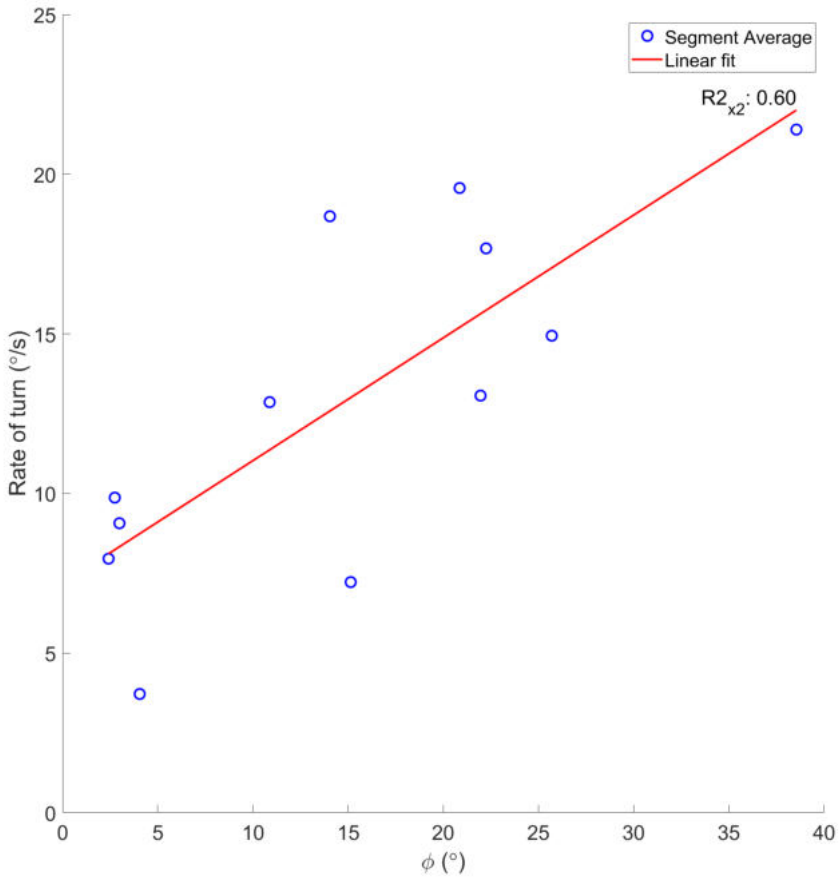

Fig. 4.17 Turn performance: Bank angle vs rate of turn

Figure 4.17 shows the correlation between bank angle; as estimated from the body pose, and rate of turn; as calculated using the kinematic expression (Equation 4.4), and a correlation ($R^2 = 0.60$) is shown.

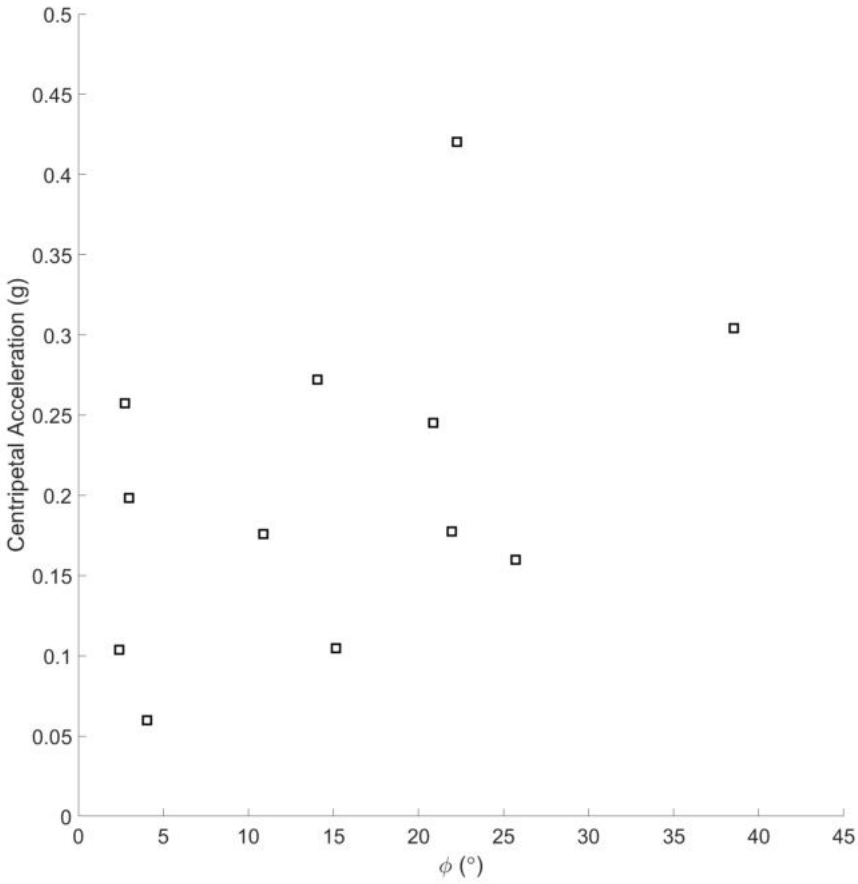

Fig. 4.18 Bank angle vs lateral load factor

The relationship between bank angle, not corrected for the non-horizontalality of the turning plane and the centripetal acceleration, subject to large propagated errors as a result of the double derivative of the position data, are show in figure 4.18 and show a very poor correlation ($R^2 = 0.22$). The test appears to have a null result, however, the flight paths as recorded by the RSV rig are not representative of totally level turns constrained to the horizon for which the equations are derived.

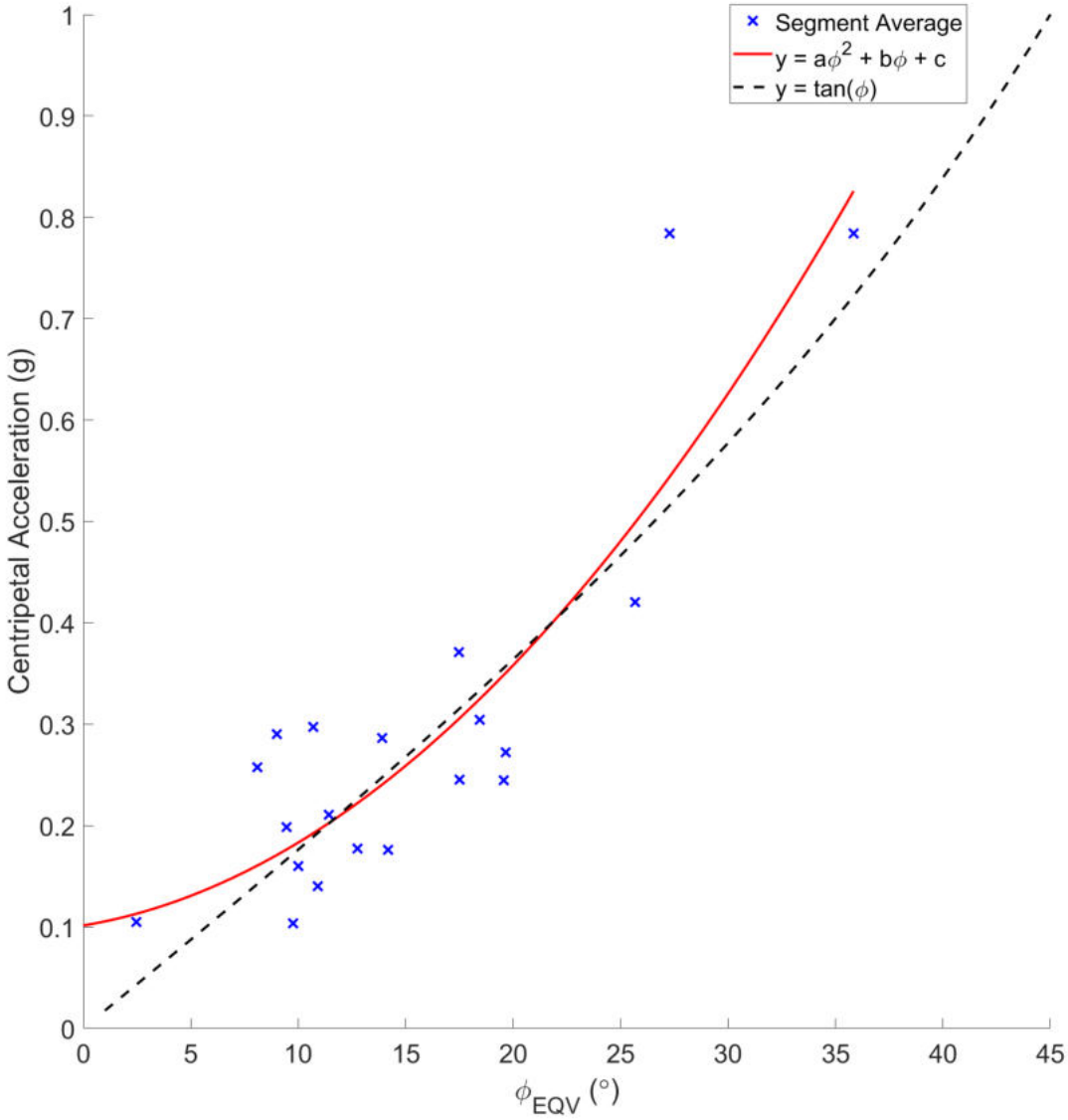

Fig. 4.19 Equivalent bank angle, relative to the turning plane vs lateral load factor

Figure 4.19 plots an equivalent bank angle defined by the turning plane. Using this definition the rigid body model $n_{a_c} = \tan\phi_{EQV}$ has significance and is determinate ($R^2 = 0.73$) but in this case the relationship between the data is also well fit using a quadratic model $n_{F_c} = a\phi_{EQV}^2 + b\phi_{EQV} + c$ with a higher coefficient of determination ($R^2 = 0.81$).

4.6 Discussion

4.6.1 Flight Envelope

Gulls are flight generalists that have different flying gaits which they use for different purposes. Generally a gull will take to the wing to commute or find food. The results in this chapter show a glide polar which is in line with existing theoretical glide polars found in the literature. By examining the kinematics of the flight paths (Figure 4.20 and Figure 4.21) it is possible to construct a flight envelope (Figure 4.22) for the gulls based on framework provided for the certification of aircraft.

Using biometric data for the lesser black-back gull population of Bristol, UK [96] where the average mass and geometric properties of 13 individuals as presented in Table 4.2 it is possible to construct a flight envelope velocity - loading (V-n) diagram for the gull using the design requirements of EASA certification specification CS-23 Normal,Utility, Aerobatic and Commuter aeroplanes [97]. Choosing to work to the regulation of a Utility category aircraft, chosen because whilst gulls do perform some aerobatic manoeuvres, 80% of the measured load factors as seen in Figure 4.20 are less than the utility category limit load of 4.4g the Vn diagram looks as in Figure 4.22.

Table 4.2 *Larus fuscus* biometrics. Average measurements from thirteen gulls taken from the Bristol population in summer 2017 [96]

Wingspan (m)	**Mass (kg)**	**Wing area (m^2)**
1.1	0.7	0.2
Aspect ratio	**Mean aerodynamic chord (m)**	**Frontal area (m^2)**
7.8	0.15	0.007

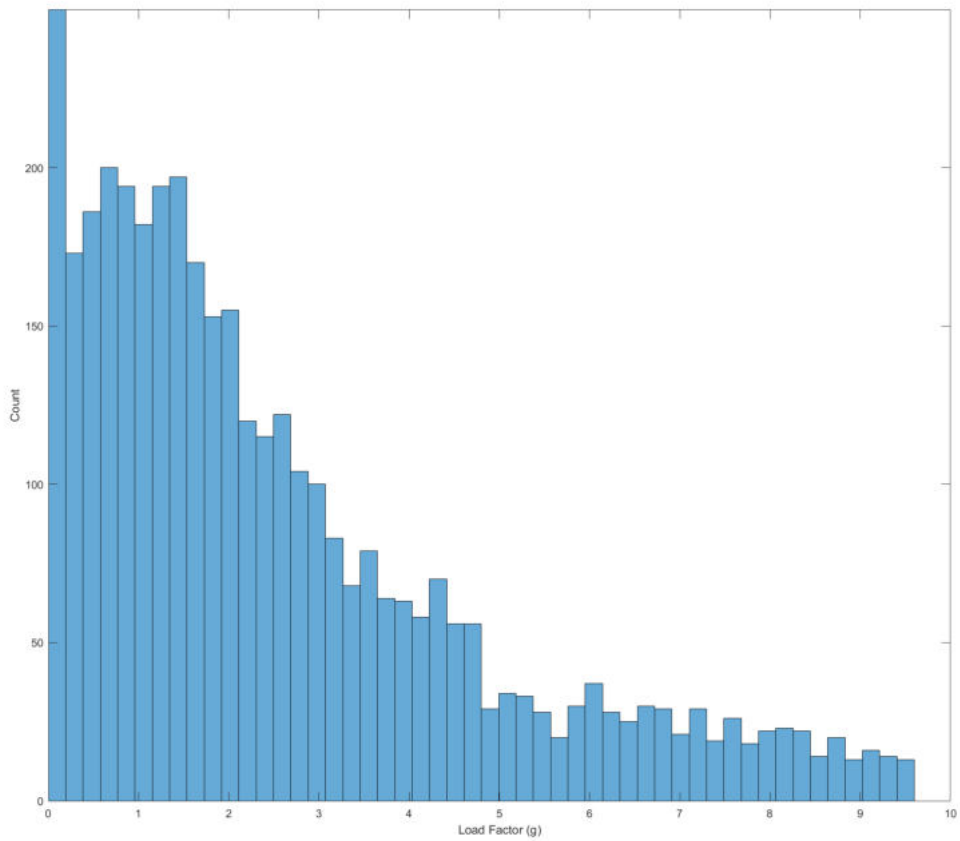

Fig. 4.20 Histogram of absolute acceleration as measured in terms of g. 81.5% of acceleration measurements are < 4.4g, the limit load for utility category certification.

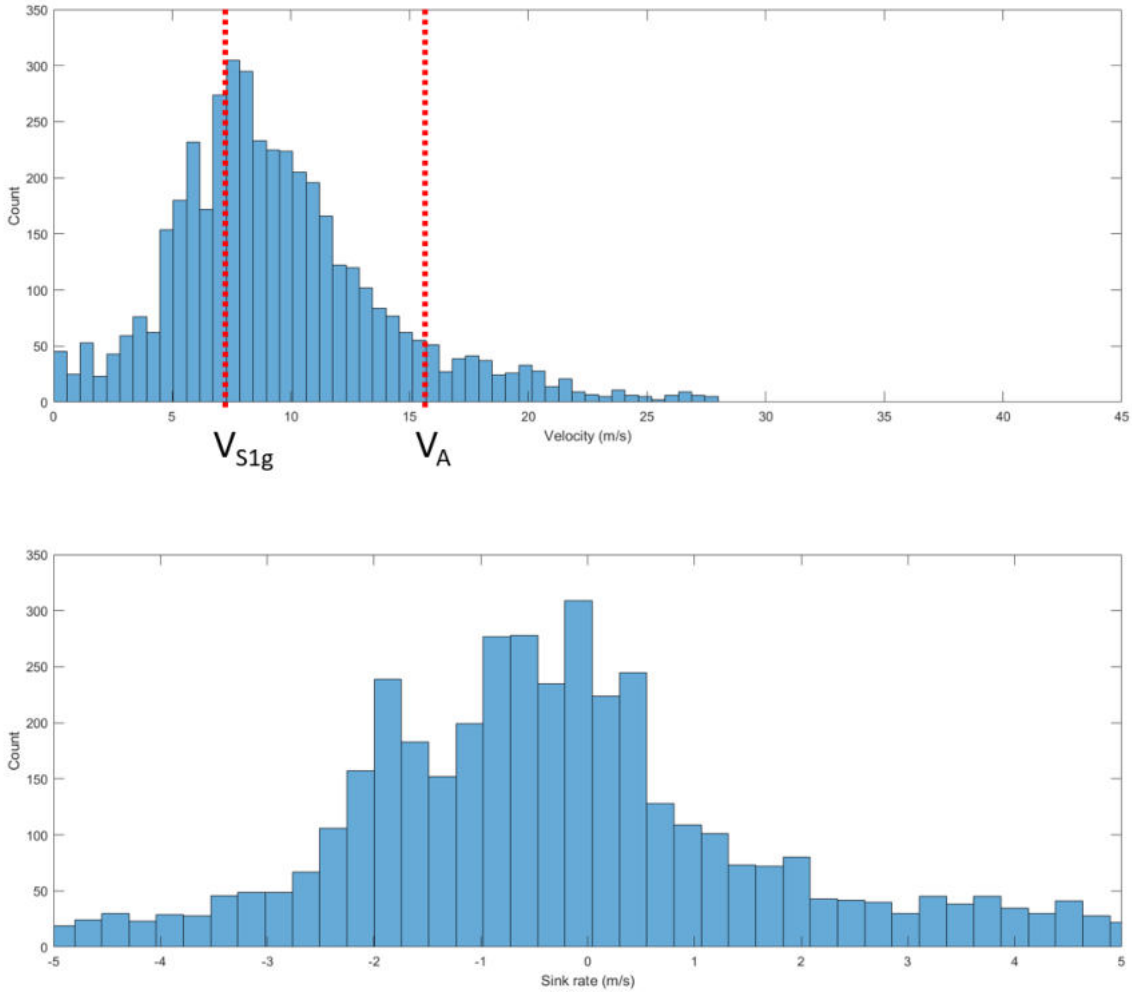

Fig. 4.21 Histogram of instantaneous velocity measurements.

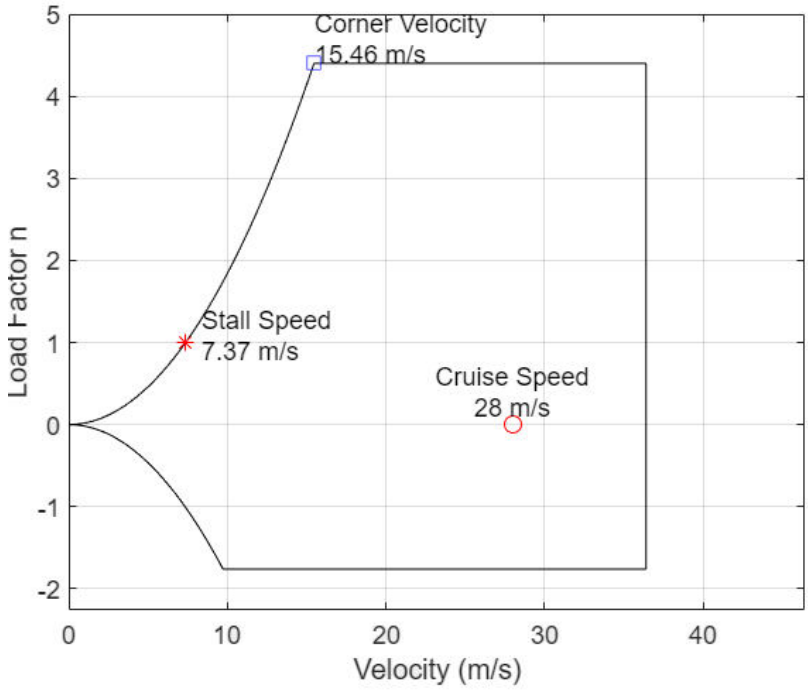

Fig. 4.22 Equivalent V-n diagram for *Larus Fuscus* as built using EASA CS23.335.

Figure 4.22 is a Velocity - Load factor design diagram (V-n) typical of a UAV of comparable mass and plan-form to the gulls. When comparing the histogram of the velocity measurements from all the gull flight datasets (Figure 4.21) to the V-n diagram it can be seen that 89% of flights are taking place at velocity less than the assumed maximum manoeuvring speed as calculated using EASA CS-23 [98]. Furthermore velocity values below the equivalent 1g stall speed are consistently measured. This is caused in part by the addition of relative wind to the dataset, which will reduce measured flight velocities below the calculated stall speed but also because of the birds ability to flap. By redirecting thrust to counteract the weight the amount of forward velocity needed to support the birds weight through aerodynamic lift is reduced. Expanding of the flight envelope, particularly at low flight speeds and high load factors highlights the importance of flapping and of variable wing geometry to the birds.

The maximum recorded velocity of 28 m/s falls within the established flight envelope and is approaching the calculated value of maximum manoeuvring speed so a fixed wing platform modelled on the characteristics of the lesser black-backed gulls, whilst the minimum velocity of 0 m/s and all values of velocity that fall below the calculated fixed wing stall speed for the gulls (V_S = 7.3 m/s) are likely due to the effects of flapping and of the tail spread. Flapping directs a component of thrust in opposition to the weigh the weight of the bird, while flapping flight cannot be considered as steady, the downwash induced by the combination of aerodynamic lift on the surface and the direction of the thrust mean that the traditional calculation of stall speed has no bearing on flapping flight and as such when flapping it is expected that the bird could fly substantially below the traditional stall speed. Tail spread is seen in almost all low speed flights, this modifies the downwash from the main wing and will contribute it's own aerodynamic force. It is likely increasing the total lifting surface area of the gull and it has been found to act as a high lift device [57] further increasing the value of C_{Lmax} as used in the fixed wing model. The modal value of flight velocity is 7.5 m/s and sits between the velocity for minimum sink (V_{ms}) and the velocity for best glide ($V_{L/D}$) although the error on the polar fit is such that it could be either of these values. Given that the flights were deliberately recorded on calm wind days to minimise the influence of the wind on the measurements it is difficult to infer what effect increased headwind or tail wind would have on the gulls propensity to fly at different speeds in accordance with established soaring theory [99]. The high load factors recorded in the flight path might be attributed to instances of flapping flight. Flapping induces momentary and substantial out of plane forces which will cause high levels of acceleration and jerk acting on flight path. These effects are not accounted for in traditional fixed wing design where load factors are typically considered as a long period, low frequency effect which must be sustained rather than as momentary transients as seen in this dataset. The behaviour captured is clearly not representative of the peak performance of the animal but instead of loitering and soaring as might be expected due to the location of data capture in the Bristol Harbourside and that the measured velocities and accelerations fall largely within the flight envelope as established for a fixed wing utility category vehicle based on the mass and geometric properties of the gulls suggests that using fixed-wing flight mechanics for modelling this part of the gulls flight regime is a reasonable proposition.

4.6.2 Forward motion of the wings and control of flight path angle in gliding flight

Unlike man-made air vehicles birds do not have discrete control surfaces, relying instead on the morphing of their main lifting surfaces to change the distribution of forces about their bodies and induce moments to control their flight path. Autopilot systems will typically used closed loop feedback control with inner (flight control) and outer (flight guidance / management) loops to control the flight dynamics and guidance of the vehicle. When analysing inner loop control systems it is common to think of them as decoupled systems with primary and secondary effects. For example, controlling longitudinal motion about the lateral axis in steady flight could be thought of either as a demand for a given pitch angle or a specific angle of attack. In some manoeuvres it may be more desirable to target a specific pitch rate or constant load factor. In practice it is usually some combination of these parameters depending on the phase of flight and desired manoeuvre or autopilot state. The controller will then modulate the control surface to achieve this. With discrete control surfaces this provides a simple feedback arrangement where the position of the surface can be measured and fed-back as part of the control response.

Here positive ζ represents a sweep back of the wing-line and aft movement of the centre of pressure of the wing (Figure 4.23).

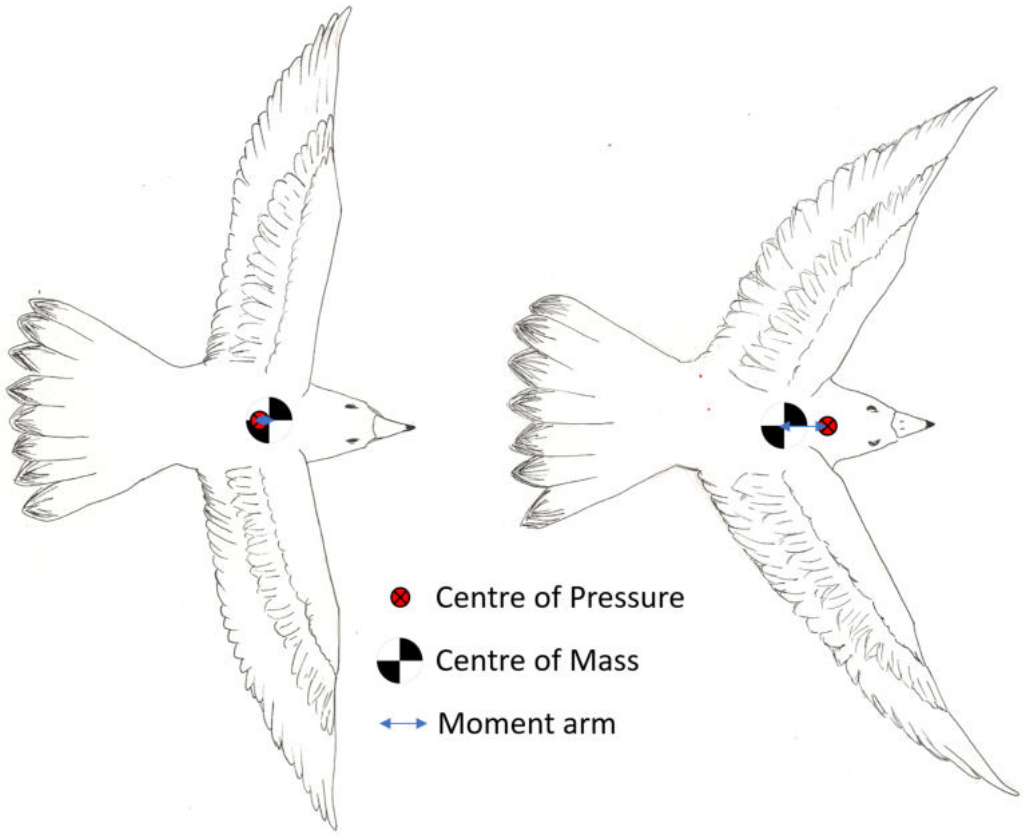

Fig. 4.23 Change in centre of pressure with wing sweep. As the wing sweeps forward the centre of pressure moves ahead of the centre of mass.

Figure (4.23) shows a forward (negative) sweep angle. This arrangement of net aft sweep and slight positive dihedral is as would be found on stable designs of small unmanned air vehicles SUAVs with similar characteristics. This forward movement of the centre of pressure increases the couple about the centre of gravity and increases the pitch up moment of the bird. It is understandable then that there is a correlation between values of wing-line sweep and flightpath angles. The same affect is seen when sweeping the wing aft, where a positive, rearward sweep, reduces the couple and induces a nose down pitching moment. As a result we should expect to see this variable coupled in some way to the pitching effect, or in the case of the bird where the wing and body do not have a fixed setting angle, a change to the longitudinal flight path angle. However from the free-body diagram it is clear that the change in the

geometry affects the pitching moment which in turn will affect the pitch rate of the bird. Such a result is interesting as it is in direct opposition to the way the majority of conventionally arranged aircraft achieve the same result.

Conventional aircraft with a main wing and empennage arrangement control their longitudinal dynamics using discrete flight control surfaces affixed to the trailing edge of the horizontal stabiliser or by total actuation of the stabiliser as part of an all-flying tail [100]. This arrangement provides a long moment arm for the control surface and thus reducing the size and weight of the control surface and minimising the control loads experienced by the pilot or actuator. Whilst secondary flight control surfaces on the main wing: flaps, slats and spoilers do directly effect the pitching moment of the wing and thus the longitudinal dynamics, these effects are typically small in relation to the size of the control surface and are considered a secondary effect and not the main reason for actuation of these surfaces. The upside to the gull's use of the main wing for longitudinal control is that it provides enormous control power from such a larger surface and it frees the tail from the requirement of control. Gulls already have large muscle groups powering the wing and by using these for control it would alleviate the need to have additional powerful muscle groups at their tail [101]. Additionally the skeletal structure of the bird supports a large range of motion in the main wings, being adapted forelimbs, far more than is possible with the tail. This likely improves the sensitivity of the controller to small changes in flight path whereas the tail serves more as a gross trim control being in a furled state, producing relatively little lift and hence pitch-down moment, or unfurled, acting as a high-lift device, reducing total wing loading and providing a pitch down moment.

Gliding is a selective flying gait whose purpose is to minimise energetic cost by being aerodynamically efficient. By gliding with a furled tail (unused for flight control) the gulls can reduce their static margin, minimise induced drag and glide further for a given loss of height. This seems a likely scenario given that the tail is typically observed to be furled when in a steady glide.

4.6.3 Variable dihedral and changes in vertical speed and stability

The morphing main wing allows for large changes in geometry, span, chord, aspect ratio, camber and wetted area whilst largely maintaining the thickness of the wing. These changes in the wing effect the total lift and drag produced and will effect the control and stability of the bird. The hypothesis here is that this might perform two functions. Firstly that by increasing the angle of the main wing (either in dihedral or anhedral) the bird quickly redirects the aerodynamic force vector to counteract a vertical gust. In doing so it offsets any increase / decrease in lift and maintains it's flight path with minimal perturbation. Secondly, by varying the wings elevation angle the bird can vary the lateral - direction stabilising dihedral effect (Figure 4.24). This effect tends to roll the bird out of a slipping condition, restoring coordinated flight. Changes to lateral stability with regards to the change in the wing-line sweep and rise are not easy to assess with the information available from the RSV device and so are examined analytically in Chapter six. It has been hypothesised that birds use the rotation and inertia properties of their wings to offset gust response [102]. The rotation of the shoulder absorbs the changes in lift distribution in response to a gust. The exact mechanics of the response depends on the location of the centre of mass and the centre of pressure relative to the wing root, in essence the centre of pressure must lie in the wings "sweet spot", also known as the centre of percussion. In this case the expected result in Figure 4.16 would be a variation in wing-line rise with little variation in either vertical velocity or changes to the flight path. The results here supports this hypothesis but the conditions under which the data was collected was not ideal or necessarily representative of the conditions required to properly test this hypothesis in the lesser black-back gulls.

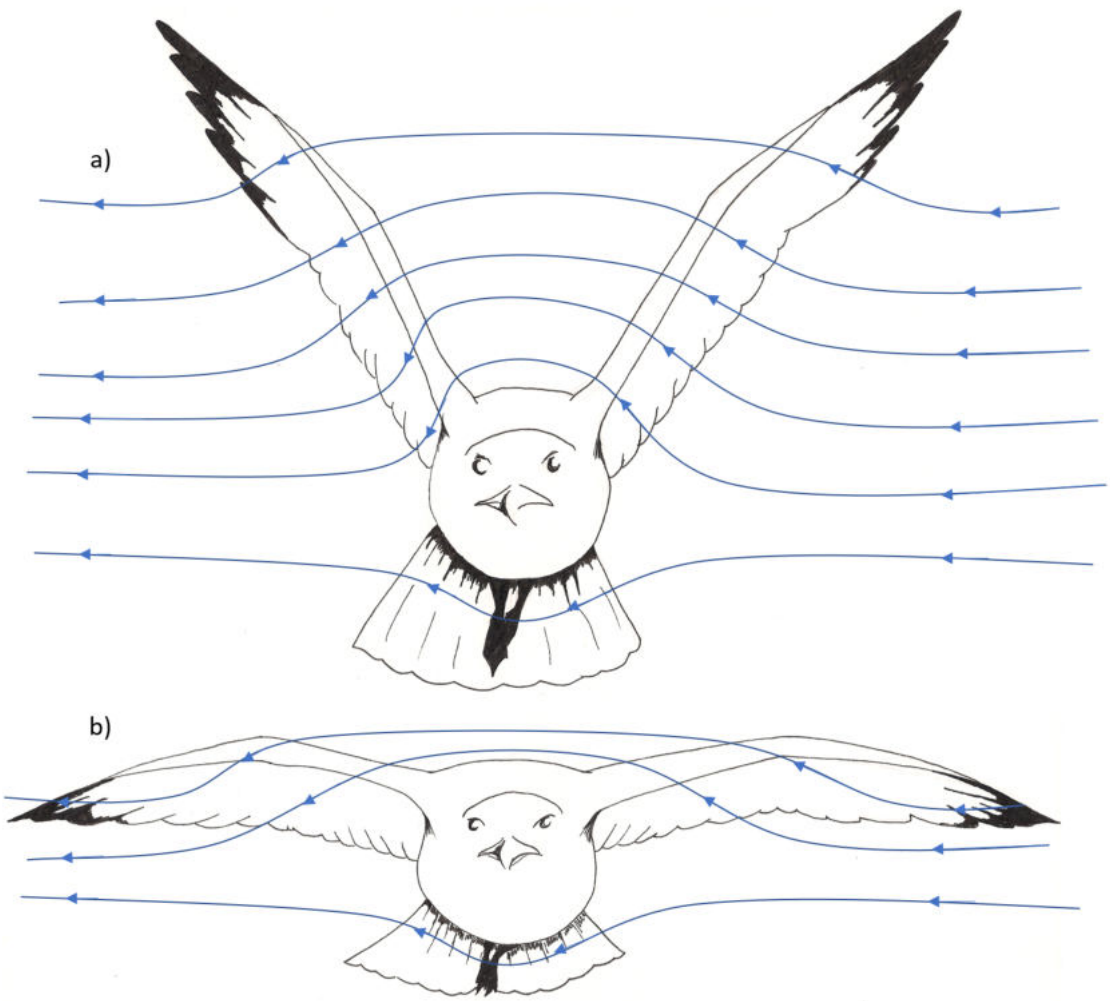

Fig. 4.24 Change in dihedral effect with wing rise. As the wing rise angle increases the stabilising dihedral effect increases.

Increasing dihedral angle (Figure 4.24 - a)) increases the lateral-directional stability of the bird in the presence of a side-slip. The into slip wing sees a local increase in effective angle of attack whilst the trailing wing sees a reduction in local angle of attack. This span-wise lift imbalance creates a rolling moment which will tend to oppose the motion of the side-slip thus reducing it. A similar effect is established in the presence of a high-wing configuration (Figure 4.24 - b)). Here the up-wash over the into slip wing is due to the presence and interference of the body below the wing line, the span-wise lift asymmetry causes an into slip stabilising rolling moment in the same way a wing with positive dihedral does. Birds, with their articulated shoulders have a wide range of possible dihedral angles and thus may modulate their static lateral-directional stability when gliding.

4.6.4 Turning mechanics

Using the kinematic analysis described earlier in the chapter it is possible to determine the turning mechanics of the lesser black-backed gulls. Previous works examining different species of birds have found that the bank angle (ϕ) is the primary control variable when describing turning performance [103], this result is also seen in other flying animals such as dragonflies [104] which also make use of bank angle for high speed turns whilst retaining the yaw turn (analogous to a rotorcraft's pedal turn) for slow speed manoeuvring. Throughout fixed wing flight mechanics, equations of motion relating to turning use the bank angle as the fundamental control to initiate and maintain a steady turn. The bank angle (ϕ) is poorly defined for non-rigid and non-fixed wing aircraft and in this case birds. In a fixed wing aircraft the bank angle is defined at the angle included between the lateral axis and the horizon. Rolling is initiated through a span-wise imbalance of lift generated through asymmetric deflection of aileron surfaces. This definition is pertinent as the body is assumed to be rigid, and the wings to be fixed such that the relationship between any two points on the geometry remains constant at all times. However these assumptions do not hold true for a bird or any aircraft where the wings are neither fixed, or the body is substantially non-rigid. In this case the relationship of the lift vector is independent of a coordinate system affixed to the birds body or head, indeed many species of bird actively stabilise these to remain horizon-locked for sensory purposes [105]. Instead the parameter of interest is the angle between the resultant lift vector and the world-fixed normal axis. Birds and flex-wing aircraft still initiate a roll through a rotational moment, however this moment could either be induced through a span-wise imbalance of lift, for example by twisting the wing surface or by offsetting the centre of pressure and resultant lift force against the centre of gravity by shifting weight to generate a rolling moment. Estimating this resultant lift vector is done by assuming it is the cross product of the body line and the perpendicular vector joining the port wing-tip to the starboard wing-tip. Both the wing-tips are resolved by the RSV system and so the bank angle (ϕ) discussed here is not the roll angle as is used in the fixed-wing derivations, but instead the included angle between the resultant lift force, assumed to be perpendicular to the average wing-line between the wing-tips, and the world normal axis.

According to fixed wing flight mechanics (Equation 4.4), the rate of turn using small angles approximation should be proportional to the bank angle. This correlation in Figure 4.17 agrees with the expected proportionality and suggests that it is appropriate and possible in this case, to model the turning mechanics of the gull using the flight mechanics equations for fixed wing aircraft using rigid body assumptions. Furthermore by finding the expected relationship it suggests the assumption of calculating the bank angle using the average lift vector between the two wing-tips is a good method to use where the relationship between the wing and lateral axis is not rigidly defined. However if this was a perfect definition then you would also expect to see a strong correlation between the lateral load factor and the bank angle in figure 4.18. This is not the case and it shows a poor correlation ($R^2 = 0.22$). However this is not due to the assumed direction of action of the lift vector, it is instead to do with the definition of the plane in which the turn takes place. The equations of motion assume a steady turn constrained to the horizon plane but in this data set the gulls turns may be climbing and descending. The projection of the flight path onto the horizon plane distorts the path and the radius of curvature.

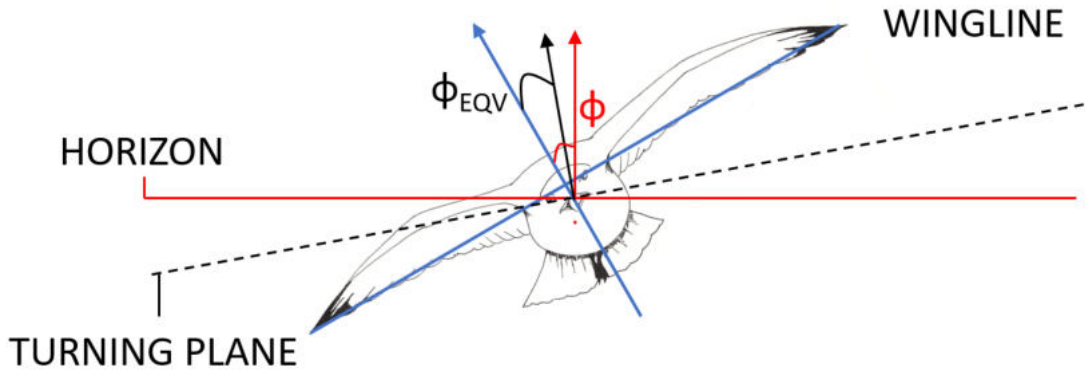

Fig. 4.25 Definition of bank angle (ϕ) and Equivalent bank angle (ϕ_{EQV}) for a gull whose wing is not rigidly defined in relation to it's body lateral axis.

Adjusting the definition of the bank angle from the included angle that exists between the resultant lift vector and the world normal axis, to instead define an equivalent bank angle ϕ_{EQV} defined by the angle included by the resultant lift vector and the axis perpendicular to the average centripetal acceleration experienced in the turn (Figure 4.25), the equivalent bank angle accounts for the out of plane rotation of the world normal axis due to the inclination of the plane of turn due to any climbing or descending in the turn. Plotting the new equivalent bank angle against the centripetal acceleration (Figure 4.19) reveals the expected strong correlation between the two variables.

For gliding turns the manoeuvres performed by the gulls are based on the roll angle as estimated by the average wing-line. This geometric stand-in for a properly defined lateral body axis serves to allow the implementation of fixed-wing mechanics when describing the performance of a non-rigid body aerial system, be it a bird or an aerial vehicle equipped with a morphing wing. By defining this equivalent roll angle in relation to an offset axis, normal to the plane of the turn, it is possible to apply equations derived for steady level turns to climbing and descending turns, providing the velocity stays substantially constant or the calculation is iterated at an appropriate rate.

4.7 Conclusions

In this chapter, multi-point flight path tracking using Rotational Stereo Videography (RSV) is used to assess the kinematics and flight mechanics of the lesser black-backed gull (*Larus fuscus*) and this chapter demonstrates marked relationships between the bi-variate description of the wing morphology and the control of the birds flight path using measurements taken from free-flying wild animals in an uncontrolled natural environment with minimal impact on the behaviour of the animal. Using a wireframe model fit four individually tracked points it is possible to construct a bi-variate model describing the morphing wing of the gull in flight in terms of the wing-line sweep and wing-line rise. A portion of the gulls glide polar is presented and the manoeuvres measured are mapped to an equivalent fixed-wing aircraft flight envelope, of the manoeuvres captured, all the the velocities measured were below the equivalent fixed-wing manoeuvring airspeed and >80% of the acceleration data was less than the +4.4g limit, no negative g-loads were recorded. The range of motion of the gulls wings as a function of the bi-variate wing-line model was bounded at $\pm 60°$ for wing-line sweep and $\pm 30°$ for wing-line rise The gulls used fore-aft movement of the wing-tips, as represented by changes in the wing-line sweep to control their rate of change of flight path angle (equivalent to pitch rate) during straight glides. No correlation was found between wing-line dihedral and control of vertical flight dynamics but it is noted that this would be the case in the event that the bird is using this degree of freedom to absorb perturbations, no definite conclusions could be made in this case. Gliding turns are roll-based, as defined by the equivalent measure of roll as the angle between the average wing-line and the horizon. By using equivalent variables it is possible to apply flight mechanics equations derived for fixed-wing rigid body aircraft to describe the flight mechanics of a non-rigid body in gliding flight.

In some specific instances the gulls flight is well modelled by fixed-wing equations of motion and the flight of the bird could be considered to be similar to a fixed wing vehicle. These instances are when the bird is strictly not flapping. In straight gliding flight the birds longitudinal trajectory is in part effected by the sweep angle of the main wing. This is very different from elevator based control on traditional aircraft and more similar to the sorts of control schemes seen on rotary wing vehicles. However when turning, whilst the method of initiating the roll is different, the turn performance is well modelled by traditional methods as the redirection of the lift vector is common

between both birds and fixed wing aircraft. The ability to flap expands the flight envelope beyond what is possible with traditional fixed wing, particularly in the low speed regime where flapping helps mitigate against high angles of attack on a rigid wing allow the birds to fly well below what would be considered a traditional stall speed.

Chapter 5

Bird-inspired control schemes using the main wing for flight control

5.1 Chapter Summary

Birds and aircraft have very different configurations and control schemes. Different species of birds adopt different flying gaits and depending on their environment have different approaches to flight. The gulls reviewed in Chapter 3 are robust and flexible and use a variety of flying styles but can be predominantly seen to be using a flap-glide and a gliding / soaring gait. They have a main wing and tail which may be furled or spread depending on the phase of flight. In gliding flight the tail is typically furled and the main wing is used for flight control. In this chapter a series of control schemes were developed using only the main wing for flight control. The control schemes are based on actuating the main wing about the three principle axis, where the wing is assumed to have a perfect 3D ball joint at the wing root - fuselage conjunction. The main wing can be swept about the normal axis, twisted about the lateral axis and flapped about the longitudinal axis. The control schemes were assessed in simulation using a 3D vortex panel method, with conditions which match wind tunnel experimentation and uses simplified models of physical base airframes upon which the modified wing is tested. Three seperate mechanisms were designed and manufactured and sit upon two base airframes, a Bix3 and WOT4. Wind tunnel testing of the vehicles is used to validate the analytical models. All experimental models were capable of free flight. An articulating wing opens up a new set of control strategies which extend flight control beyond traditional three axis control using discreet flap control surfaces and allow for novel manoeuvres which would not be possible otherwise. The primary findings were that sweeping the main wing is a powerful tool for altering the aircraft's flightpath on the longitudinal plane, whilst having an effect on the aircraft's longitudinal stability and that varying the dihedral of the main wing allowed for an adjustment to the lateral-directional stability in flight, particularly effecting the spiral mode.

5.2 Chapter Structure

This chapter introduces an articulating main wing as a means of controlling flight. The main wing is hinged at the wing root and can be articulated about three principle axis. The articulating wing is a function of the morphology of the modified forearms that birds use for flight. An articulated wing control scheme is comparable to rotary wing flight control which also use discreet or flexible hinges at the wing root. This chapter introduces the articulated wing control schemes and the two experimental airframes upon which the modified wing is built. Reference data for unmodified airframes are established for the Bix3 and WOT4. The three modified wings are configured for wing sweep, wing twist and variable wing dihedral. Results are presented for the control schemes from analytical modelling and validated using experimental wind tunnel data. Three novel control schemes are presented: wing sweep for pitch control, wing twist for roll control and direct lift control and variable dihedral for variable stability.

5.3 Introduction

This chapter builds upon the control laws identified in Chapter 3 and examines the control effectiveness of manipulating the main wing. From the analysis of the flight paths of the lesser black backed gull *Larus fuscus* it has been determined that the gull uses fore-aft movement of the average wing line to effect control of its flight path angle and to climb and descend. It has also been shown that like rigid body aircraft the gulls use roll, as measured from the average wing-line to generate the forces necessary to initiate and maintain a turn. Whilst it was not possible to quantify exactly how the roll was initiated in terms of control surfaces from the flight path tracks, qualitatively it can be said that such turning behaviour occurs whether the tail is in a furled or unfurled state and thus the main wing is being used in some way to generate the rolling moments. Similarly birds lack the traditional vertical stabiliser seen in almost all human piloted aircraft (with no artificial stability assistance) and so some level of lateral directional stability and control is being achieved through the actuation of the main wing.

This Chapter looks at how an articulated main wing, with three degrees of freedom, hinged at the wing root, can be incorporated into the traditional three-axis control scheme and what benefits and drawbacks such a system has for small unmanned aerial vehicles. The articulated wing is an example of rotational wing morphing as introduced in Chapter 2. By articulating the wing at the root it is possible to actuate the wing through three rotational degrees of freedom, modifying the wings' sweep, twist and dihedral. The effect of modifying these three parameters and how it relates to the control of the flight is to be examined and related to the concept of flight control using a morphing wing using the average wing line two variable reduced order model as discussed in Chapter 3.

Three different hinge designs are presented that are incorporated into Bix3 and WOT4 airframes that are capable of free flight.

5.4 Methods

By articulating the main wing, the centre of pressure and thus the position of the resultant lift and drag vectors can be moved relative to the airframe and importantly in relation to the centre of mass of the vehicle about which the aircraft will rotate in free-flight. It is worth noting that by moving a large structure like the main wing the centre of mass of the vehicle will also move to follow the wing. This is due to the translation of the wings centre of mass in accordance with the rotation seen at the wing root. The effect of this motion of the centre of mass and thus the centre of rotation in the same direction as that of the lifting surface will act in opposition to the desired change in moment arm between the centre of pressure and the centre of mass. This effect will be most pronounced where the mass distribution of the aircraft is such that a high proportion of the mass is located in the wings and furthermore where this mass is concentrated towards the wing-tips at the most distal point from the point of articulation at the wing root. Such a configuration is not uncommon in larger scale aircraft which rely on large quantities of liquid fuels stored in wing tanks, where it is desirable to store fuel in outboard wing tanks to assist with load alleviation at the wing root in the form of wing bending relief. These vehicles would not be considered appropriate for wing root articulation due to the comparatively high loads at the wing root when considering that material properties do not scale linearly with increasing vehicle mass.

This wing root articulation is inspired by flying insects and birds, creatures whose mass is typically concentrated in their bodies with the wings being a small fraction of total body mass. It is therefore acceptable to apply this technique to any air vehicle whose mass distribution fits this model whereby the mass is concentrated in the fuselage with relatively light wing structures. This configuration is similar to those seen in small UAVs utilising electrical power for propulsion. These utilise batteries located in the fuselage for energy storage, and have relatively light wing structures. Because the material properties at low mass scales means that wing root load relief and wing bending alleviation is not required, mass is not placed outboard in the wing tips at the distal point that would have maximum effect on the change in centre of mass.

The effect of wing root articulation on airframe control is decomposed into rotation about a three hinge axis centred on a joint at the wing root, fuselage junction. Here the wing can be articulated fore and aft, rotating about a normal axis, parallel to the body normal axis and located at the wing root - fuselage junction and positioned at 50% chord. The wing can be 'flapped' up and down, rotating about a longitudinal axis, parallel to the body longitudinal axis and located at the wing root - fuselage junction and positioned at 50% thickness. Rotation of the wing about the lateral axis, as defined to be perpendicular to the plane defined by the prior two axis, varies the angle of incidence of the wing in relation to the fuselage, this twisting of the wing occurs about the axis positioned at 50% thickness and 50% chord.

5.4.1 Wing root articulation

The wing root articulation is based on the concept of an unrestricted ball and socket joint located at the wing root and fuselage junction. Such a joint would not be suitable for a production vehicle incorporating all three degrees of rotation but serves to standardise the origin and orientation of the axis as defined above.

Wing sweep for pitch control

Rotation about the wing root normal axis varies the effective sweep of the wing and alters angle at which the incoming flow meets the leading edge, the effective aerofoil cross section as viewed from the body lateral axis and marks a reduction in the span as measured wing-tip to wing-tip. Rotation about this axis will shift the centre of pressure of the wing fore and aft, as well as moving the centre of mass of the vehicle fore and aft (Figure 5.1). In this model the wing is sheared instead of rotated which will have implications regarding the effective washout and aerofoil sections however it is expected that this will have limited effect on the trends of the results.

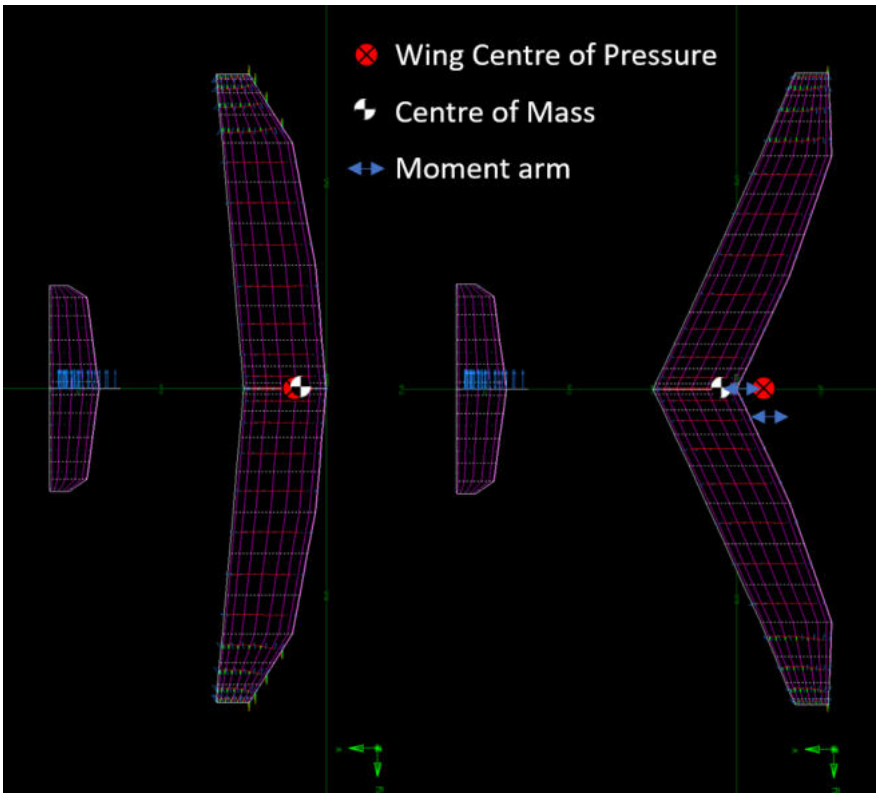

Fig. 5.1 Movement of the centre of pressure with wing sweep

This change in the moment arm between the centre of pressure and the centre of mass along the longitudinal axis will change the control derivatives and the specifically the pitching moment imparted to the vehicle and also effect the conditions of stability due to the movement of the neutral point and the change in stability derivatives which are a function of the mass distribution and the aerodynamic derivatives.

Wing twist for roll control and direct lift control

Dynamically changing the angle of incidence of the wing in relation to the fuselage (wing setting angle) by rotating the wing about the lateral axis allows for a rapid variation in the angle of attack of the main wing. This twisting of the wing allows for an angle of attack change and can be performed asymmetrically to generate a rolling moment about the fuselage due to the asymmetry of lift production between the two wings, or the angle of attack change may be performed symmetrically to adjust the setting angle of the wing in-flight (Figure 5.2).

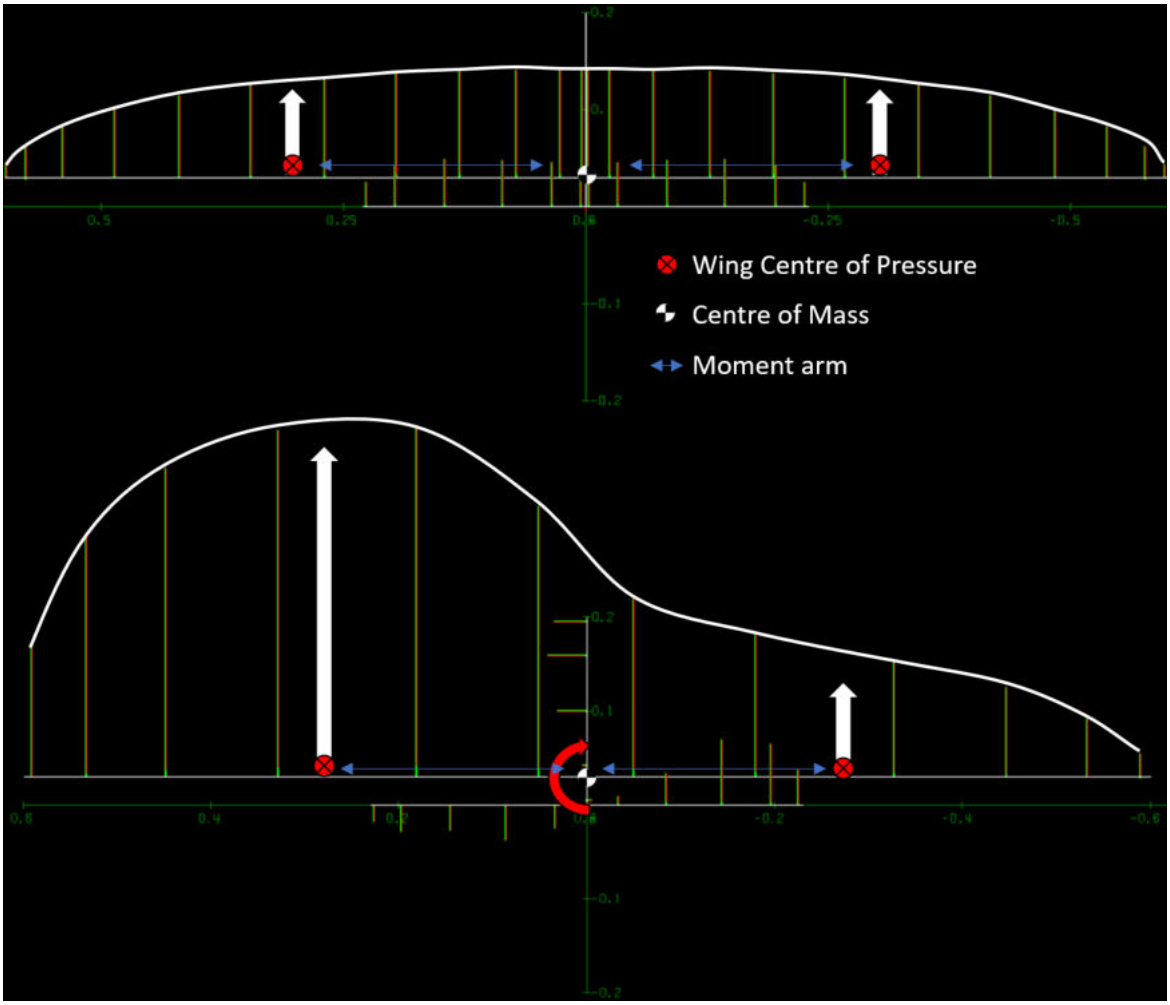

Fig. 5.2 Rotation of the wings to affect the span-wise lift distribution

The asymmetric actuation of the wings may be thought of as the extreme case of an aileron surface whereby the whole wing deflects to generate a lift asymmetry along the wingspan. Symmetric actuation allows for the adjustment of the angle between the wing and the fuselage in flight. Such an adjustment will have a transient dynamic effect and an effect on the pitch trim condition of the wing. The initial dynamic response will depend on the speed of actuation due to the inertia of the aircraft maintaining the effective relative wind at high actuation speeds, driving the wing to a higher or lower angle of attack will directly affect lift production allowing for direct control over the vertical translation or heave, with a coupled pitch response due to the effect of the pitching moment with respect to angle of attack, $C_{m\alpha}$. Additionally the static trim condition of the aircraft will change allowing for the nose to be effectively pointed in pitch, independently of the main wing and the vehicle response in pitch. Such a condition may prove useful for sensor pointing in critical flight phases.

Variable dihedral for variable stability

Flapping the wing, that is rotating the wing about the longitudinal axis symmetrically varies the dihedral or anhedral of the main wing. Asymmetric actuation establishes rotation of the total resultant lift vector about the longitudinal axis and an offset from any other secondary lifting surface (i.e. for a conventional aircraft the horizontal stabiliser) (5.3).

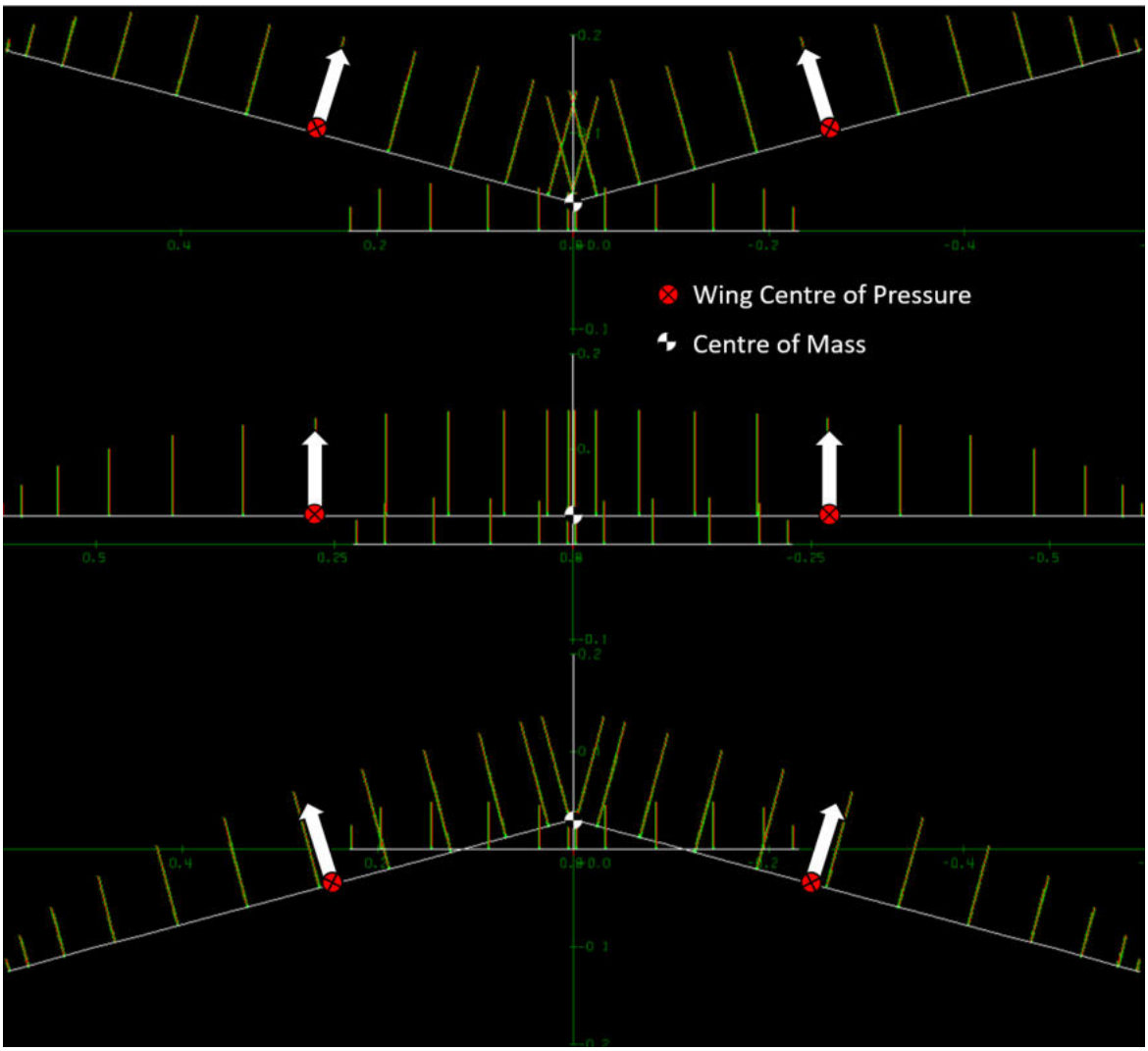

Fig. 5.3 Flapping of the wings to move the lift vector

Dihedral or anhedral governs the lateral stability of the aircraft and is a key parameter to meet handling requirements in roll. The spiral and Dutch roll modes are governed by the relative levels of lateral and directional stability. By varying the dihedral / anhedral of the main wing it is possible to vary the levels of stability and excite different dynamic responses. Asymmetric actuation introduces an unbalanced sidewards component of force which will initiate a yawing moment and resulting side-slip, along with a coupled roll response depending on the airframe configuration. The magnitude of this effect will be small in comparison to directly inducing a roll moment due to an imbalance of lift forces but may be useful for fine-scale control.

The modelling here has the wing root and centre of gravity being coincident and the wing rotates around this point. This is not the case in the birds as measured nor in the physical model wherein the wing root is offset from the fuselage. This offset means that the moment arm between the wing's effective centre of pressure and the centre of gravity is not constant, and varying the dihedral will change both the magnitude and moment of the resultant pressure force. This will further effect the rolling moment induced about the centre body but for the purposes of this symmetric analysis the effect is of no concern. When deflected symmetrically for the purposes of altering lateral stability the effect on the moment arms is equal and opposite and so cancels out as to not induce a rolling moment.

5.4.2 Control schemes

Utilising a wing root articulation, the motion of the main wing relative to the fuselage and the centre of mass can be adjusted to effect the control of the flight path and the stability properties of the aircraft. Many vehicles have explored the concept of wing morphing to control flight [106]. These three degrees of rotational freedom are examined independently to one another and examined where the wings motion is controlled both symmetrically and asymmetrically. When selecting appropriate control schemes attention is given to both control of the flight path about a major axis and also the effect that articulation in a given plane will have over the stability of the vehicle. The following control schemes are examined to assess the capability of wing root articulation as an addition or alternative to traditional three axis control utilising aileron, elevator and rudder control surfaces.

Wing-sweep for pitch control:
By exploiting the change in moment arm created by the translation of the centre of pressure along the longitudinal axis when the wing is symmetrically swept, and assuming in this case a quasi-stationary centre of mass due to the relatively low mass fraction of the wing surfaces, this control scheme examines the pitching moment due to wing sweep $C_{m\delta}$ and the effect sweeping the wing has on the C_L and C_D. Whilst this isn't explicitly inspired by the work of chapter 4, due to the fact that the birds pitch attitude was seen to be held somewhat constant, it is a development of the idea for a vehicle with a wing root articulation in only one degree of freedom to sweep.

Wing-sweep for variable stability:
The fore and aft movement of the centre of pressure changes the position of the neutral point and the moment arm between the main wing and centre of mass. Both static and dynamic pitch stability are effected by changes in these parameters as is the spiral stability of the platform. Being able to adjust the longitudinal stability of an aircraft in flight can be highly desirable as different flight phases and manoeuvre profiles have different requirements. Traditionally conventional aircraft have used mass transfer in the form of fuel trim tanks to adjust the longitudinal stability of the aircraft in-flight, something that would require a very different setup with solid-state energy sources for electrical power trains.

Wing twist for roll control:
Twisting the wing about the wing root, or more specifically varying the local angle of attack along the span with a constant interval in an independent and asymmetric sense will induce a rolling moment on the airframe $C_{m\delta}$. This effect is consistent with the application of an aileron control surface except in this case the whole wing serves as the control surface. As such actuation angles are correspondingly less than an equivalent aileron control surface would require for the same magnitude of rolling moment. Because the whole wing is being actuated and not just a discrete trailing edge surface, consideration of the $C_{L\alpha}$ curve is required to avoid pushing the wing into a region of separated flow (stalling the wing) wherein control reversal may occur. This situation may be expected in flight regimes with initial high angles of attack.

Wing twist for direct lift control and trim change:
Symmetric rotation of the main wing allows for dynamic adjustment of the wing setting angle and rapid transient changes in angle of attack. This allows for direct lift control, something which a conventional aircraft cannot really achieve although some approximation can be made through the actuation of slow moving large flap surfaces and the use of upper surface spoilers or air brakes, all of which directly effect many aerodynamic parameters simultaneously and do more than just drive the wing up and down the $C_{L\alpha}$ curve directly. Direct lift control allows for transient control in heave, responding to changes in relative wind to maintain a consistent loading on the wing would allow for smoother flight in areas of turbulence. Long period actuation of symmetric wing twist will adjust the pitch trim characteristic of the aircraft. This will allow for fixed sensor pointing independent of the wing angle of attack. It will also allow for other relative positions of fixed geometry to be adjusted for different phases of flight, for example tail-strike protection on take-off or landing.

Wing dihedral for roll control:
Independent actuation of the wing rotating about the longitudinal axis, the flap hinge, creates a small rolling moment about the body longitudinal axis until the aircraft finds equilibrium again with the other lifting surfaces. This motion additionally generates a yawing moment due to the sidewards component of lift, produced either at the main wing, or at the horizontal stabiliser depending on the state of equilibrium. This side-load will cause a side-slip to occur, exciting the lateral directional dynamic modes. Properly tuned it may be possible to exploit this modal control behaviours [107] to initiate and maintain controlled turns and side-slips. Such independent behaviour of the wing may also help to actively account for the apparent directional stability in birds that exhibit stable flight whilst lacking a vertical stabilising tail surface as seen on all conventional aircraft.

Wing dihedral for variable spiral stability:
Further developing the idea of modal control through explicit excitation of specific lateral directional modes it would be beneficial at times to adopt different configuration to change the stability of the aircraft. Aircraft with relatively high levels of directional stability as opposed to lateral stability tend to exhibit an unstable spiral mode. This is typically the case with straight wing aircraft with no stability augmentation systems. Spiral modes tend to have long periods and be non oscillatory making them easy to control by either a manned pilot or a simple controller. In contrast higher levels of lateral stability opposed to directional stability tend to exhibit an unstable Dutch roll mode. This is often the case with swept wing aircraft, or aircraft with high degrees of dihedral. An easily excited Dutch roll mode can make for flight with oscillatory and variable accelerations about all three axis. Typically the Dutch roll mode is eliminated using artificial stability systems as the phase lag between control input and response makes it difficult for a manned pilot or simple controller to account for it.

The six control schemes outlined in Table 5.1 form the basis of the testing and analysis in this chapter.

Table 5.1 Control schemes with an articulated 3 degree of freedom shoulder hinge. 3-Axis, 6-Axis and secondary effects

Freedom:	**3-Axis control**	**6-Axis control**	**Secondary effects**
Sweep (δ)	Pitch		Longitudinal stability
Twist (ω)	Roll	Roll	Direct lift control
		Heave	Gust rejection
		Surge	Trim condition
Flap (γ)	Roll	Sway	Lateral-directional stability
	Yaw		Turning flight

Three axis control in a traditional aircraft refers to the control of the aircraft in rotation about it's three principle axes: roll, pitch and yaw using discreet surfaces to generate moments about the vehicles centre of gravity. Six axis control refers to direct control over translation along the principle axes: heave, surge and sway. Heave is the relative motion along the aircraft normal vector, surge involves changes in the relative forward motion of the aircraft aligned with the free-stream and sway is the lateral component of motion. These control schemes differ from a more traditional three axis control scheme which incorporates ailerons, elevators and rudders for primary axis control and secondary flight control surfaces such as slats, flaps and spoilers for flight augmentation. Comparisons between the two schemes are interesting but it is important to note that wing root articulation and multi-jointed wing articulation can be complementary to existing control systems and can be used in conjunction with existing flight controls to extend the flight envelope beyond what is currently achievable.

5.4.3 Control scheme analysis

The theoretical wing root ball and socket joint is analysed as three separate rotational degrees of freedom with no interdependencies. The origin of the coordinate system is fixed at the wing root - fuselage junction at 50% thickness and 50% chord. The local longitudinal and normal axis are aligned with the vehicles body longitudinal and normal axis, with the lateral axis being perpendicular to the plane between the other two axis. Analytical aerodynamics tools XFOIL [108] and AVL [109] are used to model the effects of the individual degrees of freedom on a model airframes, the HobbyKing Bix3 [110] and Chris Foss WOT4 [111]. The simulations are used to examine the effect of control deflection and angle of attack on a variety of aerodynamic and stability derivatives. Wind tunnel testing is used to validate the results of the analytical anlysis tools and all the test airframes are configured to be capable of free flight. The purpose of the independent testing of the separate degrees of freedom is to demonstrate a notable increase in aerodynamic control power for a given airframe and to explore the potential for control in an additional axis and of the use of variable stability for modal control.

5.4.4 Airframes

Bix3

The HobbyKing Bix3 (Figure 5.4) is a high-wing, pusher prop, tailwheel design designed from the outset with an electric propulsion system. The wing is a high aspect ratio, tapered wing with polyhedral wing-tips. It is a popular entry level remote controlled hobby aircraft and has docile handling characteristics.

BIX3 Specifications	
Propeller	11 x 8'
Wingspan	1550mm
Chord	200mm
Length	948mm
Weight	890g
Aileron throw	± 30mm
Elevator throw	± 20mm
Rudder throw	± 30mm

Fig. 5.4 BIX3 Aircraft

WOT4

The Chriss Foss WOT4 (Figure 5.5) is a high-wing, puller prop, tailwheel design with a large wing area and square section fuselage. The airframe was designed to be powered by a variety of power units and can be configured for either electric or gas motor power-plants. The wing is a low aspect ratio, constant chord design which utilises a thick section flat bottom aerofoil giving it very good high angle of attack characteristics. It is an intermediate level fully aerobatic remote controlled hobby aircraft with large powerful control surfaces and a wide flight envelope.

WOT4 Specifications	
Propeller	11 x 8"
Wingspan	1205mm
Chord	200mm
Length	1050mm
Weight	1100g
Aileron throw	± 9mm
Elevator throw	± 15mm
Rudder throw	± 45mm

Fig. 5.5 WOT4 Aircraft

The analytical and experimental models for assessing the sweep degree of freedom are based off of the Bix3 model. This model was selected for continuity with existing datasets within the University of Bristol Flight Laboratory. However the Bix3 model has several flaws. It's all foam moulded construction requires extensive internal modification to house the additional mechanical components necessary to facilitate the wing hinge, the fuselage is low volume and has a complex curve cross section making the model difficult to mount into a wind tunnel assembly. The high aspect ratio wing is of solid foam construction and has a one third length spar and is highly flexible without extensive modification.

Given the downsides of the Bix3 as described a different platform was selected for modelling and testing the twist and flap degrees of freedom. The WOT4 possessed a square section high volume fuselage which requires minimal modification for the installation of additional components. The wing is hollow planar, with a constant chord and far stiffer thanks in part to a full-span carbon fibre tubular main spar. The thicker wing cross section made mounting hardware more accessible and structurally sound. The WOT4s thick, flat bottom aerofoil possesses excellent high alpha characteristics and performs well in free flight. The aircraft's overall design is more rugged and is suitable for repeated free-flight testing.

Onboard flight control and data logging is performed by a Pixhawk flight controller running the PX4 open source autopilot. The system is modular and records data from a variety of sensor suites including two inertial measurement units (IMUs), magnetometers, pitot sensors, barometers and global positioning system (GPS) receivers. These sensors encode aircraft attitude information at 25Hz, inertial acceleration information at 50Hz and pressure based airspeed and baro information at 10Hz. The PX4 also logs the position of the control surfaces and the pulse width modulation (PWM) signals sent to each control servo actuator. The onboard clock signal records a timestamp that is useful for the synchronisation of datasets.

Wing sweep - Bix3

Wing sweep has been traditionally employed as a passive design feature in wings. By sweeping the wing rearwards the aerofoil has a reduced effective rate of change of curvature, this helps to reduce the rate expansion and associated pressure drops that create localised shock waves and increased drag in transonic flow regions. Hence it is a common design feature of transonic aircraft [112]. The span-wise flow towards the wing-tip in swept back wings creates a thicker boundary layer near the wing tips which can cause the tips to stall before the inner wing. Forward wing sweep is typically employed to enhance manoeuvrability at high angle of attack. Air is encouraged to flow span-wise in the direction of the wing root, where the wing chord is generally larger and the fuselage acts as a wing fence, the result is a reduction in lift induced drag and an increase in C_{LMax} hence improving manoeuvrability. A forward swept wing will tend to stall earlier inboard, preserving the effectiveness of the outboard ailerons into the stall [113]. Variable wing sweep has been employed to great effect in transonic combat aircraft which necessitate varying the wing plan-form for different phases of flight (i.e. The Panavia Tornado – Low swept wing for take-off, landing and low speed flight, increasing rearward wing sweep for high speed cruise) typically such systems have discrete positions and are not continuous in operation [77]. Actuation speeds are typically too slow for control applications.

The wing sweep vehicle uses a plywood wing-box and wing root inserts which clamp onto the main spar (Figure 5.6).

Fig. 5.6 Wing sweep - Bix3 aircraft with a plywood wingbox and wing spar stub extensions

Bending loads are transferred through the wing-box by dorsal and ventral beams. The hinge line is coplanar with the wing root - fuselage junction and the actuation pushrod runs on a roller bearing. The assembly is driven by a pair of Hitec HS-M7990TH servo actuators which are geared through a four bar linkage to convert the rotary motion of the servo in to linear actuation and back into rotational torque at the wing root to increase the torque available to actuate the wing. The actuator has ability to drive the wing through $\pm 25°$ of anterior and posterior sweep.

Wing twist - WOT4

Wing twist is the original control scheme. The Wright brothers [114] used wing-warping to asymmetrical adjust the lift distribution across the wing for roll control, as materials and construction techniques moved away from fabric wings the technique was dropped in favour of discreet control surfaces. Passive wing twist is often added to a wing to improve the aircraft's low speed handling and stall characteristics. Wash out or a reduction in local wing incidence is often applied to set the ailerons (typically near the wing tips) at a lower angle of attack than the wing root, encouraging flow separation to begin at the root, helping to maintain roll control at low speeds and the onset of stall. Active aircraft control is achieved through imbalanced forces about the centre of rotation. By actuating the twist parameter of each wing asymmetrically the pilot has local control over the relative difference in angle of attack as seen by each wing / section that is actuated. When actuated symmetrically the local wing setting angle relative to the fuselage can be adjusted to change the aircraft's trim position. Such actuation is often employed in the empennage, either to adjust tail plane setting angle for trim control, an all flying tail for pitch control, or asymmetrically for roll control.

The wing twist vehicle uses a modified tubular carbon fibre main spar where the port spar stub has a reduced cross-sectional diameter and runs concentrically inside the starboard spar stub supported by cylindrical bearings at each rib station (Figure 5.7). This set-up is desirable as it maintains the continuity of the main spar through the wing box, transmitting the loads from one wing into the other, meaning the aircraft loads are reacted by the opposing wing without loading a single point in the central wing box.

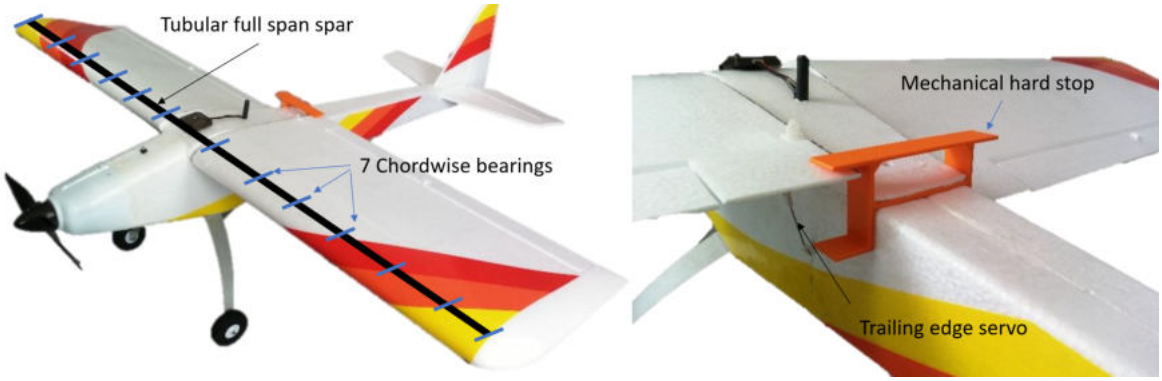

Fig. 5.7 Wing twist - WOT4 aircraft with wing root inserts and modified wing spar

Actuation is achieved by a pair of Hitec HS-M7990TH servo actuators mounted in the fuselage and connected to control horns which push/pull on hard-points mounted to the wing root trailing edge. The trailing edge is reinforced with a one third span spar plate to transfer the loads evenly into the wing structure. Mechanical hard stops exist at the trailing edge of the wing root to limit the wings movement in the event of a control horn failure The actuators have the ability to drive the wing in twist from to the upper and lower hard-stops. The hard-stops limit rotation of the wing to $\pm 25°$. In the event of a servo or control horn failure the wing's pitching moment will drive the trailing edge towards the upper hard-stop.

Wing flap - WOT4

Dihedral and anhedral are classical design tools used to deliver the desired lateral-directional stability of an airframe. Typically, the amount of dihedral is fixed or is some function of the wing loading for very flexible wings. Global dihedral is defined as the angle formed between the line joining the wing-tip to the wing root relative to the horizontal when the aircraft is level. Positive values (dihedral) represent the wing tips being raised compared to the wing root and negative values (anhedral) represent the wing tip being set lower than the wing root. Dihedral acts to improve the lateral directional stability of an aircraft by increasing the restoring roll response due to side-slip. This occurs because of the reduction in angle of attack seen by the up-going wing in a roll perturbation relative to the down going wing means that there is a restoring force against the direction of perturbation. Even so most aircraft have an unstable spiral mode, although the period is usually so long that it is easily controlled by the pilot or autopilot system. Aircraft with large dihedral value are very stable in roll and are typically less manoeuvrable as a result. Many low wing general aviation and civilian aircraft employ dihedral or polyhedral wings. Conversely anhedral acts to reduce the passive stability of an aircraft, it is typically employed in high swept wing because of the inherent stability provided by the keel effect and swept wing, in this configuration anhedral improves manoeuvrability. When actuated symmetrically, variable dihedral will affect the level of passive lateral-directional stability, this may be beneficial in different phases of flight. Gusty conditions can excite the lateral-directional modes very rapidly and having increased damping in these modes is beneficial in inclement weather. When actuated asymmetrically the effect is similar to a weight-shift, by inclining the main wing plane to the horizon and offsetting the centre of gravity the aircraft can be commanded to enter a banked turn as the total lift vector rotates about the centre of gravity. The offset lift vector also induces a side-load component which will cause the aircraft to develop a side-slip. Equally any offset of the centre of pressure and the centre of mass along the longitudinal axis will induce a yawing moment.

The wing flap vehicle uses a heavily modified wing box structure. The main wings have been offset from the central wing box and are mounted on large main and drag pins, the wing is free to rotate about this offset root (Figure 5.8).

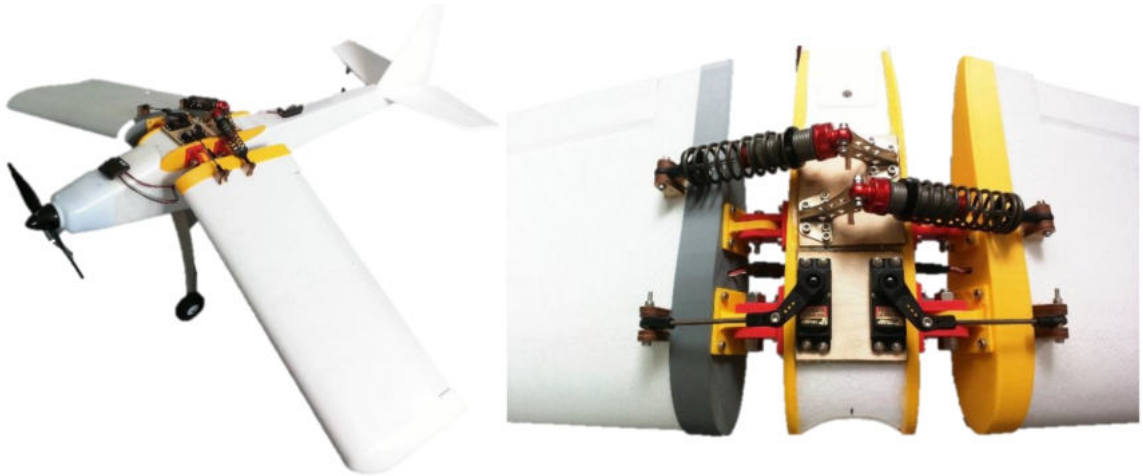

Fig. 5.8 Wing flap - WOT4 aircraft with a modified wing-box supporting a spring damper and actuator system

Flight loads are carried by a spring mass damper system as part of the rear drag pins. Spring stiffness and preload are selected to limit the dihedral angle to 0° in a 1g flight condition and to +25° at 3 g's. Negative flight loads are not reacted. The wings are mechanically limited to -25° by hardstops. Actuation is achieved through a pair of Hitec HS-M7990TH servos mounted on the central wing box, push rod connections are made to the main wing through root mounted control horns acting about the main pins. Part of the aerodynamic loads were offset by a pair of sprung fluid dampers which were sized and tensioned to support 1g wing loads in level flight.

5.4.5 Analytical Modelling

Modelling the Bix3 and WOT4 aircraft for simulation requires a digitised geometry. The Bix3 and WOT4 are hobby level remote control aircraft and there is no existing CAD model that is readily accessible. Before using flow simulation tools the geometry is digitised using a laser scanning technique provided by a FARO EDGE scan arm. The arm encodes the position of the scanning head and uses a non-contact scanning laser sheet to encode the wing as a digitised point cloud (Figure 5.9). Using the point cloud the aerofoil cross section can be extracted at each wing station and the mean camber line is extracted as an input for the 3D flow solver.

Fig. 5.9 Faro laser scan of Bix3 aircraft converted to a point cloud - Aerofoil section are extracted to determine the mean camber line for use in XFOIL and AVL analysis

The 2D flow analysis tool used is XFOIL. XFOIL allows for viscous / inviscid analysis and uses the superposition of known analytical solutions of the Navier-Stokes equations for a free-stream flow and vortex sheet to model flow around a 2D aerofoil. This 2D technique was used to better analyse the typical loads and moments that a wing comprised of a specific aerofoil section was capable of generating to inform choices for experimental design. XFOIL outputs plots of C_L, C_D amd C_M for specified Reynolds number and Mach number.

3D flow analysis is performed using AVL. AVL is a 3D vortex lattice method which models aerodynamic surfaces as a thin vortex sheet. The modelled aerofoil is reduced to a mean camber-line to fulfil the single layer vortex sheet requirements. The user sets the geometry and flight parameters and AVL computes the loading coefficients and stability axis derivatives. The outputs form the basis of an analytical model of the aircraft.

AVL cases were run as batch executables which defined the parameters for each run. The model geometry was generated from five sets of aerofoil data. A horizontal tail and a vertical tail whose aerofoil section is constant with reducing chord and three main wing aerofoils defining the different cranked portions of the wing. The plan-form is defined by section positions an linearly interpolated between each section. Section transitions are defined at the wing root, change in leading edge sweep, start and finish points on the control surface and the wing tip. For the control surfaces the hinge position as a percentage of wing chord is also defined.

In order to change the morphing position of the main wing a CAD model was generated in Siemens NX an used to compute the new positions of the section transition points in 3D space and then these points were transcribed into the AVL geometry files. A finite number of geometry files were defined and run to cover the full range of test positions in sweep, and flap. Wing twist was applied by setting the angle of incidence at each section transition and assumed constant over that section. By using this method each case is represented by a static geometry and assessed under assumed steady flow conditions.

5.4.6 Windtunnel testing

The wind tunnel tests made use of the University of Bristol 7ft by 5ft closed section wind tunnel at 10-15 m/s (Figure 5.10).

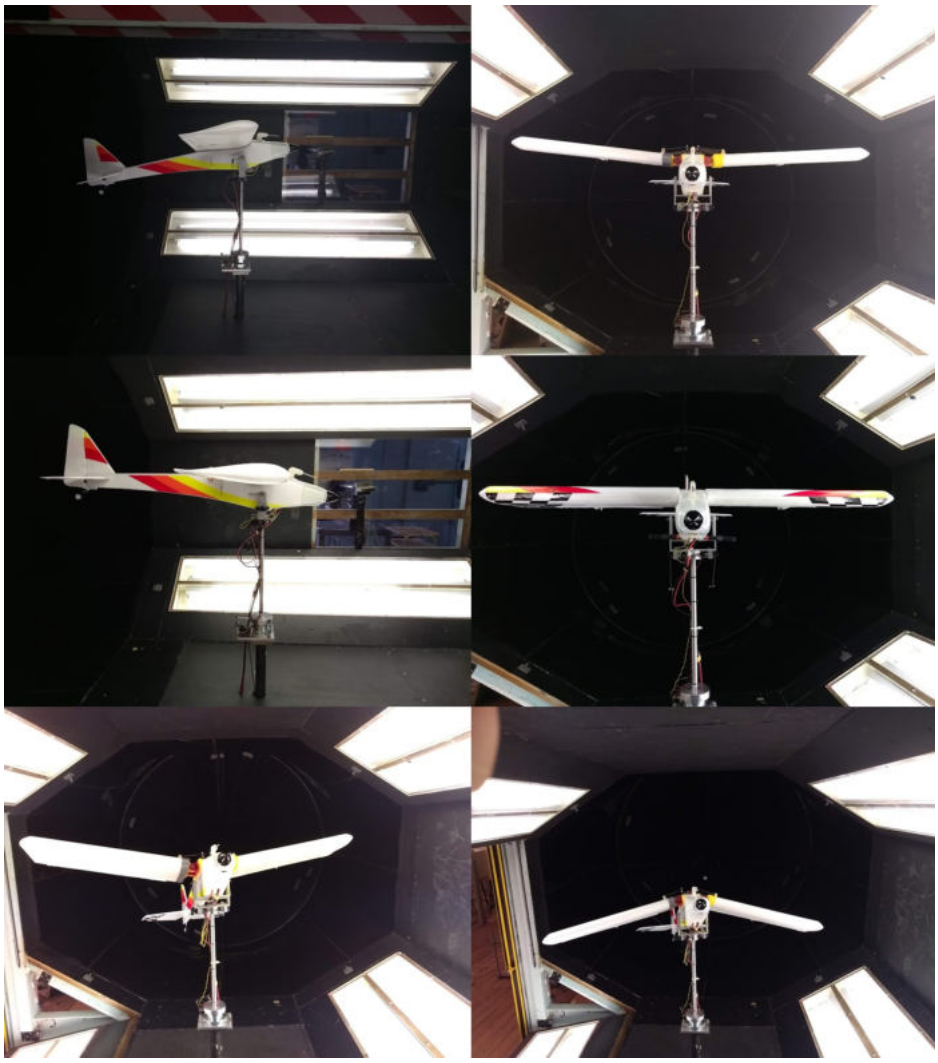

Fig. 5.10 7 X 5ft Closed section return wind tunnel with the various iterations of the WOT4 aircraft installed on the instrumented aircraft cradle

The wind tunnel was equipped with removable gust vanes which were removed for these experiments. Data capture was done with two data-logging systems, synchronised with a common clock from a main workstation. The first system was onboard the aircraft and was the PX4 data-logger [115]. This data-logger reads multiple sensor sources at different sample rates as discussed above and logs the output to a data file. The open source software is highly modular and will readily accept additional input on

standard protocols. A clock signal for data alignment was provided using the universal serial bus interface from the main workstation. This system records aircraft state parameters including roll, pitch, yaw, and rates, airspeed and barometric readouts, control surface positions and demanded positions. The second system was comprised of an aircraft mounting spike affixed to a six axis load cell (Mini 45, ATI Industrial Automation).

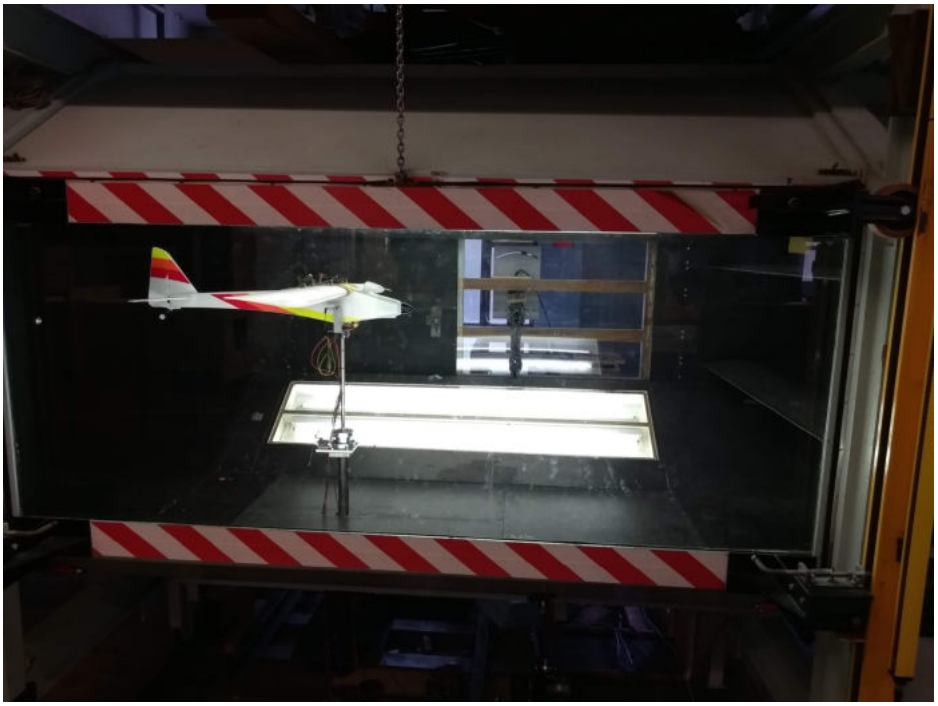

Fig. 5.11 Pitch / Yaw mounting spike with 2 degrees of freedom: angle of attack and side-slip angle.

The spike (Figure 5.11) had two degrees of freedom and can set the angles of attack and side-slip of the aircraft. It could be configured to work in one of two modes, a fixed setting mode that gives direct control of Angle of Attack and Side-slip, it restrains the model to record control moments imparted by control surfaces and a free-flight mode in which the aircraft is free to pitch and yaw which is used to record trim positions in "free-flight". The load-cell records three axis force components and three axis torque components at a 100Hz sample rate. The data was logged using the main workstation running Labview [116]. It was written to a .csv file and timestamped with the common clock.

Data concentration, transformation and alignment was performed in post using Matlab [117]. A simple script loads in the multiple data sets, aligns them using the common timestamp and resample the data to a common sampling frequency of 25Hz. Higher frequency load-cell and IMU datasets are downsampled and low frequency airspeed (which is being controlled to a constant value) and barometric / temperature information (which are being logged for normalisation purposes) are upsampled. An example of an aligned time-series dataset is presented in (Figure 5.12)

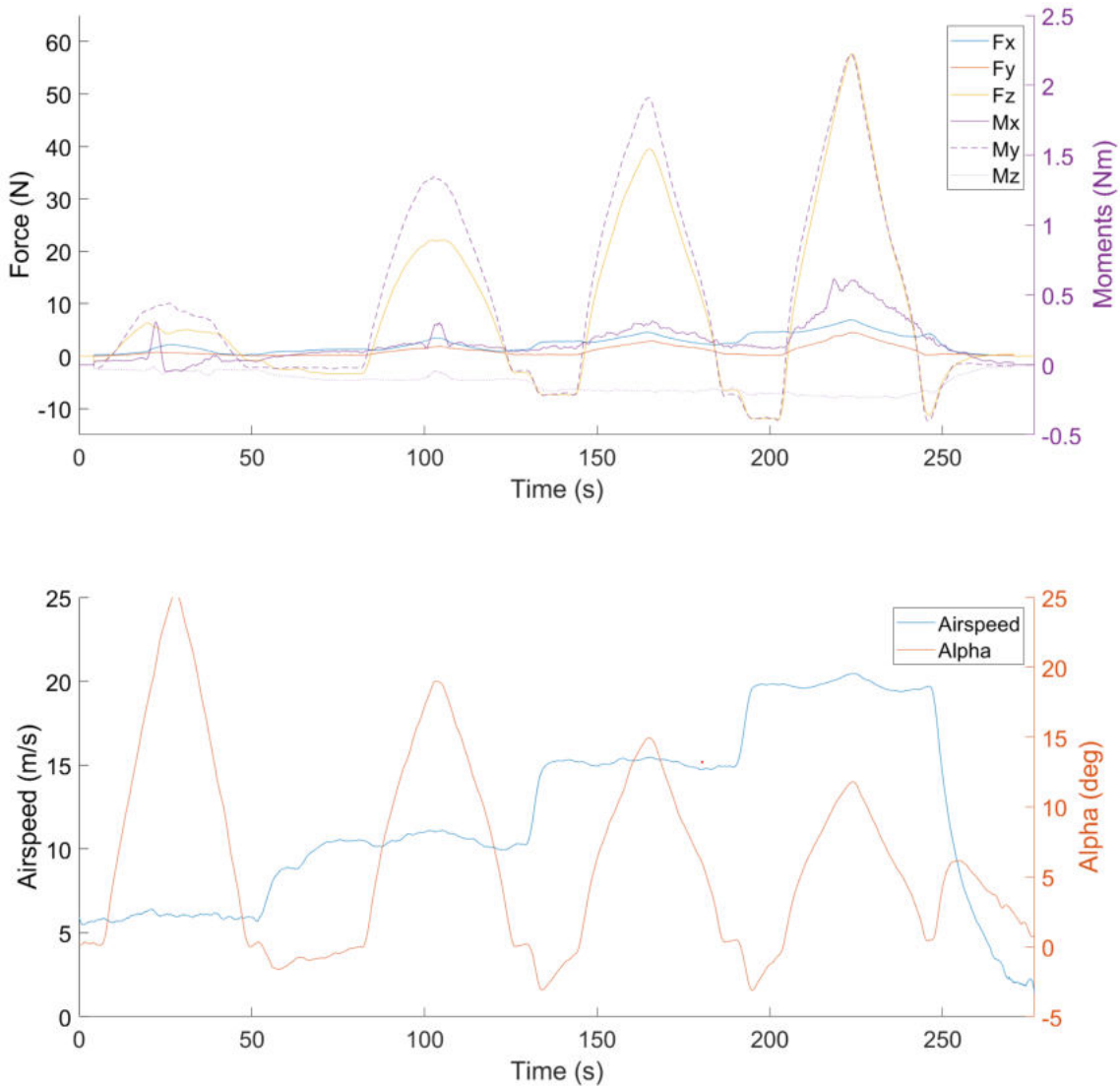

Fig. 5.12 Raw time-series data from the ATI load-cell (Top) and PX4 (Bottom) aligned, resampled and filtered

Each airframe was subject to a series of angle of attack (AoA) sweeps and control surface sweeps (δ), AoA sweeps were performed discretely at 5-20 m/s and control sweeps were performed at 10m/s and discrete angle of attack (α) of 0-10 degrees, control surface positions were continuously swept through.

Table 5.2 Vehicle wind tunnel testing schedule

Test	**Aircraft**	**U (m/s)**	$\alpha(^o)$	$\delta(^o)$
AoA sweep	WOT4 / BIX3	5	sweep	-
		10	sweep	-
		15	sweep	-
		20	sweep	-
Control sweep	WOT4 / BIX3	10	0	sweep
		10	5	sweep
		10	10	sweep

The AoA sweeps were used to characterise the vehicles polars and the control surface sweeps covered: elevator, aileron, rudder, wing sweep, wing twist and wing dihedral in accordance with Table 5.2. Wing sweep, twist and dihedral runs were conducted with symmetric and reduced order asymmetric control deflections so as to protect the vehicle cradle from significant rolling moments. Each run involved sweeping through the control parameter at 1°/s. Test runs at 0.5^o/s demonstrate no change in recorded measurements. Each run was repeated three times and the results averaged.

5.5 Results

The results presented here are a combination of datasets made using computer simulation analysis in XFOIL and AVL and experimental results from the wind tunnel models, two base model reference aircraft, the Bix3 and WOT4 and 3 modified articulated wing platforms based on the reference aircraft.

5.5.1 Bix3 reference data

The Bix3 model (Figure 5.14) which has has a tapered thin section wing whose aerofoil (Figure 5.13) is optimised for low profile drag (Figure 5.15). Viscous parameters match wind tunnel experimental conditions, Reynolds number = 300000 and Mach number = 0.1.

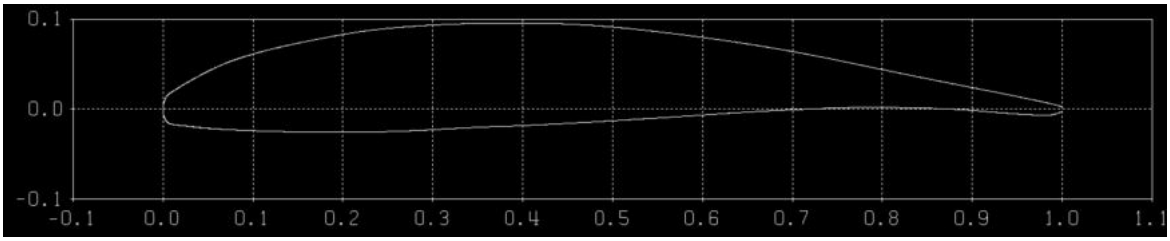

Fig. 5.13 BIX3 Aerofoil cross-section

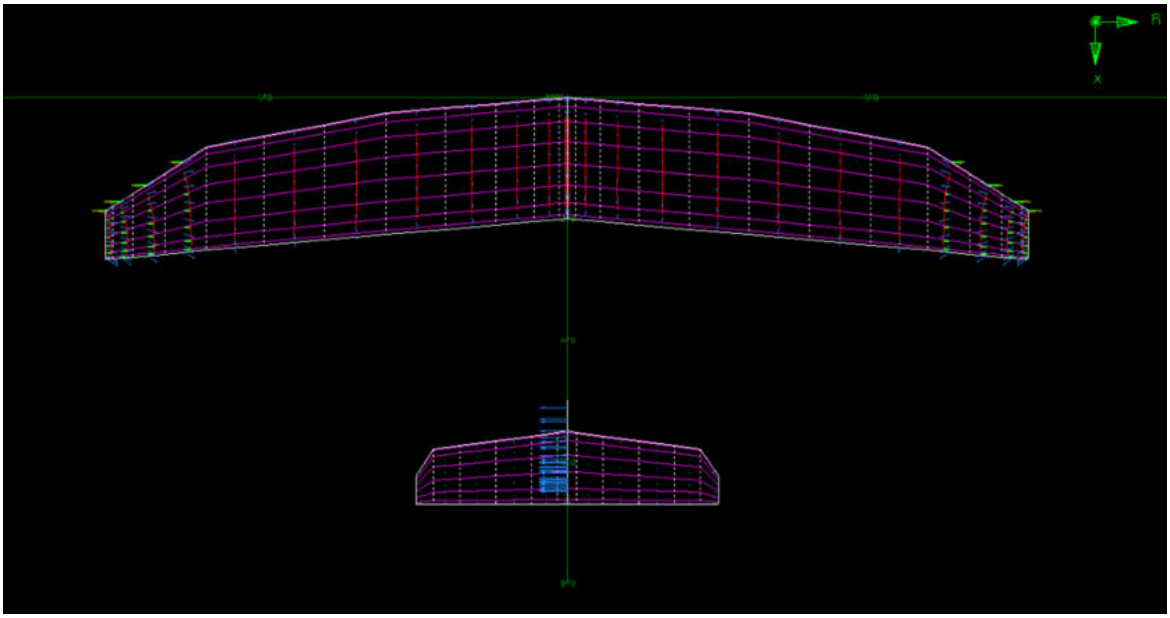

Fig. 5.14 BIX3 AVL plan-form showing polyhedral wing and tail geometry. The fuselage is reduced to a slender beam element

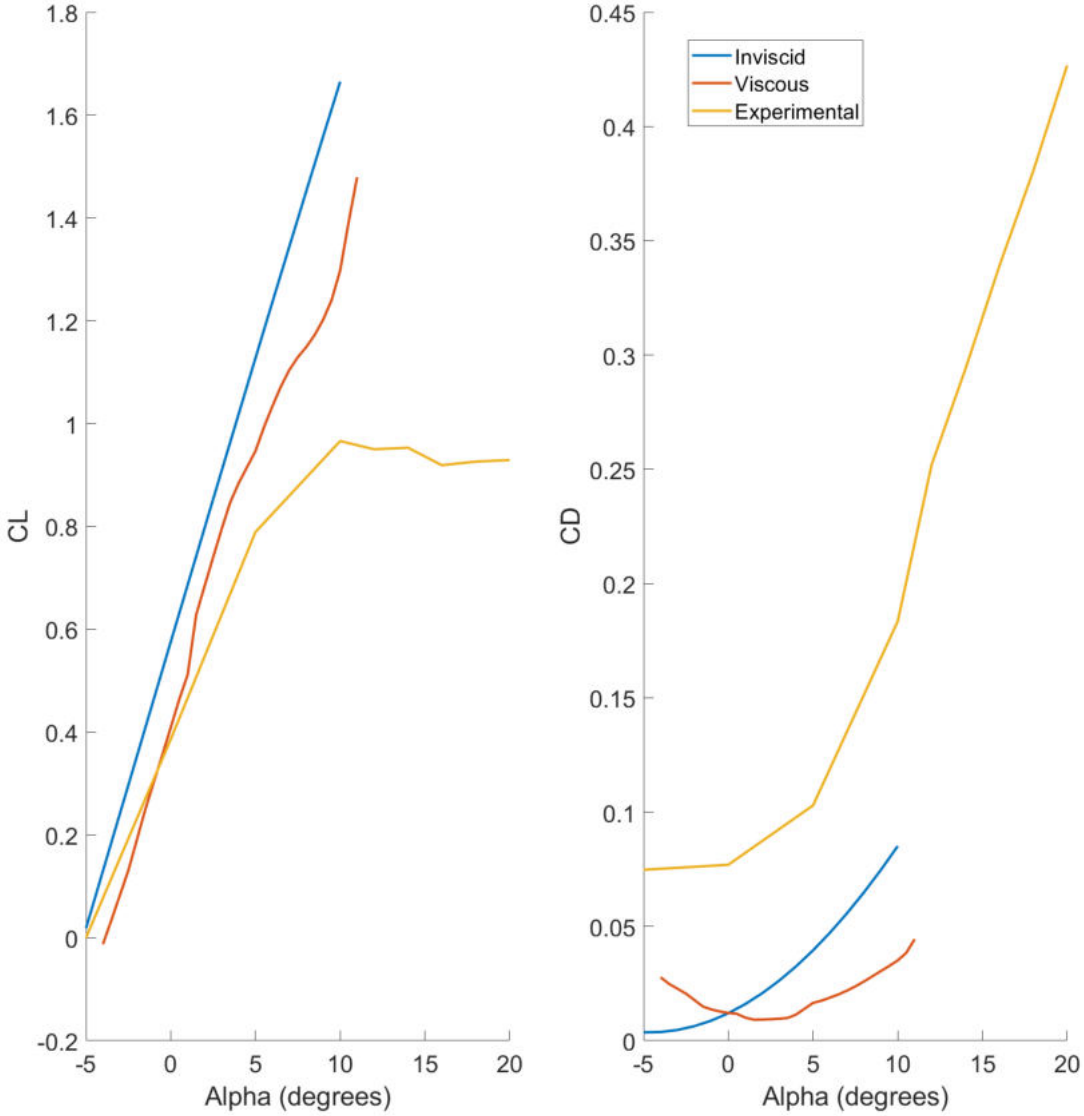

Fig. 5.15 BIX3 Aerofoil analysis: CL, CD vs Alpha (Experimental polar from whole aircraft data)

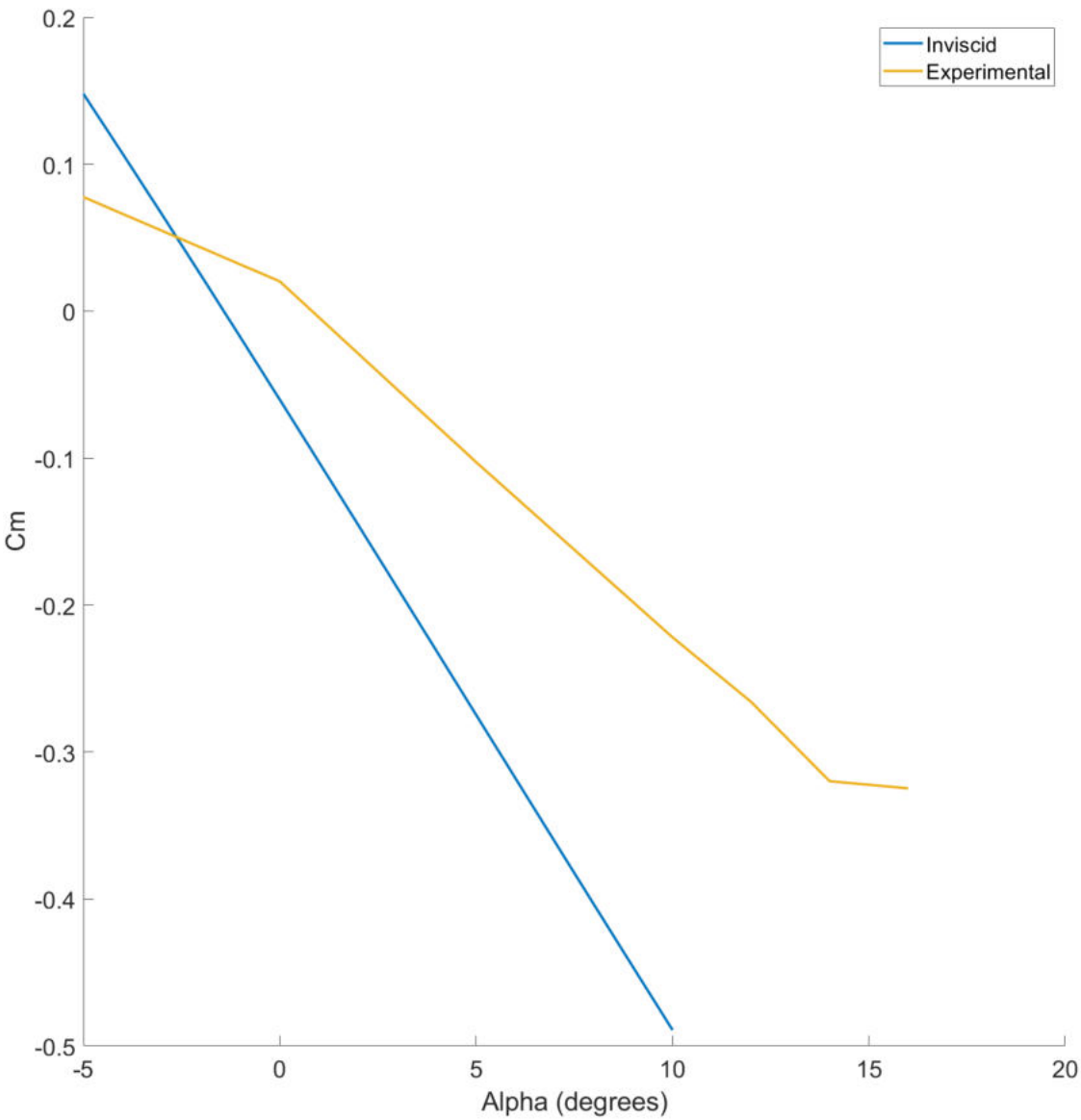

Fig. 5.16 BIX3 Aerofoil analysis: CM vs Alpha

The aerofoils linear $C_{L\alpha}$ provides a smooth lift response and the C_D curve demonstrates a drag bucket minimising viscous drag at low angles of attack (3 - 5 degrees) pursuant to the typical cruise angles of attack of the aircraft. The aerofoils' pitching moment response is stable with a negative $C_{M\alpha}$ slope.

5.5.2 WOT4 reference data

The WOT4 model 5.18 which has a straight thick section wing whose aerofoil (Figure 5.17) is optimised for benign stall response an lift at high angles of attack (Figure 5.19).

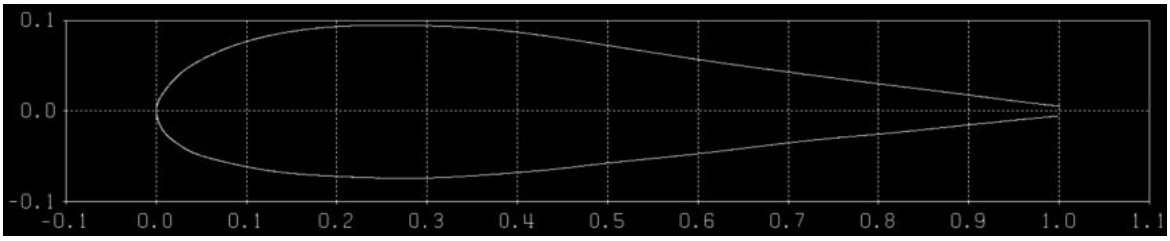

Fig. 5.17 WOT4 Aerofoil cross-section

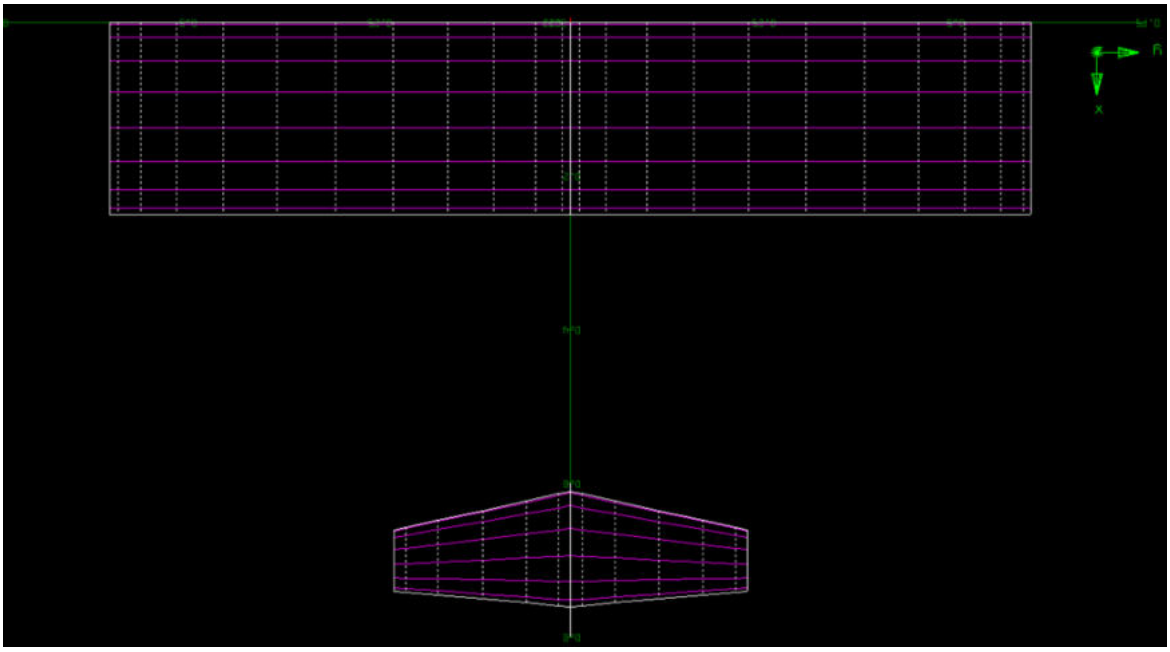

Fig. 5.18 WOT4 AVL plan-form showing rectangular wing and trapezoidal tail geometry. The fuselage is reduced to a slender beam.

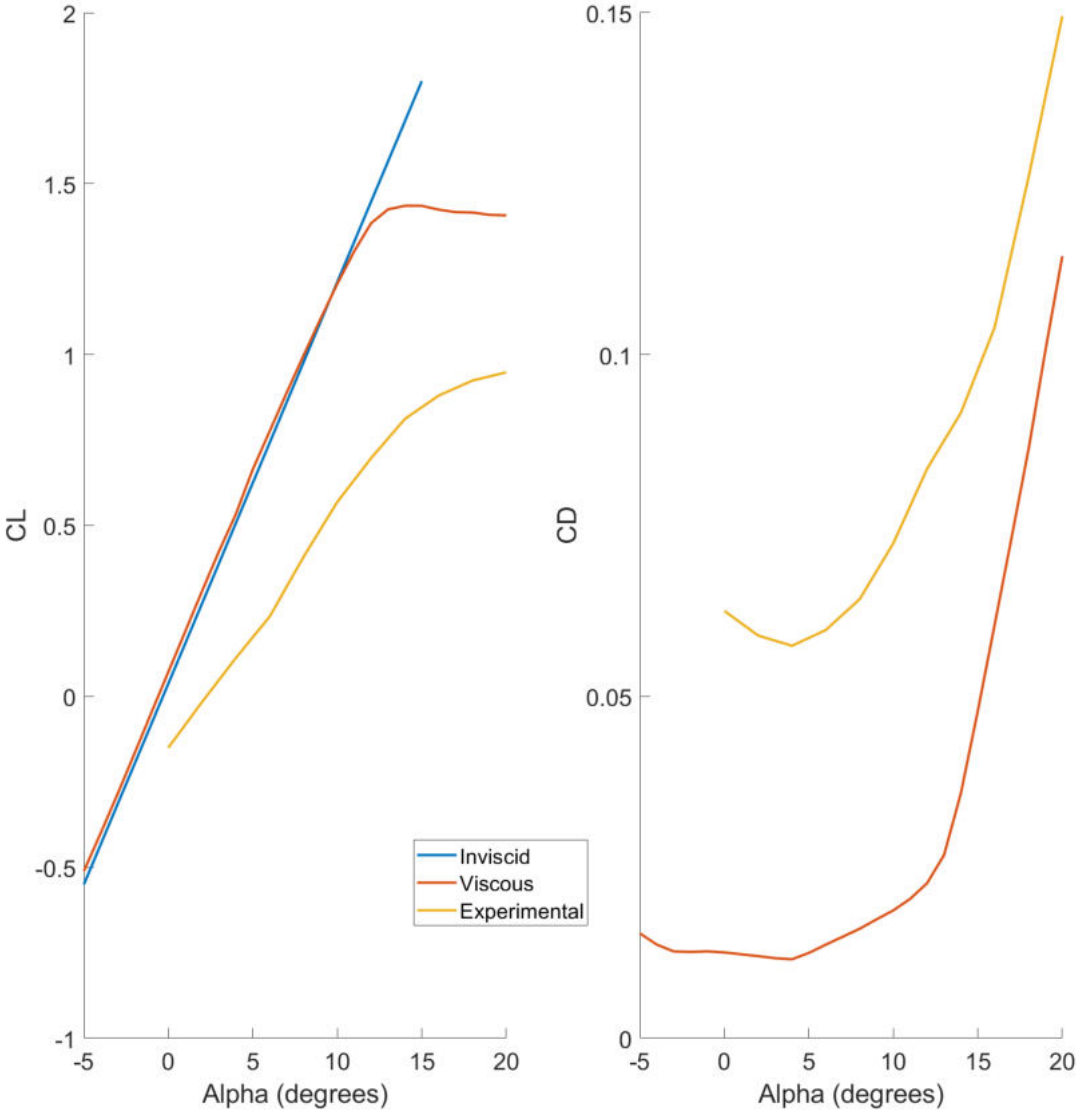

Fig. 5.19 WOT4 Aerofoil analysis: CL,CD vs Alpha

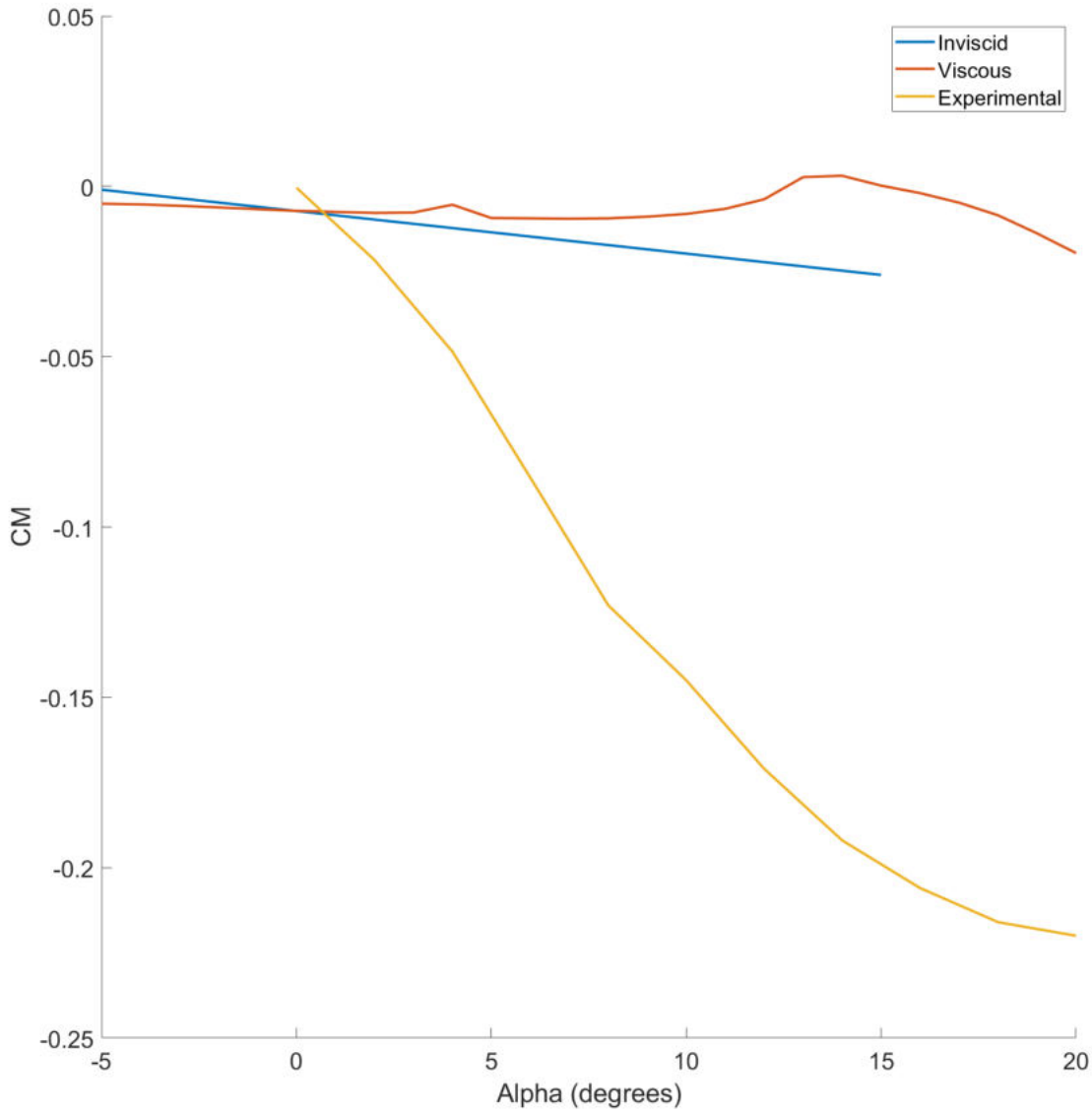

Fig. 5.20 WOT4 Aerofoil analysis: CM vs Alpha

The aerofoils $C_{L\alpha}$ is linear between -5 and 10 degrees angle of attack and has a noticeable plateau above 10 degrees, maintaining lift up to 20 degrees angle of attack. This provides a benign stall response making the aircraft very capable at high angles of attack, preserving lift well beyond the peak C_{LMax} found at 13 degrees angle of attack. The C_D curve demonstrates a flat response up to the critical angle before sharply rising as the adverse pressure gradient grows quickly above 15 degrees angle of attack. The aerofoils' pitching moment response is stable at low angles of attack with a negative $C_{M\alpha}$ slope. Above the critical angle the response is non-linear.

5.5.3 Wing sweep - Bix3

Sweeping the wing on the Bix3 changes the properties of the aerofoil in relation to the chord-wise flow. These variations result in changes to the aerodynamic coefficients of the aerofoil as measured in AVL. The effective aerodynamic moments are shown in Figure 5.21 and Figure 5.22 where the effect of wing sweep (dashed lines) is compared to traditional elevator control (solid lines). Measurements were made from three different initial angles of attack: Alpha = 0 (red), 5 (green) , 10 (blue) degrees. Pitching moment is defined as being positive with a nose up tendency. Elevator angle was defined as being positive with upwards deflection (producing a nose up pitching moment) and wing sweep is defined as being positive with forward deflection (producing a nose up pitching moment). Note the definition of positive wing sweep in this Chapter is different to the convention used in Chapter 4 where forward sweep was defined as being negative. This change in convention was made to keep the results aligned with other sources of reference for each body of work.

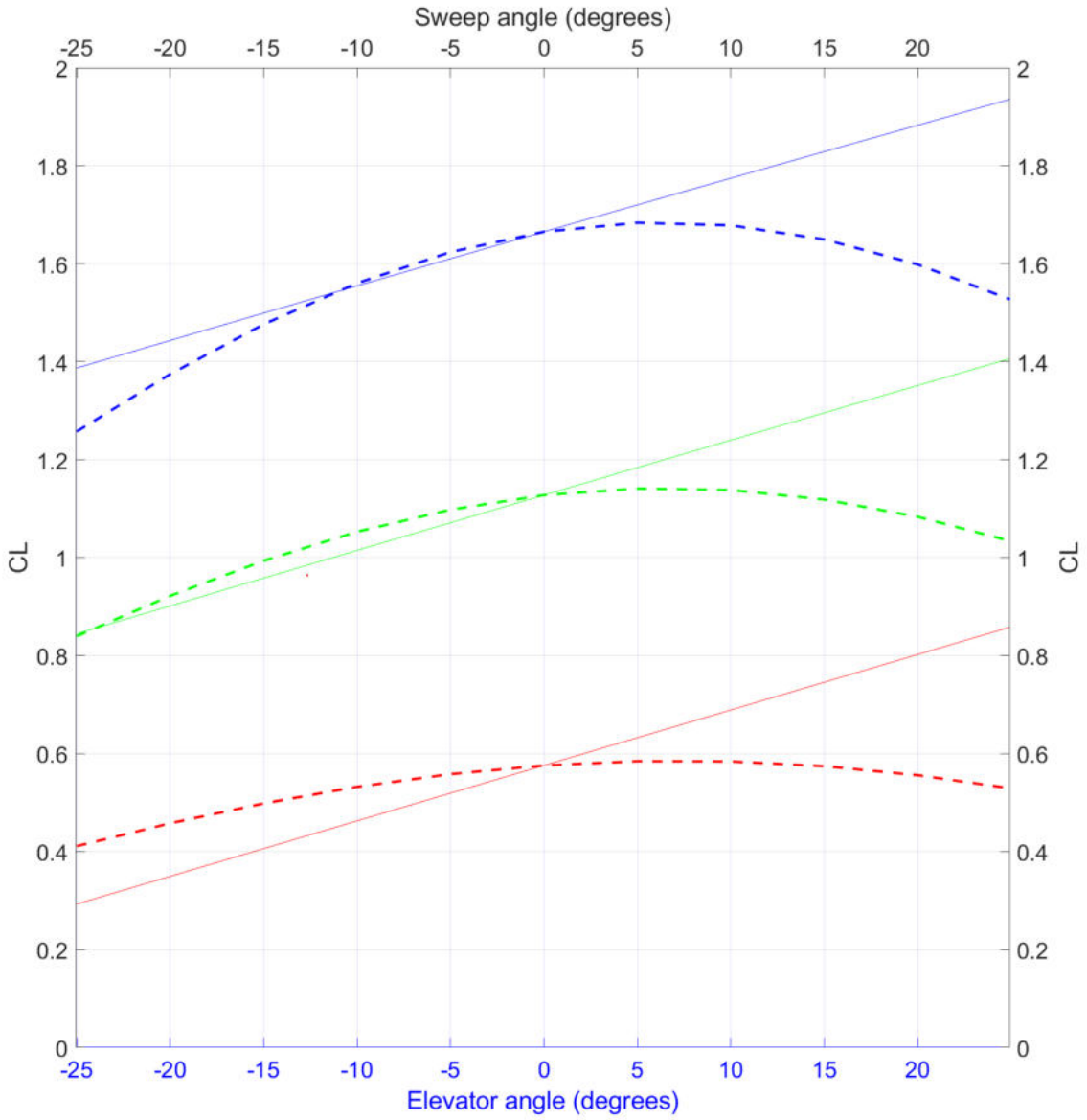

Fig. 5.21 Elevator (solid) and wing-sweep control (dashed) - BIX3 analysis: CL vs Elevator, Sweep, V = 10m/s, Alpha = 0 (red), 5 (green) , 10 (blue) degrees

Figure 5.21 shows the change in lift coefficient with changes in elevator deflection (solid line) and wing sweep deflection (dashed line). The $\frac{dC_L}{d\delta_{elevator}}$ is positive and linear from -25 to 25 degrees of elevator deflection. This corresponds with the primary effect of the elevator control which is to effect a change in angle of attack of the main wing which drives the change in lift coefficient. The pitching moment coefficient shows a similar behaviour in figure 5.22. The gradient $\frac{dC_m}{d\delta_{elevator}}$ is positive and crosses the origin between 2 and 12 degrees of elevator deflection depending on the angle of attack (more elevator deflection being required to generate a nose up pitching moment at a high angle of attack or corresponding low flight speeds). Sweeping the main wing to effect longitudinal control demonstrates a very different response.

Figure 5.21 shows the parabolic response in the lift coefficient as the wing is swept away from the ideal value. As the wing sweeps the lift coefficient achieves a peak of 1.68 at 5 degrees forward sweep before dropping off either side of this peak value. Due to the taper on the Bix3 main wing the leading edge is angled back approximately 5 degrees in the base configuration which corresponds to 0 degrees of wing sweep angle. As such the peak value of C_L is seen when the leading edge is perpendicular to the free-stream flow and this occurs at approximately 5 degrees of forward sweep for all angles of attack. As the wing is swept away from this position the magnitude of the lift coefficient falls by up to 30% depending on the degree of sweep and the angle of attack.

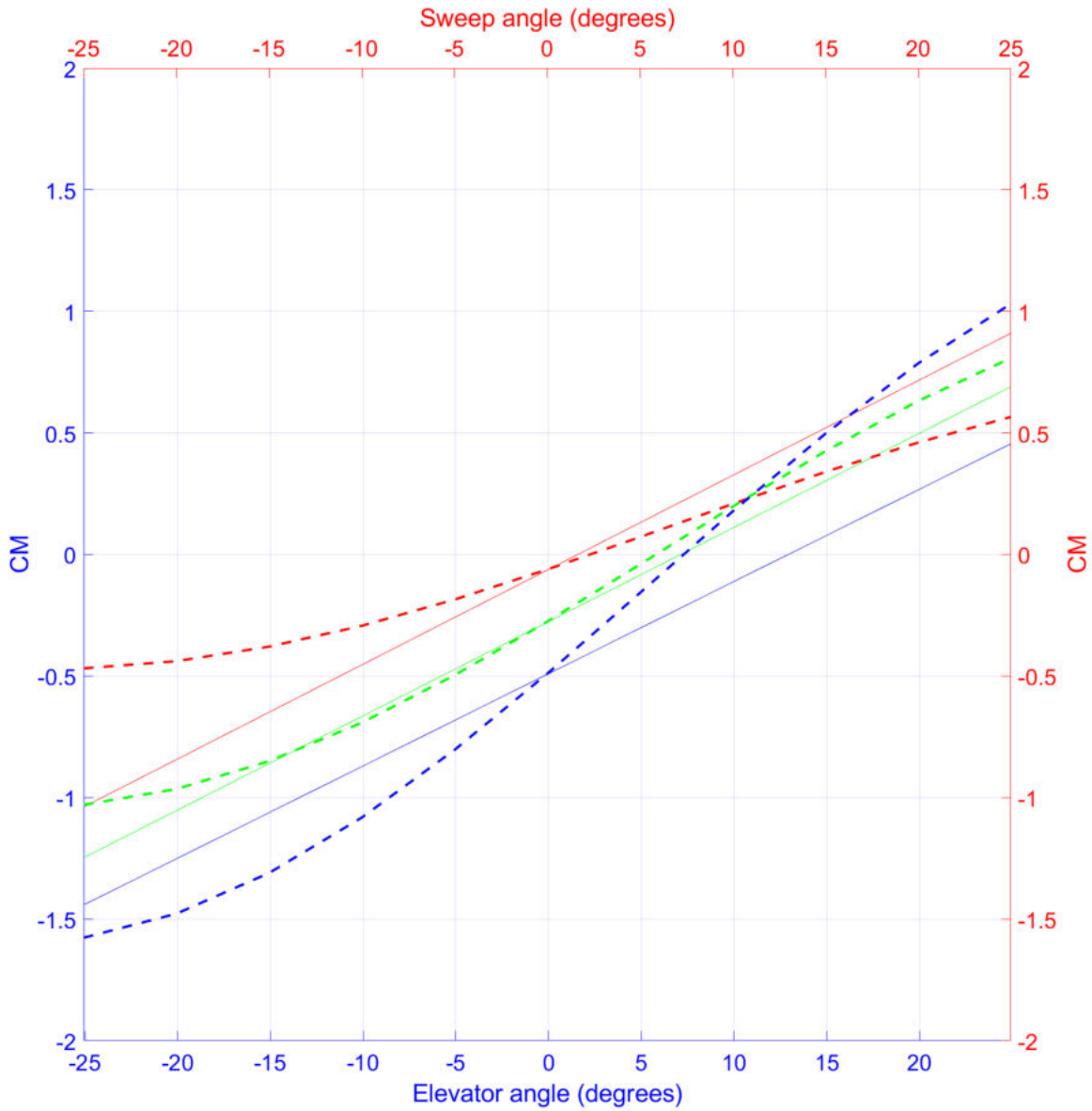

Fig. 5.22 Elevator and wingsweep control - BIX3 analysis: CM vs Elevator, Sweep, V = 10m/s, Alpha = 0 (red), 5 (green) , 10 (blue) degrees

The pitching moment due to wing sweep $\frac{dC_m}{d\delta_{sweep}}$ seen in figure 5.22 is similarly non linear. Because the main wing in being actuated sweeping the wing produces larger changes in both positive and negative pitching moment at higher angles of attack. This results in a cross over of the $\frac{dC_m}{d\delta_{sweep}}$ curves for different angles of attack at a constant value of approximate 12 degrees of forward sweep. Above this value the main wing sweep develops a more positive pitching moment for increasing angle of attack and below this value the main wing develops a more negative pitching moment for increasing angle of attack. In this configuration the centre of pressure of the main wing is coincident with the the aerodynamic centre and so at this point the pitching moment is constant and $\frac{dC_m}{dC_L} = 0$ It also marks the point whereby the aircraft configuration goes statically unstable. For all angles of attack when the wing sweep is less than 12 degrees forward an increasing angle of attack generates a more negative pitching moment, lowering the angle of attack and restoring equilibrium. Above 12 degrees forward sweep an increase in angle of attack generates a more positive pitching moment resulting in an unstable increase in angle of attack. The pitching moment generated by sweeping the wing is most effective at high angles of attack.

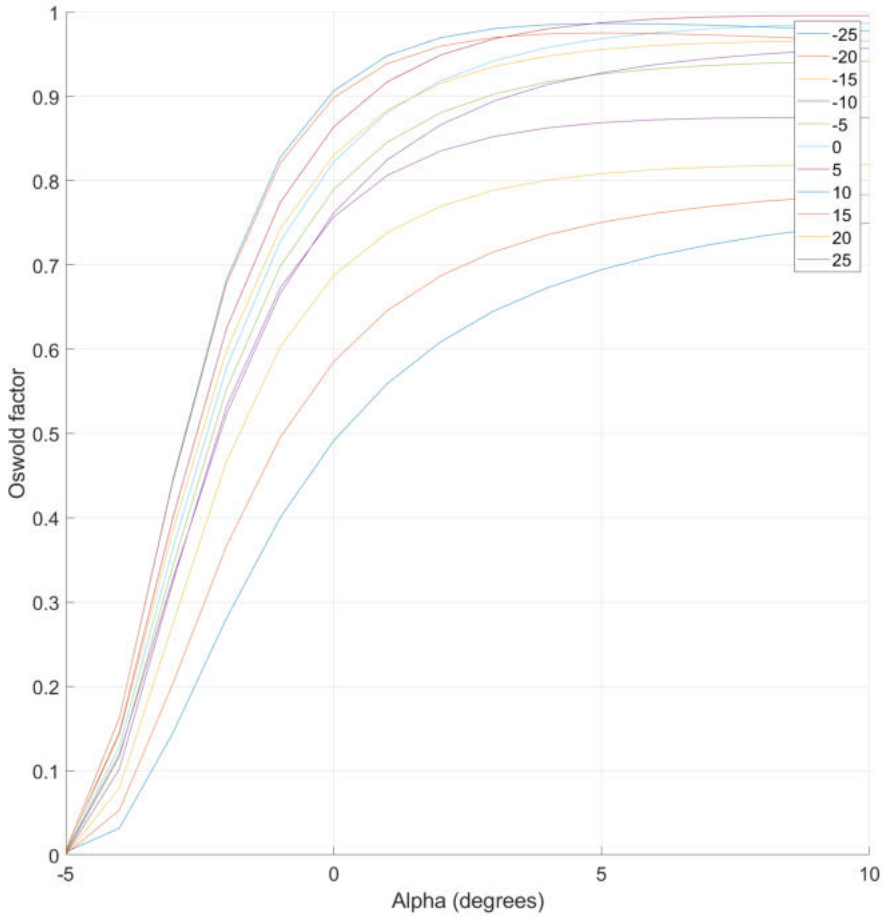

Fig. 5.23 Sweep control - BIX3 Inviscid analysis: Oswold factor

The efficiency of the wing when compared to an ideal wing with an elliptical lift distribution is given as the Oswold factor (Figure 5.23). Where an Oswold factor of 1 equals an ideal wing. The Bix 3 achieves the maximum efficiency above angles of attack of 5 degrees and with a 5 degree forward sweep. Sweeping the wing moves the position of the centre of pressure in relation to the centre of mass and this effects the longitudinal static stability of the configuration (Figure 5.24). The Bix3 with 0 degrees wing-sweep is longitudinally stable. Sweeping the wing aft increases the longitudinal static stability (split between the lines) and the cross over point at which the aircraft becomes unstable is 11 degrees of forward sweep. This change in static stability at 11 degrees is independent of angle of attack.

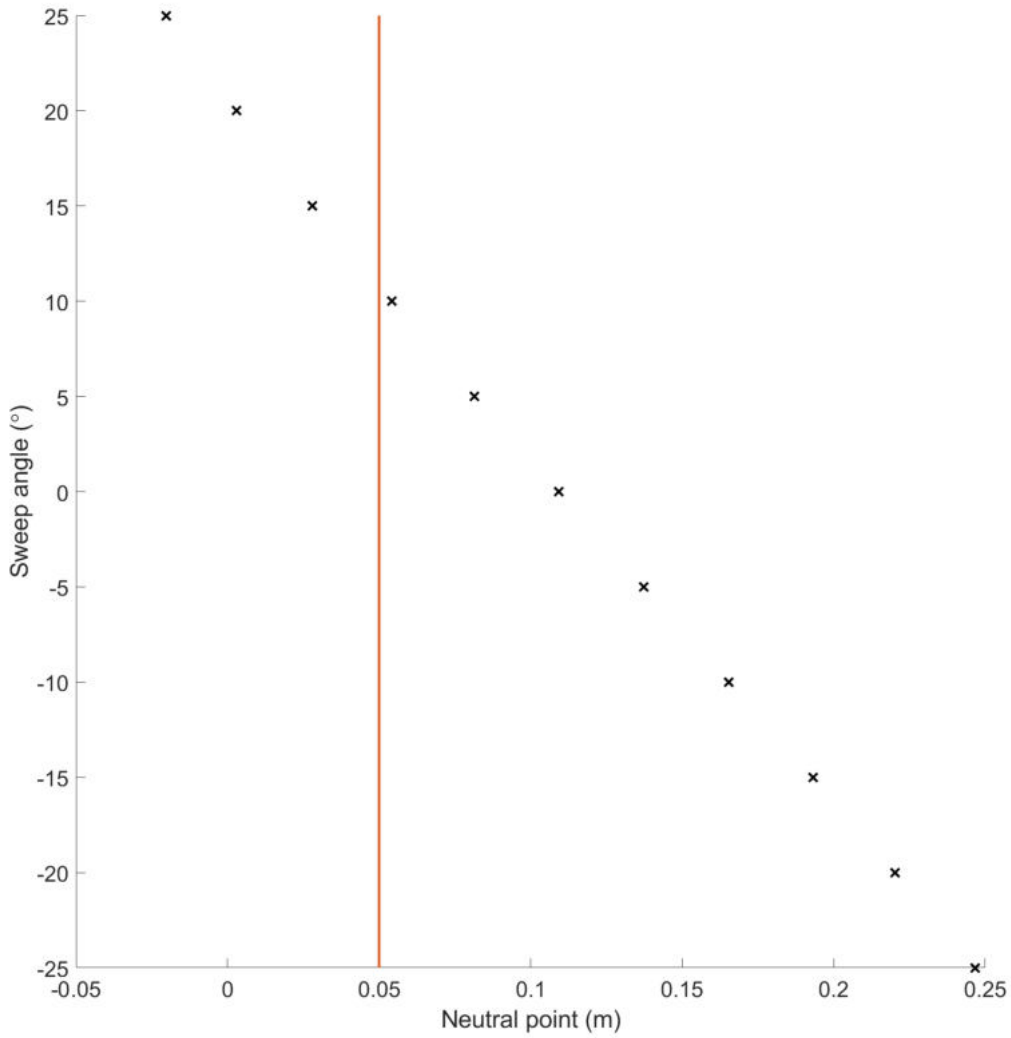

Fig. 5.24 Sweep control - BIX3 Inviscid analysis: Neutral Point

Figure 5.24 shows the point of neutral stability at approximately 13 degrees forward sweep for the lines corresponding to $\alpha = 0°$. The same general result is true for $\alpha = 5°$. However when $\alpha = 10°$ the stability remains positive and the pitching moments remains more negative across the test envelope. This is likely due to the dynamics of the test causing the Bix3 wing to exceed its critical angle of attack at approximately 11 degrees as seen in the wind tunnel test data in figure 5.19. Any loss of lift due to flow separation will result in a nose down pitching moment. The fall over point in static stability equates to the neutral point being coincident with the centre of mass at 0.05m reference position (rear of the wing root chord).

The Bix3 airframe has an unstable spiral mode as determined by the ratio of lateral stability to directional stability:

$$\frac{C_{l\beta}C_{nr'}}{C_{lr'}C_{n\beta}} \tag{5.1}$$

This condition indicates an unstable spiral mode when the result is less than one. The Bix3 airframe has an unstable spiral mode at all positions of wing sweep at the cruise angle of attack (4 degrees) (Figure 5.25).

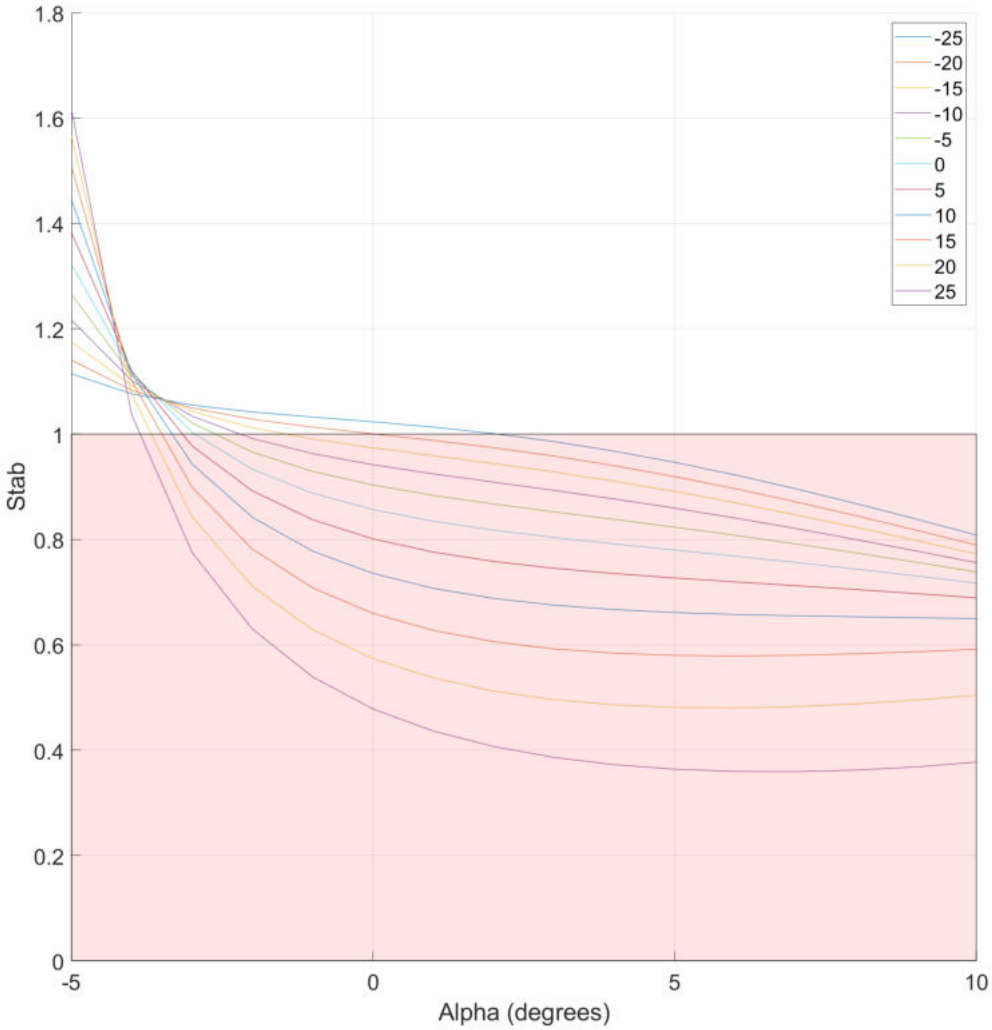

Fig. 5.25 Sweep control - BIX3 Inviscid analysis: Spiral stability

5.5.4 Wing twist - WOT4

Twisting the wing changes the local effective angle of attack as experienced by the wing. The wing can be twisted symmetrically to alter the setting angle of the wing in relation to the fuselage, short term dynamic response from fast actuation of the wing symmetrically is manifested as a short term change in angle of attack, long term response is a trim change due to the change in wing setting angle. The dynamic response can be exploited for direct lift control and the long period response is beneficial as a trim change. Because twisting the wing symmetrically simply effects the local angle of attack it drives the wing up and down the angle of attack curves presented in the WOT4 reference data.

Twisting the wing asymmetrically changes the span-wise lift distribution. This variation in span-wise lift distribution induces a rolling moment about the centre of mass. The effectiveness of twisting the whole wing to induce a local change in lift coefficient and rolling moment compared to traditional aileron control surfaces are presented in Figure 5.26.

The rolling moment due to twist in this particular experiment does not show an improvement over the existing aileron. However, it is expected that benefits would be more apparent at very low flight speeds where the increased surface area of the whole wing would offset the increase in flow speed over a smaller control surface. It's worth considering that considering the rolling moment induced without a full consideration of how such a morphing wing would increase undesirable parameters such as drag doesn't present a complete picture but it does identify its potential use for roll control in the absence of aileron surfaces.

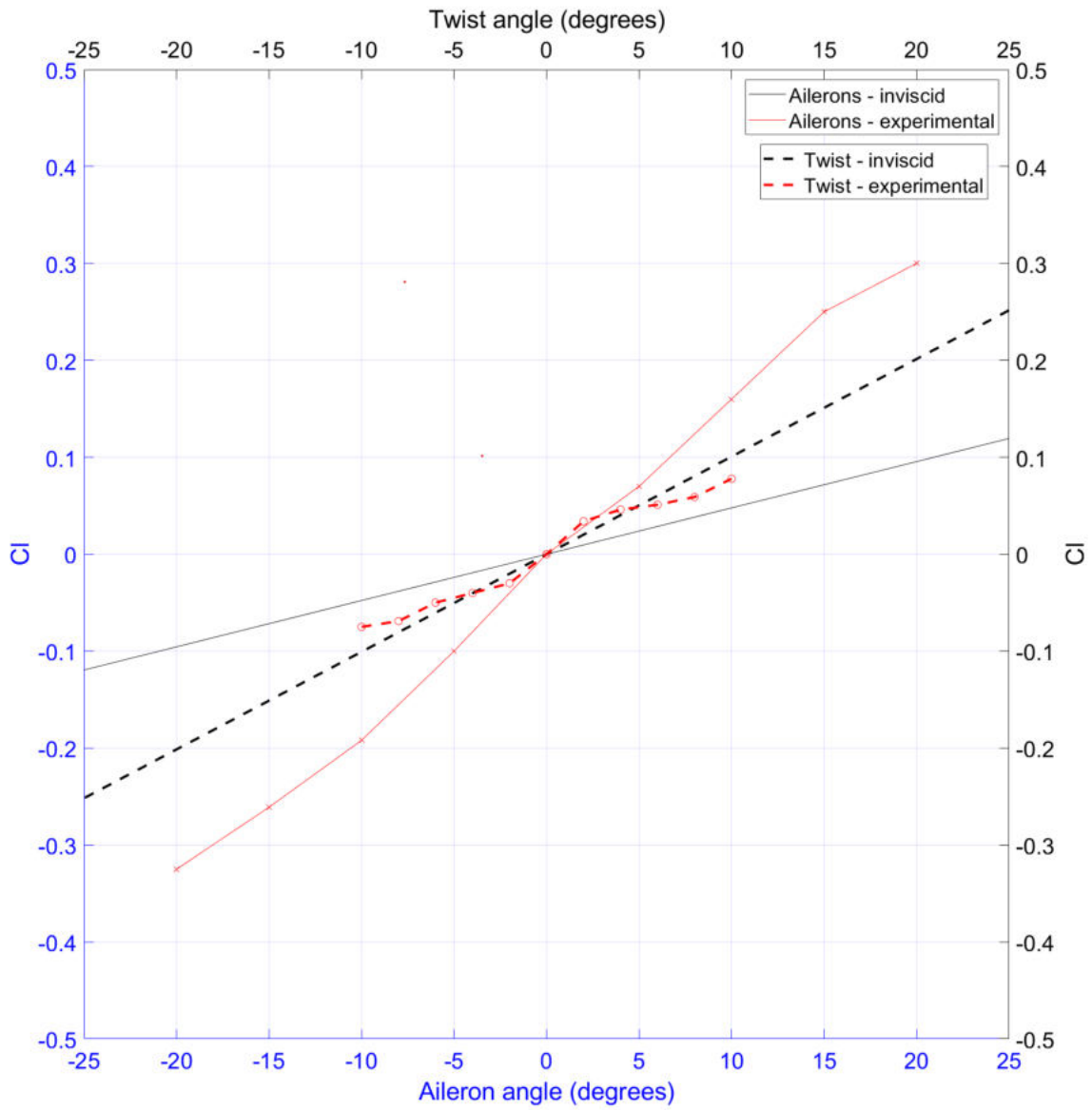

Fig. 5.26 Aileron control - WOT4 Aileron and Twist analysis: Rolling moment vs Control deflection

5.5.5 Wing flap - WOT4

Rotating the wing about the longitudinal axis symmetrically varies the dihedral / anhedral of the aircraft. This varies the C_{LMax} of the wing as a function of dihedral angle. The peak value of lift coefficients occurs when the wing has 0 degrees dihedral (Figure 5.27).

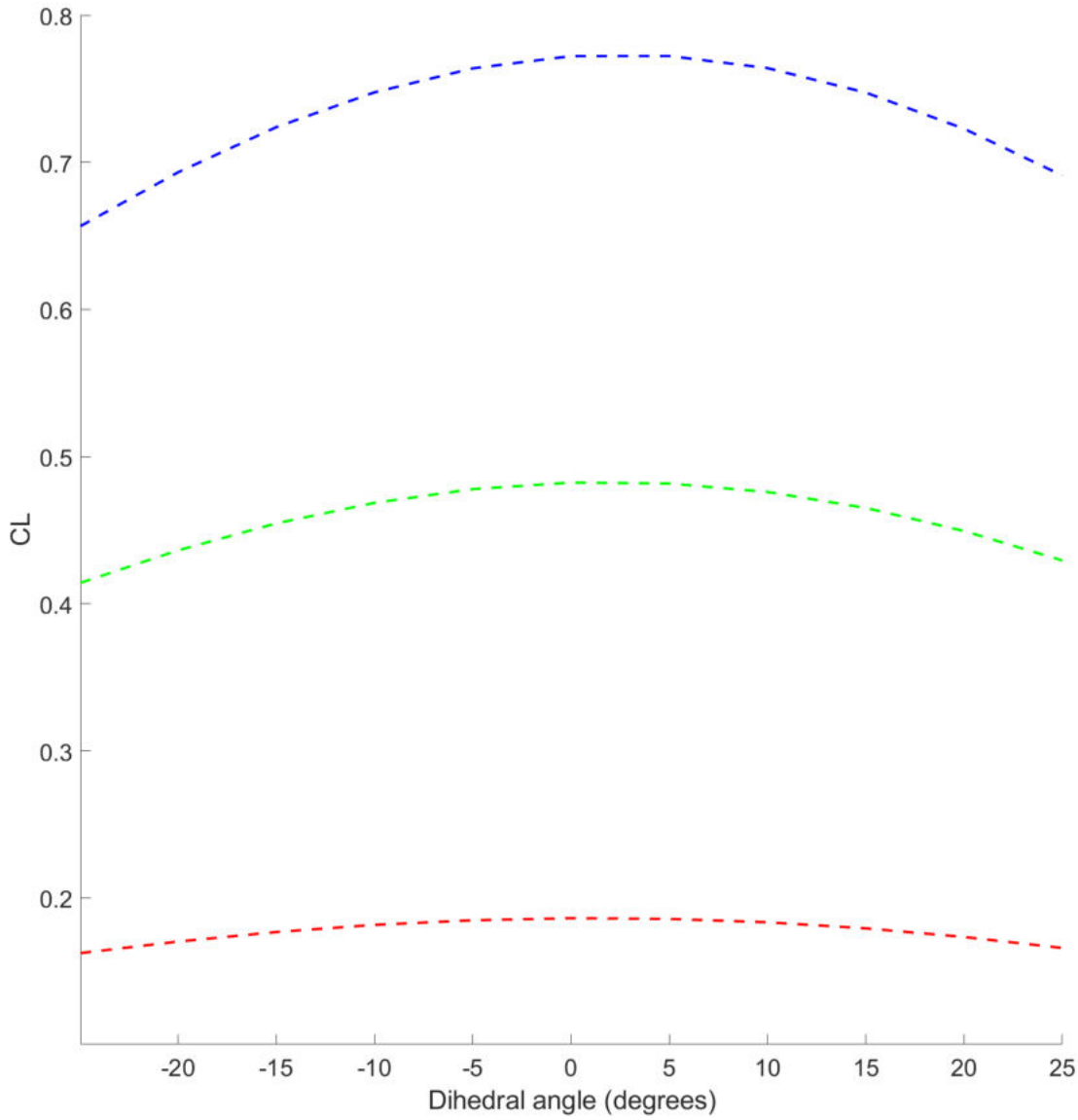

Fig. 5.27 Symmetric Dihedral control - WOT4 Inviscid analysis: CL vs Alpha, V = 10m/s

The primary reason for applying dihedral and anhedral to a wing is to adjust the relative lateral-directional stability of the aircraft by adjusting the aerodynamic rolling and yawing derivatives with respect to side-slip. The spiral stability of the aircraft is modeled using (Equation 5.1) as previously stated. Figure 5.28 shows how the spiral stability of the WOT4 platform varies with changing dihedral / anhedral angle.

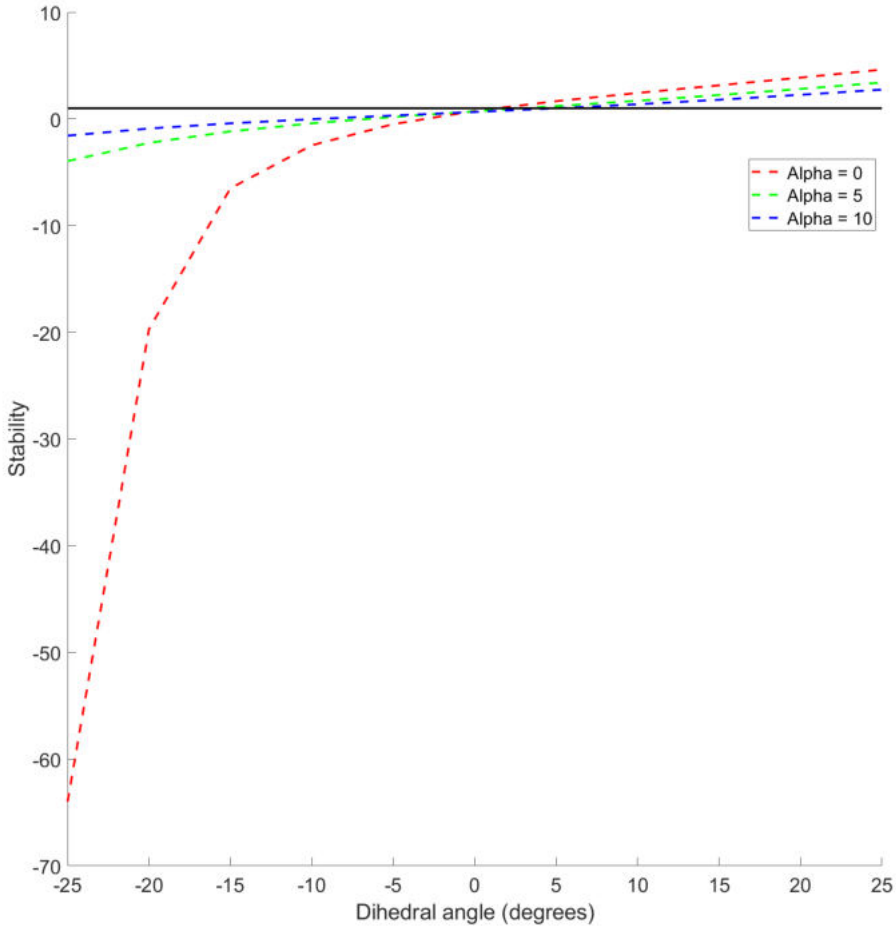

Fig. 5.28 Symmetric Dihedral control - WOT4 Inviscid analysis: Spiral stability

The point of neutral stability depends on angle of attack is found between 1 and 5 degrees dihedral. Greater values of dihedral imply positive spiral stability (and a less stable Dutch roll mode) whilst any anhedral is enough to excite the unstable spiral mode at all positive angles of attack.

5.6 Discussion

Fixed wing aircraft have been operating using a three-axis control scheme since their inception. Early experimentation with whole wing morphing was typically constrained by the material properties of the time. Whilst variations on the classical arrangement of elevators, ailerons and rudder have been developed, utilising mixed surfaces (e.g. elevons, stabilators) most of these still use discrete moving surfaces which deflect along the trailing edge of the wing. The work here looks at the actuation of the main wing for flight path control. This is similar to the weight shift control utilised in flex-wing microlight aircraft as it moves the centre of pressure of the lifting surfaces relative to the centre of mass of the vehicle, thereby inducing a force couple and a controlling moment on the aircraft's trajectory. Total control of the main lifting surface is also employed in the control of rotary wing vehicles, helicopters and gyrocopters, the wing actuation axis are inspired by the hinge setup found in rotor hub systems, incorporating a pitch, flap and lead-lag hinge. In this body of work the fore-aft motion of the wing about a normal axis is referred to as wing sweep, the rotation of the wing about a lateral hinge axis as wing twist and the vertical motion of the wing-tip rotating about the longitudinal axis as variable dihedral or wing flap.

5.6.1 Variable wing sweep and control in pitch

Moving the wing fore and aft about the root affects the longitudinal dynamics of the vehicle. Sweep affects both the mechanics and aerodynamics of the main wing which in turn effect the flight path. Looking first at the mechanics of sweeping the wing forward (Figure 5.29).

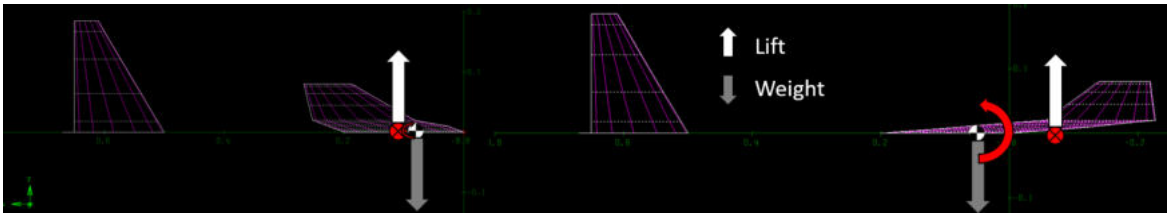

Fig. 5.29 Mechanics of forward wing sweep and the effect on the longitudinal dynamics

Moving the centre of pressure forward relative to the centre of mass of the vehicle induces a pitch up moment. Simultaneously it reduces the static margin to a point where in the vehicle become statically unstable in pitch, increasing the pitch up in response to a perturbation. The forward sweep of the wing moves the wing root aft of the wing tip, the favourable span-wise pressure gradient that exists encourages inboard span-wise flow from the tips towards the wing root. This redistribution of the pressure pattern towards the wing root reduces the effect of the wing-tip vortices, with the fuselage acting as a wing fence. With a stronger adverse pressure gradient inboard at the wing root the wing will tend to stall at the root first. This preserves flow over the outboard wing-tip and ailerons, increasing their effectiveness deep into the stall condition. The result of these effects are increased controllability at higher angles of attack deeper into a pitching manoeuvre at high pitch rates and high angles of attack. The longitudinal dynamics depend on the degree of forward sweep and whether there is a reversal in the static stability of the aircraft but as a general result, forward wing sweep will excite the short period and phugoid mode and tend towards dynamic instability. Lateral-directional stability is also effected. The effective forward sweep is increased on one wing and reduced on the other in the presence of a side-slip condition (Figure 5.30).

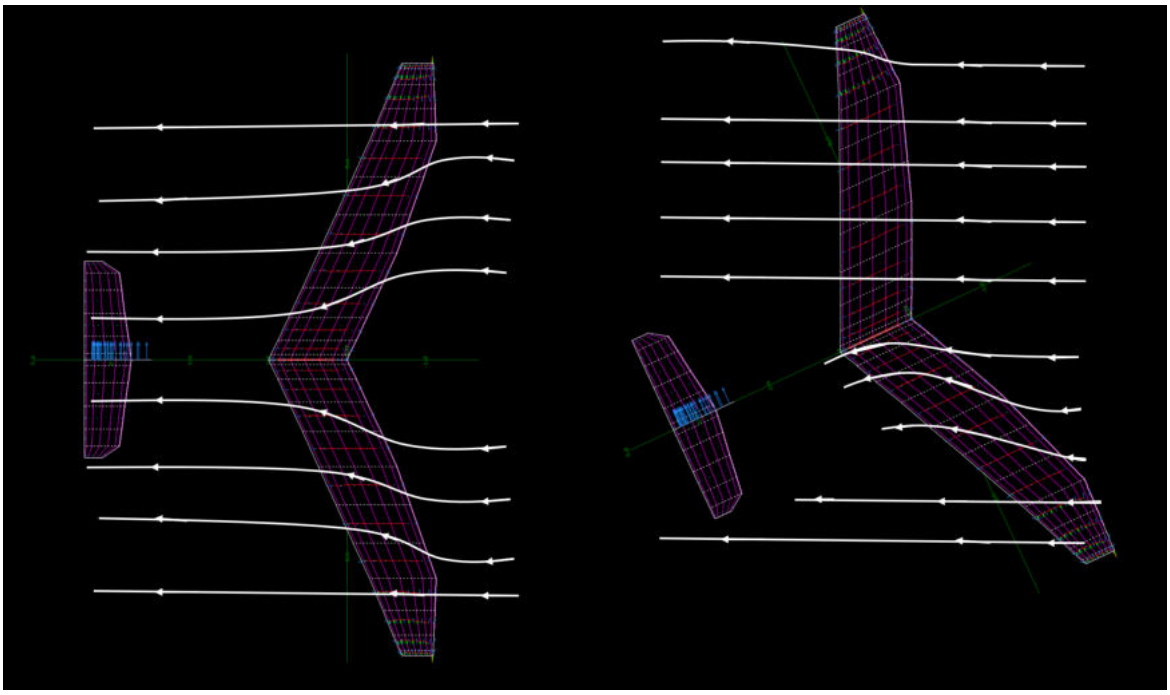

Fig. 5.30 Mechanics of forward wing sweep and the effect on the lateral dynamics. The advancing wing experiences an increased sweep angle whilst the retreating wing sees a reduced effective sweep angle

The rear sweeping wing as effectively reduced sweep, which will increase the lift and drag coefficients on the retreating wing. The increase in lift will induce a roll towards the side-slip and the increase in drag with further increase the side-slip condition, these two effects will excite lateral-directional instability.

Rearward wing-sweep has the opposite effect on the mechanics and dynamics and is already commonly used on transonic vehicles to reduce the effective Mach number. The rearward motion of the centre of pressure induces a nose-down pitching moment, this effect is exacerbated by the immediate reduction in lift as the wing sweeps rearwards. With rearward sweep the wing will tend to stall at the tip first, the manoeuvrability is reduced, the static margin is increased and the short period and phugoid modes are more heavily damped. Lateral-directional stability is effected with a tendency to excite the Dutch roll mode and damp the spiral mode.

5.6.2 Whole wing twist for roll control

Rotating the wing about the wing root changes the local angle of attack of the wing. This effective twisting or pitching of the wing can be used asymmetrically to generate a couple about the longitudinal axis to generate a rolling moment. Symmetric twisting of the wing alters the setting angle between the wing and the fuselage junction. The static residual of this is to change the longitudinal pitch trim of the vehicle whilst the dynamic response will drive a change in the angle of attack and directly control the lift generated by the main wing.

Asymmetric deflection works in the same fashion as existing aileron surfaces but effects the whole wing. The up going wing sees an increase in the local angle of attack and the down-going wing sees a reduction in the angle of attack. This asymmetry of lift sets up a couple and the vehicle will roll about the longitudinal axis. The aircraft will continue to roll until equilibrium is re-established by equalising the lift produced by the port and starboard wings. Unlike ailerons which only effect the local angle of attack about the small region of the wing where they are situated twisting the thing from the root effects the whole wing. Most aircraft have their primary ailerons situated outboard to maximise the distance component of the force couple, meaning the ailerons can be as small as possible. This means that the effectiveness of the control surface is reduced when the wing is more highly loaded towards the wing root, such as when flaps are deployed for low speed approaches. Large civil transport category aircraft typically have secondary inboard aileron control surfaces to assist in roll control in these configurations and at high speed when control forces are larger due to the increase in velocity component. Twisting the wing effects the whole lift distribution and will improve roll control in these situations.

AVL analysis predicts a linear control response for both the aileron surfaces on the WOT4 and for asymmetric wing twist (figure 5.26). Testing reveals that the ailerons have a linear response up to approximately 15 degrees beyond which there effectiveness begins to plateau (figure 5.26). The control gradient $\frac{dC_l}{d\delta_{aileron}} \approx 0.017$ as measured in wind tunnel testing is approximately double that which is predicted by AVL where $\frac{dC_l}{d\delta_{aileron}} \approx 0.007$. This might well be to do with 3D effects resulting in the ailerons having a greater influence on the global flow of the wing when compared to the vortex lattice simulation approach used by the AVL software. Twisting the wing effects the

aerodynamics quite differently in the wind tunnel compared to the simulated results. The control response is non-linear in nature. The control gradient $\frac{dC_l}{d\delta_{twist}}$ is non-linear with multiple inflection points which might correspond with changes in the flow. Between 0 degrees and 15 degrees of twist the slope is increasing up to an initial peak rolling moment of 0.3. The WOT4 wing has a thick section aerofoil that has a flat lift curve slope above the critical angle. The critical angle is found to be $\alpha_{crit} \approx 14°$ using a viscous panel method and $\alpha_{crit} \approx 16° - 18°$ experimentally in the wind tunnel. Combining the steady state $\alpha_{freestream}$ and the twist deflection means that the wing is reaching its critical angle at approximately 15 degrees of twist. The first inflection peak at 15 degrees seen in the wind tunnel analysis matches the approximate values predicted by AVL. Beyond which AVL predicts a linear continuation due to it not modelling the stalling behaviour. Above this value the control response curve demonstrates a noisy flat response which corresponds with the up-going wing being stalled. In this condition the up-going wing will stall before the down-going wing, with the WOT4s flat stall response there is no immediate loss of lift and so no change in the rolling response. On another aerofoil with a sharp loss of lift at the critical angle the lift of the up-going wing might sharply fall resulting in a control reversal at high twist angles meaning this approach might now be suitable for all wings. A second inflection point can be seen beyond 20 degrees of wing twist. At this point both the up-going and down-going wings will be deeply stalled and post stall dynamics will be affecting both wings. Additionally at this point the wing box is under considerable torque and the stiffness of the foam material construction of the WOT4 means that there is considerable deflection of the wing structure in this condition so the resultant changes in the rolling moment will be affected by the change in the aerofoil shape and wing structure under load.

5.6.3 Variable dihedral and variable stability

Changing the dihedral symmetrically effects the lateral directional stability derivatives with respect to side-slip angle; $C_{l\beta}$ and $C_{n\beta}$. It does this with small changes in lift and drag coefficient for small angles of dihedral. Some bird families like the pigeons *Columbidae* adopt a high positive dihedral in the glide. This configuration provides a method to passively stabilises the lateral direction mechanics and modes which would otherwise be actively controlled in flapping flight. This configuration is useful to alleviate the workload on a control system or pilot in phases of flight that demand high levels of stability (e.g. a straight glide through known turbulence).

AVL analysis (figure 5.27 predicts a flat $\frac{dC_L}{d\delta_{dihedral}}$ and $\frac{dC_D}{d\delta_{dihedral}}$ curves around small angles of dihedral both positive and negative before a reduction in both lift and drag at more extreme dihedral / anhedral angles ($> \pm 5°$. However the wind tunnel analysis shows a flat response in lift and drag up to angles of $\pm 15°$ with the drag curve having a hysteresis loop due to the dynamic nature of the wind tunnel control sweeps.

Figure 5.28 shows the plot of the lateral-direction stability metric vs dihedral deflection. The stability metric is described by the ratio of the relative magnitudes of the product of the rolling moment due to side-slide and the yawing moment due to yaw rate and the rolling moment due to yaw rate and the yawing moment due to side-slip. If metric is greater than one then the configuration has relative strong positive lateral stability against weak directional stability, this relationship will damp the spiral mode but may excite a Dutch roll response. If the metric is less than one then the configuration has relatively weak positive lateral stability and strong positive directional stability, this relationship will excite the spiral mode as the aircraft 'winds up' into a tightening turn. Because spiral modes tend to have longer time constants than the Dutch role modes they are easier to control either through direct piloting or through an inner loop controller. However in the cases where the Dutch roll modes are already damped due to airframe design stabilising the spiral mode will reduce the requirements of the control system. The WOT4s spiral mode sits on the cusp of stability depending on the angle of attack and achieves stability between dihedral angles of $\delta_{dihedral} = 2° - 5°$ with $\alpha = 0° - 10°$. The base wing has no dihedral or anhedral and this design decision likely achieves a sufficiently long time constant for the unstable spiral mode whilst sufficiently damping the Dutch roll mode to meet handling quality

requirements. The vehicle is also designed to fulfil the requirements of a basic aerobatic trainer, which include requirements for inverted flight and as such the straight section wing with no dihedral or anhedral is a sensible selection for the flight envelope. Symmetric variable dihedral can be both passive and active.

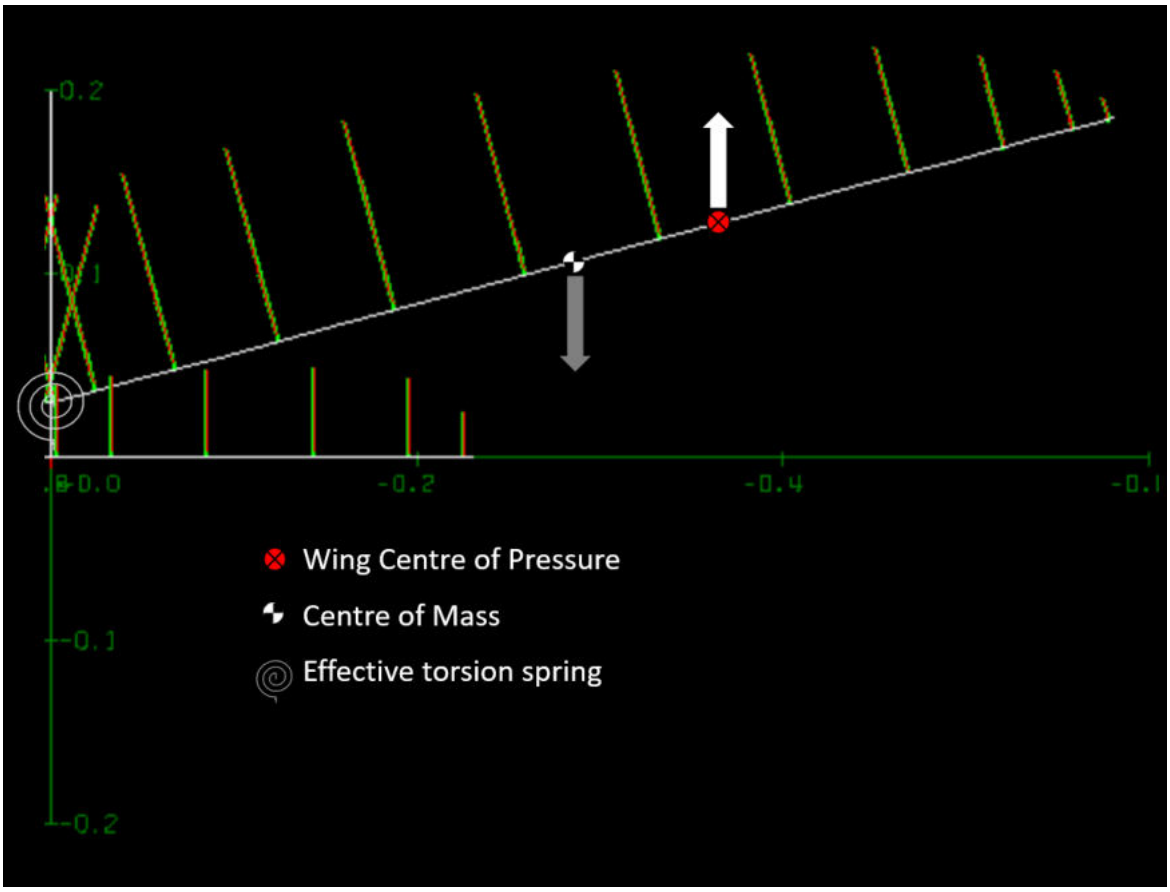

Fig. 5.31 Passive dihedral deflection acts as a suspension system in the body normal direction

If deployed in the passive sense the wing can be modelled as a spring mass-damper system with separate rotational freedoms about each wing (Figure 5.31). This will allow the wings to travel and rotate in the presence of a gust load perturbation, increasing the rise time in the body response and to the change in the flight path. This is a form of passive suspension which increases the time to perturbation and would allow the bird / vehicle time to make a control input whilst also reducing the normal acceleration or shock loading felt by the airframe, particularly as a wing root bending moment.

5.6.4 Asymmetric dihedral and turning

The main wings are independent of each other and as such the dihedral can be varied asymmetrically across the full span. This can be achieved in two ways, firstly the total dihedral angle between the two wings can be kept constant as they rotate around the body, or secondly, the relative half angle of one wing can be maintained constant with reference to the body whilst the other wing moves, this will change to total effective dihedral between the two wings.

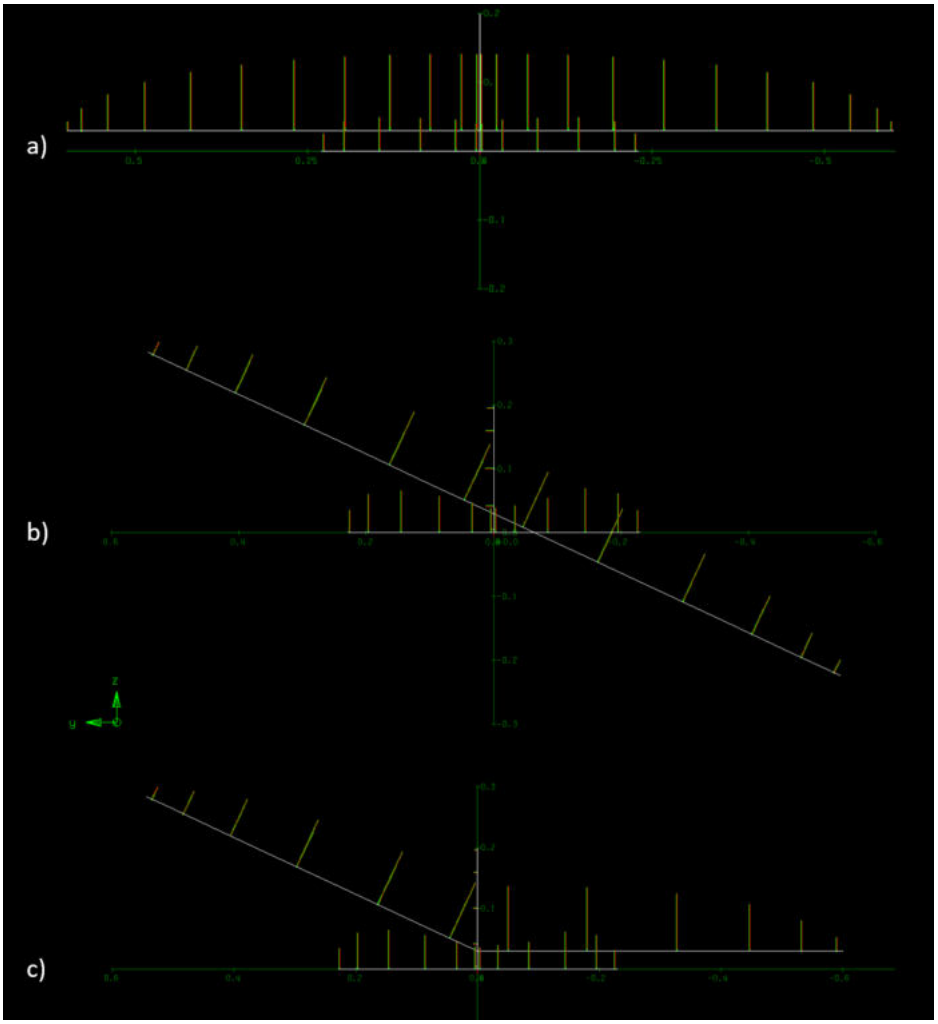

Fig. 5.32 Asymmetrical Dihedral effect: a) Conventional symmetrical wing, b) total angle constant - rolling the wing w.r.t the tail, c) half angle constant - raising one wing to induce lateral turning force

The first case (Figure 5.32 - b) is equivalent to the main wing rolling and the tail twisting in opposition, this tail twist is discussed in the next chapter. The change in

effective bank angle of the main wing whilst preserving the total dihedral angle will induce a normal dihedral response and a corrective rolling moment due to the change in span-wise lift distribution which will tend to roll the wing back so that the total lift force vector is vertical albeit now with the effects of the twisted tail.

This allows the motion of the wing-line angle relative to the world axis to be independent to that of the body and the tail and allows the wing to be somewhat decoupled from the inertia of the body. This will increase the rise time of any perturbation about the established flight path and allow the bird / vehicle more time to make a control input. Depending on whether the response is active or passive the wing could be modelled as a torsional spring - mass damper system with rotational freedom about the body (Figure 5.31). This allows the wing to act as a torsional suspension system, damping out span-wise asymmetric gust loading.

The second case (Figure 5.32 - c) acts to induce a rolls response in accordance to the increased effective dihedral angle. This will cause a restoring roll moment and simultaneously establish a larger dihedral angle and increase lateral stability. The airframe will tend to roll such that the total lift force vector is balance and vertical. This will leave the airframe with some residual angle of twist between the main wing and the tail. The effect of twist is discussed in the next chapter. In essence the response is the same as the first case whilst also changing the magnitude of the response as the total dihedral angle changes.

5.6.5 Comparison with traditional three axis control

The control schemes presented in this section are quite different to traditional three axis control schemes using discrete moving surfaces to locally effect changes in the lift coefficient. With the exception of wing twist the other two methods, wing-sweep for pitch control and variable dihedral, results in only small changes to the lift coefficient. Instead it is the change in the position of the centre of pressure and changes to the stability derivatives which are used to effect control and make changes to the flight path. The benefit of using existing lifting surfaces for control includes the elimination of discrete panels and the additional interference drag these generate. These mechanisms have exposed parts and gaps between the aero surfaces, in an optimised system the mechanism would be internal and any gaps sealed with compliant skins to full realise the benefits. By manipulating the main lifting surfaces the control forces can be very large and in some instances greater than is achievable with discrete surfaces. By using alternative control strategies it is possible to decouple the primary effect of controlling the flight path from the body orientation as is required using traditional control systems. For example when using the elevator to control pitch angle, the secondary effect is to make changes to the angle of attack of the main wing. As such a manoeuvre which demands a high positive pitch rate will be coupled with an increase in lift and subsequent increase in altitude. A manoeuvre such as a nose over tail tumble with only a small change in altitude is not possible in a rigid body aircraft with traditional three axis control. The application of elevator needed to generate sufficient nose up pitch rate would also drive an increase in lift resulting in a looping manoeuvre and subsequent changes in kinetic and potential energy. A wing-sweep for pitch control system can generate a large nose up pitching moment with only a small change in lift coefficient making such a manoeuvre possible. Symmetric twisting of the main wing can be used to effect global lift coefficient without effecting the pointing of the fuselage, allowing for gust rejection by 'spilling' excessive lift. Asymmetric twisting of the main wing acts up to the critical angle as a powerful roll control surface increasing the total roll power particularly in the low speed, high angle of attack regime. Twisting the wing beyond the critical angle would induce local flow separation and stall the wing leading to a possible control reversal as the stalled wing rapidly looses lift. This effect was not explored due to limitations in the experimental setup. This heave control without effecting the trim is not something that is possible with a three axis control system.

By considering the application of existing design features for control, additional functionality can be achieved for minimal penalties with regards to weight, cost and complexity. For example modern long-haul airlines are using folding wing-tip structures [118] to increase the aspect ratio of the main wing whilst still fitting the geometric constraints of airport gates. These folding wing-tips would allow for local changes in dihedral at the wing-tip, a feature that may be exploited for use in roll control [119] and a use case changes to stability and gust-rejection [120] has been shown. Of course there are disadvantages to such control schemes. Actuating major lifting surfaces means that the loads on the actuators may very large, resulting in heavy costly structures. The major lifting surfaces are typically a large proportion of the mass fraction of the aircraft. Whereas the demonstration aircraft used here have a foam wing and whose structure is very light weight, larger scale aircraft often use there wing structure to house fuel. Moving these surfaces would therefore contribute to considerable changes in the inertial properties of the vehicle, some of these change might well be useful in the form of weight shift control, moving the vehicles centre of gravity and by changing the vehicles rotational moments of inertia as the mass distribution can be moved towards and away from the centre of gravity. However some of these changes to the inertial properties may produces undesirable effects or indeed negate the desired control effects altogether. Taking the major lifting surfaces into post-stall aerodynamic regions may be undesirable and the design rules for these regions are not well defined. The aerodynamics in post-stall regions are highly geometry dependent and may be unpredictable. Whilst using a different control scheme opens up doors to previously unachievable manoeuvres it may also make some flight manoeuvres more difficult to perform.

Whilst such control schemes come with pros and cons it clearly pushes the envelope achievable through existing three axis control schemes. Coupled with other secondary control surfaces and thrust vectoring systems, main lifting surface actuation has the potential to increase the agility of certain types of aircraft operating at the limits of the three axis control envelope. By combining these control strategies with existing three axis methods it may be possible to move towards complete six axis control systems for aircraft; controlling rotation about the three principle body axis and the three translational motions (heave, surge and sway). Incorporating whole lifting surface control actuation into future control schemes should therefore be considered in the case of winged aerial vehicles with high agility requirements.

5.6.6 Review of methods

This section explores the potential of main lifting surface actuation for flight control. The approach involves using a 3D vortex panel method (AVL) to assess to effects of moving the main lifting surfaces. AVL is a program for the flight dynamic analysis of Rigid body aircraft and uses a linearised aerodynamics model combined with an inertial mass model. The configuration file which defines the main flight control surfaces is generated from a 3D CAD model and analysed in steps to recreate the effect of actuating the lifting surface. As such each step is a snapshot of a rigid body configuration and it does not account for the dynamic effects of actuating the model. Any dynamic effects are thus excluded and hysteresis behaviour is impossible to determine using this approach. This lack of time series information regarding control surface actuation is the main weakness of this method because time variant 3D flow structures are likely to dominate in the high alpha regime, an area which the vortex panel method does not model well. In order to validate the model for a range of deflections wind tunnel models are used based of the Bix3 and WOT4 airframes. The inconsistencies in the model used is unfortunate but was a necessary consequence of the Bix3 model fuselage being unsuitable for housing twist and dihedral actuation and the Bix3 wing being unsuitable to support the increase in asymmetric bending loads. The wind tunnel used in testing, the University of Bristol A1 wind tunnel is a closed return tunnel equipped with flow straightening gauzes. The working velocity range for the tunnel is 10 - 60 m/s in the working section so the tests conducted here are at the bottom of the speed range. The pitch-yaw rig used to test the airframes constrains the airframes in roll whilst having free and driven modes in pitch and yaw. Because of the nature of the roll constraints and the large bending moments generated at the wing-root when subjected to an asymmetric lift distribution, the degree of rolling moment that could be imparted to the airframe had to be minimised to preclude the risk of wing box failure. As such the full rolling power of the whole wing twist could not be fully explored. Given unlimited access to the wind tunnel facilities further testing could be used to better validate the AVL models however subject to the constraints of shared facilities the necessary validation runs have been presented in this chapter. To improve the validity of the results and to extend the analysis to more extreme dynamic manoeuvres the use of a common airframe and full computational fluid dynamic techniques, combined with improved airframe mounting for wind tunnel testing and associated free-flight testing would be recommended.

Fig. 5.33 Flight track of an approach and landing conducted using wing sweep for pitch control at Fenswood farm

It is worth noting that the requirement for free-flight testing was part of the design of the wing-box and actuation systems for all of the flight test vehicles presented here. All three vehicles have flown successfully and demonstrated the associated whole lifting surface actuation in free flight (Figure 5.33), but on these flights there were not instrumented to record the necessary information for presenting along side wind tunnel and simulated analysis. Should the requirement for free flight be removed the wing box and actuation structure could be considerably improved and instrumented more completely.

5.7 Conclusion

In this chapter, whole lifting surface actuation is proposed as an alternative and augmenting flight control system as inspired by the flight control laws presented in chapter 4 and chapter 5. Three different vehicles based on two different airframes have been modified to demonstrate the effect of wing sweep for pitch control, whole wing twist for roll control and direct lift control and variable wing dihedral for variable lateral directional stability and control. Simulations of the flight dynamics of these vehicles is conducted using AVL, a 3D vortex panel method and these simulations are validated using wind tunnel testing in the University of Bristol A1 wind tunnel on a two axis aircraft carriage instrumented with a 6 degree of freedom ATI F/T Mini 45 load-cell. The time series datasets are processed an presented using traditional rigid body flight mechanics and the effect of the whole lifting surface actuation is compared to three axis flight control schemes. The wing sweep for pitch control was found to be a powerful tool for controlling aircraft pitch, especially at high angles of attack, subject to additional changes in stability and loss of lift. However this control reconfiguration does effect the longitudinal stability of the aircraft, making a stable airframe unstable with just 12° of forward sweep. Whole wing twist for roll control seems to match the performance of aileron based roll control, but the limitations of the test rig are discussed and the additional capabilities of direct lift control are advantageous. Varying the wings dihedral / anhedral dramatically changes the lateral-direction stability of the platform and the effect on the spiral mode is particularly pronounced. By implementing whole lifting surface actuation control and using it to augment existing flight control systems it may be possible to move towards full six degree of freedom control system for winged aircraft and unlock new manoeuvring capabilities and extend the flight envelope for small aircraft with demanding agility requirements.

Chapter 6

Lateral control using a variable twist tail

6.1 Chapter Summary

Different species of birds use their tails in very different manners as part of their flying gait. This difference can be starkly contrasted between gulls (*Larus fuscus*) as covered in Chapter 4 and in the Red Kites (*Milvus milvus*) presented here. Some species, like the gulls, use flap-glide gait and fly for the most part with their tails furled. In this configuration the tail feathers are contributing very little to any controlling moments and the tail remain furled throughout gliding manoeuvres, only spreading during the most dynamic motions when the wings are typically being flapped as well. Other birds such as the red kites use a primarily gliding or soaring gait, with wings stretched and tails at full spread. These low and slow gust soaring specialists can be observed making many active inputs with their tail to control their flight. In this chapter the Rotational Stereo Videography method, as previously discussed in Chapter 3, is used to track a set of seven control points on the red kites bodies and fit these to a wireframe model whose relative positioning can be used to infer the position of the various lifting surfaces and make estimates of control inputs. Red kites make active use of their tail to steer and control their lateral flight by using it both independently and in conjunction with their main wing to induce and fortify lateral forces and moments. The applicability of a bird tail inspired control scheme is assessed in simulation using a 3D vortex panel method based on modified models of the airframes used to test the articulating wings in Chapter 5. The forces and moments are generated by a tail which is free to articulate about a ball joint at it's leading edge and has motion about a offset axis, aligned to the principle body axis and whose origin is at the conjunction of the fuselage and horizontal tail. The analytical results allow for an assessment on the design characteristics required for a small unmanned aerial vehicle to make full use of an articulating tail control scheme. Pitching the tail generates large pitching moments and alters the static balance of the bird. Twisting the tail is an effective in fine control of the total side force generated by the bird in a banked turn and

also contributes a yawing moment. Tail wag, or in-plane lateral deflection of the tail moves the centre of pressure and the line of action of the tail drag to contribute a stabilising yaw moment about the bird. An all articulating tail surface allows for additional coupled control schemes beyond the traditional three-axis scheme seen in most traditional small aircraft.

6.2 Chapter Structure

This chapter introduces the concept of the twisting tail and it's role in flight control. The lack of a vertical stabilising surface is a major difference between all bird species and many aircraft, requiring active control to stabilise the lateral directional modes, various stabilising strategies are presented. The results from fifty separate manoeuvring Red Kites are presented with the manoeuvres classified into three categories: Straight glide, Left turns and Right turns. Rotational stereo videography is used to fit a wireframe model to seven control points on the birds. The control surface positions are extracted; direction, range of motion and line of action were assessed and related to specific flight parameters. The relationships between the morphological variables and the flight path were used to infer the control schemes being used by the birds. An analytical model of a 3D pitching,twisting and wagging tail is developed adapted from the configuration of the Bix3 airframe. The tail model is assessed in straight and level glide to reveal the types of forces and moments it is capable of producing. The differences between the Red Kites and the Bix3 configuration are discussed and the revelations regarding how a small unmanned aerial vehicle might be designed to take full advantage of a twisting tail are presented based on the findings in this Chapter.

6.3 Introduction

When examining the turning performance of the gulls in Chapter 4, the rate of turn was found to be correlated to the bank angle of the bird in the glide. Qualitative observation suggests that for the gull species the tail plays only a small role in the control of their flight, being predominantly furled in gliding flight and unfurling during slow flight and flapping flight. Other species seem to use their tails very differently. Suggesting that just as legged animals display different gaits and locomotion, wing-borne animals may also have different flight strategies. The Red Kites extract every energy from turbulence in the lower atmosphere to soar for minimal effort. Their flight paths tend towards circling patterns and they appear to make substantial use of their tails to control their turning flight. The tails are typically unfurled (as seen in other species in the slow flight regime) and are twisted in relation to the body and the main wing throughout the turning manoeuvre. This twisting tail is a form of control quite different to anything employed in manned aircraft. In a traditional aircraft, turns are initiated by using a span-wise asymmetric lift distribution to role the aircraft into the turn, offsetting the total lift vector into the turn and inducing a lateral component of force into the direction of the turn. This turn is then maintained in level flight by increasing the angle of attack on the main wing so as to increase the total lift force, such that the component in the gravity axis matches the weight of the aircraft. This means the rate of turn of the aircraft is by necessity coupled to the bank angle and the method of inducing roll has secondary effects, yawing the aircraft which must be coordinated with additional control surfaces in the form of a vertical tail comprising a vertical stabiliser and a rudder. Birds obviously lack any form of vertical tail and so their approach to initiating and controlling a turn is clearly quite different. This chapter looks at the role of the tail in the flight of Red Kites and how this mechanism might be adapted for use in small unmanned aerial systems.

6.3.1 The role of the tail in bird flight

Conventional aerodynamic theory suggests that the highest efficiency wing, in terms of maximising the lift to drag ratio of a body in slow flight, is achieved by a single high aspect ratio wing [121]. The morphology of a single wing with no additional aerodynamic surfaces is seen in nature, bats have this morphology, but it is not typically seen in birds [122]. However, birds that spend a substantial time gliding on the wing do tend to a high aspect ratio main wing with smaller auxiliary lifting surfaces. This isn't always the case for species under selective pressure to optimise for flight performance [123]. Swifts and Swallows are aerial insectivores which rely on exceptional flight performance for survival and in these birds the tail feathers make up a substantial component of the lifting surface area.

So why do birds have tails? The tail is a consequence of evolution from reptiles, whose tails served a variety of purposes. The birds tails also serve a variety of purposes, not all to the benefit of flight performance. Sexual dimorphism is common in avian species, with tail ornaments being a common dissimilar trait which are used in behavioural and social interactions. The tail can also be seen to be used in ground locomotion for balance. The purpose of the tail under consideration in this chapter is it's role as an aerodynamic device and there are several ways the tail is employed to augment the birds flight control.

6.3.2 The birds tail as an aerodynamic device

In much the same way that terrestrial animals have different gaits, wing-borne animals also have different flying gaits and use their tails in different ways. Presented here are the four most commonly accepted theories of the role of the tail in flight control and how they relate to aircraft. Split flaps are an aerofoil modification for enhancing lift and drag. The lower surface of the trailing edge hinges downward from a point towards the leading edge while the upper surface stays fixed. This creates a large region of separation and stagnated flow immediately aft of the split. This affects the pressure distribution on the aerofoil and causes large changes to longitudinal trim. At max deflection the split flap acts much like a lower surface spoiler and contributes to a significant increase in the drag coefficient as well as a small increase in lift. It's purpose is primarily to increase the drag on an airframe to allow the body to decelerate and approach with higher power settings (important for missed approaches and escape manoeuvres). Some species of bird are thought to use their tails in this manner when approaching to land, unfurled tails vastly increase drag and help the bird to decelerate as they approach to land. ([124]) A pitch stabiliser uses a trim force to balance the longitudinal moments on a flying body to maintain straight and level flight. Passive stabilisers are found on aircraft which are statically stable and active stabilisers, using the control surfaces, are found on unstable aircraft. The question of static stability in birds is heavily debated [125]. It is likely species dependant and configuration dependant. It is known that some species of bird utilise a lifting tail, a configuration unlike a conventional aircraft. It is possible to be statically stable in this configuration providing that the lift curve slope of the tail is greater than that of the main wing, however there is no requirement for passive longitudinal stability as configuration changes and control inputs can actively stabilise flight. In slow flight (high alpha), the tail is unfurled which shifts the centre of area of the combined lifting surface aft. This increase the moment arm and the total area available to produce force. The centre of mass of the bird is not a fixed position and may span the centre of lift as the bird changes configuration. All of these characteristics imply a need for active pitch stabilisation and the need for an auxiliary surface through which to generate additional trim forces. Many aircraft make use of multiple lifting surfaces. The flow around a secondary wing effects the flow around the primary wing. Upwash ahead of the rear wing changes the effective angle of attack of the fore wing, reducing the fore wings contribution to the total drag whilst also contributing to total

lift production. Whilst this layout is not as aerodynamically efficient as a single high aspect ratio wing, if other requirements require a secondary lifting surface aft of the primary lifting surface, this configuration can be optimised for an improvement in lift to drag ratio. Many species of birds fly at low speeds with an unfurled tail and in this configuration the tail surface is acting as a drag reducing flap, increasing lift whilst also acting as a longitudinal trim control. Traditional aircraft have a vertical and horizontal tail as part of the empennage. The vertical tail is used for lateral directional stabilisation and control. Birds notably lack a vertical tail, suggesting active control and stabilisation of the lateral directional modes. Whilst the main wing can contribute to the lateral-directional control, the tail contributes a significant moment arm. There are different models of how the tail can be used in the control of the lateral directional mechanics. Some species appear to actively use the tail twist to induce control forces and it's that mechanism which is explored in this chapter ([68].

6.3.3 Aircraft empennage - Vertical tails

Vertical tails are an important part of a conventional aircraft's lateral-directional control and stability and are notably absent in natures fliers. The vertical stabiliser primarily performs four main functions for aircraft:

1. Directional stability - The vertical stabiliser provides a restoring moment in the presence of transient uncommanded side-slip.

2. Coordination of adverse yaw - Aircraft roll control creates asymmetric spanwise drag which induces an unwanted yaw component about the centre of mass, rudders are used to counteract this adverse yaw and maintain coordinated flight.

3. Directional control on take-off and landing - Aircraft require long ground rolls on take-off and landing, necessitating infrastructure that isn't always aligned with the direction of the wind, the rudder controls help to maintain positive directional control on take-off and landing in the presence of a crosswind condition.

4. Balance Asymmetric thrust and counteract engine torque and P-factor - The rudders provide a lateral force to oppose those generated by an asymmetric thrust condition, either in multi-engine aircraft with one engine inoperative or for the offset thrust line found in propeller powered aircraft due to the effects of torque and P-factor.

Of these four important functions only the first two generally apply to birds, where long ground rolls are not required for take-off and landing and asymmetric thrust is a function of flapping flight which is beyond the scope of this chapter.

6.3.4 Differences in lateral control strategy between species

With the role of the tail in bird flight being undefined and variable between different species. Gulls are flight generalists who use multiple flying gaits; flapping, gliding and flap-glide. Red kites are low altitude soaring scavengers who are typically seen to be gliding and soaring at low level using small updraughts to maintain height. Gulls typically fly with there tails furled without making visibly active use of it, whereas the red kites typically soar with an unfurled tail and can be seen to make active use of a twisting tail in their control of turning flight. The results presented here are discussed with particular attention on the implications that a bird inspired tail has for the design of small unmanned aerial vehicles.

6.4 Methods

Depending on the species the tail comprises a large fraction of the total lifting surface area of the bird. Actuation of the tail undoubtedly influences the flight control of the bird and this chapter looks at the different mechanics of tail actuation for flight control. Because of the distal position of the tail, lying on the longitudinal axis with symmetry about the vertical plane, forces can be generated by pitching and twisting the tail. Pitching the tail about a parallel lateral axis will change the effective angle of attack experienced at the tail. This mechanism is analogues to an all-flying tail or the trimable horizontal stabiliser found on aircraft. By varying the lift produced at the tail the bird would have control over it's pitch trim. Twisting the tail around the longitudinal axis moves the surface out of the vertical plane of symmetry it occupies. This action offsets the lift vector at an angle to the body normal axis. The force vector would still act predominantly though the centre of mass about the longitudinal, so would not directly induce a rolling moment. However the offset force vector will affect the total resultants of aerodynamic force acting to oppose the weight on the bird, and any centripetal accelerations in turning flight. By using this twisting mechanism the bird might be varying the total lift production to counteract small transient changes due to gusts. This gust offset could be used either to reject vertical acceleration in level flight or moderate the radius of turn in circling flight. Rotation about the third principle normal axis is the final rotation considered in this chapter. Wagging the tail around the normal axis also breaks the symmetry of the vertical plane. This wagging modifies the effective side-slip angle as seen by the tail and offsets the tails centre of pressure laterally off the longitudinal body axis. The increase in side-slip will tend to reduce the aerodynamic efficiency of the aerofoil and reduce lift whilst increasing drag. It does this by increasing the position and magnitude of the effective thickness of the aerofoil as experience by the flow. Offsetting the centre of pressure will exert a coupled roll and yawing moment as the lift and drag resultants are laterally offset. The rolling moment is is opposition to the tail wag whilst the yawing moment is in the same direction as the tail wag creating an adverse couple. This chapter builds on the techniques used in chapter 3 and chapter 4 to measure an analyse the effect of an articulated tail.

6.4.1 Rotational Stereovideography

In order to simultaneously record the flight path and flight control input parameters of the tail the rotational stereo videography (RSV) method developed in chapter 3 is used. In this situation where the emphasis is on the control input made by the tail, additional control points are used to establish and additional flight control vector in the form of the average tail line. Seven control points are tracked, (six measured and the seventh body centroid calculated) on the bird positioned as in figure 6.1.

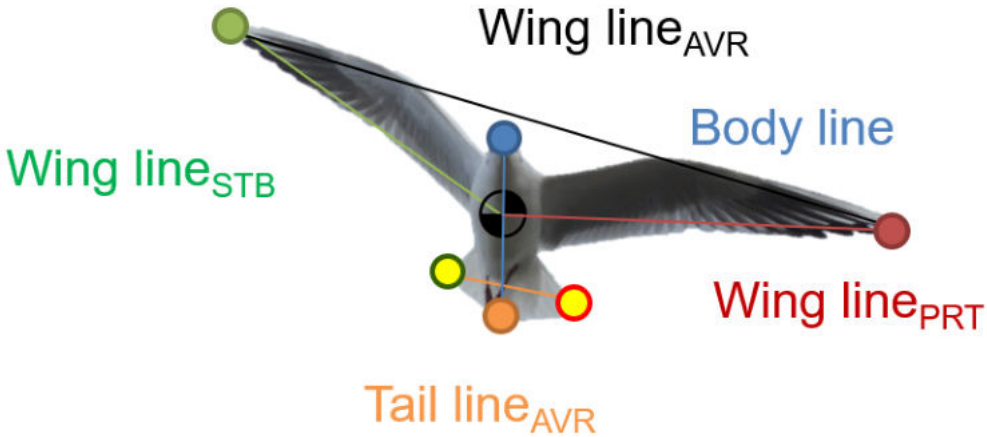

Fig. 6.1 The seven control points as established to make measurements of the tail geometry

The control points are grouped to establish the various morphometric vectors which are transformed to the body and world axis to establish the flight control parameters. The body axis are defined as before using the beak and tail centroid positions to establish the longitudinal axis with the lateral axis being parallel to the average wing-line and coincident with the centroid control point. The average wing-line is defined as the vector between the port wing-tip and the starboard wing-tip. The port wing-line is between the port wing-tip and centroid, and the starboard wing-line is between the starboard wing-tip and the centroid. The average tail line is established between the port side tail tip control point and the starboard side tail tip control point.

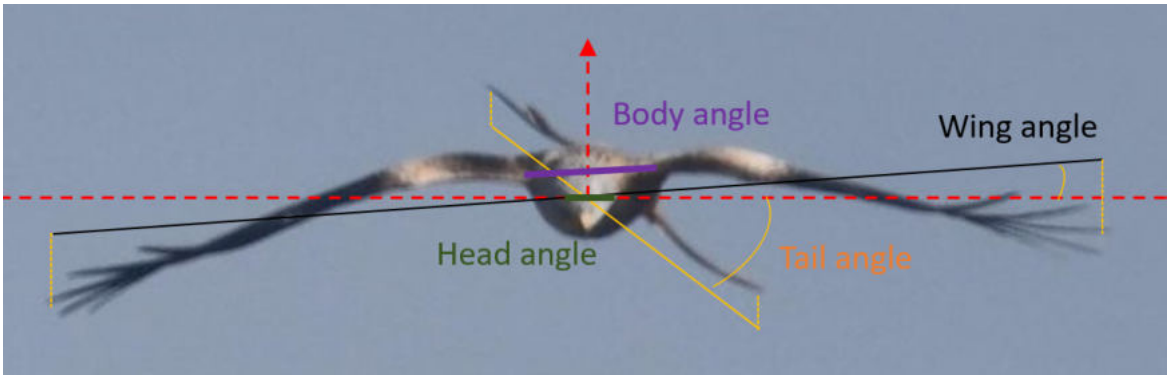

Fig. 6.2 Morphology parameters of interest with regards to performance

The lines defined by the seven control points are related to the horizon to establish the coordinate transform between the birds aero-surfaces and it's flight path (6.2). Where the tracked sequence allows, four additional control points where used to measure the head angle and body angle. Two points at the shoulder joints define a lateral body vector whose roll is independent from the wings, tail and head. The two eye points define a head lateral vector to measure head angle against the horizon. Body angle was measured to establish the relationship between this parameter and the wing geometry. Head angle is of interest for navigation purposes as other hawk species are known to use head stabilisation for flight guidance ([126]). Flight path parameters and air data are estimated from the derivatives of the positional data as previously discussed in chapter 3.

6.4.2 Field study

The results in this chapter are of a field study into the flight control of Red kites (*Milvus milvus*) and the role their tail plays in controlling the excitation of lateral directional dynamics. The red kite study quantifies the deflections of the aerodynamic surfaces and inspires a similar control scheme based on using an articulated tail for three axis control. The Red Kite is indigenous to the United Kingdom, an opportunistic carrion feeder which will occasional hunt small animals. It's range covers the whole of the United Kingdom, with the most successful colonies throughout the Welsh mountains and South Central England.

Fig. 6.3 The study location in Cholsey, Oxfordshire, UK

The birds recorded here were filmed soaring in Cholsey, Oxfordshire over the summer of 2021 6.3. The RSV camera system was positioned on the south side of the field with the field of view directed North to preclude the sun from shining directly onto the reflecting mirrors or camera lens. The birds manoeuvred along the tree line and out into the field. Each manoeuvring sequence is a selected flight manoeuvre either being a straight glide, left turn or right turn. To improve consistency and to reduce the signal to noise ratio in the measurement each manoeuvre is averaged over 25 frames (0.5 seconds at 50 frames per second). The average position of the seven control points is recorded and the average body morphology vectors are established. The relationship between changes in the position of the wing and tail surfaces and the effect on the flight path is noted. Fifty discreet manoeuvring sequences were extracted from twenty individual flights recorded in three separate recording sessions.

6.4.3 Analytical modelling

AVL modelling is used to assess the effectiveness of each control strategy as applied to a small unmanned UAVs. The vehicle on which the model is based is Bix3 model used earlier in chapter 5 the tail sizing is consistent but has the ability to rotate. In the AVL model the empennage is modified to allow for three axes of rotation about a point located on the vehicle centre line at a point coincident with the leading edge root of the vertical stabiliser. Model geometry is shown in figure 6.4.

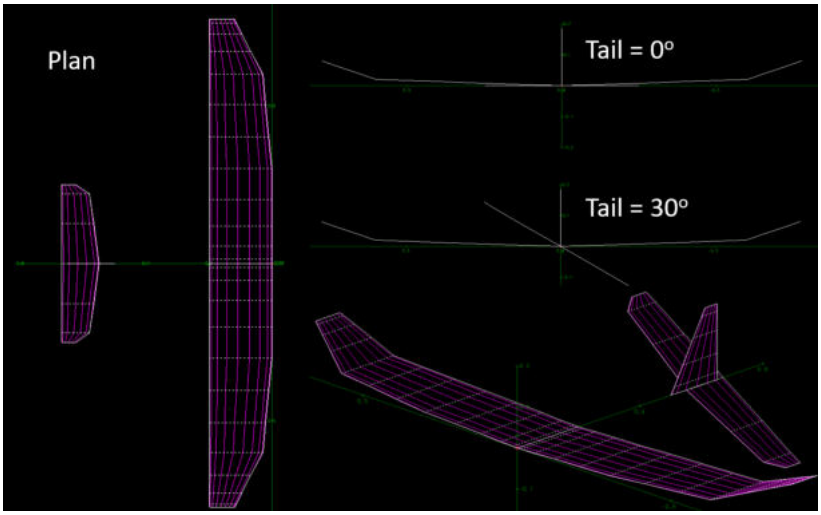

Fig. 6.4 AVL model of the Bix3 with a modified three-axis all flying tail.

The AVL geometry is updated and batch run against predefined flow characteristics to compute the resultant forces and moments acting on the vehicle. This analysis is used to assess the type of control available to the vehicle using the following control schemes. The articulated tail study presents the results of analytical modelling and the results are grouped by longitudinal and lateral-directional functions.

A new parameter for the assessment of tail effectiveness is the tail side-force coefficient.

$$C_{Y_{ff}} = \frac{Y}{\frac{1}{2}\rho V^2 S} \tag{6.1}$$

The side-force coefficient is the lateral component of the total body aerodynamic force normalised for dynamic pressure and surface area. This is measured by fluid accelerations in the far-field through a Treffz plane.

6.5 Results

The following results are extracted from RSV datasets similar to those already presented in chapter 3 and 4.

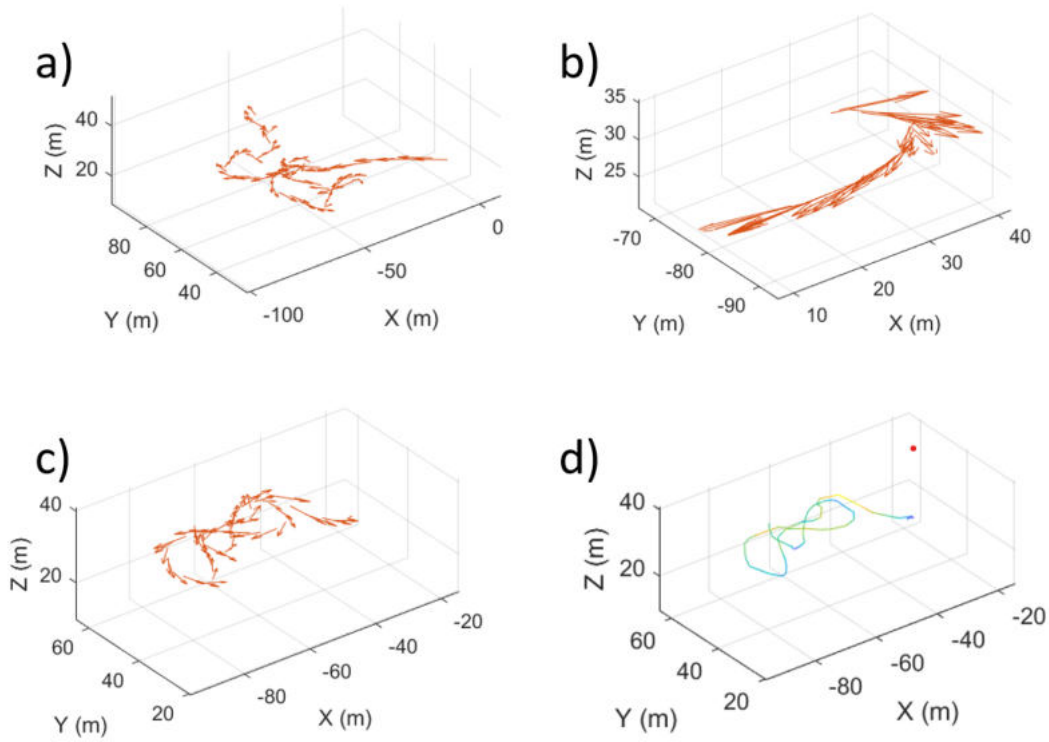

Fig. 6.5 Example soaring flights of Red Kites in Cholsey. a), b) and c) show examples of manoeuvring flight with instantaneous velocity vectors. d) shows the flight path of c) colour-coded by absolute acceleration

Figure 6.5 shows an example soaring flights of the kites from which manoeuvring data was extracted.

The envelope for each flight control metric can be displayed as a histogram, this gives some idea of the range of the main wing and the tail and of the relative motion between them. For each histogram positive values indicate a port side wing low and negative values indicate starboard wing low.

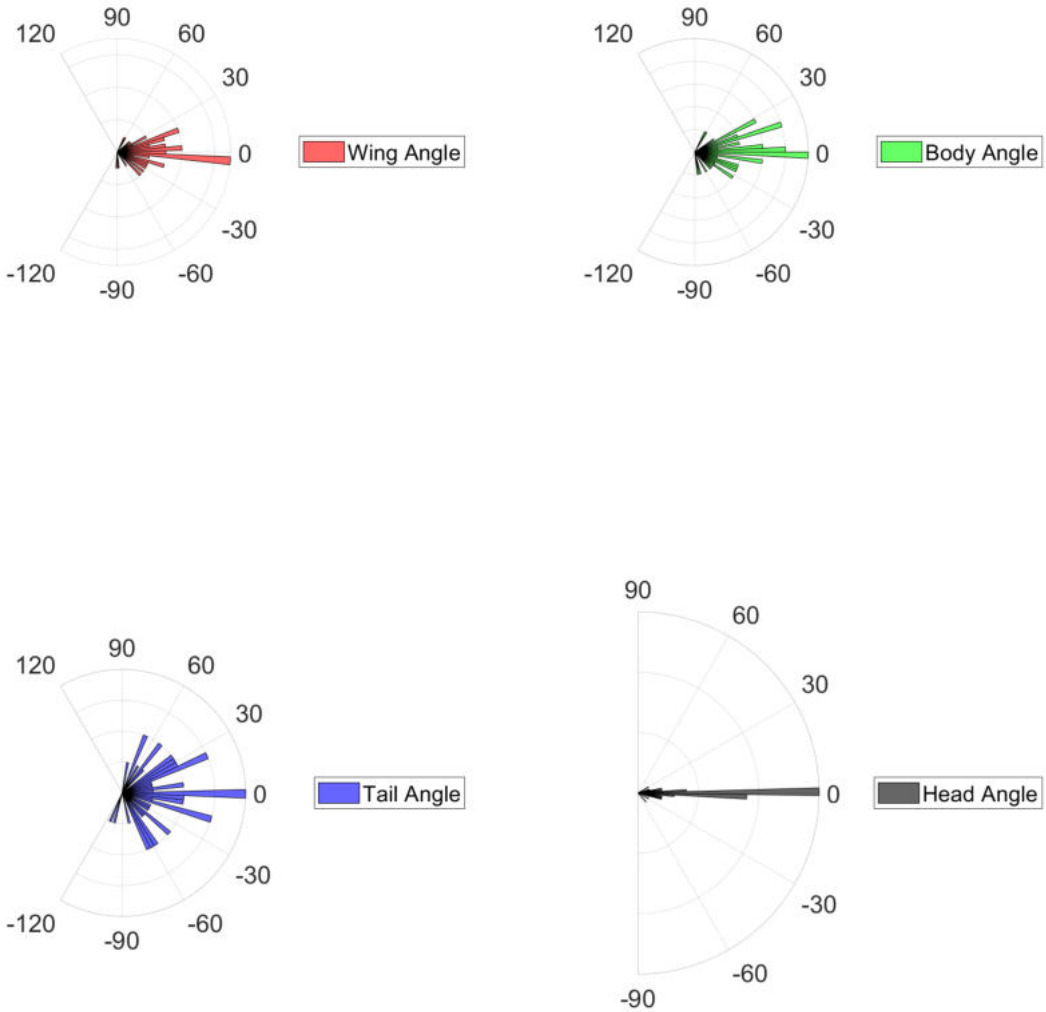

Fig. 6.6 Histogram of Wing, tail, body and head angles as measured from Red kites in flight

Plotting the wing angle against the tail angle reveals the augmentation of the tail.

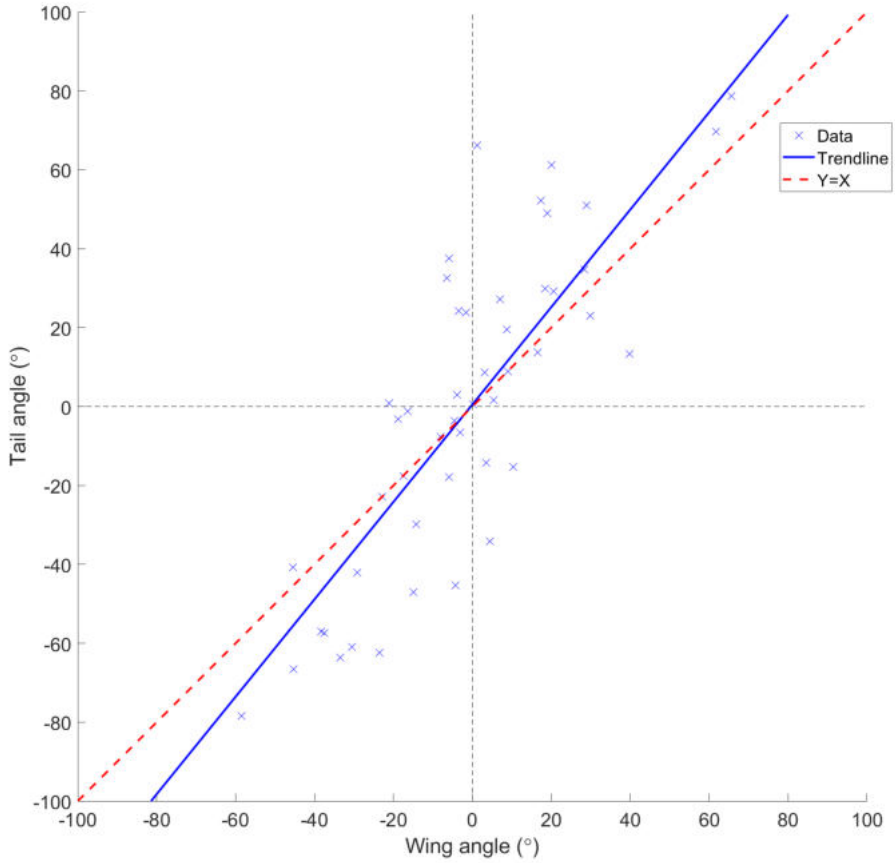

Fig. 6.7 Main wing vector against tail wing vector showing the pro and counter rotation of the tail

For positive wing angles, tail into turn is indicated by all points above the equal function (y=x) line and for negative wing angle into turn deflections are below this line. All other points are considered to be counter rotated tails acting out of turn. Note the spread around small angles of the main wing (bank) which shows the tail deflecting in straight flight. In the positive-positive quadrant, points above the y=x line indicate an increase in effective bank angle and pro turn tail deflection, in the negative-negative quadrant points beneath the line show pro-turn tail deflection.

Plotting main wing angle against the relative angular displacement between the main wing and tail reveals the envelope of the coupled flight control scheme, enclosed by a diamond pattern, showing greater achevable relative tail deflection at low angles of bank reducing with increasing bank angle towards zero relative deflection at approximately 60 degrees angle of bank.

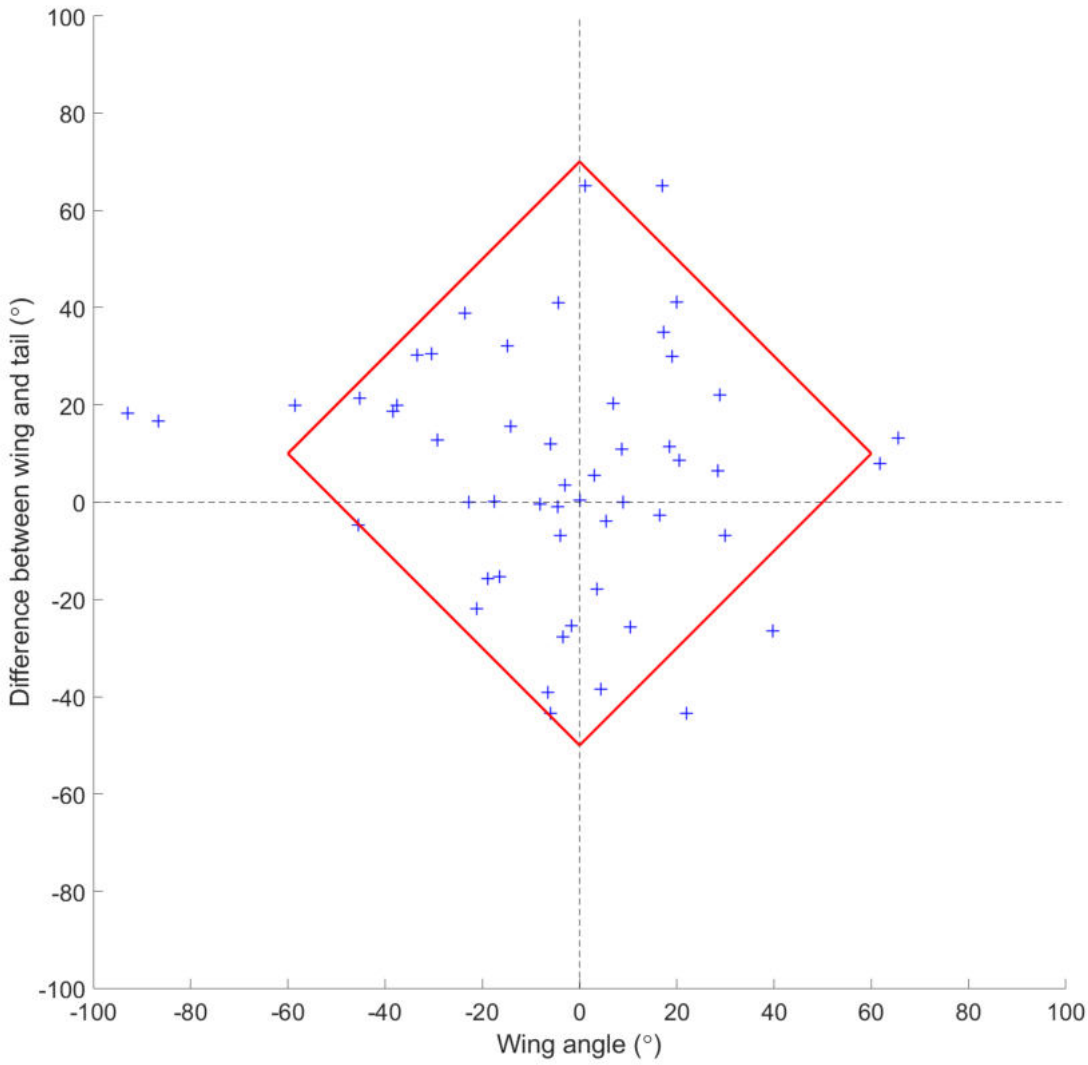

Fig. 6.8 Main wing vector measured in the world axis vs the relative angular displacement between the wing and tail - The flight control envelope

6.5.1 Tail pitch for longitudinal control

The articulated tail can be actuated in pitch to control the longitudinal dynamics. This is similar to an all-flying tail or stabilator arrangement. The lift, drag and pitching moment coefficients can be compared to an equivalent discreet elevator based control scheme.

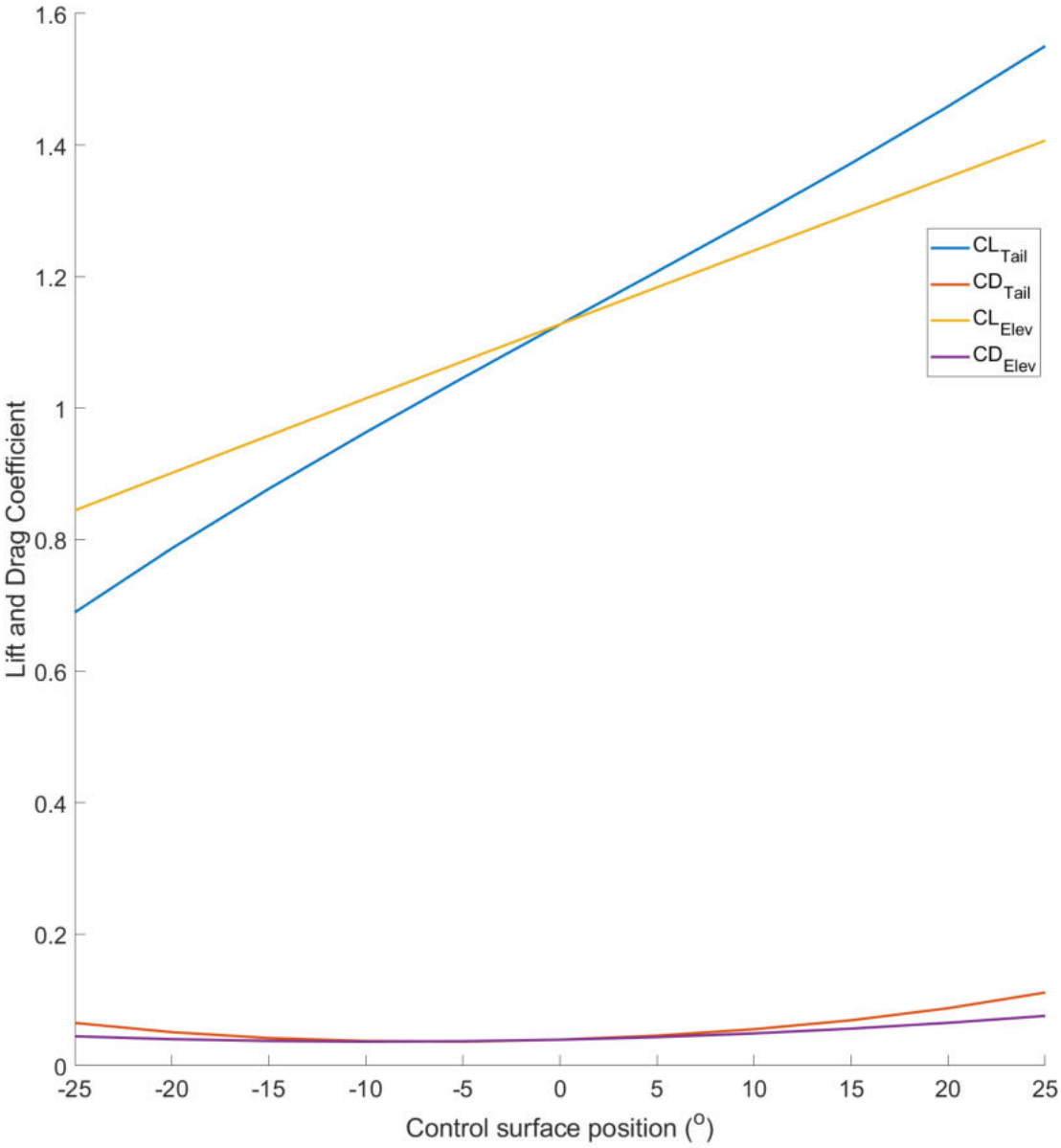

Fig. 6.9 Lift and Drag coefficients against control angle deflection for a pitching tail and elevator model.

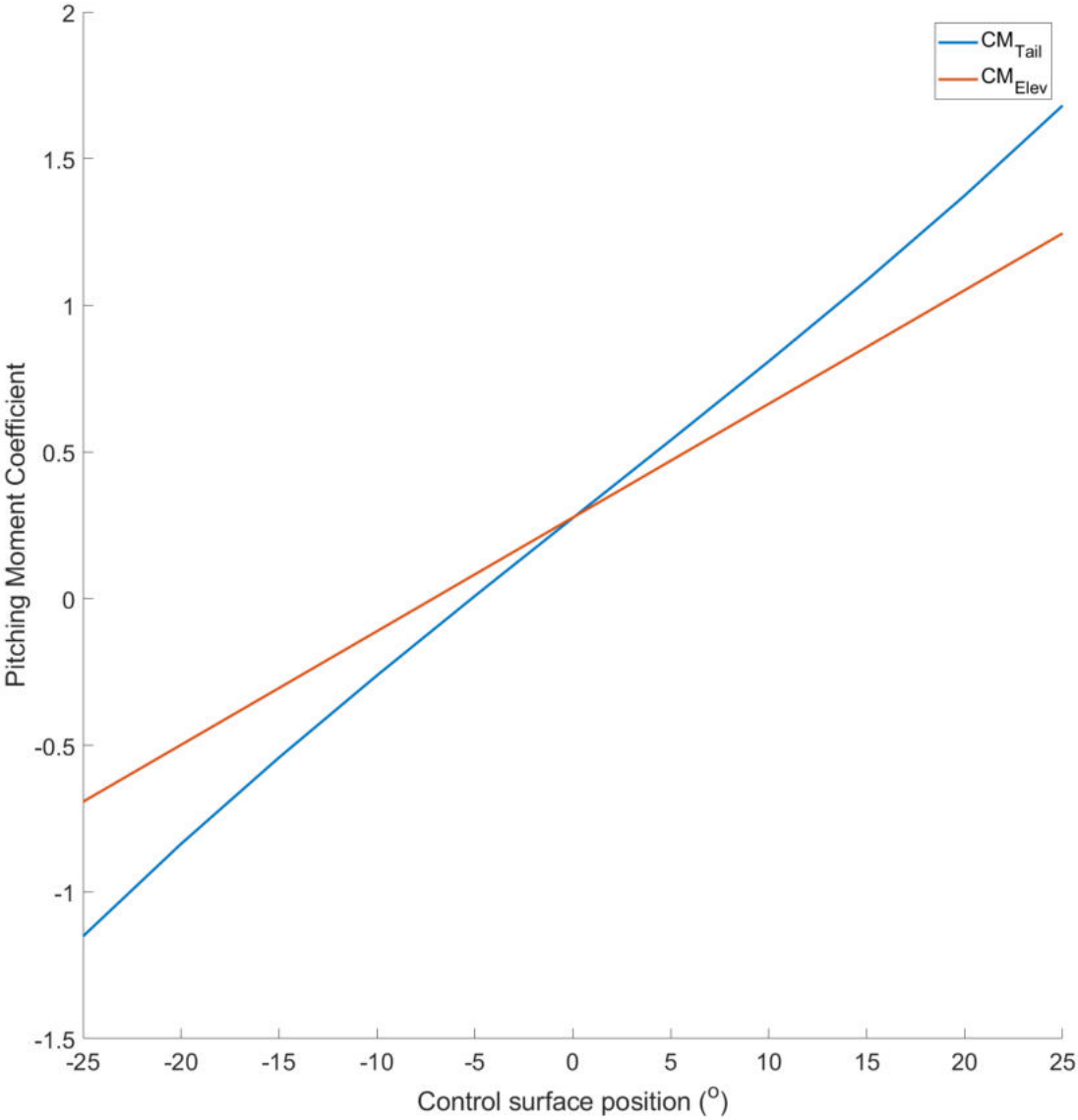

Fig. 6.10 Pitching moment coefficients comparing a pitching tail to an elevator

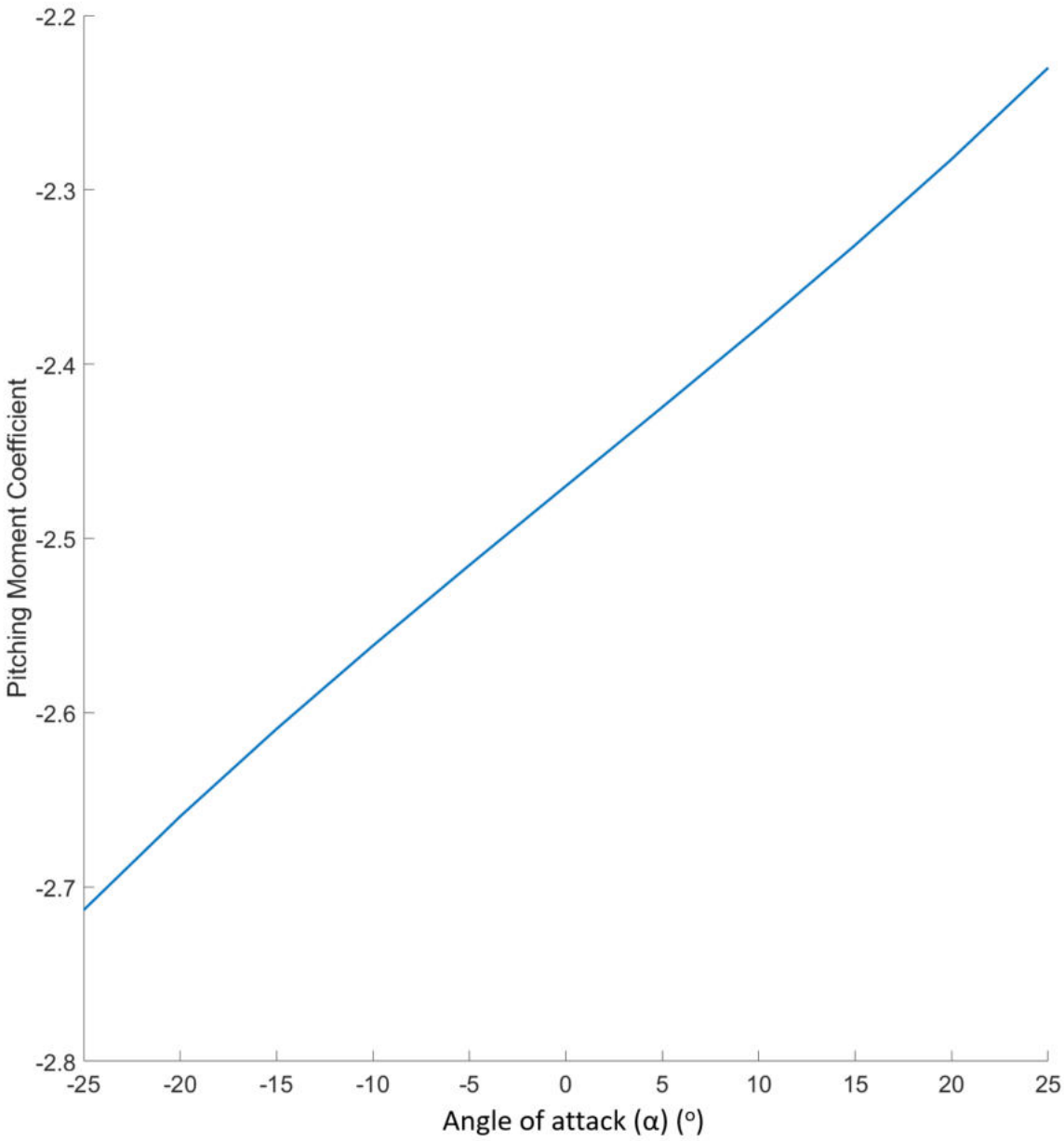

Fig. 6.11 Pitching moment coefficients for a pitching tail with respect to angle of attack

The all flying tail shares the exact same geometry with Bix3 horizontal tail with a continuous surface and no hinged discreet elevator. The larger wetted area of a full flying tail modelled here results in greater control power as seen in Figure 6.9, Figure 6.10 and Figure 6.11. These figures plot total vehicle lift, drag and pitching moment curves comparing the effectiveness of the all pitching tail to that of a conventionally sized elevator control surface. In this model the all flying tail simply acts as a larger control surface in relation to a fixed wing. The tail curves have similar shapes to that of the elevator with increased slopes indicating the increase in control power which is expected when increasing the size of the control surface. Figure 6.11 shows a stable trend in pitching moment, the $C_{M\alpha}$ is negative for all angles of tail pitch. Post-stall behaviour of the different control surfaces are not reached.

Whilst the two surfaces share the same geometry there are limitations to direct comparisons between them. Whilst total lift and pitching moment induced by the all flying tail at a given angle of attack are both larger in magnitude than for the elevator the drag is also substantially increased. The pre-existing elevator control surface would have been sized for a particular set of aerodynamic characteristics to meet a set of aircraft performance requirements. For example improving pitch control with the all flying tail could also be achieved through a larger elevator sizing, however a direct comparison is not the purpose of this analysis. Instead this analysis highlights that large control moments can be generated without any need for substantial geometry changes and all flying surfaces do extended the magnitude of the induced control moments. The main limitation in this method is that the geometry is defined from a model designed for a discreet elevator surface, further improvements may be had when designing for an all flying tail from the offset.

One of the main differences between the pitching tail and elevator control scheme is the amount of surface that can be substantially deflected into the flow, changing the flow physics acting on the surface.

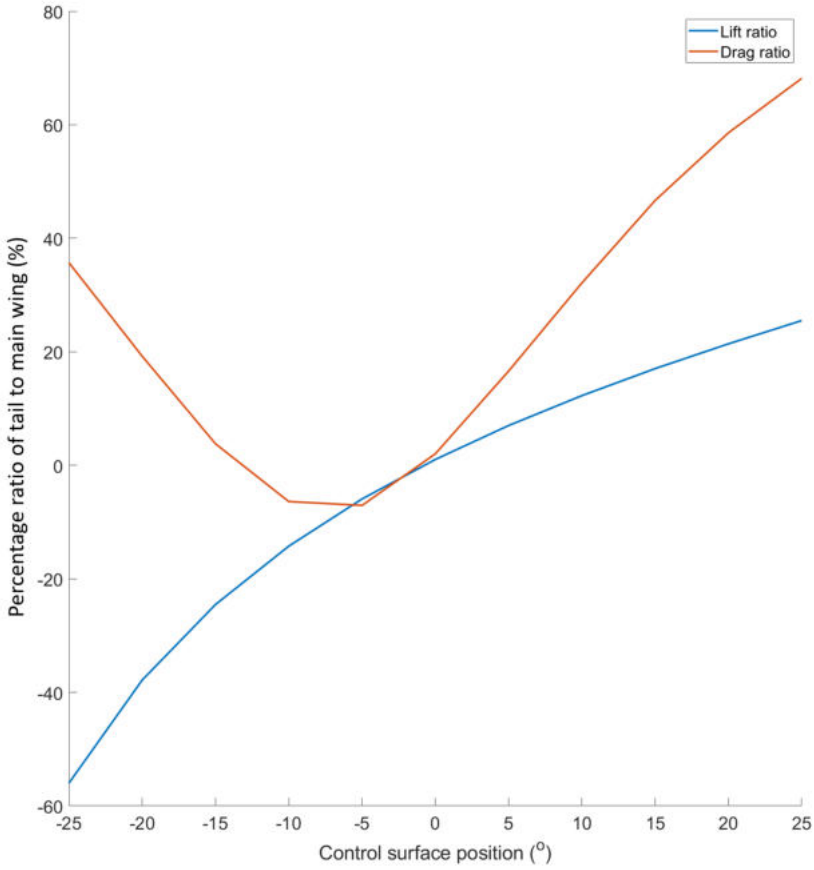

Fig. 6.12 Main wing and tail lift and drag coefficients as a percentage of the total lift and drag of the body

Figure 6.12 shows the percentage ratio of lift and drag expressed as a percentage (0 - 100%) provided by each surface and also shows how the global centre of pressure shifts as the surfaces are deflected. An optimum configuration for gliding where the tail produces the least amount of drag exists when the tail is slightly deflected up by five degrees. In this configuration the tail is producing near zero lift, contributing very little to the total drag and the combined aero surfaces are acting like blended wing body.

6.5.2 Tail twist for lateral directional control

The tail can be articulated about two separate axes to induce lateral directional control. Twisting the aircraft about the longitudinal axis primarily creates a side-force to oppose / induce a side slip.

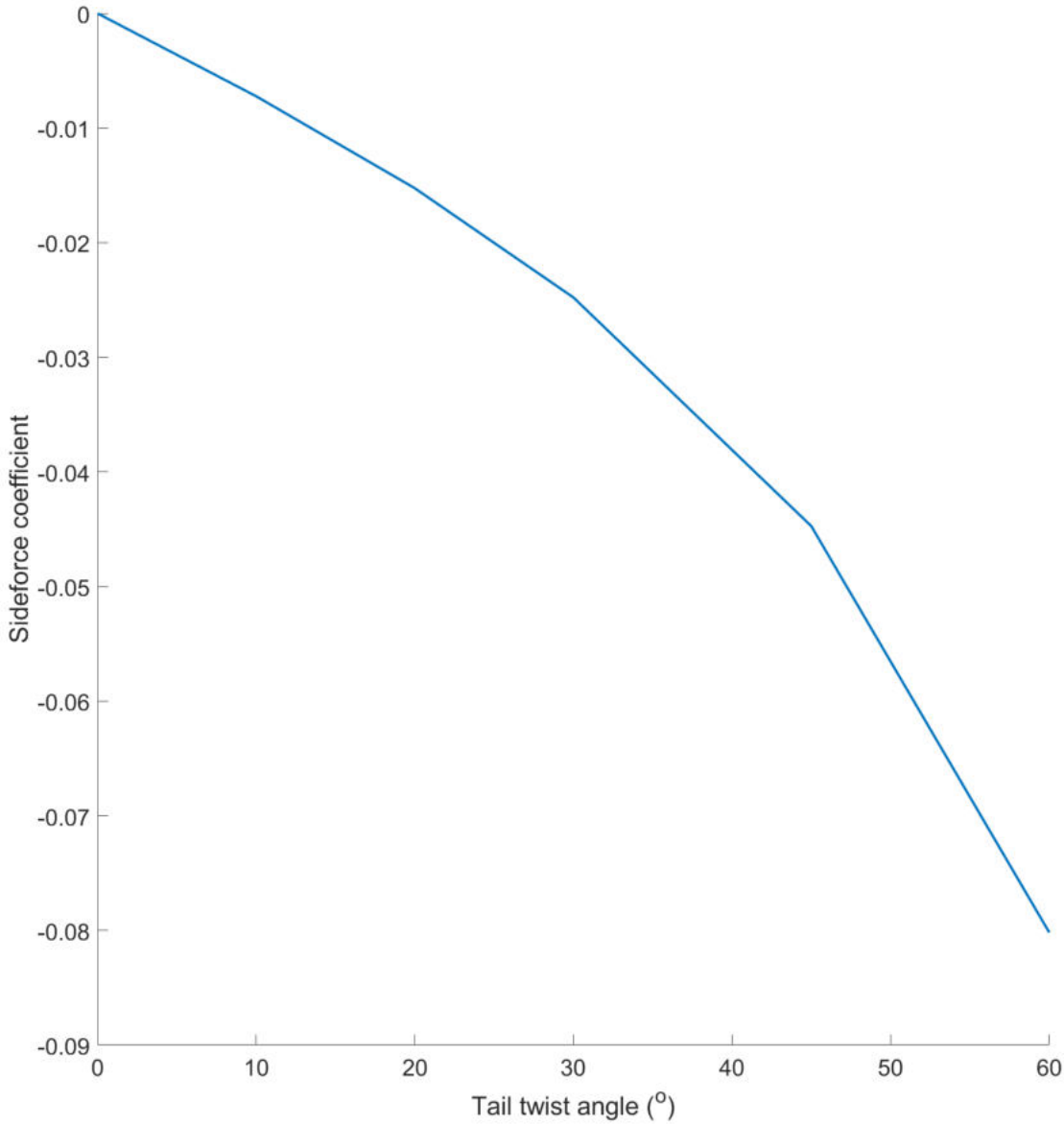

Fig. 6.13 Side-force as measured in the Treffz Plane as a function of tail twist angle

Figure 6.13 shows the coefficient of side-force as measured in the downstream wake. This residual measurement is indicative of the side-force as measured in the aerodynamic stability axis and is indicative of the lateral directional performance, both in terms of turn radius and in as to initiate / oppose a side-slip. The force is non-linear with respect to tail twist angle.

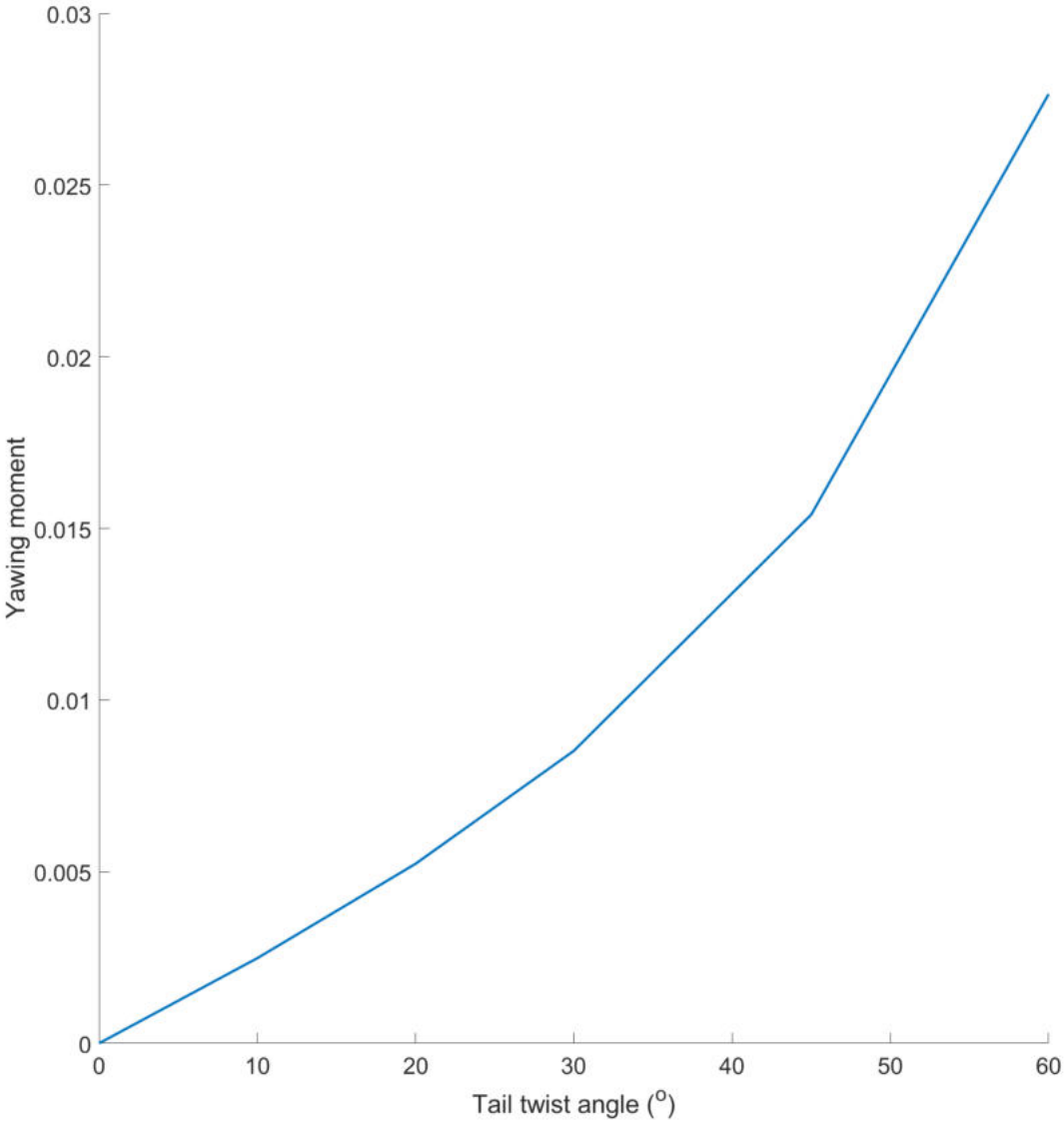

Fig. 6.14 Yawing moment induced by twisting the tail

The side-force induced at this position contributes a yawing moment which is proportional to the cosine of the tail twist as shown by the curve in figure 6.14.

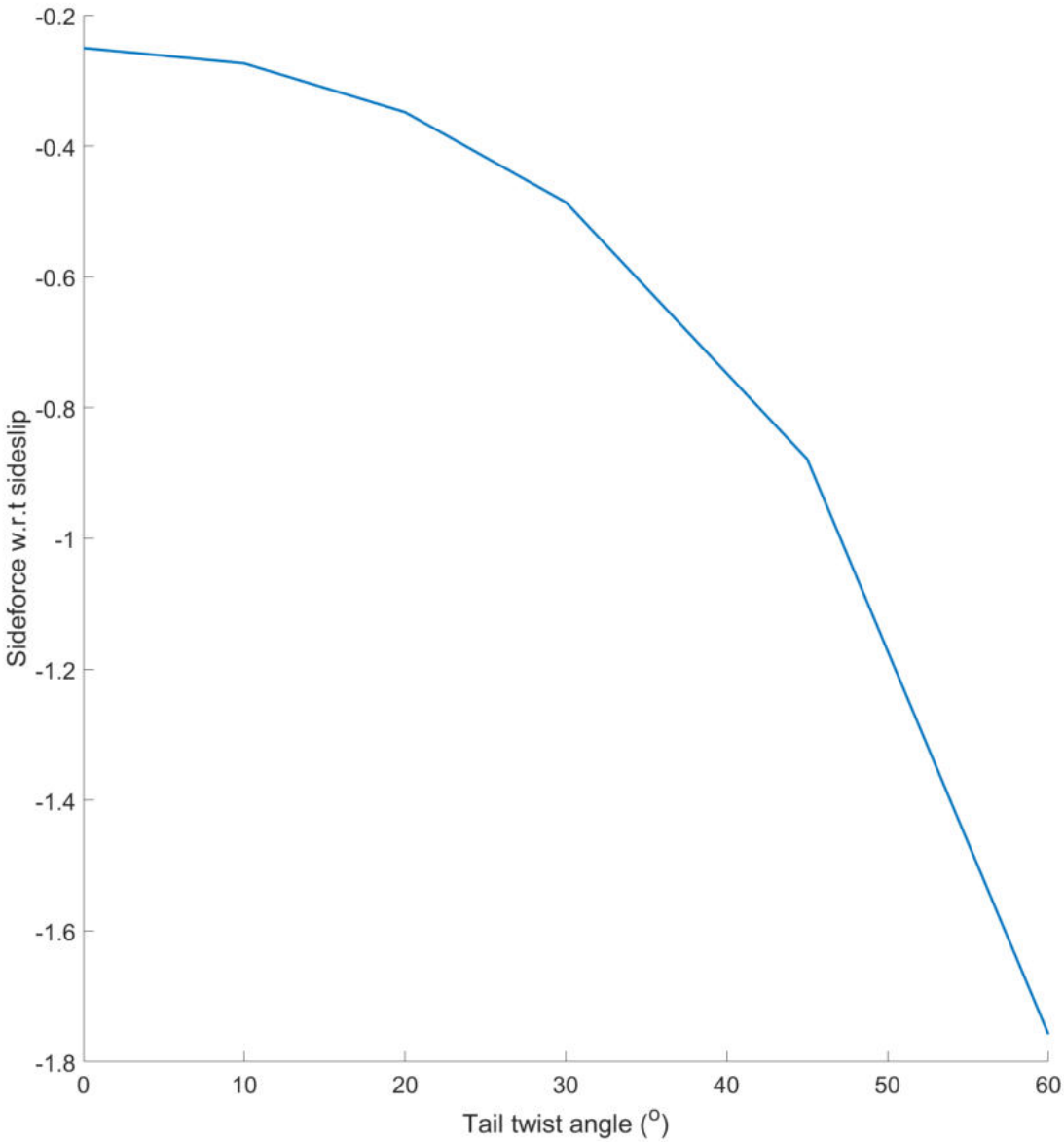

Fig. 6.15 Coefficient of side-force with respect to side-slip angle (β)

In Figure 6.15 the gradient of side-force grows as a function of side-slip with increasing tail angle. This function will be maximum at 90 degrees at which point the twisted tail has become a vertical stabiliser with respect to the aerodynamic axis.

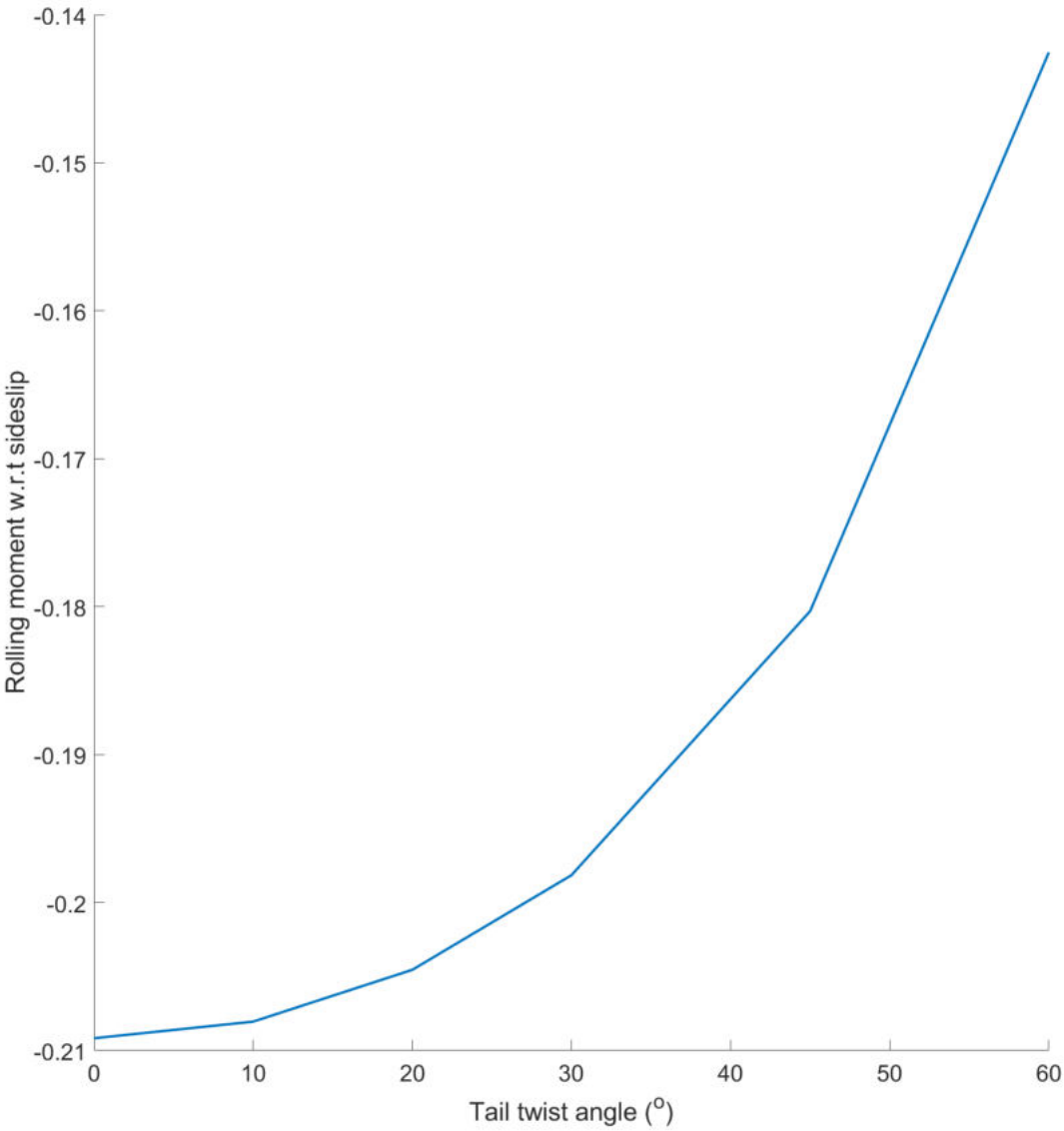

Fig. 6.16 Coefficient of rolling moment with respect to side-slip angle (β)

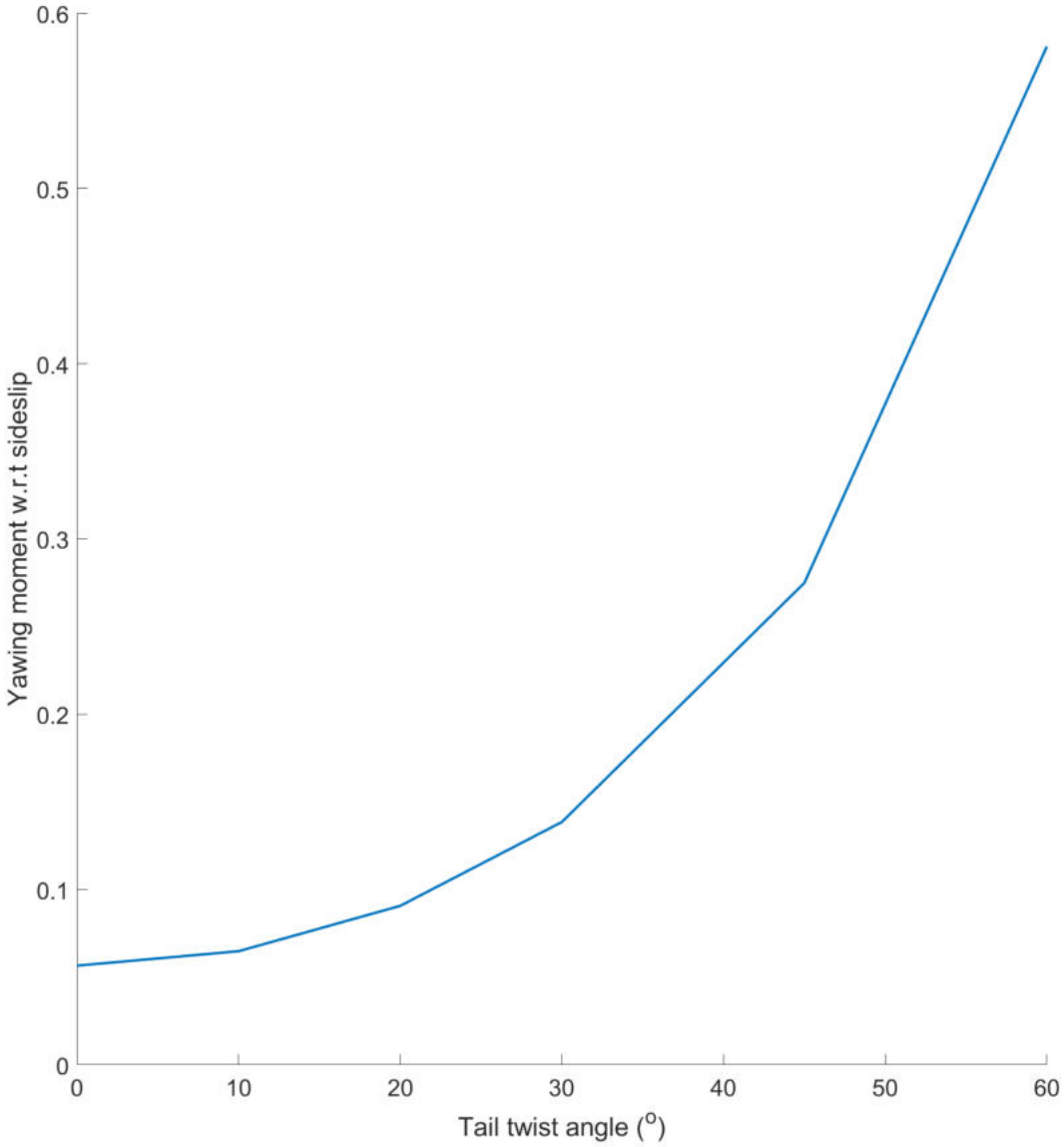

Fig. 6.17 Coefficient of yawing moment with respect to side-slip angle (β)

The coefficients of rolling ($C_{l\beta}$) and yawing ($C_{n\beta}$) moment with respect to side-slip angle are effected by the tail twist angle. Figure 6.16 and Figure 6.17 show how both of these derivatives increase in relation to the increasing tail twist.

The rolling moment with respect to side-slip (Figure 6.16) is non linear and acts in opposition to the direction of tail twist. The magnitude of the moment decreases as the tail twists towards the vertical. As the tail twists towards ninety degrees the effective angle of attack experienced by the tail as a function of side-slip is reduced, in turn reducing the counteracting rolling moment towards zero.

The yawing moment due to side-slip (Figure 6.17) has a positive relationship which increases as the tail twist angle approaches ninety degrees. At ninety degrees the tail is effectively a vertical stabiliser who's centre of pressure is after the centre of mass and the restorative moment of the tail is at a maximum. The fact the tail sits aft of the centre of mass means that there is a positive non-zero restoring yawing moment with respect to side-slip even at zero angle of tail twist but this increases considerably as the tail twists away from the vertical.

Tail wag comprises a rotation about the normal control axis, the effect is to offset the centre of drag away from the plane of symmetry and to establish a yawing couple. The effect is subtle and configuration dependant. The Bix3 isn't suitably configured to benefit from this effect and so it is discussed further in the next section.

6.6 Discussion

The results presented in this chapter examine the role of the birds tail in manipulating flight. The role of the tail can be qualitatively identified as being species dependant. Gulls and Red kites use there tails quite differently as part of their flying gaits. Whereby the gulls tend to fly with furled tails, the red kites soar with spread tails and make large active corrections with their tail. The objective is to better understand the mechanics of the tail in flight and how it can be used to inspire control schemes that offer benefits over the traditional three-axis systems based on discreet flight controls. The red kites tail makes up a large proportion of its lifting surface and it is configured in a positive lifting arrangement in opposition to how most traditionally stable manned aircraft are configured, with the horizontal tail producing negative lift. When examining the role of the tail in traditional aircraft the tail is split into a horizontal and vertical surface which perform a number of functions.

The horizontal tail provides longitudinal trim and control based on the actuation of either the whole surface or a discreet part of the surface to modify the local angle of attack and production of lift. The vertical tail provides lateral directional stability and control, to overcome adverse yaw, asymmetric flight and to maintain direction on take-off and landing in the presence of a cross wind. Whilst birds are not totally unique when compared to an aircraft's configuration they are certainly unconventional. Tailless aircraft exist and achieve lateral-directional stability by means of active control. However birds are not simply tailless, merely lacking in a vertical tail. This is a configuration not widely seen in aircraft, most tailless aircraft employ a single flying wing design. Perhaps the best known example of a tailless aircraft which is not a flying wing and does not rely on any auxiliary vertical stabilising surfaces in the X-36 'Tailless Fighter Agility Research Aircraft' [127] an experimental X-plane developed by McDonnell Douglas in the later 90s. This design still differs substantially from a birds platform with forward canards and used thrust vectoring for directional control and operates in a radically different flight regime.

Presented in this section are the main contributions of this work into understanding how one species of bird (*Milvus milvus*) use their tail as part of their lateral directional control scheme and provides some considerations as to how this might be implemented on a small unmanned aerial vehicle.

6.6.1 Why birds don't need vertical tails

A vertical tail or surface is not a requirement for lateral directional stability [66]. Providing the rolling and yawing moments with respect to side-slip $C_{l\beta}$ and $C_{n\beta}$ are sufficiently large then yaw stiffness and damping are managed and the spiral dynamic mode is stable. Most species of bird have a high level of dynamic stiffness about the yaw axis. This is due to the relative effectiveness of the yawing moment of inertia and the restoring aerodynamic moments at small physical scales. The yawing moment of inertia reduces more quickly that the aerodynamic moments at the scale of birds. The other prime consideration for lateral direction control is that of adverse yaw, or indeed the control of desired side-slip. Adverse yaw is typically the resultant of an asymmetric span-wise increase in lift induced drag acting distal from the body producing a yawing moment which opposes the rolling moment generated by the asymmetry in lift. For tailless aircraft it is desirable to also be able to induce pro-verse yaw through the manipulation of the span-wise aerodynamic forces and this effect is particularly pronounced if the wing adopts a bell-like lift distribution to allow the wing tips to produce a component of thrust, such as the arrangement in the PRANTL-D wing design [128]. This effect is similar to a rotor in autorotation with a highly twisted (washed out) wing which is being driven inboard and driving (producing thrust) outboard. Adopting the bell like distribution causes the wing-tips to experience an up wash. Inboard the lift vector will be rotated aft producing lift-induced drag as is the general result from an elliptical distribution. Outboard the tips are twisted to induce a fore facing component which is described as lift induced thrust. The total net effect on the wing will be induced drag, at a magnitude which is greater than that produced by an ideal, elliptical, distribution. However the thrust components at the wing-tip can be modulated to induced pro-verse yawing moments. Such an arrangement would allow the main wing to generate the yawing moments required to drive active control about the lateral-direction axis. This effect has been exploited before in experimental flying wing designs (PRANTL-D) and is a possible method of yaw control in birds. However, there is evidence to show that in gliding flight, some species of birds adopt washed-out wing configurations [125] unlike the lift distribution required to exploit the pro-verse yaw effect. In these cases the tail must provide some input into controlling the lateral directional flight and the general results for red kites are discussed here.

6.6.2 Tail articulation for control in Red Kites

Red kites use tail twist to control their flight. The red kite is a low and slow soaring specialist. They are primarily carrion feeders but are also opportunistic predators and will feed on small mammals and birds if presented with an opportunity. This lifestyle necessitates long periods of low level loitering, slow speed flight in turbulent conditions. The kites appear to extract energy through gust soaring in the lowest levels of the atmosphere, the exact mechanism is out of the scope of this thesis. Figure 6.6 presents the range of motion of the aerodynamic surfaces measured across fifty instances of flight manoeuvres: 11 Straight glides, 17 left turns and 22 right turns. The range of motion of measured average wing-line and tail line are taken between the port and starboard wing and tail tips. They are measured in the world axis this is equivalent to the rigid body bank angle of the bird. Notably the bird is seen to achieve angles of bank $> 60°$ with two manoeuvres having an 'overbank' in excess of $90°$. The majority of manoeuvres however see the bird limiting the main wing bank angle to $30°$ or less. The body measurement, taken between the shoulders of the bird and establishes the lateral body axis of the bird, shows similar results. Whilst the wing-line measurement gives an effective aerodynamic bank angle, this measurement is indicative of a geometric body reference bank angle. Generally these two values are of comparable magnitude and direction, the largest difference being a $12°$ whereas the mean difference across 50 manoeuvres is $3°$. The tail of the red kite is actively twisted to control flight. The former plots the average tail-line angle as measured with reference to the world axis. It is a pseudo bank angle specific and effective at the tail. The total range of motion of the tail is greater than that of the main wing which can also be seen when referencing figure 6.7. This figure plots the average angle of the wing line subtracting the average angle of the tail, accounting for the relative direction of motion is shows a histogram plot of the angular difference between the two surfaces. This is the range of angular twist of the tail in relation to the main wing, which has been shown to remain close to the lateral axis of the body. The maximum angular separation is $65°$. This was experienced in a straight glide.

Whilst the histograms indicated the established envelopes of the surfaces the plot of wing angle vs tail angle 6.7 show the pattern which reveals some information about the control scheme being employed. For a rigid body aircraft whose wing and tail maintain a rigid body relationship where the two surfaces are parallel to each other the expectation would be that all points would lie on the line of equivalence (y=x) depicted in solid red. Accounting for noise the overall trend line, presented here as a dashed blue line, has a steeper gradient. This indicated that the tail has a greater range of motion than the main wing and tends to be actively twisted with respect to the wing.

Figure 6.8 Shows the bounding on the relationship between the main wing and the relative angle to the tail. The tail sees maximum rotation relative to the main wing when the main wing is at a low angle of bank and less relative rotation as the main wing moves towards a higher angle of bank. This indicates a shift in the effectiveness and control preference when moving from a low bank angle turn (where use of the twisting tail is preferable) to high bank angle turn (where the lift of the main wing is dominating the turn performance).

For all points lying on the positive side of the equivalence line in the positive x axis and on the negative side of the line in the negative x axis, the tail is twisted pro-verse to the wing 6.18, deflecting further into the turn.

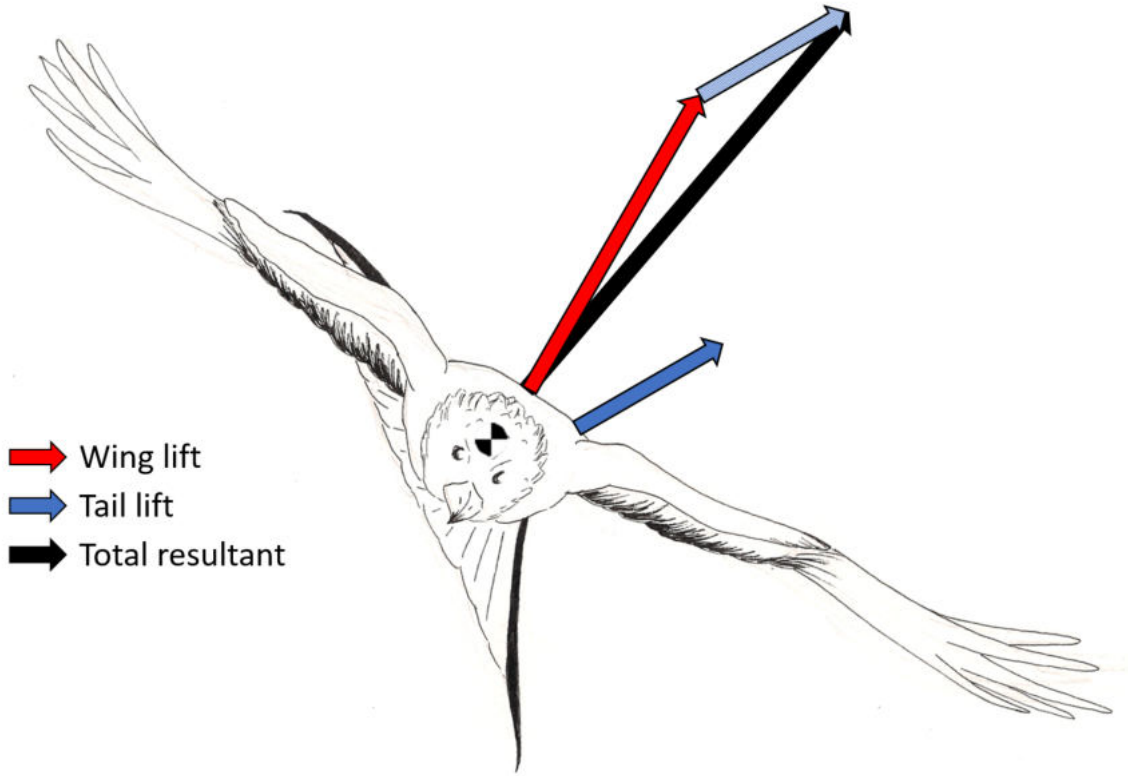

Fig. 6.18 Depiction of a simplified wing-tail arrangement in a left turn as viewed head on. The tail is pro-versely twisted into the direction of turn

For all points on the opposing side of the line in each half of the graph the tail is twisted adverse to the main wing 6.19, deflecting out of the turn.

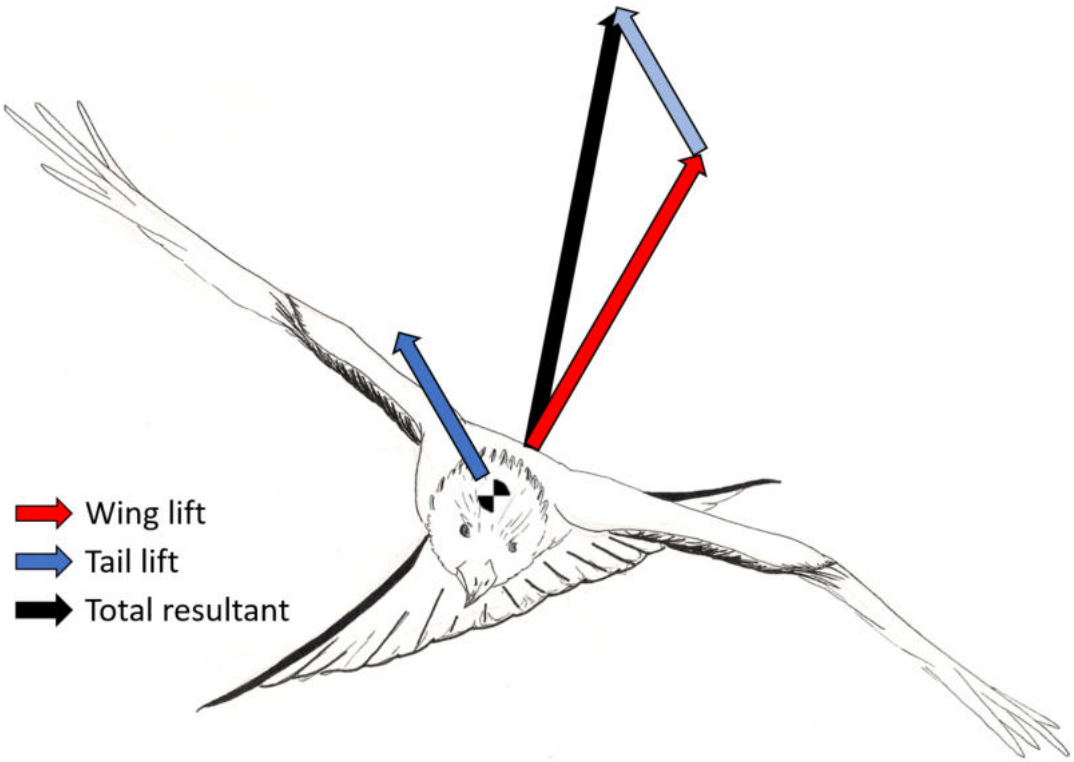

Fig. 6.19 Depiction of a simplified wing-tail arrangement in a left turn as viewed head on. The tail is adversely twisted against the direction of turn

The general result for the average overall trend is that the points tend to lie in pro-verse segments of the graph, indicating that in these manoeuvres the tendency was to use the tail as a pro-verse deflection and increase the deflection into the direction of turn. Deflecting the tail into or against the turn changes the direction of the total effective aerodynamic force vector on the bird. By twisting the tail the angle of the lift vector relative to the vertical changes, twisting the tail into the turn rotates this vector into the turn and twisting the tail out of the turn reduces the angle of the effective lift vector to the vertical. The mechanics changes the effective lift vector and modulates the side-force experienced by the bird. Side-force is important as it induces and opposes side-slip and controls the radius of turn for a given forward velocity. The greater the component of lateral force the tighter the turn, the faster the turn rate and the greater the effect on side-slip. The sensitivity of this effective bank angle depends on the relative contributions of the main wing and tail to the total lift contribution. The effect is more pronounced as the tail contributes more lift and a lifting tail is a general result seen in gliding raptors. Notably the magnitude of the change in effective bank angle is greatest at low angle of bank $< 30°$. The corollary of this is that for straight glides and shallow turns the red kites make more use of the tail as a principal control surface for modulating side-force and angle of side-slip. At higher angles of bank $> 30°$ the effective bank angle is principally controlled by the main wing and the tail becomes relatively less effective. In these conditions the main wing is used for coarse corrections and the tail becomes a method of fine tuning the desired turning and lateral performance. This is best visualised in figure 6.8, plotting the relative angle of the tail against the bank angle. The diamond shaped envelope shows peak tail motion in straight glides and shallow turns up to 30°, slowly reducing towards a minimum tail input at 60° angle of bank. The envelope is symmetric about the y axis, indicating this mechanism is present in both left and right turns and it's principle lateral component is positive and non-zero which indicates that the general result is a proverse, into turn deflection even at higher bank angles.

6.6.3 Mechanics of a twisting tail

The red kites achieve control using their tails. A small unmanned vehicle could achieve flight control using a similar system whereby an all flying control surface is used to modulates the relative aerodynamic and control coefficients. The system modelled here is based on the Bix3 airframe as previously described in preceding chapters. The difference is that the empennage is articulated about an assumed perfect 3D ball joint, mated to the fuselage at the leading edge of the horizontal stabiliser. The vertical stabiliser has been deleted and only the horizontal stabiliser remains, To simplify the analysis the motion here is broken down into three degrees of freedom:

1. Tail Pitch - Changing the relative angle of attack by rotating the tail about an axis parallel to the body lateral axis.

2. Tail Twist - Rotating the tail about the longitudinal axis to change the side-force generated at the tail.

3. Tail Wag - Moving the tail in the lateral plane by rotating about the normal axis, shifting the aero forces generated at the tail off axis and creating an aerodynamic asymmetry.

Pitching the tail for longitudinal control The first axis of articulation is about an axis parallel to the body lateral axis, coincident with the tail junction. Pitching the tail surface about this axis will change the local angle of attack at the tail, changing the magnitude of the lift force generated at the tail. This will change the longitudinal trim position of the vehicle and induce a pitching moment about the centre of mass. In this configuration the tail is acting as an all flying tail, a stablator, and as a trimable horizontal stabiliser.

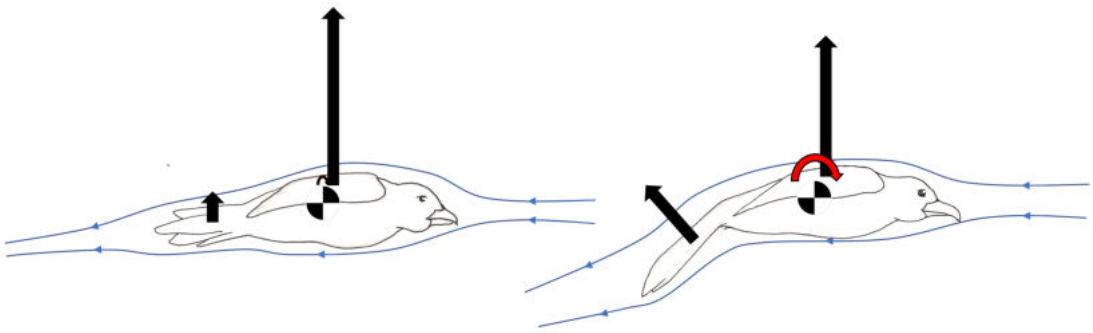

Fig. 6.20 Pitching the tail for longitudinal flight control and trim. The aerodynamic force at the tail induces a pitch couple about the centre of mass.

Figure 6.20 shows the effect of pitching the tail on the longitudinal dynamics of the vehicle. It is analogous to existing longitudinal control surfaces such as stabilators and trimable horizontal stabilisers.

Tail twist for rate of turn control Lateral control can be achieved by varying the lateral component of force in a turn. Twisting the tail rotates the tail lift vector about the longitudinal axis and redirects the total aerodynamic force acting on the tail. This variation in the direction of the total force will change the lateral component of the force in the turn. Angle of attack and side-slip are maintained at the tail. An increase or decrease in rate of turn is induced due to the change in the effective bank angle of the vehicle as the sum of the resultant lift forces changes the lateral component of force. This may be used to modulate rate of turn for a fixed body and main wing roll angle. Due to the aft offset position of the centre of tail lift a small adverse yawing moment is also induced.

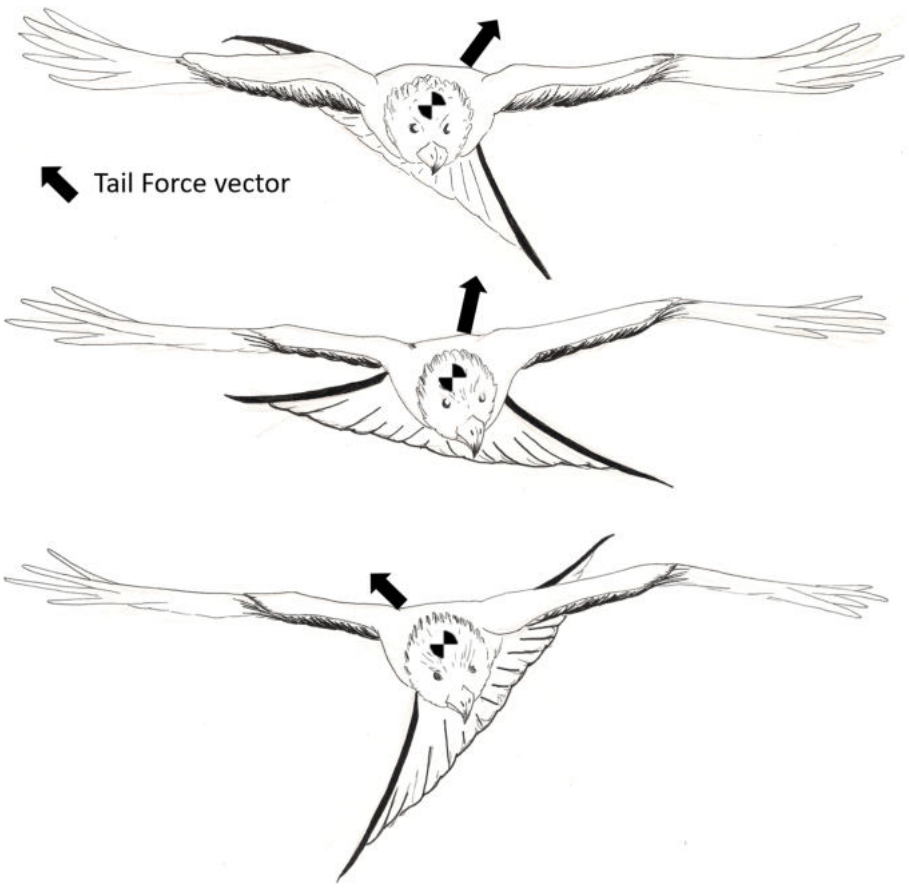

Fig. 6.21 Twisting the tail for lateral flight control and rate of turn through effective bank angle modulation

Figure 6.21 shows how twisting the tail induces a change in the lateral component of force which effects the turning performance. By steering the tail through the air, the bird develops a lateral component of aerodynamic force aft of the centre of gravity. Assuming that the birds tail is producing positive lift the steering of the tail has two effects:

1. The lateral component of force provided by the tail sums with the main aerodynamic force being provided by the lift of the main wing. If the tail is deflected the same way as the wing the lateral force will be increase and if it is deflected in the opposite direction from the main wing then the total lateral force will be decreased. The bird may use this fast twisting of the tail to augment and help to trim the relatively slower change in lift vector that comes from rolling the main wing.

2. The aft position of this lateral force will induce a yawing couple about the centre of gravity. If the tail is deflected in the same direction of the main wing then the tail will create and adverse yawing moment, further increasing the side-slip on the bird. If the tail is deflected in opposition to the main wing it will create a coordinating yawing moment, reducing the side-slip. This yawing moment is only the contribution from the lateral twist of the tail and a restoring yawing moment may be coordinated through the action of tail wag.

Offsetting tail drag using tail wag to induce yaw The tail can also contribute to the yawing moment when 'wagged' to offset the centre of pressure away from the body longitudinal axis. By moving the centre of pressure off axis the drag force couples to produce a yawing moment. This yawing moment as a result of the drag force can be used to coordinate and offset the adverse moment induced by twisting the tail to change the effective bank angle. When used in this manner the tail alone can initiate, control and coordinate turning flight independent of the main wing.

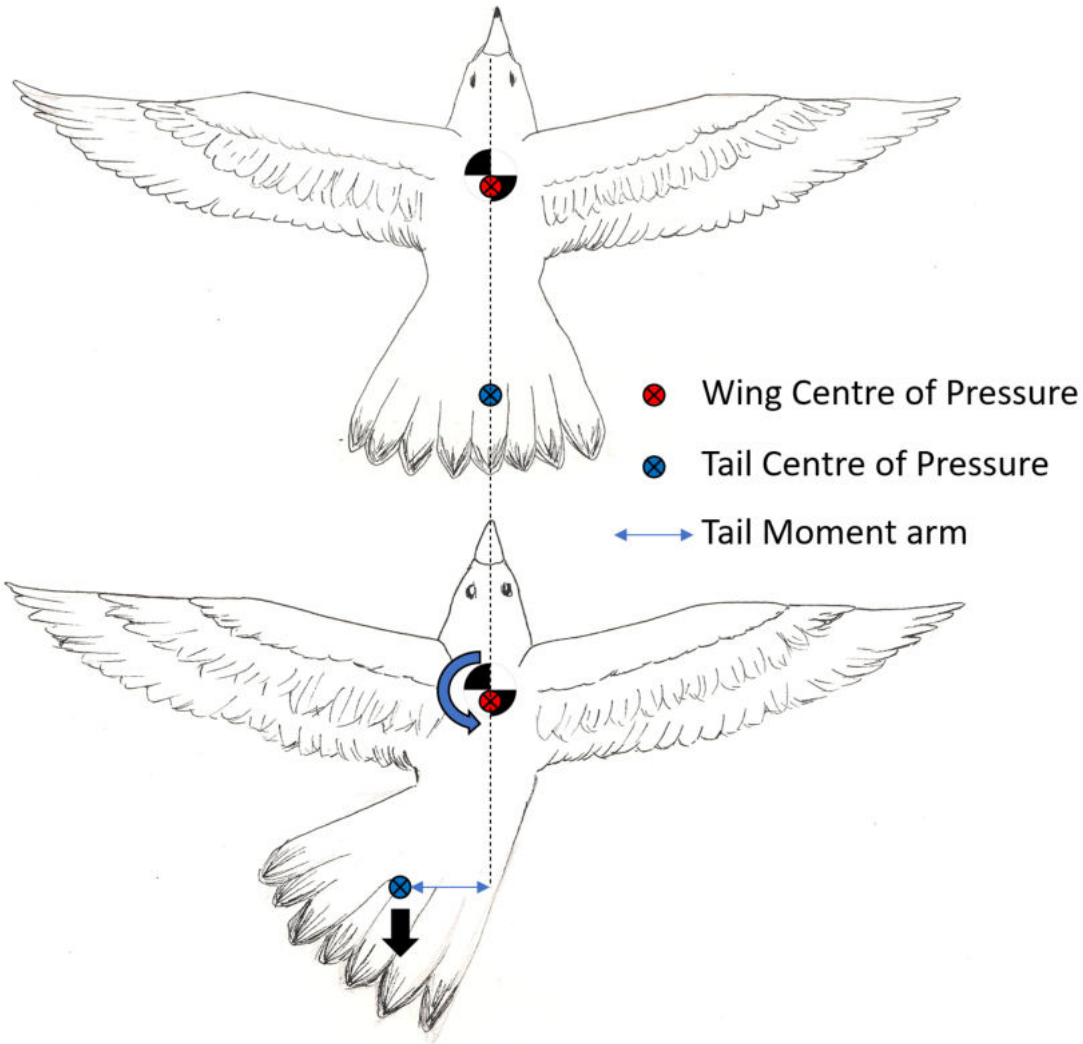

Fig. 6.22 Wagging the tail offsets the drag force and induces a yawing moment on the aircraft

Figuire 6.22 shows how offsetting the centre of pressure of the tail sets up a yawing moment as a product of the drag force and the lateral offset of the centre of pressure

from the centre of mass on the body longitudinal axis. This allows the tail to produce pro-verse yawing moments which can be used to coordinate turns and enhance turning performance beyond what the main wing can provide on its own.

By combining these three control schemes the tail can be used to provide complete control over the flight by initiating rotations about all three principle axes. In this manner the tail provides independent and redundant control of the longitudinal and lateral directional flight dynamics.

Figure 6.9 and figure 6.10 show a comparison between using a pitching tail (Blue) to control longitudinal dynamics and using an elevator control scheme (Red). The larger aerodynamic surface of the tail means for a given deflection the changes to the aerodynamic coefficients C_L and C_D and the pitching moment C_M is greater.

Perhaps of most interest is how the ratio of lift and drag generated between the main wing and tail changes as the tail pitches. Figure 6.12 shows this behaviour. The ratio of tail lift coefficient to total lift coefficient shows the strong inverse relationship between negative tail pitch and the main wing angle of attack. As the tail deflects up (negative) the pitching moment drives the wing to a high angle of attack and a relatively larger lift coefficient, however the relatively large negative lift coefficient of the tail (almost 60% that of the main wing and in opposition at $-25°$) means it's possible to generate large pitching moments with a smaller change in total C_L than is achievable for an elevator style control system. This somewhat decouples the effect of pitching and increasing lift, possibly allowing for interesting out of plane manoeuvres and increased control of pitch attitude at high angles of attack. The effect is somewhat less pronounced for positive angles of tail pitch (downwards deflection). The lifting tail provides a C_L of up to 20% that of the main wing at 25° deflection. Interestingly the total lift coefficient increases (figure 6.9) whilst the nose down pitching moment also increases (figure 6.10) for an increasing downwards deflection of the tail. The drag coefficient provided by the tail is typical. The tail provides a larger component of drag as it deflects to higher angles both positive and negative. The extent of this depends on configuration and the initial setting angle but the response is approximately symmetrical about the tail at 0° incidence as seen in figure 6.12 where by the curve is axi-symmetric about the $x = -5°$ which accounts for the model tail setting angle of $-5°$.

The degree of freedom with the greatest range of motion as established by tracking the red kites is the tail twist. The twisting tail modulates the side-force and induces a yawing moment. The side-force (Figure 6.13) and yawing moment (Figure 6.14) are both non-linear and are in opposition to each other. The yawing moment is adverse to the side-force with the side-force acting to restore a side-slip and the yawing moment acting to increase it. The relative magnitudes of the coefficients indicate that the combined response is a restoring moment in the presence of a side-slip. The intended use of a twisting tail is to increase side-force, by increasing the effective bank angle and to provide yaw control by twisting the tail towards the vertical. The yaw and side-slip response is effected by the relative angle of airflow over the tail which is measured as a side-slip angle β. Figures 6.15, 6.16 and 6.17 show the effect of side-slip on the control coefficients. The side-force as a function of side-slip is non-zero when the tail is untwisted but comparatively small in value. The horizontal tail surface provides little aerodynamic damping in response to a side-slip in this position but maximises it's effectiveness about the lateral axis controlling longitudinal dynamics. As the tail twists towards 60° the tail generates more side-force. The response in non-linear with angle of twist and is an inversely proportional function of the side-slip, lift coefficient of the aerofoil and of the angle of twist. The yawing moment is non-linear and is positive in response to the side-slip, applying a restoring moment with the tails centre of pressure being positioned aft of the body's centre of gravity. As the tail twists towards the vertical it's contribution to roll damping, $C_{l\beta}$, decreases.

The twisting tail modulates the side-force and yawing moment and has a small coupling with roll moments. The closer the tail is to the vertical the more contribution it makes to later-directional control and the closer it is to the horizontal the more contribution it makes to the longitudinal control moments. By varying the side-force the tail can act to induce / oppose side-slip. It is most effective at relatively high angles of twist when the main wing is not contributing to side forces, i.e. in straight and level flight and shallow turns. It is likely that the rate of deflection of the tail is superior to the roll rate achieved by the main body and wing and so the tail is used as a fast acting control surface in straight and level flight and in shallow turns. It's effect is limited however and for tighter turns and increased rate of turns the bird / vehicle must use the more effective main wing banking to provide the turning force In this scenario the wing acts as a coarse control and the tail fine tunes the control

coefficients. In the red kites the observation was that the tail was typically used to increase the effective bank angle rather than decrease it, although this behaviour was also observed. This control scheme would be useful in environments with short period gusts allowing for fast acting control independent of long term flight guidance.

The model is also setup to wag about an axis parallel to the normal axis. This wag offsets the centre of pressure away from the plane of symmetry though the longitudinal axis. Offsetting lift and drag in this way induces small measurable roll and yawing moments. The magnitude of this effect is dependant on the configuration, the magnitude of the tail's lift and drag force and the distance the centre of pressure can be offset. A relatively small tail doesn't provide a useful control moment because of it's small size and relatively restricted displacement.

Figure 6.22 shows how this effect could be implemented and highlights the critical design parameters influencing the effectiveness of this control scheme. For this control scheme to be most effective the ratio of tail lift and drag contribution must be relatively large when compared to that of the main wing. Also the distance between the centre of pressure and the pivot point should be maximal. A maximal offset produces the most lateral asymmetry for a given angle of tail deflection. These two parameters couple to produce the largest possible yawing moments. This mechanism would be most useful for birds with oversized ornamental feathers, relatively draggy structures placed distal from the tails point of rotation.

6.6.4 Integrating tail and main wing function

Whilst not specifically evident in the dataset the observed state of the tail whilst the kites are in gliding flight imply an positive aerodynamic loading. This is consistent with findings in other bodies of work [129]. A lifting tail arrangement effects the balance and stability of the bird as a whole and the affect of furling and unfurling the tail would need to be balanced by adjustments in the main wing to offset induced moments and maintain the desired flight path. As the tail unfurls and produces lift, the main wing would need to be swept forward, moving the centre of pressure forward to balance the pitch down moment induced by the tail. This need for forward sweep to balance a lifting tail affects the longitudinal stability of the animal. This ability to adjust the stability and in turn the agility of the animal improves the flight envelope particularly when the additional benefits of the secondary effects of the tail are considered.

6.6.5 Secondary effects of the tail and considerations for UAV design

One of the main reasons to use a twisting tail over a conventional discreet flap control scheme is to exploit the beneficial secondary effects of such a configuration. A discreet flap system provides three axis control over the flight path but because it is a relatively small aerodynamic surface when compared to the main wing it's effects beyond producing control moments is somewhat limited. Having a large lifting tail, proximal to the main wing has a number of benefits. The tail can improve the efficiency of the main wing by acting as a slotted flap. As noted in previous work a proximal tail may act as a slotted flap for the main wing [130]. By unfurling the tail the aerodynamic lifting surface area can be dynamically controlled. This allows the tail to be used for direct lift control, enhancing and reducing lift quickly and without the need for a change in body attitude in the same way that a three axis rigid body aircraft would. By redirecting the aerodynamic force the tail can be used to make out of plane manoeuvres. Drag can be substantially modulated to control acceleration through the furling and unfurling out of plane. All of this moves towards six axis control, providing direct control over heave surge and sway in addition to the three rotational degrees of freedom. Such a control scheme also allows a pseudo rigid body to be somewhat decoupled in terms of aerodynamics and body attitude, something which may be useful for sensor pointing and payload protection.

To properly exploit these secondary effects, vehicle design needs to change to exploit the benefits of a twisting tail whilst maintaining positive directional control of the vehicle. An unmanned vehicle design optimised for a twisting tail would have the following attributes:

1. A large aft lifting surface whose area can be directly controlled (furled/unfurled).
2. The tail surface being proximal to the main wing to act as a trailing edge aerodynamic device and enhance the performance of the main wing.
3. Multi-axis articulation of the whole control surface, allowing aerodynamic force to be induced, spilled and redirected to produce control moments.
4. A control scheme which extends beyond 3-axis control with control laws which take advantage of the additional capabilities of a twisting tail.

A twisting tail on it's own whilst interesting doesn't provide many major benefits over a traditional discreet control system. However coupling a twisting tail with an articulated main wing as discussed in previous chapters opens some interesting potential for novel six-axis control. The birds main wing and tail posses qualities of all three types of wing morphing introduced in Chapter 2. Rotational morphing of the wing and tail at both the root and at distil positions on the wing at the elbow and wrist joints. Telescopic morphing as feather overlap exposes more or less wetted surface to the flow, and because the feathers are a permeable structure atop an impermeable layer of skin on the forearm this telescoping also changes the permeability and through-flow of the wing and tail. Compliant morphing applies to both the feathers and the skin as it is stretched over the underlying rigid bone structure. If three axis control is considered as rotation about the vehicles primary axis by the actuation of typically one set of control surfaces, by coupling controlled morphing of the wing and tail it is possible to not only control the vehicles orientation about its primary axis but its velocity relative to it. Heave, or vertical velocity changes without a change in vehicle pitch can be achieved through simultaneous rotation of the main wing - changing angle of attack and deflection of the tail - trimming out the pitch change. Lateral forces can be introduced by twisting the tail with no reduction in overall lift. Forward velocity can be modulated by varying the drag through symmetric deflection of the wings and tail. By decoupling the vehicles orientation and the flight path, morphing and dynamic reconfiguration provide a framework to move towards control of higher degrees of freedom and direct modal control.

6.6.6 Review of methods

This chapter presented control schemes using the secondary lifting tail surface for flight control. Rotational stereo videography 3D point tracking is used to make measurements of Red Kites (*Milvus milvus*), a species of raptor which are observed to use their tail to actively control lateral directional flight. The RSV system position measurement error is proportional to the square of the distance to the target and the wireframe fitting uses two points per surface to establish the reduced order model. In all cases except where the bird is directly head on / tail on to the camera the error effecting the measurement at either wing-tip/tail tip differs between the two points. This exaggerates the angular measurement error computed between the points as the total error in the computed angle is proportional to twice the error and the angle between the points. In order to minimise this error the range to the target should be minimised and kept as consistent as possible between recorded manoeuvres. The working range for the 50 flights presented here is 30 -60 m at which the stereo position error is deemed acceptable. Each aerodynamic vector requires two points to establish and in some instances the control point is out of view when occluded by another body part, this limits manoeuvres which can be tracked to those where both wing tips and tail tips are in frame. Each manoeuvre is represented as an average across 25 frames (or 0.5 seconds at 50 fps), restricting manoeuvres measured to ones at low spatial frequencies, this averaging process helps to reduce any random noise in the position measurements due to template shifting between frames. To increase the resolution of the manoeuvre measurement it would be necessary to improve spatial resolution by using a marker tracking method such as a laboratory based VICON motion capture system, and to improve temporal resolution by using increased frame rates to allow for data averaging across smaller time steps.

The greatest drawback of the RSV method is the lack of knowledge regarding the flow state surrounding the bird. Simple measurements of wind speed and direction were taken using a handheld anemometer at the RSV rig position but the birds are 30 - 60 meters away, above the tree line and are subject to a turbulent wind field. This is observable in raw video as the turn radius of the birds varies with bank angle and whilst it may be possible to infer the wind direction from this data is provides no information regarding the birds airspeed, angle of attack and side-slip which are all found to be critical parameters for flight control.

Including flow data would improve the dataset and could be established either by using a sonic anemometer mounted on a tall pole to get a better single point average wind speed and direction at an altitude comparable to the birds flight paths, or to use a laser Doppler anemometer to measure the wind gradient from the ground up. Both these methods are deficient in that they only provide an average wind distal from the birds true position, the sonic anemometer providing a 3D single point average and the laser Doppler providing a 2D planar average gradient.

The analytical AVL model requires inputs of flow speed, angle of attack and side-slip. Without any true measurements of these from the RSV dataset, sensible values are assumed and the sensitivity to changes in their values considered. Where possible control derivatives with respect to angles of attack and side-slip provide useful information as to the effectiveness of the control schemes with uncertain aerodynamics. The analytical models in this chapter have not been validated against experimental wind tunnel data with physical models unlike the previous chapter. Because there was no physical design of a functional twisting tail mechanism the effectiveness of the control scheme would likely be reduced when functional design constraints are considered.

6.7 Conclusion

In this chapter the effect of a twisting tail as a flight control surface is observed and quantified in a low level soaring falconry species, Red Kites (*Milvus milvus*). The 3D multi-point tracking technique, Rotational Stereo Videography, as presented in Chapter 3 is used to fit a seven point wire frame model to video footage tracking red kites performing straight and level glides and left and right gliding turns. This seven point model represents the kites aerodynamic surfaces as average line vectors connecting the wing and tail tips. The range of motion of the tail twist is measured and the control coupling effect in conjunction with the main wing is analysed. The kites use pro-verse tail twist to increase their effective bank angles in steep turns and use their twisting tail as a primary lateral directional control surface in straight and level flight. A control envelope for a twisting tail is presented which shows the tail to be most effective at low angles of bank, it's effectiveness reducing as the kites adopt steeper bank angles. An analytical study of a freely articulating tail is implemented and the tail is shown to be effective at inducing pitching moments about the lateral axis when used as an all flying tail. Twisting the tail about the lateral axis is effective at modulating side-force and it's effectiveness increases with higher angles of side-slip. Tail wag as a mechanism to control yaw is considered but the effectiveness of this mechanism is limited. An articulating tail is a novel mechanism which when coupled with an articulated wing provides many more degrees of freedom and the potential for a powerful full six axis control scheme which can be applied to small unmanned aerial vehicles which have been optimised to exploit the additional articulated surfaces.

Chapter 7

Summary and Conclusions

7.1 Summary and Conclusions

The aim of this thesis was to establish a method for evaluating a free flying birds flight control strategy and compare these to existing three axis control strategies. The objectives were to examine what a gull does with it's main wing and how we might apply a bird-inspired wing to a UAV and, what kites do with their tail and how a bird-inspired tail could be used in UAV design.

Quantifying the flight performance of the birds is achieved by establishing measurements of the flight path, and measurements of the the position of key points on the birds body and to use these data points to derive estimates of control parameters and examine the flight control strategy being employed by the bird. This was achieved for two species of bird: The lesser black backed seagull (*Larus fuscus*) in Chapter 4 and the Red Kite (*Milvus milvus*) in Chapter 6. The flight control schemes employed by the birds are novel and involve manipulating the primary lifting surfaces directly; are quite different to the traditional three axis control scheme employed in traditional rigid body aircraft at all scales.

In Chapter 3 an existing single 3D point tracking method, Rotational Stereo Videography, was developed and extended to support multipoint tracking and photogrammetric reconstruction of the birds geometry. The new multi-point tracking version of rotational stereo videography was built entirely from scratch and comprises custom hardware (optical mirror frame and camera system) and software (image template convolution to perform sub-pixel matching by normalised cross correlation). This is a low cost methodology which employs consumer grade camera, optics and electronics and can be employed outside of the lab in an uncontrolled environment. The software component uses control point pixel disparity to calibrate the range component of a spherical polar coordinate system whilst the hardware component consists of a pair

of 16 bit rotary encoder which record the azimuth and inclination angles which are subsequently corrected for the position of the control point in the image. High speed video files are subsampled and smoothed to reduce random error and the total position error as a function of the range is presented.

In Chapter 4 results from 117 flights from 89 video samples were used to produce a dataset comprising of the flight paths and gull morphometrics which were used for the subsequent analysis By fitting a novel wire frame model to a number of control points, a reduced order model of the birds primary flight control surfaces was established to reconstruct the position of the main wings and tail surfaces relative to the body so that their inputs could be measured to establish the effect on the flight path. The lesser black backed gulls were found to be manipulating their main wings and tail to control the longitudinal and lateral dynamics of their flight. The flight performance of the gulls can be compared to an equivalent rigid body aircraft manoeuvring diagram and all inertial measurements were found to be contained within the established flight envelope. A reduced order model established from the wire frame fit, reduced the complex wing geometry into two parameters: wing-line sweep and wing-line rise. When in the glide the gulls used fore and aft motion of their main wing, as defined by wing-line sweep, to control their longitudinal flight path angle by manipulating the relative position of the centre of lift and the centre of mass to create a response equivalent to a pitching action in a rigid body aircraft. Because the wings are not rigidly connected to the body, pitch as defined by the body axis was found to be a poor metric for flight performance in the bird, instead being replaced by the change in flight path angle which is the parameter the bird was directly controlling. In this instance rigid body mechanics do not well model the longitudinal dynamics of the vehicle and the setting angle between the wing and the body is non-constant and thought to be a variable that the birds control.

The turning performance of the gulls are better modelled by rigid body dynamics. For a steady gliding turn the bank angle as established by the average wing-line was found to be strongly correlated to the centripetal acceleration and agreed with the expected performance as computed using rigid body dynamic relationships. Gliding turns can therefore be said to be roll based (different to the Red Kites as seen in Chapter 5) and are well modelled by the rigid body equations of motion.

In Chapter 5 a series of new control schemes inspired by the gull flight data are presented and evaluated against existing three axis control methods. Whole lifting surface actuation of the main wing, actuated at the wing root is used to vary the relative position of the centre of pressure. To simplify the analysis the wing actuation is functionally decomposed into 3 separate mechanisms, each representing a single degree of freedom in rotation about the principle axis at the wing root. The three mechanisms consist of wing sweep, wing twist and wing rise (dihedral) and for each mechanism there is an associated control scheme. Each control scheme was analysed in simulation and validated using wind tunnel tests of physical mechanisms based on the Bix3 and WOT4 airframe platforms.

Wing sweep for longitudinal control allows fore and aft motion of the wing to control the longitudinal dynamics of the vehicle. This control scheme was seen in chapter 4 being used by the gulls to control their flight path angle. Wing sweep has more control power than a traditional elevator but has the side effect of changing the static and dynamic stability of the vehicle with the airframe becoming unstable with 12 degrees of forward sweep. Such changes in stability puts additional requirements on the controller to account for the change.

Wing twist for roll and direct lift control are both considered. Roll control from whole wing twist is similar to performance from the ailerons, although limitations in the wind tunnel testing rig constrained the achievable roll moment because of structural considerations. Whole wing twist forces the wing to high angles of attack beyond the critical value which limits their effectiveness so as not to invoke control reversal. Direct lift control exploits the non-rigid relationship between the main wing and the fuselage. This variable setting angle was seen in the bird flight data and is the reason why pitch is a poor metric for longitudinal flight performance in the bird data. By varying the setting angle the lift coefficient and longitudinal trim of the vehicle can be controlled directly at the wing root.

Varying the wing dihedral and anhedral symmetrically can be used to modify the lateral directional stability of the platform. The effect on the spiral mode is particularly pronounced, this mode is typically unstable albeit with a long period, however using high dihedral angles this mode can be stabilised. This may be beneficial to a gliding vehicle experiencing large lateral gusts where a spiral departure would be detrimental

to the vehicle.

Chapter 6 focuses on a raptor species, Red Kites (*Milvus milvus*), specifically on their use of spread twisting tail in the control of their turning flight. Contrary to the gulls looked at in chapter 3, the Red Kites make active use of their tail to control their lateral dynamics. Red Kites soar very differently to the gulls, they are low and slow speed gust soaring, opportunistic scavengers looking for a meal. This chapter presents the idea that the tail is used as a turning trim control, allowing the Red Kites to fine tune the amount of lateral force produced without making substantial changes to the effective bank angle of their main wing. This effect is predominantly seen at lower angles of bank where the component of lateral force induced by the twisting tail is greatest in proportion to the main wing. The deflection of the tail is predominantly pro-verse, into the direction of the turn, increasing the amount of lateral force, however their are some instances of adverse deflection out of the turn, these instances are typically seen at lower angles of bank.

The effects of tail pitch and wag are also considered although there is no evidence from this data set that either are used by the red kites to control their flight. Because of the definition of the tail control points, the points are spaced laterally across the tail and there is no control point at the tail root. The absence of a tail root control point makes it impossible to quatify tail pitch from this dataset and so it's effect cannot be properly assessed. Tail wag and the resulting yawing moment is greatly effected by the moment arm as the induced aero load will be quite small. The Red Kites do not have a long tail longitudinal moment and so the effect of wag is not measurable. Despite this the tail is clearly an active control surface and used in conjunction with the main wing to enhance the Red Kites flight control.

In summary, this thesis developed a method to make simultaneous measurements of the birds flight path and body pose and position. Using these data points it is possible to make estimates of control parameters and suggest the types of control schemes that the birds are using to control their flight. Three separate mechanisms were produced to demonstrate three different flight control strategies on a small "fixed wing" UAV, all of which were successful although the limits of their control power could not fully be explored. It remains to be seen whether simply articulating the main wing provides any substantial control benefits over existing three axis control schemes. However

when coupled with an articulating tail the two structures can work together to effect aerodynamic change in ways a three axis system cannot. When looked at as a complete system, the main wing and tail combination can be thought of as a single main lifting surface with a variable trailing edge flap system. This trailing edges has freedom to pitch, twist and wag to control the flow being shed from the main wing. Removing discreet surfaces eliminates sources of interference drag and the non-rigid nature of the wing and tail root joints means that the body is decoupled somewhat from the flight dynamics. This means that some traditional body metrics such as pitch angle become irrelevant when discussing flight performance and the control laws are focused onto the primary controlling parameters and desired outputs. Having an articulated main wing and tail makes the platform more flexible, and allows for a move towards a 6 degree of freedom control scheme, providing direct control over heave and sway independent from the body orientation.

Gulls and Red Kites are just two species of birds who adopt a gliding gait over a small portion of their flight envelope. They demonstrate remarkable finesse and control and as this thesis has shown, it is now possible to quantitatively assess their flight performance using readily available consumer grade hardware. The control schemes are based on manipulating their flying surfaces directly and they seem to offer benefits for flying in a highly dynamic environment, allowing for manoeuvres beyond what can be achieved with three axis control. Understanding these birds is an ongoing endeavour and will influence the future design of future small unmanned air vehicles.

Appendix A

Appendix A - Rotational stereo videography (RSV)

Supplemental design specifications of the rotational stereo videography system.

A.1 Datalogging

A.1.1 Microcontroller

The microcontroller (Figure A.1) is a Digilent ChipKit Max32 (Table A.1).

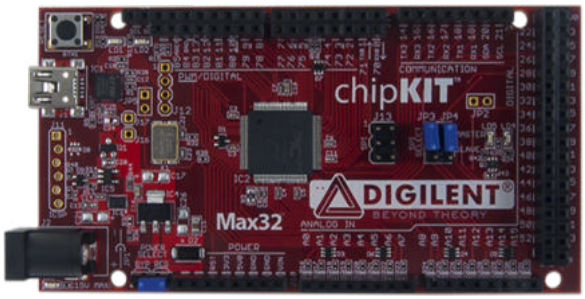

Fig. A.1 Digilent ChipKit Max32

Table A.1 Digilent ChipKit Max32 Specifications

Digilent ChipKit Max32	
Processor	PIC32MX795F512L
Flash memory	512 kB
RAM	128 kB
Clock speed	80 MHz
Controller	USB 2.0 OTG
I/O	83 pins
Dual CAN controllers	Arduino compatible

The Digilent ChipKit Max32 communicates with the SD card as a serial peripheral interface (SPI) device and makes use of specific high speed read/write hardware pins. The SD card is declared on the SPI output pin 53. On initial start up the SD card is checked for presence. If present it is scanned for the last existing file name, subsequent files are incremented on this, offering file overwrite protection in the event of a power loss. Each new data file has a unique header and is saved as a comma separated variable (.CSV) file. Data is stored in the format $(Angle_azimuth, Angle_altitude)$.

Video is recorded on the camera's internal SD card. Because of this independence the data must be synchronised in post. To facilitate this data synchronisation a microcontroller controls the camera recording start/stop and stamps the first and final frames of video which corresponds with the first and final angular measurements. These stamps are on the camera audio channel and consist of a 5ms chirp. This should span three full frames. The central frame is taken as the reference angular encoding start/stop point. The camera is physically connected to the microcontroller using two lines. These each correspond to an individual I/O pin on the ChipKIT Max32. The remote line connects using a 1/8" jack through an optocoupler to digital pin 25. The optocoupler ensures the independence of the two electronic systems which have separate power sources and do not share a common ground. The audio line connects through a standard ¼" jack directly to digital pin 5. Digital pin 5 on the ChipKIT Max 32 is PWM compatible and can emulate an analogue chirp output.

Angular data is logged to the external SD card by the microcontroller. Angular encoding measurements are made using 17bit angular encoders. These communicate with the microcontroller using the SSI protocol. SSI uses the RS485 transceiver standard to send data in response to a clock cycle, data is transmitted most significant bit first. Each encoder is connected to the microcontroller through an RS485 driver. This allows a single clock output to drive the CLOCK lines and a single data input pin to receive the DATA lines. The encoders share a common clock on digital output pin 2. The azimuth encoder sends data to digital input pin 3, the altitude (inclination) encoder sends data to digital pin 4. Data is received in Gray code format which is converted to decimal before being written into a csv file on the external SD card.

A.1.2 User interface

The user interface system (Figure A.2) comprises:

- 1 Master power on/off rocker switch

- 3 single push buttons

SET – Sets the encoder angle measurement to 0o used to set the origin in the calibration routine
REC – Start recording. This button trigger the camera and encoders to start recording, provides the first synchronisation pulse and initiates data logging.
STP – Stop recording. This button trigger the camera and encoders to stop recording, provides the final synchronisation pulse and closes data logging.

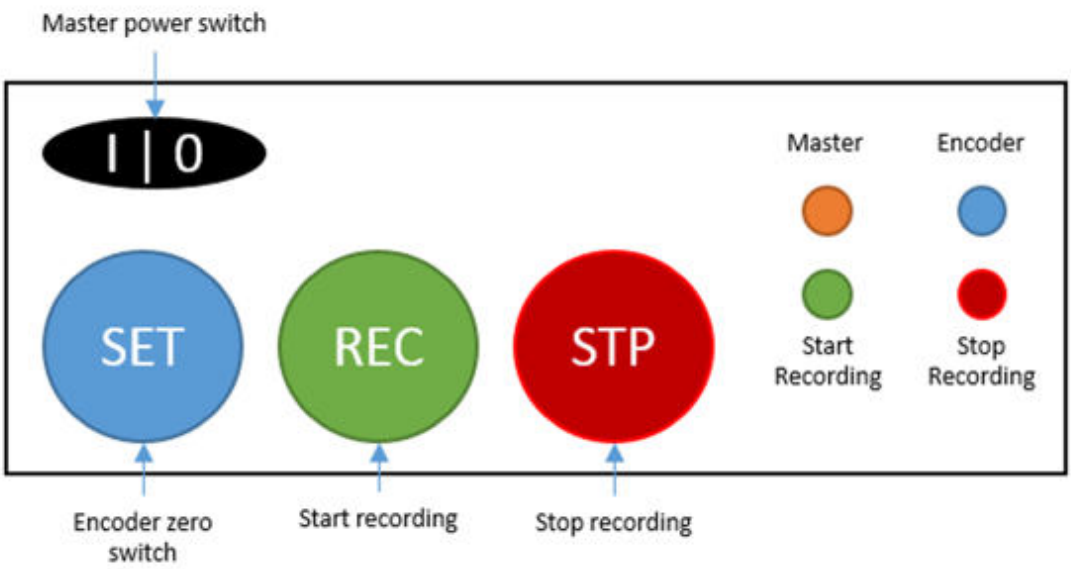

Fig. A.2 RSV control box interface

A.2 Optical system

A.2.1 Mirror sizing

Required primary and secondary mirror width are sized according to table A.2 using equation A.1 and equation A.2. Required primary and secondary mirror height are similarly calculated by adjusting the term accounting for the 45° mirror cant angle to account for the additional distance to the furthest reflective surface and the normality of the vertical plane using equation A.3 and equation A.4.

These values are based on a pin-hole camera approximation and do not account for additional light captured by the large lens barrel. A correction factor of half the Lens diameter is added to account for the additional field of view of the lens. The final mirror sizing (Table A.3) are subject to an additional 10% contingency in total area.

Table A.2 Optical sizing parameters used to determine the mirror sizing and placement for the RSV system

Parameter	**Variable**	**Value**	**Unit**
Focal length	f	0.105	m
Primary distance	b	0.320	m
Secondary distance	a	0.500	m
2K Horizontal Field of View	hfov	9.42	°
2K Vertical Field of View	vfov	5.29	°
Lens correction factor (width)	W_{lens}	0.02026	m
Lens correction factor (height)	H_{lens}	0.02625	m

Primary and secondary mirror sizing equations

$$M_{1W} = (a - f + b)\frac{sin(\frac{hfov}{2})}{sin(\frac{\pi}{4} - \frac{hfov}{2})} + W_{lens} \tag{A.1}$$

$$M_{2W} = (a - f)\frac{sin(\frac{hfov}{2})}{sin(\frac{\pi}{4} - \frac{hfov}{2})} + W_{lens} \tag{A.2}$$

$$M_{1H} = 2(a - f + M_{1W}cos(\frac{\pi}{4}))tan(\frac{vfov}{2}) + H_{lens} \tag{A.3}$$

$$M_{2H} = 2(a - f + M_{2W}cos(\frac{\pi}{4}))tan(\frac{vfov}{2}) + H_{lens} \tag{A.4}$$

Table A.3 Primary and secondary mirror sizes including lens correction and 10% contingency

Mirror dimension	**Value (mm)**
M_{2W}	52.31
M_{2H}	52.68
M_{1W}	122.14
M_{1H}	108.06

The reflective surfaces are $\lambda/4$ first surface mirrors with an enhanced aluminium coating designed for broadband applications in the visual spectrum.

A.2.2 Optical frame

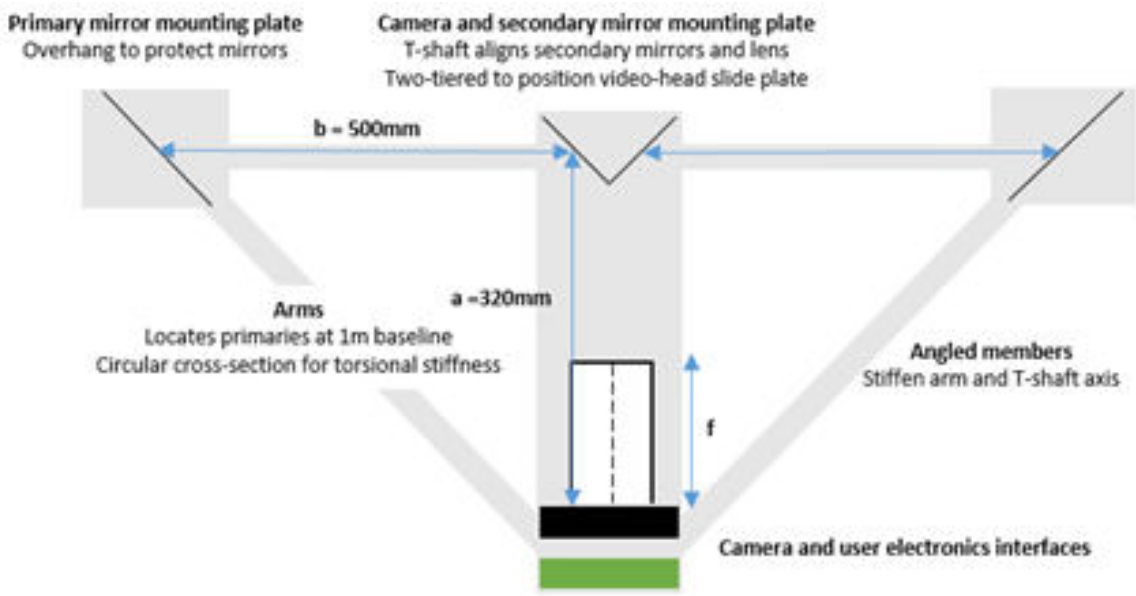

Fig. A.3 Principle dimensions of the optical frame

A T-shaped platform (A.3) is needed to locate the primary mirrors on arms distal from the camera and secondary mirrors, the mirror mounts are affixed to mounting plates connected to the arms. The mounting plates overhand the mirror mounts to provide a sacrificial layer against knocks and scrapes. Such arrangement will have poor bending stiffness along the axis joining the primary mirrors. The camera and secondary mirrors need to be affixed to a mounting plate along the t-shaft. This plate must also provide the connecting point for the video head slide plate. To eliminate any component interference or bolt clash a two-tiered plate is required, such an arrangement has the added advantage of increasing the cross-section second moment of area in the direction of bending along the T-shaft. Angled members are used to complete the T providing additional bending stiffness along the primary arms and t-shaft mounting plate. The completed triangular plan-form provides the best trade-off between structural stiffness and low frame mass. Where sensible lightening cut-outs are made in the carbon plate. To maximise the torsional rigidity of the cross arms and angled members a circular cross section in employed. The final layout is shown in figure A.4.

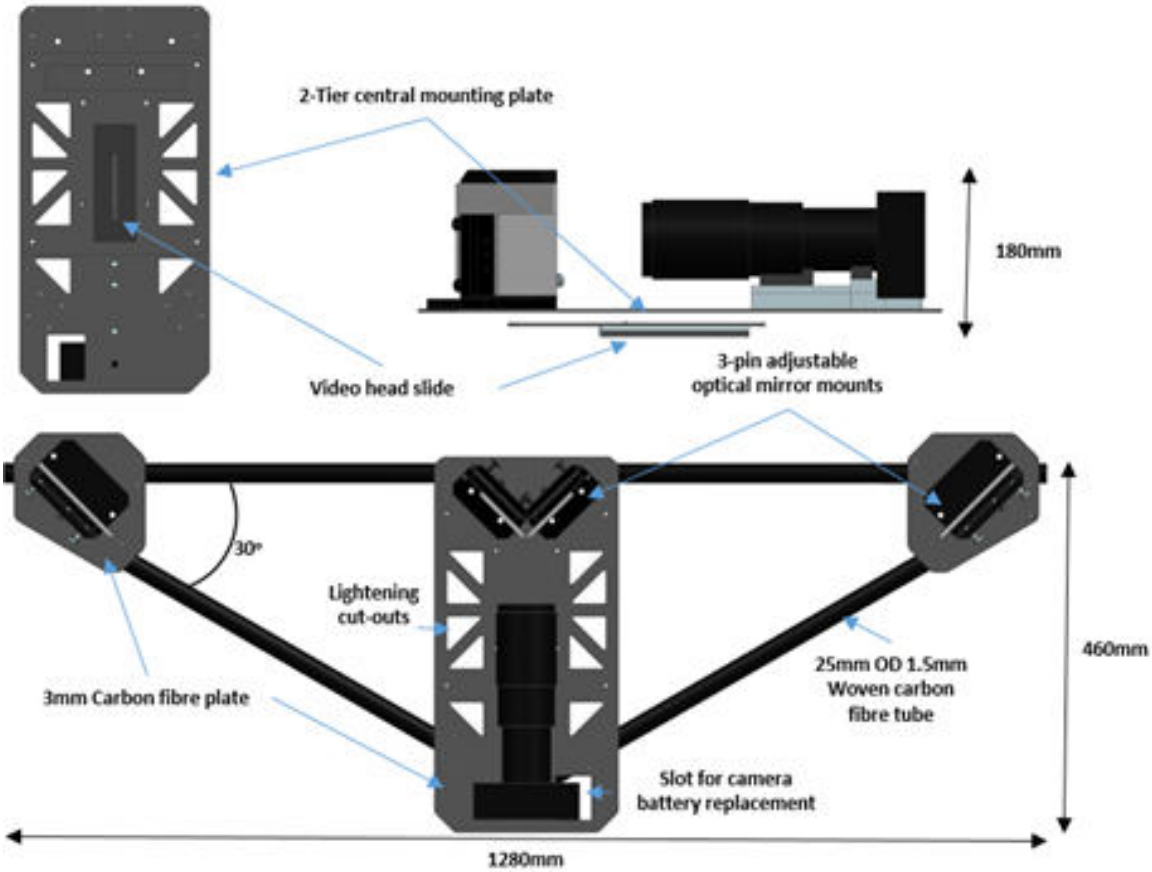

Fig. A.4 RSV production frame design

The carbon fibre material was selected to account for a compromise of stiffness, weight and availability. The design makes use of preformed carbon fibre components: rigid 7ply sheet and tri-axial woven tubing connected together using fasteners and tube clamps. This was preferred to a fully moulded frame due to constraints on tooling setup cost and time. The carbon fibre material properties are in table xx.

Table A.4 RSV Frame materials

Raw material	**Fibre layup**	**Supplier**
9ply carbon fibre sheet	Balanced 0,45,-45,90	EasyComposites
25mm OD 1.5mm t	Tri-axial 0,45,90	EasyComposites

A.2.3 Encoding system

The video head encoding system measures the azimuth and altitude (inclination) angles of the RSV's pointing axis, these measurements form two of the spherical polar co-ordinates. These coordinates are referenced to some nominal point, usually this is either true or magnetic north although this does not have to be the case. To make measurements of the azimuth and inclination angles the RSV system uses single turn optical angular encoders mounted to a video head. These devices measure the single axis rotation of the device away from the set-point around a fixed shaft, single turn means that angles 0.00-359.99 degrees are recorded before resetting to 0. The optical element is the method of digitising the angle measurement. An LED shines through a perforated patterned disc. The pattern on the disk allows light to shine through onto a light sensing array encoding the position of the device relative to a fixed shaft. In the RSV system two encoders (A.5) are needed to measure the azimuth and inclination angles. The fixed shafts are the video head mounting bolt axis (Azimuth) and the video head pivoting bolt axis (Altitude/inclination).

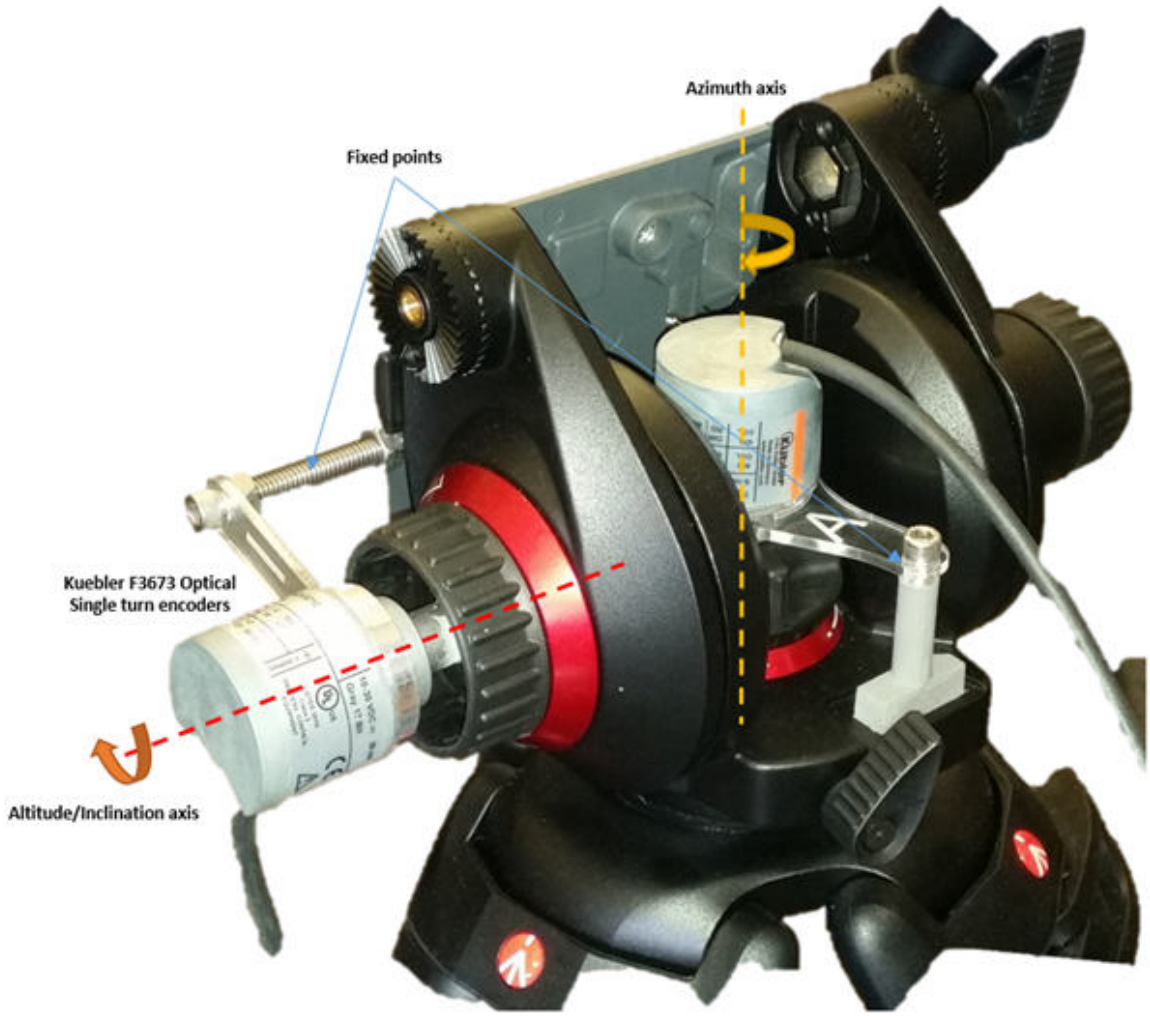

Fig. A.5 RSV encoder mounting on video head

The video head and tripod form the basis of the rotational system. They must be heavy enough to provide a stable platform but still maintain a level of portability. The video head must have space to install the encoders have fixed bolting options to mount them to. The Manfrotto 504HD video has 55mm of space between the rotational cuffs leaving ample room for the ø 40mm Kuebler encoders. All bolting points conform to industry standard ¼" 20TPI UNC threads. The video head has a fluid drag system to effect the pan and tilt velocities and a 2kg counterbalance spring which accommodates an offset c.g. position, necessary to improve the operational experience for the user. The video head is attached to a Manfrotto 546B tripod. The tripod and video head weigh in at 5.4kg, combined with a low-level spreader and adjustable level they provide a stable platform on a variety of terrain.

A.2.4 Camera system

The specifications are shown in table A.5.

Table A.5 Panasonic Lumix GH4 specifications

PANASONIC LUMIX G DMC-GH4RH	
Image sensor size	17.3 X 13.0 mm (4:3 Aspect ratio)
Lens mount	Micro four thirds
Image sensor	Live MOS
Total pixels	17.20 megapixels
Camera effective pixels	16.05 megapixels
Recording formats	MOV, MP4, AVCHD
Aspect ratios	4:3, 3:2, 16:9, 1:1
Resolution	4K, 2K
Frame rate	24, 25, 30, 50, 60, 96

The 2K full high definition (FHD) resolution (1920X1080) uses the full width of the sensor with pixel bining maximising the sensor width being utilised. By comparison although the camera is able to film at 4K ultra high definition (UHD) resolution (3840X2160) the sensor uses a 1:1 pixel readout across a smaller area of the image sensor (Table A.6).

Table A.6 GH4 video mode resolutions

Mode	**Image width (pixels)**	**Image height (pixels)**	**Aspect ratio**
4k	3840	2160	1.78
2k	1920	1080	1.78
Sensor width (mm)	**Sensor height (mm)**	**Crop factor**	**Notes**
14.4	8.1	2.5	1:1 pixel readout
17.3	9.7	2.1	Full sensor with pixel binning

A.2.5 Video resolution - working range

A variety of fixed focal length lenses are used based on the expected mean range measurement (Table A.7).

Table A.7 Range calculations for different focal length lenses based on a maximum allowable error of 0.2m

Focal length (mm)	2K Min range (m)	2K Max range (m)	4k Min range (m)	4K Max range (m)
105mm	27.97	93.49	33.60	96.69
200mm	53.27	129.02	64.00	113.59
300mm	79.91	158.02	96.00	125.71

A.3 RSV Software

A.3.1 Graphical User Interface

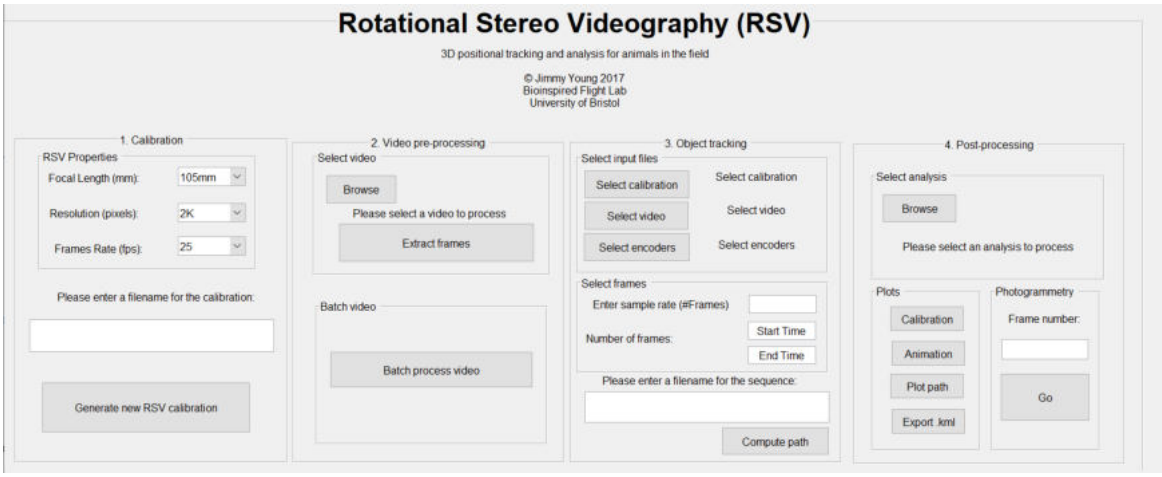

Fig. A.6 Front end graphical user interface of the RSV software component showing the available module functions

Bibliography

[1] Dale Richards. Flying high: a human perspective of unmanned aerial systems in future cities. *Theoretical Issues in Ergonomics Science*, 0(0):1–16, 2021.

[2] I Gursul. Vortex Flows on UAVs: Issues and Challenges. 108(1090):597–610, 2004.

[3] A. C. Carruthers, S. M. Walker, A. L. R. Thomas, and G. K. Taylor. Aerodynamics of aerofoil sections measured on a free-flying bird. *Proceedings of the Institution of Mechanical Engineers, Part G: Journal of Aerospace Engineering*, 224:855–864, 2010.

[4] Judy Shamoun-Baranes, Willem Bouten, E Emiel Van Loon, Christiaan Meijer, and CJ Camphuysen. Flap or soar? how a flight generalist responds to its aerial environment. *Philosophical Transactions of the Royal Society B: Biological Sciences*, 371(1704):20150395, 2016.

[5] Julie M Mallon, Keith L Bildstein, and Todd E Katzner. In-flight turbulence benefits soaring birds. *The Auk: Ornithological Advances*, 133(1):79–85, 2016.

[6] Graham K. Taylor, Kate V. Reynolds, and Adrian L.R. Thomas. Soaring energetics and glide performance in a moving atmosphere. *Philosophical Transactions of the Royal Society B: Biological Sciences*, 371(1704), 2016.

[7] Jiakun Han, Zhe Hui, Fangbao Tian, and Gang Chen. Review on bio-inspired flight systems and bionic aerodynamics. *Chinese Journal of Aeronautics*, 2020.

[8] Douglas Altshuler, Joe Bahlman, Roslyn Dakin, Andrea Gaede, Benjamin Goller, David Lentink, Paolo Segre, and Dimitri Skandalis. The biophysics of bird flight: Functional relationships integrate aerodynamics, morphology, kinematics, muscles, and sensors. *Canadian Journal of Zoology*, 93, 10 2015.

[9] Stephen M. Gatesy and Kenneth P. Dial. Locomotor modules and the evolution of avian flight. *Evolution*, 50(1):331–340, 1996.

[10] James Richard Usherwood. Physiological, aerodynamic and geometric constraints of flapping account for bird gaits, and bounding and flap-gliding flight strategies. *Journal of Theoretical Biology*, 408:42–52, 2016.

[11] C.J. Pennycuick. Soaring behaviour and performance of some East African birds, observed from a motor-glider. *Ibis*, 114, 2008.

[12] E. H. Hankin and J. D. North. On the Angle of Incidence in Soaring Flight. *Mathematical Proceedings of the Cambridge Philosophical Society*, 22(2):186–188, 1924.

[13] Eli S. Bridge, Kasper Thorup, Melissa S. Bowlin, Phillip B. Chilson, Robert H. Diehl, Rene W. Fleron, Phillip Hartl, Kays Roland, Jeffrey F. Kelly, W. Douglas Robinson, and Martin Wikelski. Technology on the move: Recent and forthcoming innovations for tracking migratory birds. *BioScience*, 61(9):689–698, 2011.

[14] Eli S. Bridge, Jeffrey F. Kelly, Andrea Contina, Richard M. Gabrielson, Robert B. MacCurdy, and David W. Winkler. Advances in tracking small migratory birds: A technical review of light-level geolocation. *Journal of Field Ornithology*, 84(2):121–137, 2013.

[15] Caroline H. Brighton and Graham K. Taylor. Hawks steer attacks using a guidance system tuned for close pursuit of erratically manoeuvring targets. *Nature Communications*, 10(1), 2019.

[16] Jorn Cheney, Jonathan PJ Stevenson, Nick Durston, Jialei Song, Masateru Maeda, Shane Windsor, James Usherwood, and Richard Bomphrey. From wing shape to fluid dynamics in the barn owl (Tyto alba). 2020.

[17] Lamber Royakkers and Rinie van Est. A literature review on new robotics: automation from love to war. *International journal of social robotics*, 7(5):549–570, 2015.

[18] E. de Margerie, M. Simonneau, J.-P. Caudal, C. Houdelier, and S. Lumineau. 3D tracking of animals in the field, using rotational stereo videography. *Journal of Experimental Biology*, (June):2496–2504, 2015.

[19] Bo Hang Wang, Dao Bo Wang, Zain Anwar Ali, Bai Ting Ting, and Hao Wang. An overview of various kinds of wind effects on unmanned aerial vehicle. *Measurement and Control*, 52(7-8):731–739, 2019.

[20] Peter Alan Davidson. *Turbulence: an introduction for scientists and engineers.* Oxford university press, 2015.

[21] HB Tolefson. An analysis of the variation with altitude of effective gust velocity in convective-type clouds. Technical report, 1948.

[22] U.S. Geological Survey. How much does a cloud weigh? *U.S. Geological Survey*, 2020.

[23] SH Abbasi and A Mahmood. Bio-inspired gust mitigation system for a flapping wing uav: modeling and simulation. *Journal of the Brazilian Society of Mechanical Sciences and Engineering*, 41(11):1–12, 2019.

[24] Paul B. MacCready. Standardization of Gustiness Values from Aircraft. *Journal of Applied Meteorology and Climatology*, 1964.

[25] Robert Sharman, C. Tebaldi, G. Wiener, and J. Wolff. An integrated approach to mid- and upper-level turbulence forecasting. *Weather and Forecasting*, 21(3):268–287, 2006.

[26] Luke N. Storer, Paul D. Williams, and Philip G. Gill. Aviation Turbulence: Dynamics, Forecasting, and Response to Climate Change. *Pure and Applied Geophysics*, 176(5):2081–2095, 2019.

[27] Abdulghani Mohamed, Kevin Massey, Simon Watkins, and Reece Clothier. The attitude control of fixed-wing MAVS in turbulent environments. *Progress in Aerospace Sciences*, 66:37–48, 2014.

[28] A. Mohamed, S. Watkins, R. Clothier, M. Abdulrahim, K. Massey, and R. Sabatini. Fixed-wing MAV attitude stability in atmospheric turbulence - Part 2: Investigating biologically-inspired sensors. *Progress in Aerospace Sciences*, 71:1–13, 2014.

[29] A. Mohamed, R. Clothier, S. Watkins, R. Sabatini, and M. Abdulrahim. Fixed-wing MAV attitude stability in atmospheric turbulence, part 1: Suitability of conventional sensors. *Progress in Aerospace Sciences*, 70:69–82, 2014.

[30] Barnes W McCormick. *Aerodynamics, aeronautics and flight mechanics*. Wiley, 1979.

[31] Gloria Stenfelt and Ulf Ringertz. Lateral stability and control of a tailless aircraft configuration. *Journal of Aircraft*, 46(6):2161–2164, 2009.

[32] Orville Wright and Wilbur Wright. Improvements in Aeronautical Machines, 1903.

[33] K P Dial. An inside look at how birds fly: experimental studies of the internal and external processes controlling flight, 1994.

[34] Gary F. McCracken, Kamran Safi, Thomas H. Kunz, Dina K.N. Dechmann, Sharon M. Swartz, and Martin Wikelski. Airplane tracking documents the fastest flight speeds recorded for bats. *Royal Society Open Science*, 3(11), 2016.

[35] Hannah J Williams, ELC Shepard, Olivier Duriez, and Sergio Agustin Lambertucci. Can accelerometry be used to distinguish between flight types in soaring birds? *Animal Biotelemetry*, 3(1):1–11, 2015.

[36] Rudolf Dvovrak. Aerodynamics of bird flight. 114:01001, 2016.

[37] Lucy A. Taylor, Dora Biro, Ben Lambert, James A. Walker, Graham K. Taylor, and Steven J. Portugal. Birds invest wingbeats to keep a steady head and reap the ultimate benefits of flocking. *bioRxiv*, pages 1–20, 2018.

[38] Christina Harvey and Daniel J Inman. Aerodynamic efficiency of gliding birds vs. comparable UAVs: a review. *Bioinspiration & Biomimetics*, 2020.

[39] Leonardo da Vinci. Codex on the Flight of Birds. 1698.

[40] T C Williams and J M Williams. Radar studies of bird migration. 1974.

[41] Bruno Bruderer and Peter Steidinger. Methods of quantitative and qualitative analysis of bird migration with a tracking radar. *NASA, Washington Animal Orientation and Navigation*, 1972.

[42] Vance A Tucker. Stereoscopic Views of Three-Dimensional, Rectangular Flight Paths in Descending African White-Backed Vultures (Gypes africanus). *The American Ornithologists' Union*, 108(1):1–7, 1991.

[43] CJ Pennycuick. The Ornithodolite. 1982.

[44] W. G. Delinger and W. R. Willis. High-precision portable instrument to measure position angles of a video camera for bird flight research. *Review of Scientific Instruments*, 59(5):797–801, 1988.

[45] Emily L C Shepard, C. Williamson, and S. P. Windsor. Fine-scale flight strategies of gulls in urban airflows indicate risk and reward in city living. *Philosophical transactions of the Royal Society of London B: Biological Sciences*, 371:20150394, 2016.

[46] Diane H Theriault, Nathan W Fuller, Brandon E Jackson, Evan Bluhm, Dennis Evangelista, Zheng Wu, Margrit Betke, and Tyson L Hedrick. A protocol and calibration method for accurate multi-camera field videography. *The Journal of Experimental Biology*, 217(11):1843–1848, 2014.

[47] M Elsbeth McPhee and K Carlstead. Effects of captivity on the behavior of wild mammals. *Wlid Mammals in Captivity: Principles and Techniques for Zoo Management*, pages 317–333, 2010.

[48] J. Y. Su, S. C. Ting, and J. T. Yang. How a Small Bird Executes a Sharp Turning Maneuver: A Mechanical Perspective. *Experimental Mechanics*, 52(7):693–703, 2012.

[49] D. T. Polet and D. E. Rival. Rapid area change in pitch-up manoeuvres of small perching birds. *Bioinspiration and Biomimetics*, 10(6), 2015.

[50] D. Lentink, U. K. Muller, E. J. Stamhuis, R. De Kat, W. Van Gestel, L. L.M. Veldhuis, P. Henningsson, A. Hedenstrom, J. J. Videler, and J. L. Van Leeuwen. How swifts control their glide performance with morphing wings. *Nature*, 446(7139):1082–1085, 2007.

[51] David Lentink, Andreas F Haselsteiner, and Rivers Ingersoll. In vivo recording of aerodynamic force with an aerodynamic force platform: from drones to birds. *Journal of the Royal Society Interface*, 12(104):20141283, 2015.

[52] Dietrich Bilo. Biophysics of the flight of small birds - I. Kinematics and aerodynamics of the downstroke of the house sparrow (Passer domesticus L.). *Zeitschrift fur Vergleichende Physiologie*, 71(4):382–454, 1971.

[53] Ch Brill, D. P. Mayer-Kunz, and W. Nachtigall. Wing profile data of a free-gliding bird. *Naturwissenschaften*, 76(1):39–40, 1989.

[54] Tianshu Liu, K. Kuykendoll, R. Rhew, and S. Jones. Avian wing geometry and kinematics. *AIAA Journal*, 44(5):954–963, 2006.

[55] Graham K. Taylor, Marko Bacic, Anna C. Carruthers, James Gillies, Yukie Ozawa, and Adrian L R Thomas. Flight control mechanisms in birds of prey. *Collection of Technical Papers - 45th AIAA Aerospace Sciences Meeting*, 1(January):347–354, 2007.

[56] Kate V Reynolds, Adrian L R Thomas, and Graham K Taylor. Wing tucks are a response to atmospheric turbulence in the soaring flight of the steppe eagle Aquila nipalensis. *Journal of the Royal Sciety Interface*, 11(101):20140645, 2014.

[57] James R. Usherwood, Jorn A. Cheney, Jialei Song, Shane P. Windsor, Jonathan P.J. Stevenson, Uwe Dierksheide, Alex Nila, and Richard J. Bomphrey. High aerodynamic lift from the tail reduces drag in gliding raptors. *Journal of Experimental Biology*, 223(3), 2020.

[58] Douglas L. Altshuler, Joseph W. Bahlman, Roslyn Dakin, Andrea H. Gaede, Benjamin Goller, David Lentink, Paolo S. Segre, and Dimitri A. Skandalis. The biophysics of bird flight: Functional relationships integrate aerodynamics, morphology, kinematics, muscles, and sensors. *Canadian Journal of Zoology*, 93(12):961–975, 2014.

[59] Bret W Tobalske. Biomechanics of bird flight. *Journal of Experimental Biology*, 210(18):3135–3146, 2007.

[60] Adrian L.R. Thomas and Graham K. Taylor. Animal Flight Dynamics I. Stability in Gliding Flight. *Journal of Theoretical Biology*, 212(3):399–424, 2001.

[61] Graham K. Taylor and Adrian L. R. Thomas. Animal Flight Dynamics II. Longitudinal Stability in Flapping Flight. 2001.

[62] Moosarreza Shamsyeh Zahedi and Mir Yaseen Ali Khan. A mechanical model of wing and theoretical estimate of taper factor for three gliding birds. *Journal of Biosciences*, 32(2):351–361, 2007.

[63] M. Fluck and C. Crawford. A lifting line model to investigate the influence of tip feathers on wing performance. *Bioinspiration and Biomimetics*, 9(4), 2014.

[64] Blake. Mechanics of Gliding Birds with reference to the influence of ground effect. 16(Columba livid):649–654, 1983.

[65] S. A. Andrews, R. E. Perez, and W. D.E. Allan. Aerodynamic implications of gull's drooped wing-tips. *Bioinspiration and Biomimetics*, 8(4), 2013.

[66] Gottfried Sachs. Yaw stability in gliding birds. *Journal of Ornithology*, 146(3):191–199, 2005.

[67] Gottfried Sachs and Mochammad Agoes Moelyadi. Effect of slotted wing tips on yawing moment characteristics. *Journal of Theoretical Biology*, 239(1):93–100, 2006.

[68] Gottfried Sachs. Tail effects on yaw stability in birds. *Journal of Theoretical Biology*, 249(3):464–472, 2007.

[69] Haider Al-Lami, Ameer Aslam, Tanya Quigley, Jack Lewis, Richard Mercer, and Prashant Shukla. The evolution of flight control systems. *Technology Development, System Architecture and Operation*, 2015.

[70] C. Gablehouse. *Helicopters and Autogiros: A History of Rotating-wing and V/STOL Aviation*. Lippincott, 1969.

[71] John J Videler. *Avian flight*. Oxford University Press, 2006.

[72] L Shyamal. Bones of wing of bird, 2007.

[73] L Shyamal. Diagram of skeletal structure and musculature of a bird's wing, 2012.

[74] VB Baliga, I Szabo, and DL Altshuler. Range of motion in the avian wing is strongly associated with flight behavior and body mass. *Science advances*, 5(10):eaaw6670, 2019.

[75] BirdForum. General anatomy and topography. 2020.

[76] Christina Harvey, Lawren L Gamble, Christian R Bolander, Douglas F Hunsaker, James J Joo, and Daniel J Inman. A review of avian-inspired morphing for uav flight control. *Progress in Aerospace Sciences*, 132:100825, 2022.

[77] Zheng Min, Vu Khac Kien, and Liew JY Richard. Aircraft morphing wing concepts with radical geometry change. *The IES Journal Part A: Civil & Structural Engineering*, 3(3):188–195, 2010.

[78] Daniel T Grant, Mujahid Abdulrahim, and Rick Lind. Flight dynamics of a morphing aircraft utilizing independent multiple-joint wing sweep. *International Journal of Micro Air Vehicles*, 2(2):91–106, 2010.

[79] Robert D Vocke, Curt S Kothera, Benjamin KS Woods, and Norman M Wereley. Development and testing of a span-extending morphing wing. *Journal of Intelligent Material Systems and Structures*, 22(9):879–890, 2011.

[80] Jiaying Zhang, Alexander D Shaw, Chen Wang, Huaiyuan Gu, Mohammadreza Amoozgar, Michael I Friswell, and Benjamin KS Woods. Aeroelastic model and analysis of an active camber morphing wing. *Aerospace Science and Technology*, 111:106534, 2021.

[81] Mujahid Abdulrahim and Rick Lind. Flight testing and response characteristics of a variable gull-wing morphing aircraft. page 5113, 2004.

[82] Desta Alemayehu, Mathieu Leng, Ryan McNulty, Michael Mulloy, Ryan Somero, and Cyril de Tenorio. Virginia tech morphing wing team fall 2004 final report. *Virginia Tech, Blacksburg, VA*, 2004.

[83] C. Harvey, V. B. Baliga, P. Lavoie, and D. L. Altshuler. Wing morphing allows gulls to modulate static pitch stability during gliding. *Journal of the Royal Society Interface*, 16(150), 2019.

[84] C. J. Williamson, A. Spelt, and S. P. Windsor. Bird-inspired velocity optimization for unmanned aerial vehicles in the urban environment. *AIAA Scitech 2020 Forum*, 1 PartF(January), 2020.

[85] John P Lewis. Fast template matching. 95(120123):15–19, 1995.

[86] William Thielicke and Eize J. Stamhuis. PIVlab – Towards User-friendly, Affordable and Accurate Digital Particle Image Velocimetry in Matlab. *Journal of Open Research Software*, 2, 2014.

[87] David Gallup, Jan-michael Frahm, Philippos Mordohai, Marc Pollefeys, and Chapel Hill. Variable Baseline / Resolution Stereo.

[88] E. Ostertagova and O. Ostertag. Methodology and application of Savitzky-Golay moving average polynomial smoother. *Global Journal of Pure and Applied Mathematics*, 12(4):3201–3210, 2016.

[89] C. J. Pennycuick. Speeds and wingbeat frequencies of migrating birds compared with calculated benchmarks. *Journal of Experimental Biology*, 204(19):3283–3294, 2001.

[90] Tyson L Hedrick, Cecile Pichot, and Emmanuel de Margerie. Gliding for a free lunch: biomechanics of foraging flight in common swifts (apus apus). *Journal of Experimental Biology*, 221(22):jeb186270, 2018.

[91] C Harvey, VB Baliga, CD Goates, DF Hunsaker, and DJ Inman. Gull-inspired joint-driven wing morphing allows adaptive longitudinal flight control. *Journal of the Royal Society Interface*, 18(179):20210132, 2021.

[92] Google maps, 2022.

[93] Emily LC Shepard, Cara Williamson, and Shane P Windsor. Fine-scale flight strategies of gulls in urban airflows indicate risk and reward in city living. *Philosophical Transactions of the Royal Society B: Biological Sciences*, 371(1704):20150394, 2016.

[94] Nguyen X Vinh. *Flight mechanics of high-performance aircraft*, volume 4. Cambridge university press, 1995.

[95] Cara J Williamson, Anouk Spelt, and Shane P Windsor. Bird-inspired velocity optimization for uavs in the urban environment. In *AIAA Scitech 2020 Forum*, page 1948, 2020.

[96] Cara Williamson. Bio-inspired Path Planning for Unmanned Air Vehicles in Urban Environments. 2020.

[97] EASA. Easy Access Rules for Normal, Utility, Aerobatic and Commuter Category Aeroplanes (CS-23) (Initial issue). page 39, 2018.

[98] EASA. Easa certification specifications for normal, utility, aerobatic, and commuter category aeroplanes cs-23, 2020.

[99] Branko Stojkovic. Generalized speed.to.fly. XVII(3), 1991.

[100] Brian L Stevens, Frank L Lewis, and Eric N Johnson. *Aircraft control and simulation: dynamics, controls design, and autonomous systems*. John Wiley & Sons, 2015.

[101] Ron A Meyers and Edward Mathias. Anatomy and histochemistry of spread-wing posture in birds. 2. gliding flight in the california gull, larus californicus: A paradox of fast fibers and posture. *Journal of morphology*, 233(3):237–247, 1997.

[102] Jorn A. Cheney, Jonathan P.J. Stevenson, Nicholas E. Durston, Jialei Song, James R. Usherwood, Richard J. Bomphrey, and Shane P. Windsor. Bird wings act as a suspension system that rejects gusts: Bird wings act as a suspension system. *Proceedings of the Royal Society B: Biological Sciences*, 287(1937), 2020.

[103] Ryan M Shelton, Brandon E Jackson, and Tyson L Hedrick. The mechanics and behavior of cliff swallows during tandem flights. *The Journal of experimental biology*, 217(Pt 15):2717–2725, 2014.

[104] David E Alexander. Wind tunnel studies of turns by flying dragonflies. *Journal of Experimental Biology*, 122(1):81–98, 1986.

[105] Douglas R Warrick, MW Bundle, and KP Dial. Bird maneuvering flight: blurred bodies, clear heads. *Integrative and Comparative Biology*, 42(1):141–148, 2002.

[106] Silvestro Barbarino, Onur Bilgen, Rafic M Ajaj, Michael I Friswell, and Daniel J Inman. A review of morphing aircraft. *Journal of intelligent material systems and structures*, 22(9):823–877, 2011.

[107] JD Simon and Sanjoy K Mitter. A theory of modal control. *Information and Control*, 13(4):316–353, 1968.

[108] Mark Drela. Xfoil: An analysis and design system for low reynolds number airfoils. In *Low Reynolds number aerodynamics*, pages 1–12. Springer, 1989.

[109] Mark Drela and Harold Youngren. Avl. *URL http://web. mit. edu/drela/Public/web/avl/. Diakses*, 14, 2014.

[110] Mohammad Badwan and Tarek A Tutunji. System identification for bixler3 unmanned aerial vehicle. In *2018 19th International Conference on Research and Education in Mechatronics (REM)*, pages 93–98. IEEE, 2018.

[111] Chris Foss. Chris foss wot 4. *URL http://http://www.chrisfoss.co.uk/wot-4/4538950500/*, 2021.

[112] Charles W Harper and Ralph L Maki. A review of the stall characteristics of swept wings. 1964.

[113] Wolf R Kruger, Thomas Klimmek, Rene Liepelt, Hauke Schmidt, Stefan Waitz, and Sunpeth Cumnuantip. Design and aeroelastic assessment of a forward-swept wing aircraft. *CEAS Aeronautical Journal*, 5(4):419–433, 2014.

[114] Fred EC Culick and Henry R Jex. Aerodynamics, stability and control of the 1903 wright flyer. 1985.

[115] Lorenz Meier, Dominik Honegger, and Marc Pollefeys. Px4: A node-based multithreaded open source robotics framework for deeply embedded platforms. In *2015 IEEE international conference on robotics and automation (ICRA)*, pages 6235–6240. IEEE, 2015.

[116] Rick Bitter, Taqi Mohiuddin, and Matt Nawrocki. *LabVIEW™ Advanced Programming Techniques*. CRC press, 2017.

[117] Desmond J Higham and Nicholas J Higham. *MATLAB guide*. SIAM, 2016.

[118] Guy Norris. Shaping up: prototype wingtip folding system tests begin as 777x passes firm-configuration milestone. *Aviation Week & Space Technology*, 2015.

[119] Fintan Healy, Ronald Cheung, Theodor Neofet, Mark Lowenberg, Djamel Rezgui, Jonathan Cooper, Andrea Castrichini, and Tom Wilson. Folding wingtips for improved roll performance. *Journal of Aircraft*, 59(1):15–28, 2022.

[120] Andrea Castrichini, Vijaya Hodigere Siddaramaiah, DE Calderon, Jonathan E Cooper, Thomas Wilson, and Yves Lemmens. Nonlinear folding wing tips for gust loads alleviation. *Journal of Aircraft*, 53(5):1391–1399, 2016.

[121] Aldo Frediani and Guido Montanari. Best wing system: an exact solution of the prandtl's problem. In *Variational analysis and aerospace engineering*, pages 183–211. Springer, 2009.

[122] Ulla M Norberg. Bat wing structures important for aerodynamics and rigidity (mammalia, chiroptera). *Zeitschrift fur Morphologie der Tiere*, 73(1):45–61, 1972.

[123] DBO Savile. Adaptive evolution in the avian wing. *Evolution*, pages 212–224, 1957.

[124] Vance A Tucker. Pitching equilibrium, wing span and tail span in a gliding harris' hawk, parabuteo unicinctus. *Journal of experimental biology*, 165(1):21–41, 1992.

[125] Nicholas E Durston, Xue Wan, Jian G Liu, and Shane P Windsor. Avian surface reconstruction in free flight with application to flight stability analysis of a barn owl and peregrine falcon. *Journal of Experimental Biology*, 222(9):jeb185488, 2019.

[126] Sofía Miñano and Graham K Taylor. Through hawks' eyes: reconstructing a bird's visual field in flight to study gaze strategy and attention during perching and obstacle avoidance. *bioRxiv*, pages 2021–06, 2021.

[127] Mark Sumich and Rodney O Bailey. X-36 tailless fighter agility research aircraft. 1998.

[128] Bradley Joseph Zelenka. *An Experimental Investigation of the Prandtl-D Research Glider's Aerodynamic Characteristics*. PhD thesis, San Diego State University, 2021.

[129] Adrian LR Thomas. Why do birds have tails? the tail as a drag reducing flap, and trim control. *Journal of Theoretical Biology*, 183(3):247–253, 1996.

[130] Adrian LR Thomas. On the tails of birds. *Bioscience*, pages 215–225, 1997.